UNIVERSITEIT VAN PRETORIA
UNIVERSITY OF PRETORIA
YUNIBESITHI YA PRETORIA

COOLING CHARACTERISTICS OF HIGH TITANIA SLAGS

by

Deon Bessinger

A dissertation submitted in fulfilment of the requirements for the degree

Magister Scientiae

In the Department of Materials Science and Metallurgical Engineering, Faculty of Engineering, the Built Environment and Information Technology, University of Pretoria

Supervisor: Professor J.M.A. Geldenhuis
Co-supervisor: Professor P.C. Pistorius

October 2000

ABSTRACT

Various aspects relevant to the cooling of high titania slags were investigated. Rapidly quenched slags contain several phases, of which the M_3O_5 phase is the most prominent and important. Other phases include rutile, metallic iron and glass phases. The M_3O_5 phase (with M being mainly Ti and Fe) is essentially a solid solution, with Ti_3O_5 and $FeTi_2O_5$ as end members of the solid solution series. Impurities such as Al, Mg and Mn are also present in this solid solution. The composition of a typical high titania slag is approximately 10 per cent FeO, 30 per cent Ti_2O_3 and 55 per cent TiO_2. It was established that there is a linear relationship between the Ti_2O_3 content and FeO content of the slag. This relationship can be explained in terms of the M_3O_5 solid solution end members, Ti_3O_5 and $FeTi_2O_5$. A linear relationship between the tap temperatures and the FeO content of titania slags was also obtained.

Decrepitation behaviour of one ton slag blocks was observed during slow cooling of the high titania slag. For the purpose of this study decrepitation was defined as the disintegration or crumbling of a material into component parts or smaller fragments. This decrepitation process was simulated on a laboratory scale by heating various slag samples in air at temperatures below 600 °C for various times. Samples heated at temperatures above 600 °C did not decrepitate. The decrepitated samples were characterised by extensive cracking of the material. Decrepitation of the high titania slag was explained by oxidation of the M_3O_5 phase to form a M_6O_{11} phase and anatase. This decrepitation, and the associated cracking of the slag, was probably caused by volume changes due to the formation of these new phases.

Key words
Titania slag, ilmenite smelting, decrepitation, anatase, rutile, pseudobrookite, oxidation, tapping temperatures, M_3O_5, slag cooling.

OPSOMMING

Verskeie aspekte relevant tot die afkoeling van titaanslak is ondersoek. Slakke wat vinnig geblus is bevat verskeie fases. Hiervan is die M_3O_5 fase die mees prominente en belangrike fase. Ander fases wat teenwoordig is sluit in rutiel, metalliese yster en glas fases. Die M_3O_5 fase (met M hoofsaaklik Ti en Fe) is 'n vaste oplossing, met Ti_3O_5 en $FeTi_2O_5$ as die eindsamestellings van die mengreeks. Al, Mg en Mn is teenwoordig as onsuiwerhede in die vaste oplossing. Die samestelling van tipiese hoë titaanslakke is ongeveer 10 persent FeO, 30 persent Ti_2O_3 en 55 persent TiO_2. 'n Lineêre verwantskap tussen die Ti_2O_3 en FeO inhoud van die slak is bepaal. Die verwantskap is verduidelik in terme van die M_3O_5 vaste oplossing eindsamestellings, Ti_3O_5 en $FeTi_2O_5$. 'n Lineêre verwantskap tussen die tap temperature en die FeO inhoud van titaanslakke is ook bepaal.

Dekrepitasiegedrag van een ton slak blokke is waargeneem tydens stadige afkoeling van die hoë titaanslak. Vir die doel van die studie is dekrepitasie gedefinieer as die disintegrasie of verbrokkeling van 'n materiaal in kleiner komponente of fragmente. Die dekrepitasie proses is gesimuleer op 'n laboratorium skaal deur verskeie slak monsters te verhit in lug by temperature onder 600 °C. Slak monsters wat bokant 600 °C verhit is het nie gedekrepiteer nie. Die gedekrepiteerde monsters het 'n groot aantal krake vertoon. Dekrepitasie van die hoë titaanslak is verduidelik in terme van die oksidasie van die M_3O_5 fase om 'n M_6O_{11} fase en anataas te vorm. Die volume veranderings in die slak (en die verwante krake) as gevolg van die vorming van die nuwe fases is die mees waarskynlike oorsaak van dekrepitasie in die titaan slak.

Sleutelwoorde
Titaanslak, ilmeniet smelting, dekrepitasie, anataas, rutiel, pseudobrookiet, oksidasie, tap temperature, M_3O_5, slak afkoeling.

TABLE OF CONTENTS

LIST OF FIGURES

LIST OF TABLES

LIST OF APPENDICES

1 INTRODUCTION

The presence of heavy minerals in South Africa has been known for several decades. During the 1950's ilmenite was mined at Umgababa as feedstock for a sulphate pigment plant located at Durban in KwaZulu-Natal (Lee and Poggi, 1978). In the late 1970's Richards Bay Minerals was founded on the east coast of South Africa. Heavy minerals are extracted from the dunes there and upgraded to produce rutile, zircon and ilmenite as the major products. The ilmenite is smelted in several electric arc furnaces to produce high titania slag and a metallic iron product. In 1997 Richards Bay Minerals had an annual production capacity of 1 million tons of titania slag (Anonymous, 1997). On the west coast of South Africa Namakwa Sands was founded in the early 1990's to extract heavy minerals from deposits situated near Vredendal. Again rutile, zircon and ilmenite are the main products. The products are transported to Saldanha where the ilmenite is smelted in DC arc electric furnaces to produce high titania slag and a metallic iron product. An increase in smelting capacity from 97 000 to 230 000 tons per annum was announced in 1998 (Anonymous, 1998). Iscor has also completed a feasibility study on the recovery of heavy minerals near Richards Bay, with approval of the project been given in the first half of 2000. This project also includes the smelting of ilmenite at a complex that will be erected at Empangeni. The capacity of this project will be 250 000 tons of high titania slag per annum.

The expansion of the titanium industry in South Africa over the last three decades shows the increasing importance of the industry to the local economy. South Africa has over this period evolved into one of the major titanium feedstock producers in the world. It is therefore important that the technical body of knowledge on the relevant metallurgical processes be expanded. This should enable the industry to optimise the processes and thereby obtain the maximum benefit for all.

This study will concentrate on aspects relevant to the smelting of ilmenite. In particular the focus will be on the following two aspects:

1. Characterisation of cooled high titania slags produced during the smelting of ilmenite. This will include the following:
   - The mineralogy of the slags.
   - The chemistry of the slags.
   - Relationships between the chemistry of the slags and the tapping temperatures of the slags.
2. The decrepitation behaviour of high titania slags after tapping.

A brief review of the titanium industry relevant to this study is given as background.

1.1 FEEDSTOCKS TO THE TITANIUM DIOXIDE PIGMENT INDUSTRY

The titanium dioxide pigment industry consumes over 90 per cent of the titanium mineral production worldwide (Stanaway, 1994; Fisher, 1997). The remaining uses for titanium minerals are as a flux for electric welding rods and for certain metallurgical and electronic applications. The most common titanium minerals that are mined are rutile and ilmenite. Rutile can be used directly in the pigment production processes to produce titanium dioxide pigment. Ilmenite is preferably treated to selectively remove the iron content in order to provide a product with a lower iron content. The removal of the iron content results in a

product with a high titanium content, resulting in less waste being produced in the processes producing the titanium dioxide pigments. The two main processes used for the upgrading of ilmenite are briefly discussed below.

1.1.1 SMELTING OF ILMENITE TO PRODUCE TITANIA SLAG

Ilmenite can be smelted at high temperatures (approximately 1650 to 1700 °C) with a suitable carbonaceous reductant in electric furnaces to produce high titania slag as the major product. In the process liquid iron is produced as a by-product. The iron product can subsequently be modified by secondary treatment (de-sulphurisation, carburisation, alloy additions) to optimise the value of the product (Lee and Poggi, 1978). The TiO_2 content (total Ti expressed as TiO_2) of the slag after reduction can range between 75 and 86 per cent. Not all the iron can be reduced, as some FeO in the slag is required to act as a fluxing agent. The final quality of the titania slag is dependent on both the quality of the ilmenite and the reductant. According to Grau and Poggi (1978) the reduction process can broadly be described by the following reactions:

$$Fe_2O_3 + C = 2FeO + CO \quad ...(A)$$

$$FeO + C = Fe + CO \quad ...(B)$$

$$2TiO_2 + C = Ti_2O_3 + CO \quad ...(C)$$

In the smelting process contact between the molten slag and the furnace refractories is prevented by the presence of a solid freeze lining. This freeze lining is required to prevent attack on the refractories by the corrosive molten slag (Grau and Poggi, 1978). Due to the high electrical conductivity of the slags (Desrosiers et. al., 1980) the electrodes are above the slag level in an "open arc" position. The high titania slag is tapped into ladles, water-cooled and crushed to produce the final products. Titania slag is used for both the sulphate and chloride process routes for the production of pigments. The criteria used for determining to which process route the slag should be allocated is determined mainly by the chemical quality and size distribution of the slag products. This will be discussed in more detail later.

Several producers worldwide use various smelting technologies to produce high titania slags. The producers are Richards Bay Minerals (RBM) and Namakwa Sands in South Africa, QIT in Canada and Tinfos in Norway. RBM and QIT use 6-in-line alternating current furnaces, while Namakwa Sands use two circular furnaces with direct current configurations.

1.1.2 SYNTHETIC RUTILE

The second type of process involves the partial or complete solid-state reduction of iron, followed by a leaching process to remove the iron content. An example of this type of process is the Becher process (Battle et. al., 1993). At present the leached iron is considered to be a waste product, although recent progress has been made in recovering this iron as a valuable product (McLoughlin et. al., 1998). A synthetic rutile product is produced containing approximately 90 to 96 per cent TiO_2. Current synthetic rutile production is

dominated by the Becher process (Grey, 1992). Other commercial processes for synthetic rutile production include the following (Battle et. al., 1993; Grey, 1992):

- The Benelite process involves a partial reduction of the iron in altered ilmenite to the ferrous state, followed by acid leaching of the iron and other impurities using hydrochloric acid.
- The Ishihara process utilises waste sulphuric acid from a sulphate-route pigment plant in Japan to leach ilmenite after partial reduction of the iron.

In Figure 1 the flowsheet of the improved Becher process are shown. This process is essentially a pyrometallurgical operation followed by a number of wet chemical process steps. It consists of the following three main process steps as described by Formanek et. al. (1997):

- Ilmenite, coal, char and sulphur are reacted in a rotary kiln at approximately 1200 °C in such a way that the iron oxide content of the ilmenite is reduced to metallic iron. This is different to the other synthetic rutile processes where the iron content of the ilmenite is only partially reduced. The sulphur is added to assist with the removal of manganese. Manganese sulfide is produced and then separated from the final product by a subsequent leaching step (Battle et. al., 1993). The reduced ilmenite is separated from the gangue materials by screening and magnetic separation. Coarse char recovered from the process is recycled to the kiln.

Figure 1: Flowsheet of the improved Becher process (from Formanek et. al., 1997)

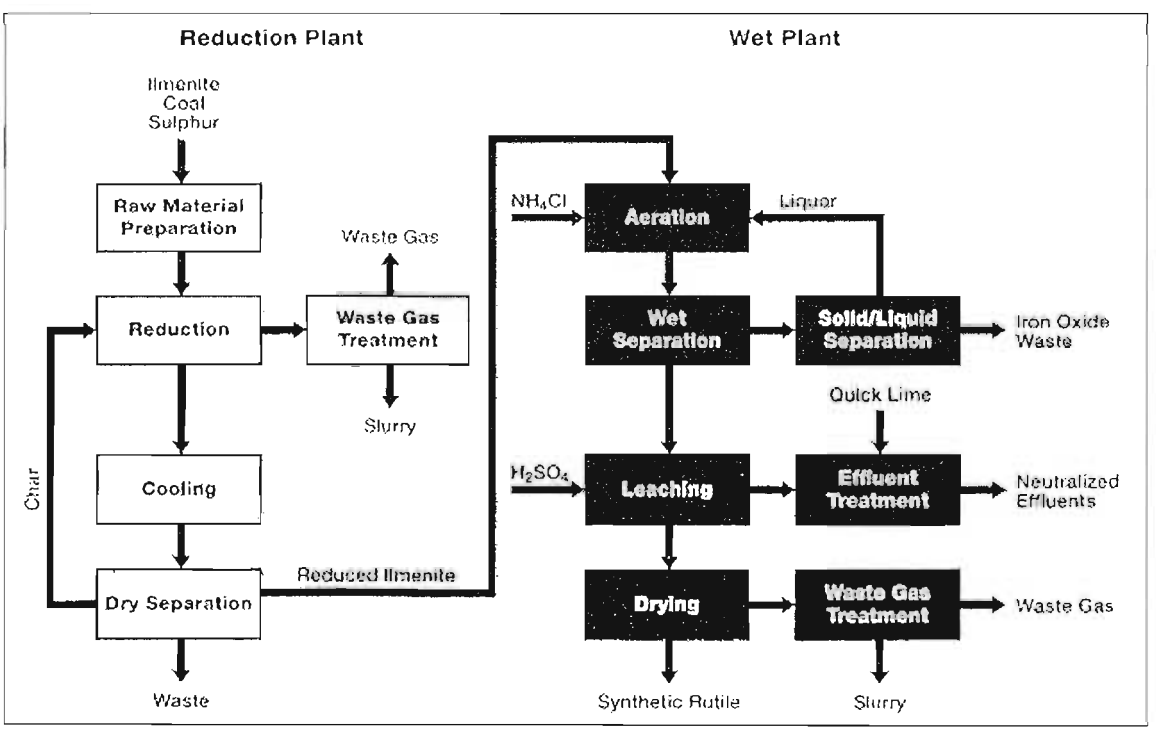

- The reduced ilmenite is aerated and stirred inside tanks in a 1.0 to 1.5 per cent ammonium chloride solution so that the iron is "rusted" from the ilmenite. The aeration process is carried out in batches. The mixture of synthetic rutile and iron oxide from the aeration step is separated in a multi-stage hydrocycloning system. At this stage the aerated product contains approximately 90 per cent TiO_2.

- The aerated product is separated from the iron oxide and leached with 10 per cent sulphuric acid to obtain a high quality synthetic rutile product. The leached product is separated from the acidic liquor in a spiral classifier. The remaining acid is removed from the synthetic rutile by counter-current washing on a belt filter. The synthetic rutile can then be dried in a flash or fluidised bed dryer. The final product contains 93.2 per cent TiO_2, with the main impurity being iron (2.4 per cent total iron). The product is porous, with a grain size similar to the original ilmenite.

The synthetic rutile product is generally sold to the chloride processing route for the production of pigments.

1.2 THE TITANIUM DIOXIDE PIGMENT INDUSTRY

Two processes are used to produce titanium dioxide pigments, these being the sulphate and chloride process routes respectively. All the high titania slag produced in the world via smelting processes is used as feedstock in one of these two processes.

1.2.1 PIGMENT MANUFACTURING PROCESSES

1.2.1.1 Sulphate processing route

The sulphate process for the production of titanium dioxide pigments was first used in Norway in 1915 (Fisher, 1997). This process is a batch process, using a number of unit operations. A flowsheet of a typical sulphate process is shown in Figure 2.

The main process steps are as follows (Fisher, 1997; Stanaway, 1994):
a) The titaniferous feed is reacted with sulphuric acid to produce titanyl sulphate. For ilmenite as feed the reaction can be written as follows:

$$FeTiO_3 + 2H_2SO_4 = TiOSO_4 + FeSO_4 + 2H_2O \ldots(D)$$

The highly exothermic reaction also emits hydrogen sulphide and sulphur dioxide as pollutants from various side reactions. Iron sulphate is removed from the solution as solid copperas ($FeSO_4.7H_2O$).
b) After the iron removal, titanyl sulphate is hydrolysed to titanium dioxide hydrate.
c) The precipitate is then chemically purified, filtered and calcined at 800 to 1100 °C to produce titanium dioxide (Habashi, 1997).

Subsequent process steps are required after this for the TiO_2 product to function as a pigment. These process steps are shown in Figure 3. These processes include milling of the particles to the required size specification and the addition of chemicals to the surface of the pigment particles to obtain the required optical and physical properties. These post-treatment processes can be similar for pigments produced by both the sulphate and chloride processes.

There is one operation in South Africa that uses this technology, this being the Huntsman Tioxide plant situated at Umbogintwini in the KwaZulu-Natal province. This plant supplies

titanium dioxide to the South African market and also exports approximately 30 per cent of its production (Tioxide Southern Africa, 1997).

Figure 2 : Flowsheet for a typical sulphate processing route (from Fisher, 1997)

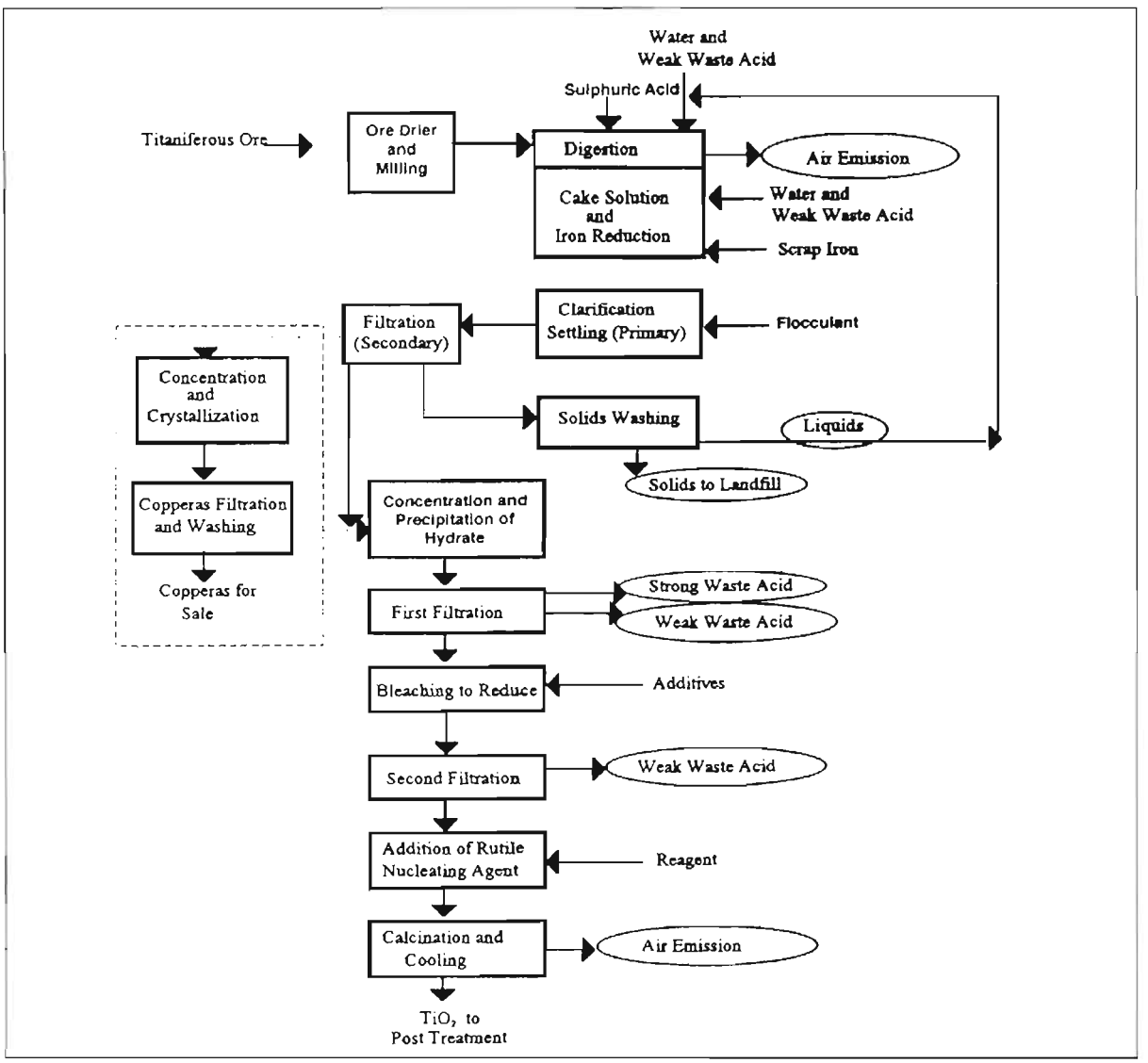

1.2.1.2 Chloride processing route

The chloride process was commercialised in the United States in 1958 (Fisher, 1997). The process is continuous and is carried out in a fluidised bed reactor. A flowsheet of a typical chloride process is shown in Figure 4. The main process steps are as follows (Fisher, 1997; Stanaway, 1994):

a) Chlorination of titanium feedstock using chlorine gas and coke to form various chloride species. The chlorination reaction is exothermic and is carried out at approximately 900 °C in a reducing atmosphere. The basic reactions can be written as follows:

$$2C + O_2 = CO \quad \ldots(E)$$

$$TiO_2 + 2Cl_2 + 2CO = TiCl_4 + 2CO_2 \ldots(F)$$

b) The volatile chloride species are separated by fractional distillation into low, medium and high boiling chlorides.

Figure 3 : A typical post-treatment process for titanium dioxide pigments (from Fisher, 1997)

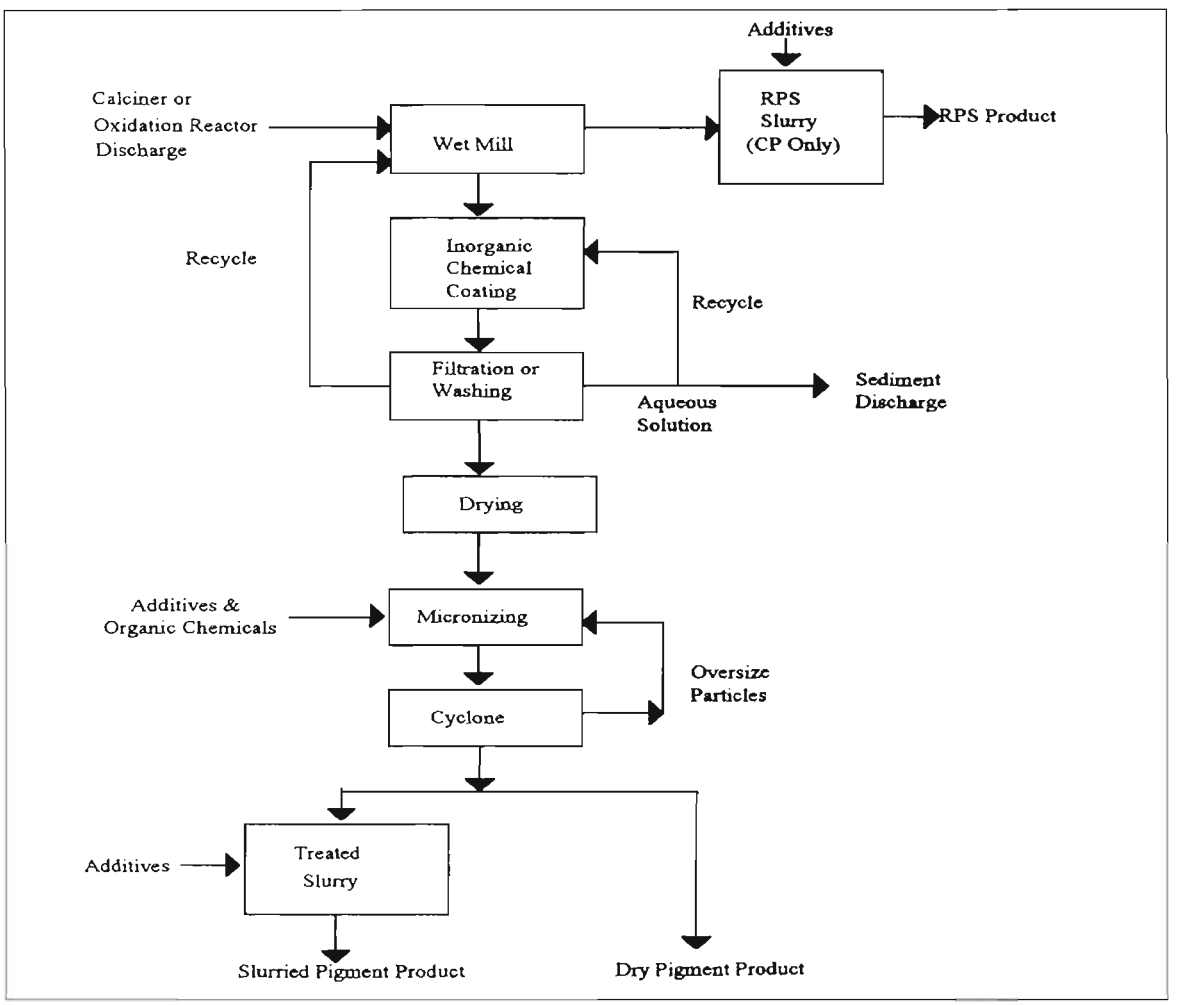

c) Titanium tetrachloride is then reacted with oxygen according to the following reaction:

$$TiCl_4 + O_2 = TiO_2 + 2Cl_2 \ldots(G)$$

The chlorine is recycled to the chlorinator, while the titanium dioxide can be processed further if required according to the flowsheet presented in Figure 3.

Because of commercial and environmental reasons the chloride processing route is preferred over the sulphate processing route. Approximately 57 per cent of all titanium dioxide pigments are produced by the chloride processing route. It is estimated that this will increase to approximately 69 per cent by the year 2010 (Fisher, 1997).

Figure 4 : Flowsheet for a typical chloride processing route (from Fisher, 1997)

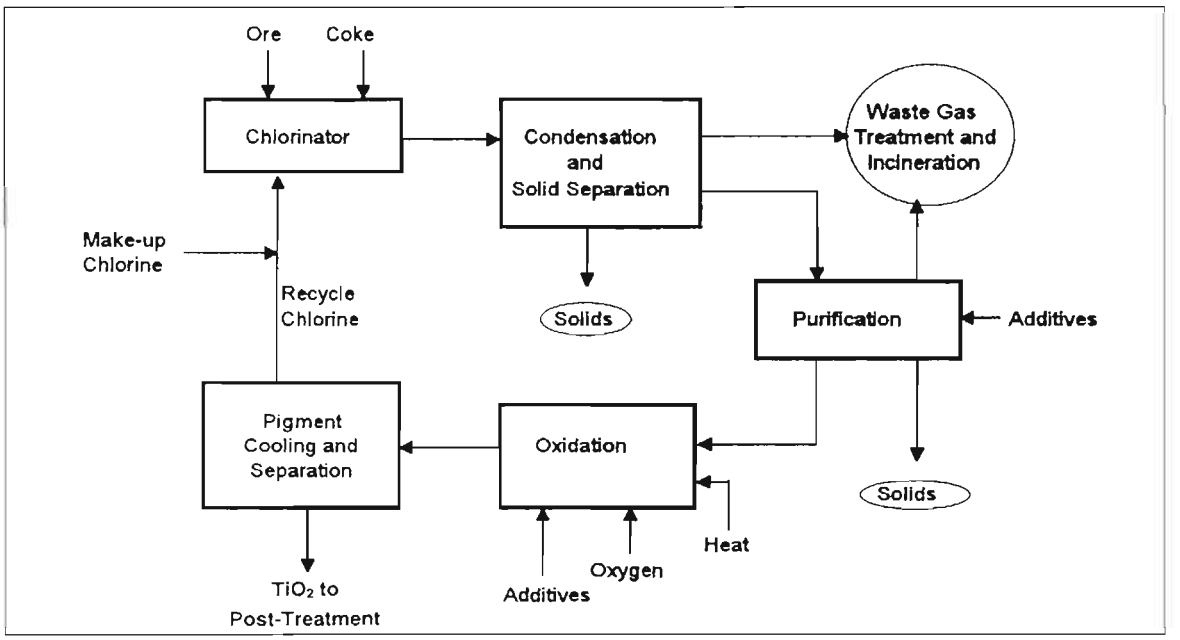

1.2.2 PIGMENT MARKETS

Titanium dioxide pigments are used across a wide range of applications. The major uses for titanium dioxide pigments are listed in Table 1 (Fisher, 1997). By far the largest use is as surface coating. In western countries titanium dioxide is now the most widely used white pigment in paints, having replaced zinc oxide, lithopone and white lead. Plastics represent the fastest growing market segment of the titanium dioxide pigment, with growth rates ranging between 5 and 18 per cent over the last two decades. Examples of some of the other uses of the titanium dioxide pigments include applications in ceramics, concrete, cosmetics, food, titanates and photovoltaic cells.

Table 1 : Global TiO_2 pigment consumption by industry (Fisher, 1997)

Use	Percentage of total world consumption
Surface coatings	59.8
Plastics	15.2
Paper	12.1
Printing inks	2.5
Fibres	2.7
Other	7.7

2 CHARACTERISTICS OF SOME HIGH TITANIA SLAGS PRODUCED IN A 3 MVA PLASMA FURNACE

2.1 INTRODUCTION

The smelting of ilmenite requires fine control of the smelting process in order to produce an acceptable slag product on a consistent basis. This section will deal with some of the characteristics of the slag product. The aims of this section of the study are as follows:

- By improving our understanding of the slag product, and the factors relevant in the production of the liquid slag, it will lead to improvements in the smelting process. In order to do this the following aspects, and the relationships between these aspects, were investigated:
  - The chemistry of the slags,
  - The tapping temperatures of the slags. This was compared to the available liquidus temperature data.
- The second aim of this section is to gain an understanding of the mineralogy and chemistry of solidified titania slag. In the next chapter the decrepitation behaviour of titania slags will be investigated. This section is to provide a basis for comparing decrepitated slag with slag that did not decrepitate.

2.2 LITERATURE SURVEY

2.2.1 MINERALOGY OF HIGH TITANIA SLAGS

According to Russian investigators as quoted by Handfield and Charette (1971) the main constituents found in industrial high titania slags in the solid state were as follows:

- A solid solution of the anosovite group (orthorhombic crystal structure). The following general formula was proposed to take into account the extensive solid solution:

$$m[(Ti, Mg, Mn, Fe)O.2TiO_2].n[(Ti, Fe, Al, Cr, V)_2O_3.TiO_2]$$

  According to this formula, iron can potentially be present as Fe^{2+} and Fe^{3+}, while titanium can potentially be present as Ti^{2+}, Ti^{3+} and Ti^{4+}.
- Minerals based on a solid solution having the Ti_2O_3 type of structure (rhombohedral). The following general formula was proposed to take into account the extensive solid solution:

$$a[(Ti, Mg, Mn, Fe)O.TiO_2].b[(Ti, Al, Cr, V, Fe)_2O_3]$$

  According to this formula, iron can potentially be present as Fe^{2+} and Fe^{3+}, while titanium can potentially be present as Ti^{2+}, Ti^{3+} and Ti^{4+}.
- The third phase consisted of glassy material with complex compositions.

For the titaniferous portion of the slags, the mutual dissolution of the elements to form a wide region of solid solutions is explained by the ionic radii of the constituent elements. This can also be explained by the small difference (in most cases less than 5 per cent) in the lattice constants of the end member phases of the solid solutions. The close ionic radii of

the cations can be seen by comparing the data of the relevant cations in Table 2 (data from Huheey, 1983). A comparison of the data for iron, manganese and magnesium illustrates this.

Table 2: Effective ionic radii of elements relevant to ilmenite smelting (Huheey, 1983)

Cation	Coordination number	Radius (Å)	Cation	Coordination number	Radius (Å)
Al^{3+}	4	0.53	Mn^{2+}	4	0.80 (HS)
Al^{3+}	6	0.675	Mn^{2+}	6	0.97 (HS)
Ca^{2+}	6	1.14	Mn^{2+}	8	1.10
Ca^{2+}	8	1.26	Si^{4+}	4	0.40
Cr^{2+}	6	0.94 (HS)	Si^{4+}	6	0.54
Cr^{3+}	6	0.755	Ti^{2+}	6	1.00
Fe^{2+}	4	0.77 (HS)	Ti^{3+}	6	0.81
Fe^{2+}	6	0.92 (HS)	Ti^{4+}	4	0.56
Fe^{2+}	8	1.06 (HS)	Ti^{4+}	6	0.745
Fe^{3+}	4	0.63 (HS)	Ti^{4+}	8	0.88
Fe^{3+}	6	0.785 (HS)	V^{3+}	6	0.78
Mg^{2+}	4	0.71	Zr^{4+}	4	0.73
Mg^{2+}	6	0.86	Zr^{4+}	6	0.86
Mg^{2+}	8	1.03	Zr^{4+}	8	0.98

HS – High spin

Handfield and Charette (1971) also discussed work carried out by previous investigators on Sorel slags. It was concluded that the main constituents in these slags were $RO.2TiO_2$ (R = Mg^{2+}, Fe^{2+} and Ti^{2+}) and $R_2O_3.TiO_2$ (R = Fe^{3+}, Al^{3+} and Ti^{3+}) phases. The opinion was expressed that these compounds are soluble in each other in all proportions and that the largest portion of the slag is a solid solution of the above compositions. It was also stated that the siliceous portion of the slag was composed of feldspathic materials (anorthite, albite and orthoclase) and mixed metasilicates of iron calcium and magnesium. A large portion of this is in a glassy state.

Handfield and Charette (1971) also concluded that melting high titania slags does not change their short range order significantly. High titania slags are also structurally different from the polymerizing silicate melts. According to Sommerville and Bell (1982) TiO_6^{8-} is the most likely ions to be present in titania slags. The reasons given for this is the clear preference of Ti^{4+} for octahedral co-ordination (compared to tetrahedral co-ordination for Si^{4+}), the observed viscosity data for high titania slags (discussed later), crystallisation characteristics and the structure of solid anosovite.

Toromanoff and Habashi (1984) investigated the mineralogical composition of a typical titanium slag from Sorel. Based on X-ray diffraction and microprobe analyses the slag was found to consist mainly of an iron magnesium titanate, armalcolite. The crystals were

cemented together by a calcium aluminium silicate phase. Trace amounts of rutile were also identified.

Also present were a small number of large metallic iron globules, some of them having a rim consisting of ferrous sulphide. These globules varied in size between 15 and 150 μm. It was assumed that these globules originated from the metal produced in the electric furnace, and were entrained in the slag during settling. Numerous small iron globules, 1 to 2 μm in size, were also observed in the slag. Because of their smaller size it was postulated that these globules had a different origin than the larger globules. The following reaction was proposed as a mechanism for the formation of the small metallic globules:

$$2Ti^{3+} + Fe^{2+} = 2Ti^{4+} + Fe^{0} \ldots (H)$$

This reaction was shown to be thermodynamically feasible.

Borowiec (1991) used a high titania slag at Tyssedal in Norway to study the sulphidisation of the solid slag. The aim of this study was to investigate the removal of impurities by this technique. Of relevance to this study are the results reported on the microprobe analyses of the phases contained in the Tyssedal slag. These results, together with the bulk analysis of the Tyssedal slag are shown in Table 3. When compared to the bulk analysis of the slag it was calculated that the slag consisted of about 88 per cent M_3O_5 phase and 12 per cent glassy silicate phase. It should be pointed out that the Tyssedal slag was made from hard rock ilmenite deposits containing high levels of impurities such as MgO, SiO_2 and Al_2O_3. The slags used in this study was obtained by the smelting of beach sand ilmenite deposists in which the impurity levels are significantly lower.

Table 3: Bulk and phase analyses of Tyssedal slag (Borowiec, 1991).

Components	Bulk analysis (mass %)	Microprobe analyses (mass %)	
		M_3O_5 phase	Glassy silicate matrix
TiO_2	75.0	64.92	11.74
Ti_2O_3	-	17.45	-
FeO	7.6	7.38	8.96
SiO_2	5.3	0.02	44.62
Al_2O_3	2.3	1.80	5.72
MgO	7.9	7.50	10.62
MnO	0.4	0.27	1.55
CaO	0.6	0.01	13.87
V_2O_3	0.52	0.60	0.06
Cr_2O_3	0.01	0.01	-

Reznichenko et. al. (1981) investigated metallic inclusions that form in high titania slags produced in Russia. Samples were taken from slag ingots that were quenched in water. These slags contained between 2 and 7.5 per cent ferrous oxide. The metal inclusions consist of two phases; metal and sulphide. A sulphide shell rim generally surrounds the metal phase, with the larger buttons containing rounded or irregular-shaped sulphide inclusions. The chemical composition for the sulphide phases was 55 to 70 per cent iron, 3 to 5 per cent manganese and 35 to 40 per cent sulphur. The authors suggest that sulphur,

introduced via the feed, has an outer electron shell similar to that of oxygen. As in the case of oxygen it can also form octahedral complexes with the iron cation. Because of the similarity of their electronic structure and the small difference in size complex oxy-sulphide compounds can form in the melt. These compounds are of the type $[FeO_xS_y]^n$, where x + y = 6. On cooling these compounds decompose to form a two-phase button as described above. It was also suggested that pure metallic iron is formed according to reaction (I), with mineralogical analysis confirming the occurrence of this reaction in the solid stage of the process. This is the same as reaction (H), except that it is written in compounds rather than ions. As the temperature decreases, ΔG^0 becomes more negative. This results in the reaction becoming thermodynamically more favourable, shifting more towards the formation of metallic iron.

$$3Ti_2O_3 + FeO = Fe^0 + 2Ti_3O_5 \ldots (I)$$

$$\Delta G^0 = -\ 110\ 667 + 19.874T \text{ (J, 700 to 1642 K)}$$

Various investigators studied the solid solution series depicted as M_3O_5, where M can be a combination of a wide number of cations. Information regarding this M_3O_5 solid solution series is relevant to this study, as M_3O_5 phases of various compositions have been identified as the main phase present in high titania slags (Toromanoff and Habashi, 1984; Borowiec, 1991). It has been shown that the M_3O_5 phase has a pseudobrookite structure, AB_2O_5 (see for example Grey and Ward, 1973; Wechsler et. al., 1976; Brown and Navrotsky, 1989). A and B represent two symmetrically distinct, octahedral cation sites within this structure, with 4 A and 8 B sites within the unit cell. The A site in general is larger and more distorted than the B site.

Grey and Ward (1973) studied the solid solution series $FeTi_2O_5$-Ti_3O_5 as a function of temperature and oxygen partial pressure. From X-ray diffraction studies they found that the solid solution is complete at temperatures above 1350 °C. For the series $Fe_xTi_{3-x}O_5$ (with $0 \leq x \leq 1$) it was found that with $x > 0.35$ the compounds had an orthorhombic pseudobrookite structure. With $x < 0.35$ the compounds had a monoclinic distortion of this structure, with the distortion increasing towards the Ti_3O_5 composition. They also reported that for $FeTi_2O_5$ approximately 72 per cent of the Fe^{2+} is found at the A site. This increases slightly to 75 per cent at a composition of $Fe_{0.75}Ti_{2.25}O_5$. For compositions close to Ti_3O_5 this value drops to approximately 60 per cent.

Eriksson et. al. (1996) compiled the Ti_3O_5-$FeTi_2O_5$ phase diagram shown in Figure 5. This shows that the Ti_3O_5-$FeTi_2O_5$ solid solution is continuous only at temperatures above approximately 1350 °C under equilibrium conditions (in agreement with the study of Grey and Ward (1973) mentioned above). The structure change at x = 0.35 is also shown.

Bowles (1988) made a summary of the site occupancies of various pseudobrookite phases. This is shown in Table 4. From this it can be seen that Fe^{2+} is concentrated in the A site, with Ti^{4+} concentrated in the B site. For Ti_3O_5 the Ti^{3+} cation mostly fills the A site, with only a small portion of the A site filled by Ti^{4+}. The series from pseudobrookite to Ti_3O_5 represents a steady replacement of Fe by Ti, with reduction first of Fe^{3+} to Fe^{2+} and then some of the Ti^{4+} to Ti^{3+}. It was also noted by Bowles (1988) that a large number of naturally occurring minerals of the pseudobrookite structure occurs.

Teller et. al. (1990, pp. 334-350) made a structural analysis of several pseudobrookite ferrous titanium oxides using neutron diffraction and Mössbauer spectroscopy techniques. Under reducing conditions it was possible to quench synthetic metastable materials that contain Fe^{2+} and Ti^{3+} cations within the same oxide lattice. These materials are thermodynamically unstable at room temperature with respect to Fe^{0} and Ti^{4+} (see reactions (H) and (I)). Two materials (approximating $FeTi_2O_5$ and $Fe_{0.5}Mg_{0.5}Ti_2O_5$) were prepared at 1200 °C, where the reducing conditions were strictly controlled. In addition two slags samples at temperatures greater than 1700 °C were prepared by the reduction of ilmenite with carbon. The stoichiometries of these samples were $Ti_{2.52}Fe_{0.33}Mn_{0.05}O_5$ and $Ti_{2.36}Fe_{0.33}Mg_{0.31}O_5$ respectively. It was found that the temperature of preparation and the conditions of reduction largely determined the distribution of the cations in the pseudobrookite stucture. For the samples prepared at 1200 °C it was found that Fe^{2+} was distributed between both the A and B sites. For the samples prepared at 1700 °C it was found that Fe^{2+} reported exclusively to the A site. These results are shown in Table 5. It was concluded that a "disordered" model best described the low temperature structures. It was also found that the Mg and Fe occupancies of the A and B sites were not identical.

Figure 5: Phase diagram of the $FeTi_2O_5$-Ti_3O_5 join (Eriksson et. al., 1996)

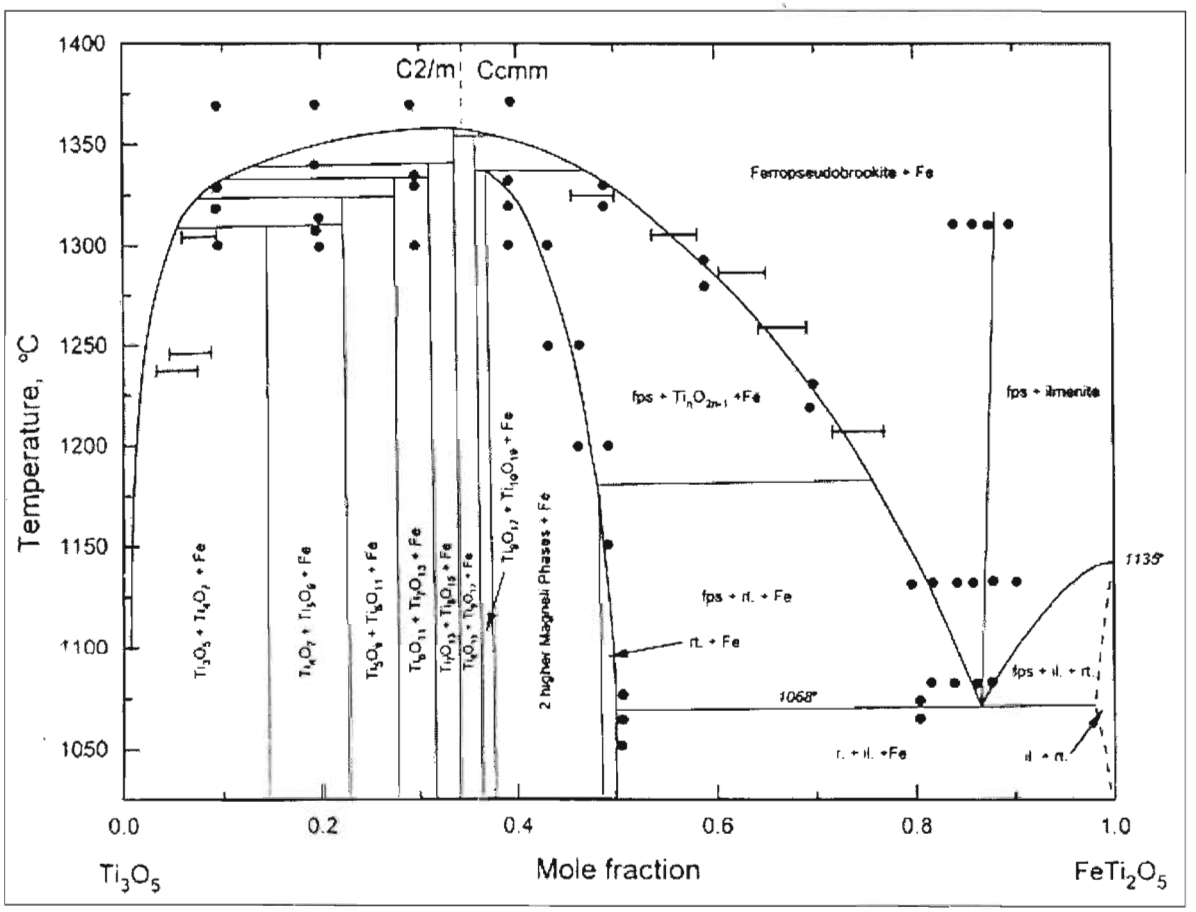

X-ray diffraction data for various samples are given in Table 6. This shows that the major peaks are found at d values of approximately 3.50 and 2.76 Å. The chemical composition of the lunar armalcolite and the Sorel slag is given in Table 7.

The unit cell parameters of various M_3O_5 samples are given in Table 8. As discussed previously Grey and Ward (1973) found in their study that the orthorhombic pseudobrookite cell transforms to a monoclinic cell at a composition of approximately $Fe_{0.35}Ti_{2.65}O_5$. This monoclinic distortion increases with increasing titanium content towards Ti_3O_5. Grey and Ward (1973) also found a slight increase in the unit cell volume (0.5 per cent) from $FeTi_2O_5$ to Ti_3O_5. The a and b parameters in their results increased towards Ti_3O_5, while the c parameter decreased. Grey and Ward (1973) believed that this occurred due to increased metal-metal bonding between Ti^{3+} cations as the amount of Ti_3O_5 is increased.

Table 4: Cation distributions in various pseudobrookite phases (Bowles, 1988)

Phase	Cations in A site	Cations in B site	Reference
$FeTi_2O_5$	$Fe^{2+}_{0.68}\ Ti^{4+}_{0.32}$	$Fe^{2+}_{0.32}\ Ti^{4+}_{1.68}$	Virgo and Huggins (1975)
$FeTi_2O_5$	$Fe^{2+}_{0.72}\ Ti^{4+}_{0.28}$	$Fe^{2+}_{0.28}\ Ti^{4+}_{1.72}$	Grey and Ward (1973)
$FeTi_2O_5$	$Fe^{2+}_{0.81}\ Ti^{4+}_{0.19}$	$Fe^{2+}_{0.19}\ Ti^{4+}_{1.81}$	Navrotsky (1975)
Ti_3O_5	$Ti^{4+}_{0.05}\ Ti^{3+}_{0.95}$	$Ti^{4+}_{0.95}\ Ti^{3+}_{1.05}$	Navrotsky (1975)

Table 5: Cation distributions for various pseudobrookite samples (Teller et. al., 1990, pp.334-350)

Sample	Cations in A site	Cations in B site
$Fe_{0.93}Ti_{2.07}O_5$	$Fe_{0.70}Ti_{0.30}$	$Fe_{0.23}Ti_{1.77}$
$Fe_{0.6}Mg_{0.6}Ti_{1.8}O_5$	$Fe_{0.5}Ti_{0.5}$	$Mg_{0.6}Fe_{0.1}Ti_{1.3}$
$Ti_{2.52}Fe_{0.33}Mn_{0.05}O_5$	$Mn_{0.05}Fe_{0.33}Ti_{0.52}$	$Ti_{2.00}$
$Ti_{2.36}Fe_{0.33}Mg_{0.31}O_5$	$Mg_{0.21}Fe_{0.33}Ti_{0.46}$	$Ti_{1.90}Mg_{0.10}$

2.2.2 CHEMICAL ANALYSES OF HIGH TITANIA SLAGS

A summary of selected high titania slag analyses is shown in Table 9. Also shown are the specifications required by the two pigment manufacturing processes. As can be seen the quality of the slag products differs significantly, with only RBM and Namakwa sands producing slag containing more than 85 per TiO_2 (total Ti expressed as TiO_2). This is mainly due to the high impurity levels of the ilmenite used by the other producers. Generally chloride grade feedstocks require high levels of TiO_2 (Fisher, 1997). This is because the high temperature chlorination reactions that occur are not selective, and most of the metal oxides contained in the feed are converted to chlorides. Intermediate processes can be used to upgrade the quality of the slag. An example of this is the UGS (Upgraded Slag) product made from Sorel slag (Fisher, 1997). In this product the undesirable alkaline elements and most of the iron oxide are selectively removed. This results in a slag product with physical and chemical properties similar to natural rutile.

Table 6: X-ray diffraction data for various M_3O_5 compounds (only peaks with I/I_0 > 10)

Anderson et. al. (1970)				Toromanoff and Habashi (1984)	
Synthetic armalcolite ($Fe_{0.5}Mg_{0.5}Ti_2O_5$)		Lunar armalcolite		Sorel slag	
d values (obs.) (Å)	I/I_0	d values (obs.) (Å)	I/I_0	d values (obs.) (Å)	I/I_0
5.019	40			5.02	20
4.879	80			4.88	30
3.493	100	3.468	100	3.50	100
2.762	80	2.763	25	2.76	60
2.452	10	2.454	25	2.45	12
2.438	5			2.44	9
2.415	10	2.414	10	2.41	13
2.233	15	2.235	15	2.23	11
		2.199	15	2.19	12
				2.19	11
1.972	17	1.958	80	1.97	10
				1.96	10
				1.87	40
				1.86	12
		1.751	10		
1.675	10	1.669	10		
1.634	28	1.632	10		
1.625	13				
1.549	18			1.55	13

Table 7: Composition of lunar armalcolite and Sorel slag samples used for X-ray diffraction analyses (see Table 6)

	Analyses (mass %)	
	Lunar armalcolite (Microprobe)	Sorel slag (Bulk analyses)
TiO_2	73.4	70-72
Al_2O_3	1.62	4-6
Cr_2O_3	2.15	< 0.25
FeO	15.3	12-15
MnO	0.08	0.2-0.3
MgO	7.70	4.5-5.5
CaO	0.01	< 1.2
V_2O_3	< 0.5	0.5-0.6
SiO_2	-	3.5-5

Table 8: Unit cell data for various M_3O_5 compounds

	Teller et. al. (1990, pp. 334-350)				Grey and Ward (1973)			Anderson et. al. (1970)	
	Samples at 1200 °C	Samples at 1200 °C	Samples at > 1700 °C	Samples at > 1700 °C	-	-	-	Synthetic armalcolite	Lunar armalcolite
	$FeTi_2O_5$	$Fe_{0.5}Mg_{0.5}Ti_2O_5$	$Ti_{2.36}Fe_{0.33}Mg_{0.31}O_5$	$Ti_{2.52}Fe_{0.33}Mn_{0.05}O_5$	$FeTi_2O_5$	$Fe_{0.50}Ti_{2.50}O_5$	$Fe_{0.32}Ti_{2.68}O_5$	$Fe_{0.5}Mg_{0.5}Ti_2O_5$	See table
a (Å)	3.7498	3.7413	3.7629	3.7828	9.790	9.798	9.823	9.752 ± 0.003	9.743 ± 0.03
b (Å)	9.8057	9.7659	9.7556	9.7938	3.757	3.781	3.785	10.048 ± 0.003	10.024 ± 0.02
c (Å)	10.0675	9.9946	10.0151	10.0280	10.079	10.020	10.000	3.736 ± 0.004	3.738 ± 0.03
Cell Vol. ($Å^3$)	370.17	365.17	367.65	371.52	370.7	371.2	371.8	366.071 ± 0.322	365.077 ± 0.619

Table 9 : Chemical analyses of various high titania slags

Compound	Analyses of various slag products (mass %)					Typical specifications for chloride grade slag[e,f]	Typical specifications for sulphate grade slag[e]
	Sorel slag[a]	Sorel slag[b]	Namakwa[a] sands	RBM[a]	Tinfos[c,d]		
Total Ti as TiO_2	77.5	71.5	86.0	85.5	75		
TiO_2	-	62.1	54.9	54.3	-		
Ti_2O_3	-	8.5	28.0	28.10	-		
FeO	10.9	11.4	10.0	10.50	7.6	Minimum	
Fe^0	-	0.8	-	-	-		
Al_2O_3	3.5	4.5	1.80	1.10	1.2 to 2.3	< 2.0	
SiO_2	3.0	4.2	1.80	1.20	5.3	$SiO_2 + ZrO_2 < 2.0$	
CaO	0.6	0.7	0.16	0.16	0.6	< 0.20 to 0.25	
MgO	5.3	5.1	0.85	1.00	7.9	< 1.0	
MnO	0.2	0.2	1.50	1.80	0.4	< 2.0	
V_2O_5	0.3	0.57	0.42	0.40	0.63	< 0.4	
Cr_2O_3	0.17	0.19	0.07	0.18	0.01 to 0.09	< 0.2	
ZrO_2	-	-	0.28	-	-		
P_2O_5	-	0.03	-	-	-		< 0.05
C	-	0.02	-	-	-		
S	-	0.06	-	-	-		

a – Pesl (1997)
b - Toromanoff and Habashi (1984)
c – Skillen (1992)
d - Borowiec (1991)
e – Stanaway (1994)
f - Battle et. al. (1993)

Other properties of high titania slags, apart from the chemical composition, also play a role in the selecting the final product for the appropriate processing technology. One such aspect is the size distribution of the slag. This will be discussed in more detail in the section on the decrepitation of the titania slags.

The following reasons for the chemical specifications for the chloride process have been given (Stanaway, 1994; Battle et. al., 1993; Fisher, 1997):

- For the chloride process route CaO can cause sticking in the fluidized bed. This is also the case for MgO and MnO, although to a lesser extent. The chlorides of these elements are liquid at the chlorination temperatures and can defluidize the bed and also cause clogging in the bed.
- The operating temperature in the typical fluidized bed is too low to convert all the silica to the chloride. The silica therefore remains in the fluidized bed, accumulating and thereby reducing the throughput. Low levels of silica are therefore specified.
- A low iron content is required to minimize iron chloride disposal problems, optimize plant capacity and minimize chlorine consumption.
- Low levels of vanadium and chromium are required due to potential toxicity problems in the iron chloride waste.
- Low tin and arsenic levels are required as these elements accumulate with the titanium chloride stream.
- Uranium, thorium and other radioactive substances concentrate in some of the waste and process streams, and are therefore undesirable.

Reasons listed for the chemical specifications for the sulphate process are the following (Stanaway, 1994; Fisher, 1997):

- A low iron content is preferable in order to minimize waste disposal, optimize plant capacity and minimize reagent consumption. Some ferric iron gives an undesirable colour to the pigment product. Some ferrous iron is however required for optimum titanium dioxide crystal formation during the precipitation stage.
- Low chromium and vanadium contents are required as these elements can colour the pigment above certain levels. These elements also cause toxicity and waste disposable problems when present in the waste products.
- High calcium and phosphate levels can hinder crystal development.
- Niobium also imparts colour to the pigment.
- Uranium, thorium and other radioactive substances concentrates in some of the waste and process streams, and once again are therefore undesirable.
- The amount of Ti^{3+} in the feed needs to be limited as this forms a Ti_2O_3 product. This Ti_2O_3 product is considered to be part of the waste materials.

For the sulphate processing route feedstocks in which the iron is in the divalent state and titanium in the tetravalent state is preferred. Ferric iron must be avoided, since these ions adsorb on the surface of the TiO_2 particles in the digestion solution and discolour the TiO_2 (Fisher, 1997). Ferric iron in the feedstock is usually reduced by the addition of iron scrap at additional cost.

As previously explained, ilmenite is reduced with a carbonaceous reductant during the reduction process. During this process most of the iron is reduced to metal, while some of the titanium is reduced from the tetravalent to the trivalent state. Increasing the reductant addition in the ilmenite smelting process, with the required energy input, decreases the iron oxide

content in the slag and increases the amount of trivalent titanium present in the slag. Based on testwork in a 150 kVA pilot furnace, Grau and Poggi (1978) illustrated the relationship between the TiO_2, Ti_2O_3 and FeO content of Sorel slag. This is shown in Figure 6, with the equivalent per cent TiO_2 being the total titanium content expressed as titanium dioxide. The relationship between the Ti_2O_3 and FeO contents was determined from the data shown in Figure 6 (data set used for calculation shown in Appendix A) and is expressed by the linear regression equation (I):

$$\% Ti_2O_3 = -(1.49)(\% FeO) + 37.17 \; ; R^2 = 0.74 \ldots (I)$$

Figure 6 : Variations in the FeO and Ti_2O_3 content of Sorel slags (Grau and Poggi, 1978)

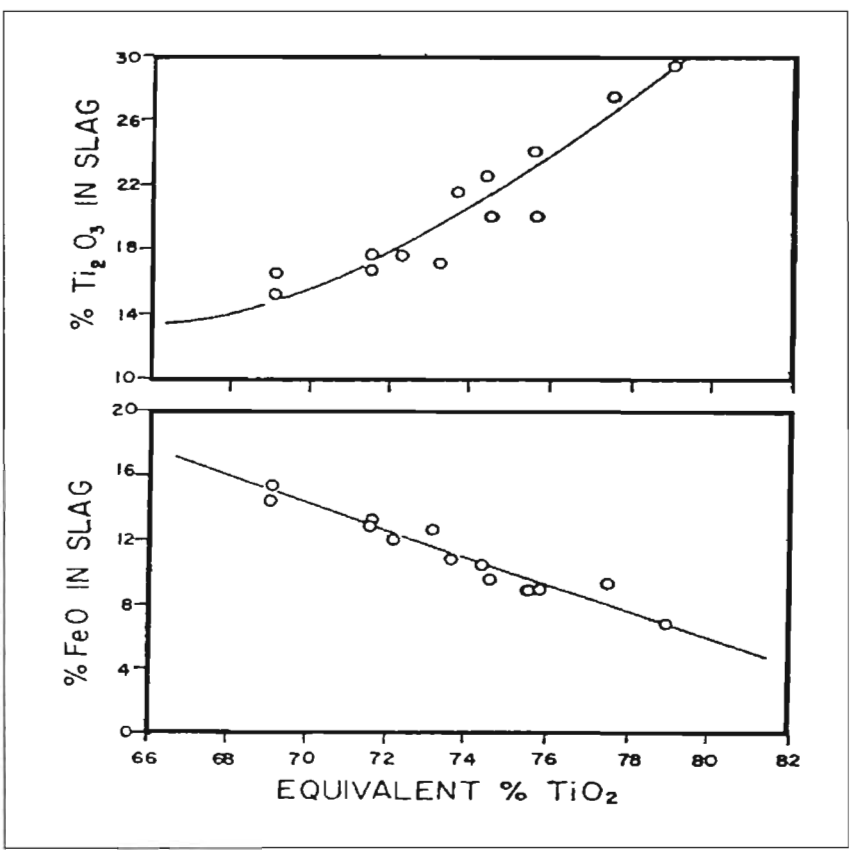

Ban (1988) investigated the smelting of Quilon ilmenite (concentrate from India) in a DC furnace. The ilmenite contained 60 per cent TiO_2 and 32.4 per cent FeO. The main impurities in the ilmenite were Al_2O_3 (1.6 per cent) and SiO_2 (0.8 per cent).

Based on Ban's small-scale smelting tests (2.5 kg batches) carried out in a DC furnace the following empirical relations were established:

$$\log (\% Ti_2O_3) = 1.781 - (0.025)(\% FeO) \ldots (II)$$

The relationship shown in equation (II) was calculated from a graphical representation of the data from Ban (1988). Ban et. al. (1988) also published data for the re-melting of Sorel and RBM slags. The following correlations were found:

$$\text{Sorel slag: } \log(\%\ Ti_2O_3) = 1.795 - (0.040)(\%\ FeO) \quad \ldots(III)$$

$$\text{RBM slag: } \log(\%\ Ti_2O_3) = 1.960 - (0.050)(\%\ FeO) \quad \ldots(IV)$$

Pistorius and Coetsee (2000) also investigated the relationship between FeO and Ti_2O_3 in ilmenite smelter slags. The following relationships were found for South African (includes slag from Iscor, Namakwa Sands and RBM) and Canadian (QIT) slags respectively:

$$\text{South African slags: } \%\ Ti_2O_3 = (-1.84)(\%\ FeO) + 50.1,\ R^2 = 0.91 \quad \ldots(V)$$

$$\text{Canadian slags: } \%\ Ti_2O_3 = (-1.39)(\%\ FeO) + 34.9,\ R^2 = 0.84 \quad \ldots(VI)$$

Pistorius and Coetsee (2000) found that the FeO-Ti_2O_3 relationship in the ilmenite smelter slags appears to follow a single pattern for different smelter furnace sizes and designs. This relationship is only affected by the impurity content of the feed materials. To quantify the effects of the impurity oxides the following set of equations were used:

$$(\%\ FeO)_{eq} = (\%\ FeO) + (M_{FeO}/M_{MgO})(\%\ MgO) + (M_{FeO}/M_{MnO})(\%\ MnO) \quad \ldots(VII)$$

$$(\%\ Ti_2O_3)_{eq} = (\%\ Ti_2O_3) + (M_{Ti2O3}/M_{V2O5})(\%\ V_2O_5) + (M_{Ti2O3}/M_{Cr2O3})(\%\ Cr_2O_3) + (M_{Ti2O3}/M_{Al2O3})[(\%\ Al_2O_3) - (\%\ SiO_2)/3] \quad \ldots(VIII)$$

M_i is taken as the molar mass of the oxide i, and the amounts of the oxides are in mass percentages. In equation (VIII) the vanadium content of the slag is expressed as V_2O_5 as this is the convention. Pistorius and Coetsee (2000) point out that the vanadium can however be expected to be in the trivalent form. The equation also shows that some of the Al_2O_3 content is not taken into account when the equivalent Ti_2O_3 content is calculated. The reason given for this is that some of the Al_2O_3 reports to a separate glass phase. It should be noted that the partitioning of other oxides (such as MnO and FeO) were not taken into account by Pistorius and Coetsee (2000). After taking into account the effect of the impurity oxides, and normalisation of the data, it was found that the slag compositions closely follows that expected for the stoichiometric M_3O_5 composition, with the end members of the M_3O_5 composition relevant to ilmenite smelting are $FeTi_2O_5$ and Ti_3O_5. The relationship between Ti_2O_3 and FeO according to the stoichiometric M_3O_5 composition can be expressed by equation (IX):

$$\%\ Ti_2O_3 = (-2.07)(\%\ FeO) + 64.28 \quad \ldots(IX)$$

2.2.3 LIQUIDUS AND TAPPING TEMPERATURES APPLICABLE TO ILMENITE SMELTING

The components most relevant to high titania slags are TiO_2, Ti_2O_3 and FeO (see Table 9). Several phase diagrams relevant to these systems have been published. Eriksson and Pelton (1993) critically evaluated the available thermodynamic and phase diagram data for all the phases in the FeO-TiO_2 and Ti_2O_3-TiO_2 systems. Their optimised calculated equilibrium diagrams for these systems are shown in Figure 7 and Figure 8.

Figure 7 : Optimised FeO-TiO_2 phase diagram (Eriksson and Pelton, 1993)

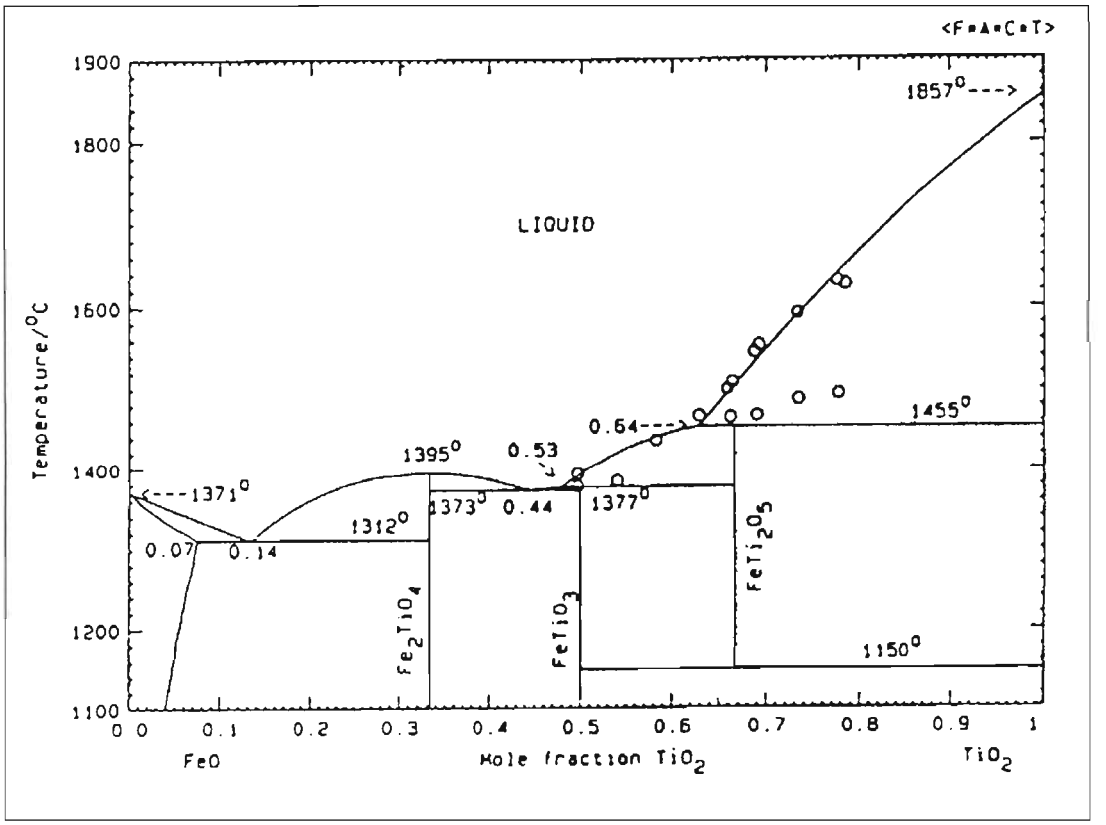

Figure 8 : Optimised Ti_2O_3-TiO_2 phase diagram (Eriksson and Pelton, 1993)

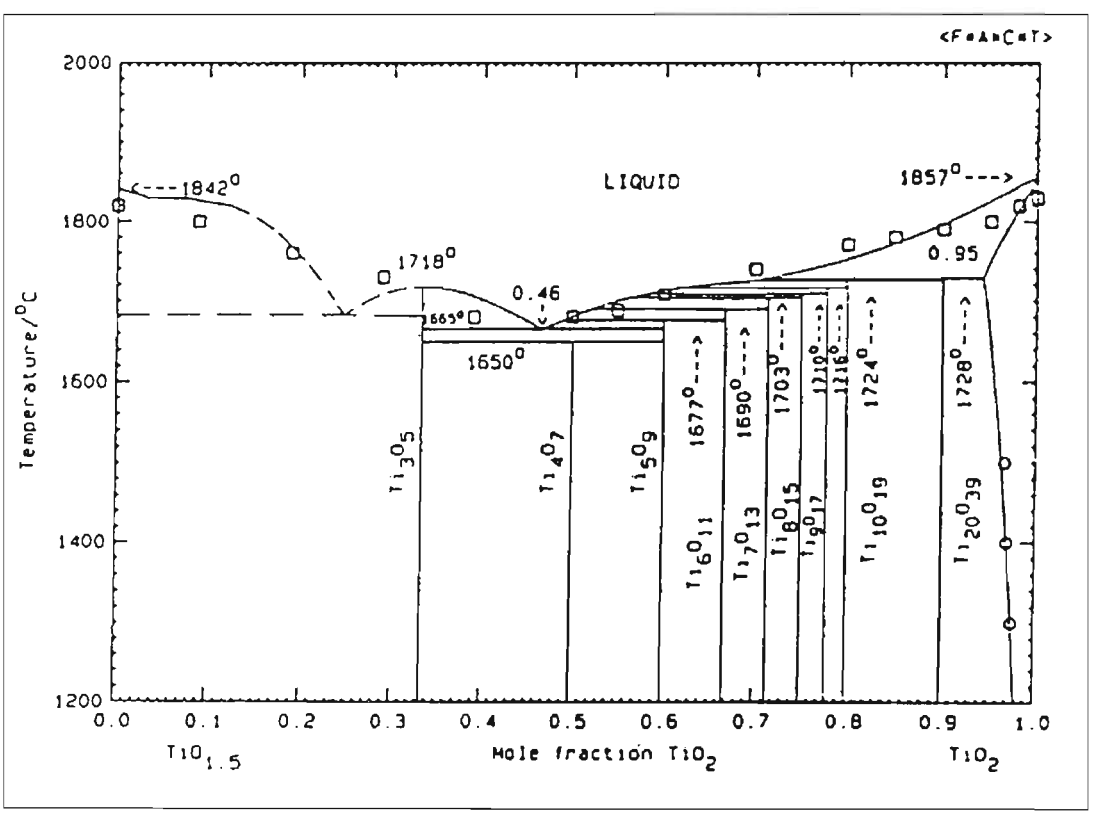

Pesl (1997) carried out isothermal experimental work on the FeO-TiO_2-$TiO_{1.5}$ ternary system at 1500 and 1600 °C. The phase diagrams for these two temperatures are shown in Figure 9 and Figure 10 respectively. Oxygen isobars relevant to the phase diagrams are also shown. The system consists of liquid slag, which has saturation boundaries with metallic iron, rutile, M_3O_5 and M_8O_{15}. For the 1600 °C isotherm it was found that the liquid slag region is enlarged substantially compared to the 1500 °C isotherm. Double saturation with respect to metallic iron and the M_3O_5 phase at 1600 °C was found to occur at 16 mol per cent FeO and 39 mol per cent $TiO_{1.5}$.

Figure 9: FeO-TiO_2-$TiO_{1.5}$ isothermal phase diagram – 1500 °C (from Pesl, 1997)

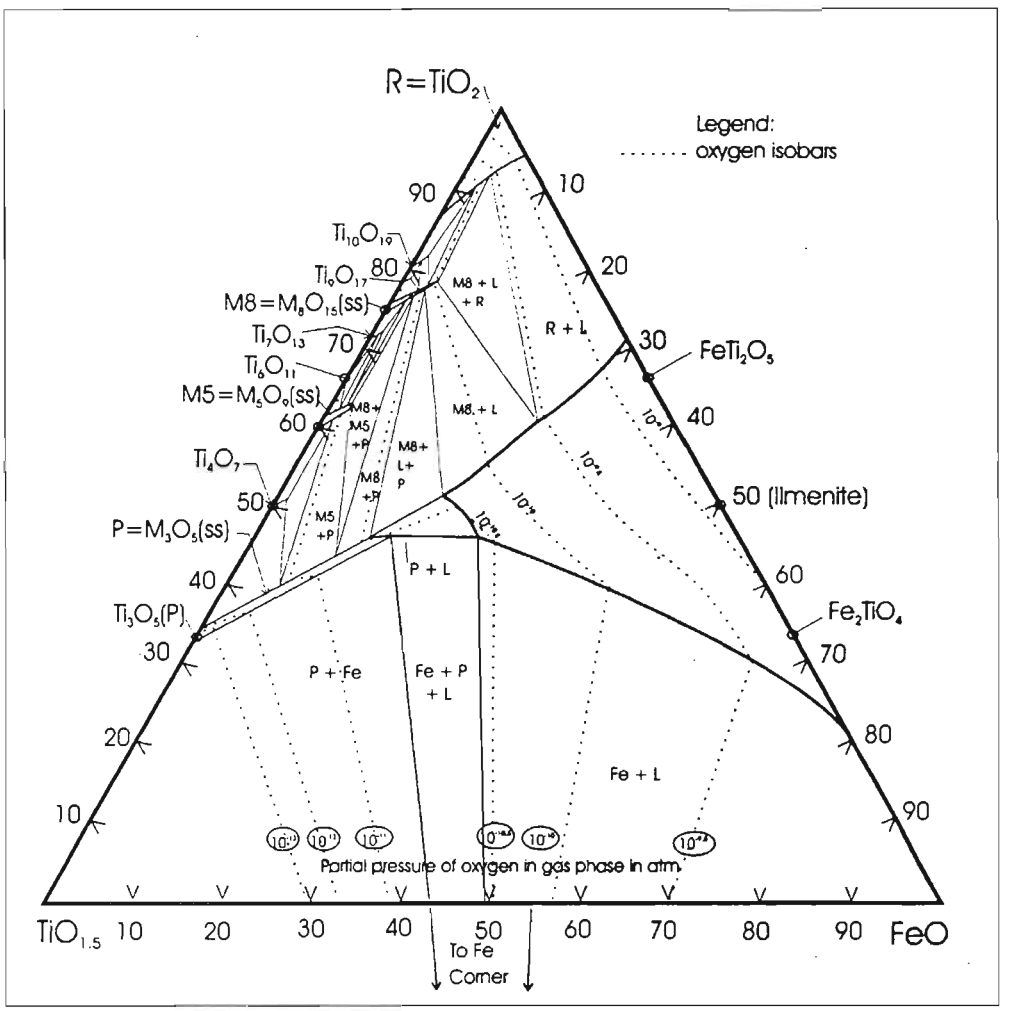

Pistorius and Coetsee (2000) presented a conjectural liquidus diagram of the system $FeTiO_3$-TiO_2-$TiO_{1.5}$, relevant to ilmenite smelter slags (see Figure 11). This diagram was based on the FeO-TiO_2 and Ti_2O_3-TiO_2 binary diagrams of Eriksson and Pelton (1993), as well as data from Pesl (1997). Quasichemical model parameters for the liquid slag region taken from Eriksson and Pelton (1993) were used to calculate the slag composition in equilibrium with iron. Based on this diagram it was proposed that the formation of Ti_2O_3 does have a beneficial effect of lowering the liquidus temperature of the slag.

Grau and Poggi (1978) described the Sorel slag tapping data they obtained from smelting testwork in their 150 kVA pilot furnace. These results are shown in Figure 12 as a function of

the equivalent per cent TiO_2 (total Ti expressed as TiO_2). Also shown in Figure 12 are the melting point data of the Sorel slags.

Figure 10: FeO-TiO_2-$TiO_{1.5}$ isothermal phase diagram – 1600 °C (from Pesl, 1997)

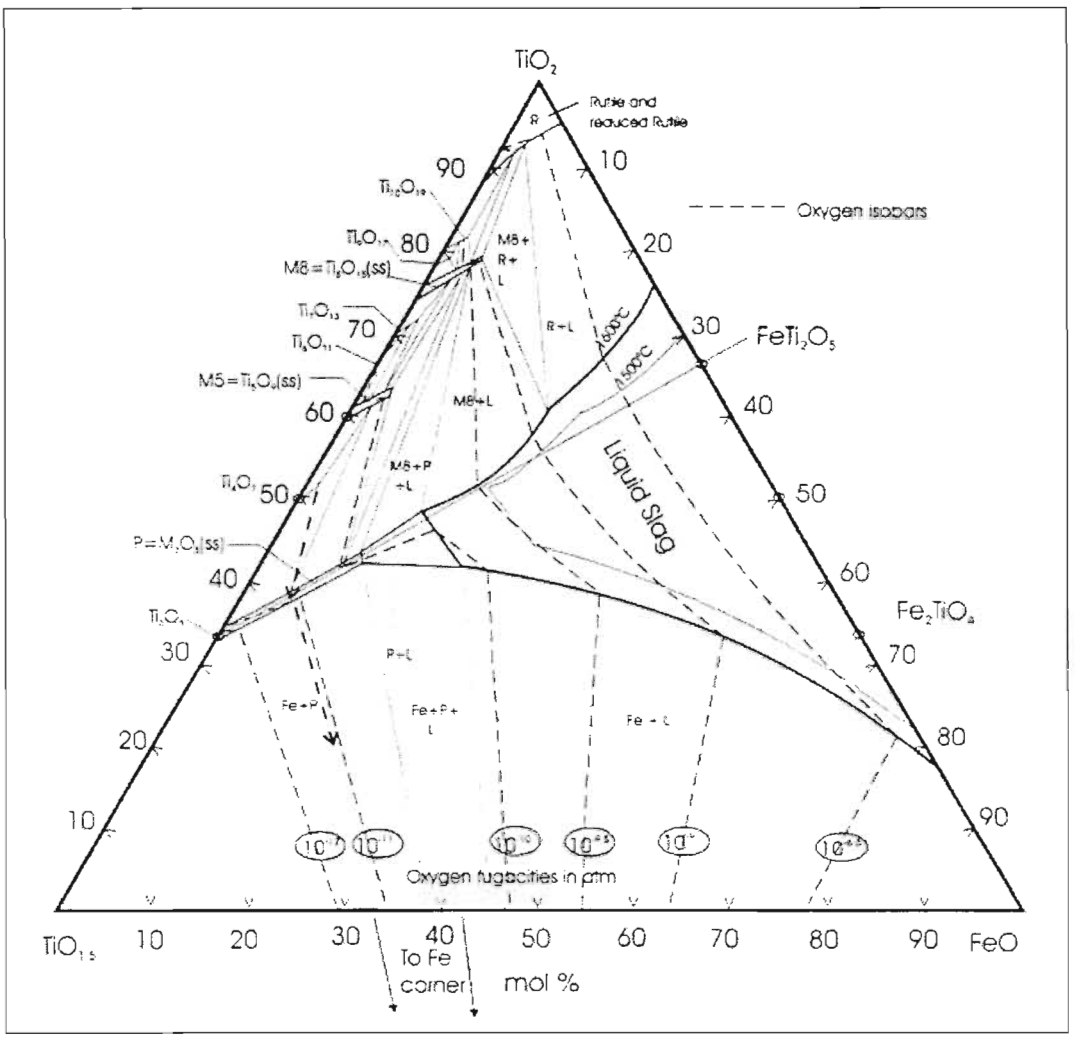

These melting points were determined by the cooling curve technique. With this technique slag temperature is continuously recorded during a cooling cycle, with a temperature arrest during cooling indicating the start of solidification. This was taken as the melting point, or liquidus temperature, of the particular slag. The results show that the slag melting point increases approximately linearly with the equivalent TiO_2 content of the slag. The comparison between the slag tapping temperatures and melting points indicates that the difference between the two becomes less as the degree of reduction of the slag increases. The difference between the two values can also be described as the "degree of superheat" within the slag.

In his work Ban (1988) suggested that by relating the liquidus temperature increase of the slag to the FeO content in high titania slags, the melting temperature follows the liquidus line in the $FeTiO_3$-TiO_2 system given by Grau (1979). Based on this Ban (1988) provided the following equation for the liquidus temperature of the slag:

$$\text{Liquidus temperature} = (-8.02)(\%\ \text{FeO}) + 1780 \quad \ldots(X)$$

Figure 11: Conjectural liquidus diagram of the $FeTiO_3$-TiO_2-$TiO_{1.5}$ ternary system (Pistorius and Coetsee, 2000)

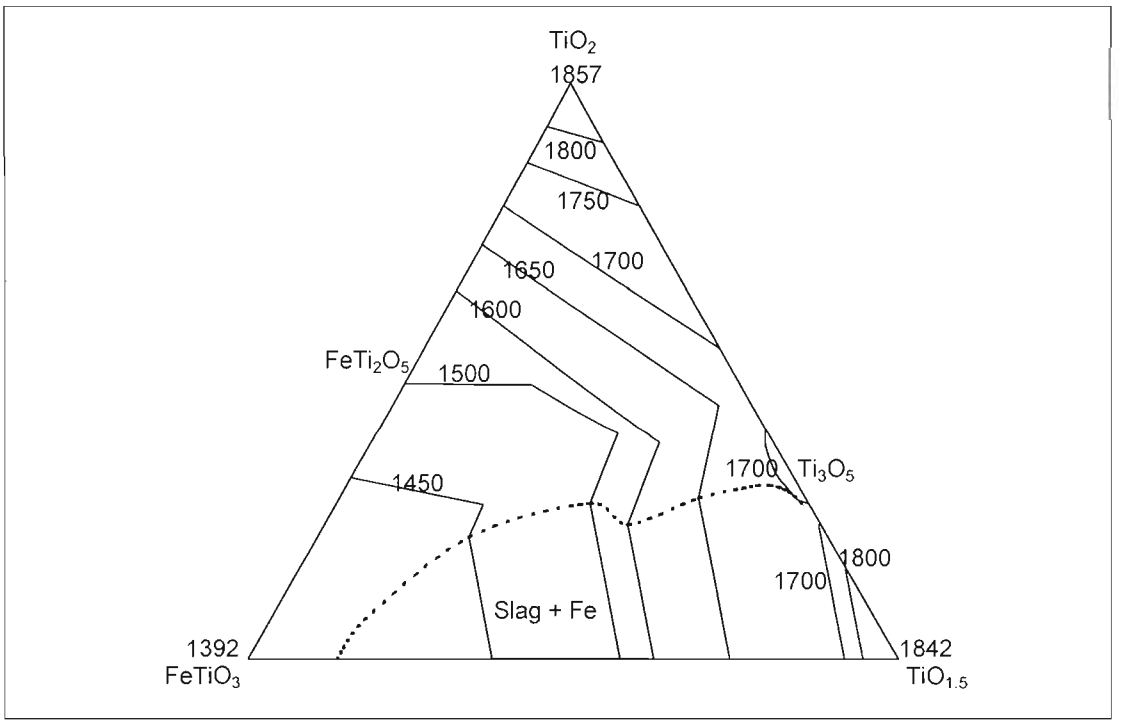

Figure 12: Sorel slag tapping and melting temperatures (Grau and Poggi, 1978)

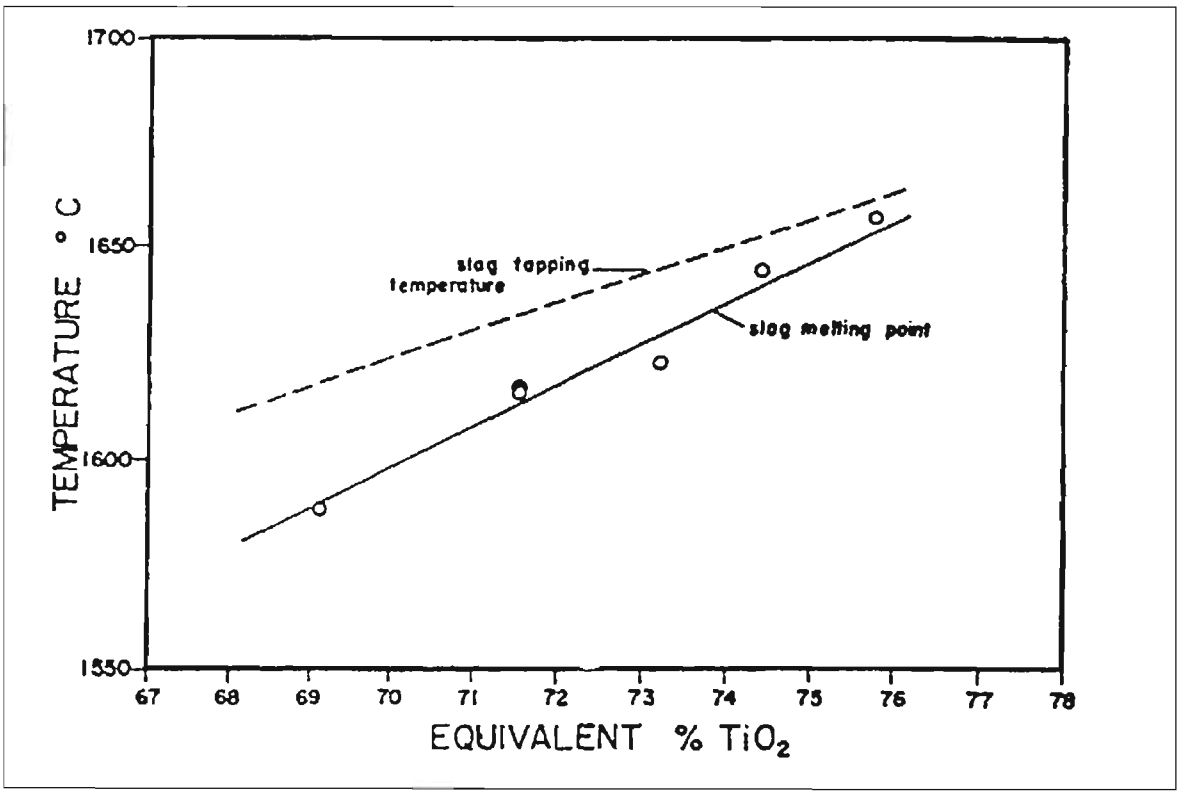

Du Plooy (1997) investigated the melting points of TiO_2-rich slags using a thermal analysis technique. The liquidus temperatures of several industrial slags in various atmospheres were determined as a function of the FeO content of the slags. These results are shown in Figure 13. The total titanium content of the slags (expressed as TiO_2) ranged from 80 to 92 per cent. The oxygen potentials for the various slags were calculated to be approximately the following order of magnitude (the actual values differed somewhat as a function of temperature):

- Ar – Oxygen partial pressure of $10^{-5.9}$ atm.
- CO - Oxygen partial pressure of 10^{-15} atm.
- CO_2 - Oxygen partial pressure of 10^{-2} atm.
- CO/CO_2 - Oxygen partial pressure of 10^{-7} atm.

Figure 13: Liquidus temperatures of various industrial titania slags as a function of the FeO content (Du Plooy, 1997)

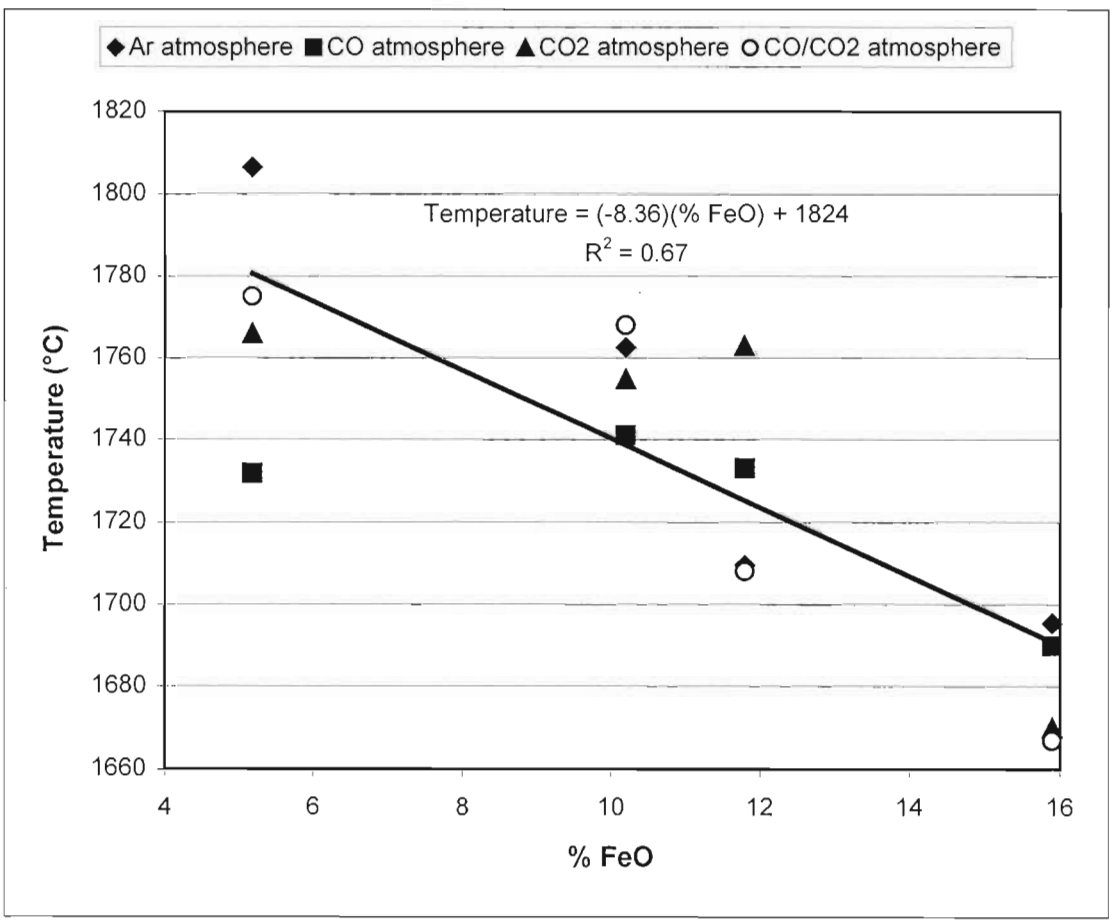

Also shown in Figure 13 is the calculated linear regression line for all the data points.

2.2.4 OTHER ASPECTS OF HIGH TITANIA SLAGS

As the viscosity and electrical characteristics of titania slags are also important in the ilmenite smelting process, a brief review on the available information is given here.

2.2.4.1 Viscosity of titania slags

In the seventies some pioneering work was carried out in determining the viscosity of high titanium slags (Handfield and Charette, 1971; Handfield, Charette and Lee, 1971). They measured the viscosity of Sorel slags (67-80 % TiO_2, 3.3-15 % FeO) using the rotation method. A commercially available viscosity meter (Brookfield Rheolog) was used in the studies. With this method a cylinder is immersed in a crucible containing the slag. The inner cylinder (spindle) is driven by a synchronous motor through a calibrated spring. The deflection of the spring caused by a viscous drag opposing the rotation of the spindle is an indication of the viscosity of the slag. Both the crucible and spindle were made of molybdenum for these studies.

A literature survey conducted by Handfield and Charette (1971) on the viscosity of oxide mixtures containing more than 50 % TiO_2 could not find any papers published prior to 1957. After 1957 the U.S.S.R. Academy of Sciences published a series of articles dealing with the electric melting of titanium slags. Their main conclusions were that the slags investigated had low viscosities when molten. Ti_2O_3, Al_2O_3 and MgO additions increased the viscosity of the slags, with Ti_2O_3 having the largest effect. It was also found that FeO, MnO, CaO and Cr_2O_3 decreased the viscosity of the titanium slags. The composition range over which these results were obtained is not clear from the article.

In their own research Handfield and Charette (1971) used eleven Q I T slags. The composition ranges of the slags were as follows:

TiO_2	67-80 %	Ti_2O_3 as TiO_2	5-26 %
FeO	3.3-15 %	Fe as metal	0.1-1.3 %
SiO_2	3.4-5.4 %	CaO	0.75-0.89 %
MgO	5.2-5.7 %	C	0.02-0.31 %

Figure 14 shows typical results obtained by the researchers. These results show that the viscosity of titania slags is low when completely molten, with values of approximately 30 centipoise.

Smelting of Australian ilmenite was carried out by Swinden and Jones (1978) using an electric arc furnace. The chemical composition of the slags produced was approximately as follows:

TiO_2 (total)	89 %	TiO_2 (actual)	56 %
Ti_2O_3 (actual)	30 %	FeO	10 %
Al_2O_3	1.3 %	MnO	1.5 %

The ternary plot in Figure 15 shows that the slag compositions obtained during the testwork lie on or about the $FeTi_2O_5$-Ti_3O_5 tie line. For the purposes of their study, the small amounts of gangue were grouped together with the FeO content in the slags. It has been found that there is complete miscibility between $FeTi_2O_5$ and Ti_3O_5 above 1346 °C (Grey and Merrit, 1981). This is also shown in Figure 5.

Figure 14 : Viscosity of two typical Sorel slags and of a CaO-TiO_2 mixture (Handfield, Charette and Lee, 1971)

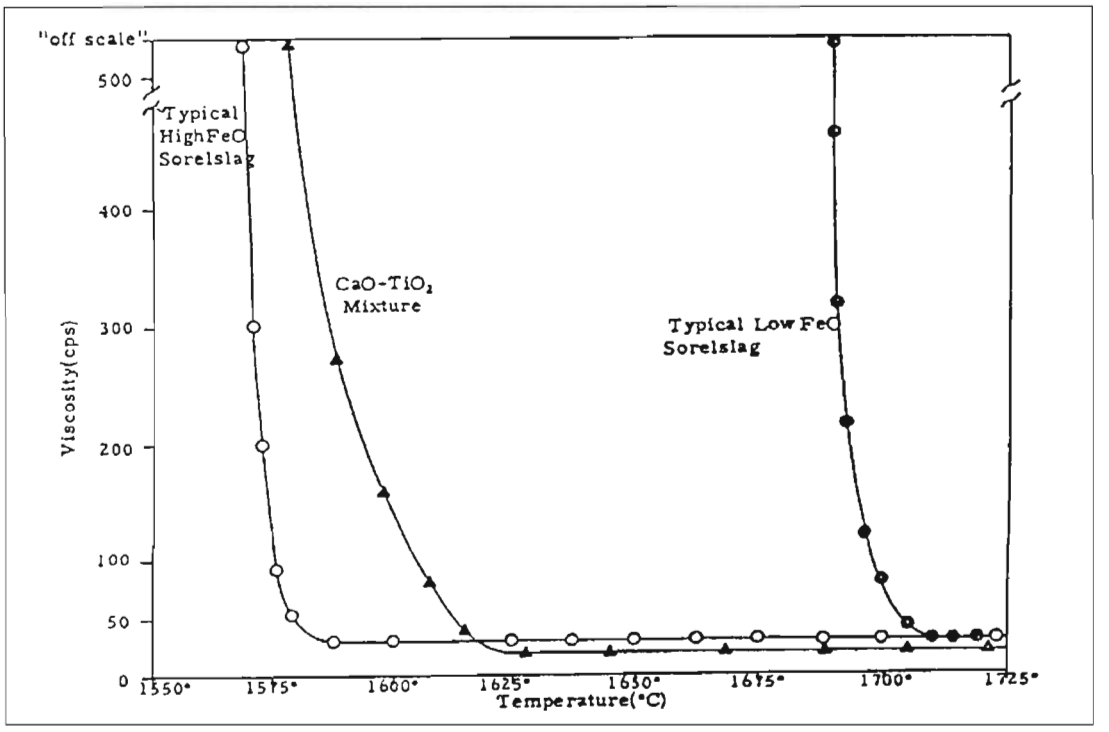

Figure 15 : Slag compositions from the smelting of ilmenite. Fluidity values (mm channel length) adjacent to points (Swinden and Jones, 1978)

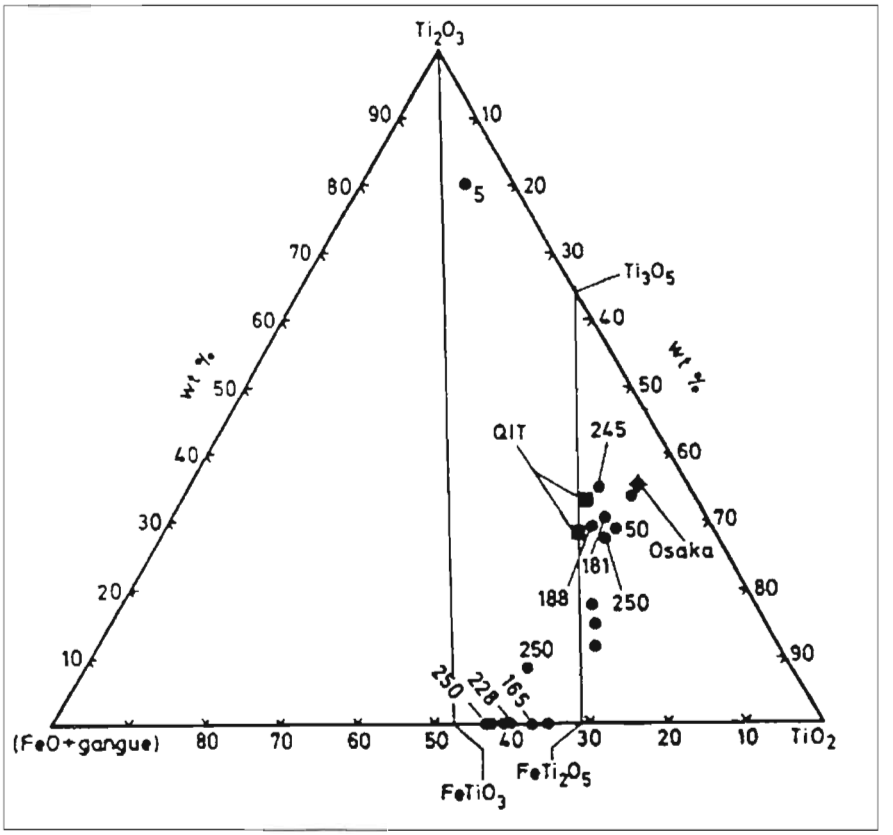

The fluidity of the various slag compositions was determined by pouring the slag into a steel mould with a horizontal tubular channel of 6 mm diameter. The more fluid slags ran further along the channel before solidifying. The fluidity values are therefore expressed as mm channel length. From the few results shown in Figure 15 it seems that in the early stages of the reduction process the melt becomes more viscous as the composition changes from $FeTiO_3$ to $FeTi_2O_5$. As the slag moves along the M_3O_5 solid solution line the slag fluidity seems to increase again. Swinden and Jones (1978) speculated that this could be due to the increasing Ti^{3+} content or to the enrichment of impurities such as MgO and MnO, which act as network breakers in the slag structure. In the Ti_2O_3 corner of Figure 15 the fluidity is extremely low. This suggests that a high slag fluidity might be because of the impurity content and not the Ti^{3+} content.

It is expected that the viscosities of the high titanium slags in this study will be of the same order (30 cps).

2.2.4.2 Electrical conductivity of titania slags

Studies on the electrical conductivity of high titanium slags were carried out by Desrosiers et. al. (1980), using Sorel and RBM slags. Measurements were carried out between 1527 and 1702 °C, with slag compositions ranging between 65 and 90 % TiO_2. Alternating current resistance measurements were made by an impedance bridge at a frequency of 1 kHz. The slag samples were contained in a molybdenum crucible that also acted as a fixed electrode (attached to the bridge by a molybdenum assembly). A molybdenum electrode was placed in the slag to make the necessary measurements. The experimental results obtained by Desrosiers et. al. (1980) are shown in Figure 16.

These results show that the slags are highly conductive, and that the conductivity of the slags increases with increasing TiO_2 content. The RBM slags are significantly more conductive compared to the Sorel slags due to a lower gangue content. In conclusion it was found that the slags were characterized mainly by electronic conduction. The implication of the highly conductive titanium slags is that the best way of operation is in an open-arc mode, with the electrode positioned above the surface of the slag. In such a process the resistive heating of the slag represents a small fraction of the energy delivered to the furnace. Most of the energy is dissipated within the arc and the thermal efficiency of the process relies on the heat transfer from the arc to the molten bath (Grau and Poggi, 1978).

2.3 EXPERIMENTAL DETAILS

2.3.1 SLAG SAMPLES

Various slag samples were obtained during smelting campaigns carried out at the Iscor direct current pilot plant furnace in Pretoria (electrical rating of 1.5 MW). A series of campaigns of varying duration (between 2 to 6 weeks) were carried out between 1995 and 1998. In these campaigns ilmenite was smelted with various carbonaceous reductants to produce high titania slags, with iron metal as a by-product. The titania slag was tapped from the furnace at regular intervals into ladles. The size of each tap ranged from approximately 500 kilogram to approximately one ton. Spoon samples were taken directly from the slag tap stream and

quenched in water, or allowed to cool in air. No differences, chemically and mineralogically, were found between these two types (cooled in water or air) of spoon samples. For the purpose of this study no distinction was made between the two types of spoon samples. These spoon samples were approximately one kilogram in size.

Figure 16 : Variation of electrical conductivity with increasing equivalent TiO_2 content at 1973 K (Desrosiers et. al., 1980)

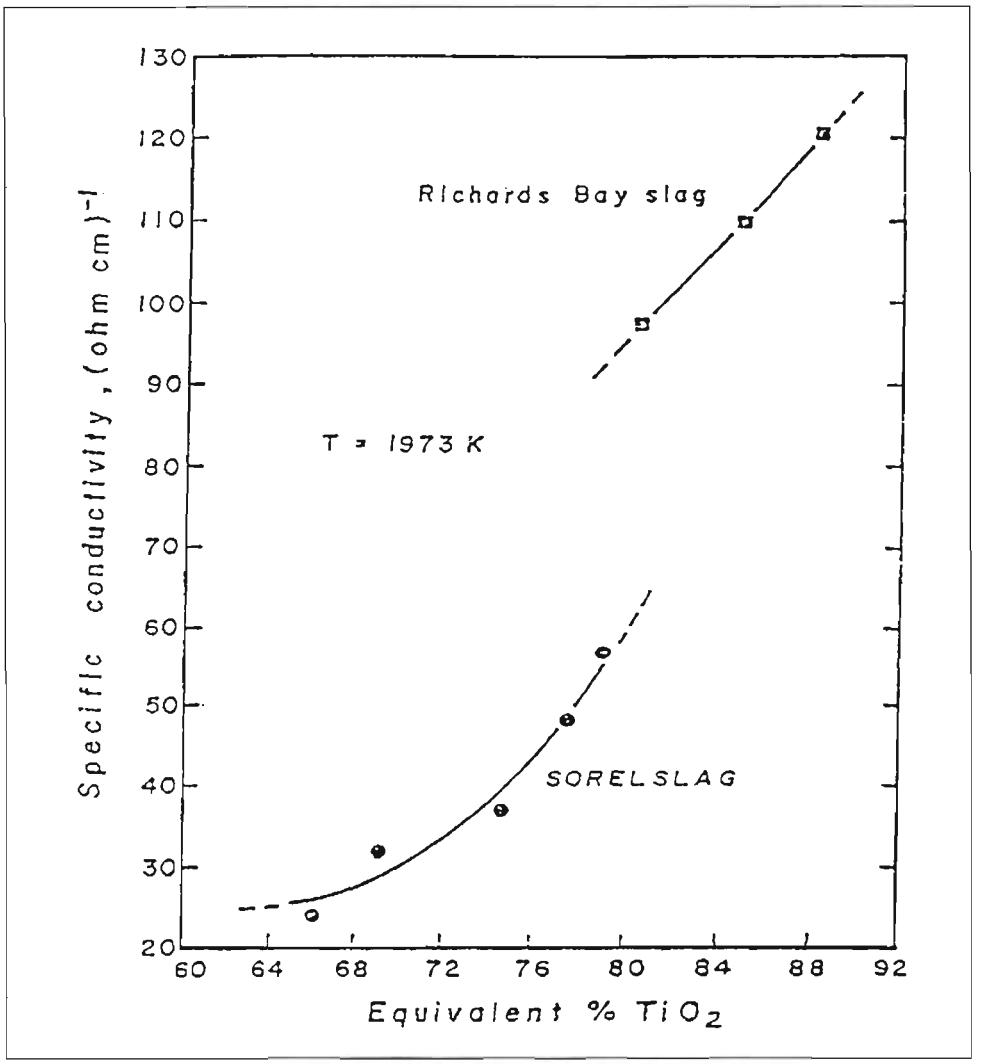

At each slag tap the temperature of the slag was measured with Electronite thermocouple devices (rated to 1730 °C). The temperature of the slag was measured in the ladle, when the ladle was approximately half filled.

2.3.2 ANALYTICAL TECHNIQUES

Chemical analyses of all the samples were carried out using inductively coupled plasma (ICP) or X-ray fluorescence (XRF) instruments. The oxidation states of iron and titanium in the slag samples were determined by using a wet chemical analytical technique (Du Plooy, 1997). X-ray diffraction analyses were also carried out on all the samples. In some instances an internal quartz standard was used to correct the data. In these instances both the M_3O_5 and quartz cell

constants were refined, together with the zero point. The cell constants of quartz were used as a control in these instances. Polished sections were also prepared for standard reflected light microscopy techniques.

2.3.2.1 Scanning electron microscopy and wavelength dispersive analyses

Polished sections of all the relevant samples were made. These polished sections were evaluated by scanning electron microscopy (SEM) and electron microprobe analyses. Photographs of the sample are of back-scattered electron images (unless otherwise indicated), providing contrasts on the basis of atomic numbers.

Suitable areas on the relevant phases were marked on selected polished sections prior to the wavelength dispersive analyses (WDS). An ARL-SEMQ electron microprobe at Mintek was used for the analyses. The elements that were analysed are shown in Table 10. Also shown are the standards that were used for calibration.

Table 10: Standards used for the wavelength dispersive analyses

Element	Standard	Element	Standard	Element	Standard
Mg	Spinel	Zr	ZrO_2 (synthetic)	V	V_2O_5 (synthetic)
Mn	Hausmannite	Al	Spinel	O	Rutile
Ti	Rutile	Fe	Hematite	Cr	Cr_2O_3 (synthetic)
Si	Quartz	Ca	Wollastonite	S	Anhydrite

Rutile was used as standard for oxygen, as most of the samples had both high Ti and O values. For these phases the shifting of the peaks (changing of wavelength of the oxygen X-rays generated and forming of peaks) was not found to be a significant problem. This is an inherent problem with the analyses of the light elements such as carbon and oxygen, where the wavelength of the generated X-rays depends on the bond length between the oxygen atoms and the cations. With this standardisation approach the analysed value for oxygen in the following standards was found to be too low:
Hematite (69.1 per cent Fe): 2.7 per cent too low
Ilmenite (36.2 per cent Fe): 2.1 per cent too low
Quartz (46.7 per cent Si): 5.2 per cent too low.

The error in the analysis of the oxygen content also has implications for the calculation of cation oxidation states. For example, for the calculation of the abundance of Ti^{3+} and Ti^{4+} in a M_3O_5 phase the Ti^{4+}/Ti^{3+} ratio can be greatly understated, depending on the value used for the oxygen analysis. In this study no corrections were applied to the actual observed results for the various phases analysed.

2.3.2.2 Mössbauer spectroscopy

Mössbauer spectroscopy measurements were carried out at the laboratory situated within the Department of Physics at the University of the Witwatersrand. Iron containing samples in powdered form were provided to the laboratory. The ^{57}Fe Mössbauer measurements were carried out in conventional transmission geometry at room temperature. A K3 Austin

Associates linear motor, driven by a triangular reference wave form, were used to scan the resonance profile. A Xe-CO_2 proportional counter was used to detect the transmitted 14.4 keV resonance radiation from a 5-10 mCi $^{57}Co(Rh)$ radioactive source. Typically 40-50 mg.cm^{-2} of sample was used. This was considered the optimal thickness in order to ensure the following:

- Avoid spectral lineshape distortions.
- Ensure acceptable transmission of the incident radiation when taking into account electronic absorption effects.
- Have adequate quantities of the ^{57}Fe isotope in the sample to ensure satisfactory signal-to-noise ratios after typical 12 to 24 hour data accumulation periods.

Data analyses were done by using a non-linear least squares Mössbauer analysing program NORMOS (supplied by WISSEL Starnberg-Germany). The fitting program was used for theoretical fits of the data with Lorentzian lineshapes to deconvolute various sub-components (phases) in the spectrum. A minimum number of sub-spectra (doublets and sextets) was used to obtain the best fit to the total spectrum. Final parameters of the fitted components were compared with the accepted literature values for the various oxides to enable phase identification. Mössbauer interaction parameters of selected Fe-Ti-O compounds relevant to this study are shown in Table 11 (data from Mulaba and Hearne, 1999). These parameters were determined at room temperature. Oxidation states of iron in the various phases were determined from the combination of values of fitted δ (isomeric shift) and Δ (quadrupole splitting) parameters obtained for quadrupole doublets, or from the B_{hf} (internal magnetic field) value of magnetically split sextets.

2.4 RESULTS AND DISCUSSION

2.4.1 MINERALOGICAL ANALYSES OF THE SLAGS

Four main mineralogical phases were identified to be present in the various slags. The amount of the phases varied from slag to slag depending on the chemistry of the slag, as well as the conditions under which each slag was cooled down. Differences were found for example between samples taken from slag blocks (cooled relatively slowly) and spoon samples (cooled relatively quickly).

2.4.1.1 The M_3O_5 phase

The major phase present in the various high titania slags was found to be the M_3O_5 phase. This is illustrated by the micrograph of a typical slag shown in Figure 17, with the M_3O_5 phase indicated by the symbol t. Identification and characterisation of the M_3O_5 phase were done by X-ray diffraction, microprobe analyses and Mössbauer spectroscopy. The bulk compositions of some of these slags characterised by these techniques are shown in Table 12. The phase analyses for these samples were determined from the elemental analyses of the respective phases. The analyses were normalised in order to obtain the number of cations for every five oxygen atoms. The calculated M_3O_5 phase compositions are as follows (full details given in Appendix B):

- DB100 – $Mg_{0.07}Al_{0.04}V_{0.01}Mn_{0.01}Ti_{2.61}Fe_{0.27}O_5$ ($M_{3.01}O_5$)
- DB152 – $Mg_{0.07}Al_{0.09}V_{0.01}Mn_{0.01}Ti_{2.84}Fe_{0.07}O_5$ ($M_{3.09}O_5$)
- DB156 – $Mg_{0.05}Al_{0.08}V_{0.01}Mn_{0.01}Ti_{2.65}Fe_{0.20}O_5$ ($M_{3.00}O_5$)

Table 11: Mössbauer hyperfine interaction parameters of selected Fe-Ti-O compounds at 300 K (Mulaba and Hearne, 1999)

Chemical formula	Mineral name	Ionic state of iron	δ_{Fe} ($mm.s^{-1}$)	Δ ($mm.s^{-1}$)	B_{hf} (T)	Comments	References
Fe	Iron	0	0	0	33.0	bcc metal	-
$FeTiO_3$	Ilmenite	3+	0.27	0.29	-	-	Stevens et. al. (1998)
		2+	1.04	0.70	-		
Fe_2O_3	Hematite	3+	0.37	-0.20	51.1	-	Stevens et. al. (1998)
Fe_2TiO_4	Ulvöspinel	2+	1.16	1.52	-	Inverse spinel where Fe^{2+} is found in "A" site and $Fe^{2+}Ti^{4+}$ in "B" site	Stevens et. al. (1998)
Fe_3O_4	Magnetite	3+ (A)	0.28	0.0	48.7	Tetrahedral – "A" site	Stevens et. al. (1998)
		3+ (B1)	0.66	0.08	45.4	Octahedral – "B" site	
		2+ (B2)	0.63	-0.16	45.7	Octahedral – "B" site	
Fe_2TiO_5	Pseudobrookite (ferric)	3+	0.39	0.70	-	-	Shirane et. al. (1962)
		3+	0.38	0.90	-	When some Fe^{3+} replaces Ti^{4+}, these hyperfine parameters may be obtained	Stevens et. al. (1998)
		3+	0.38	0.56	-		
$FeTi_2O_5$ (with Mg as impurity)	Pseudobrookite (ferrous)	2+	1.05	3.15	-	Tetrahedral - "A" site	Stevens et. al. (1998)
		2+	1.02	1.96	-	Octahedral – "B" site (less intense)	
$FeTi_2O_5$ (with Mn as impurity)	Pseudobrookite (ferrous)	2+	1.05	3.20	-	Tetrahedral - "A" site	Stevens et. al. (1998)
		2+	1.02	2.18	-	Octahedral – "B" site (less intense)	
$FeTi_2O_5$ (with Mn as impurity)	Pseudobrookite (ferrous)	2+	1.17	2.83	-	Tetrahedral - "A" site	Teller et. al. (pp. 351-367, 1990)
$Fe_{0.5}Mg_{0.5}Ti_2O_5$	Armalcolite	2+	1.05	3.15	-	Tetrahedral - "A" site	Stevens et. al. (1998)
		2+	1.03	2.01	-	Octahedral – "B" site (less intense)	
$Fe_2Ti_3O_9$	Pseudorutile	3+	-	-	-	No parameters have been reported	-

δ_{Fe} – Isomeric shift

Δ - Quadrupole splitting

Figure 17: Micrograph of a typical high titania slag

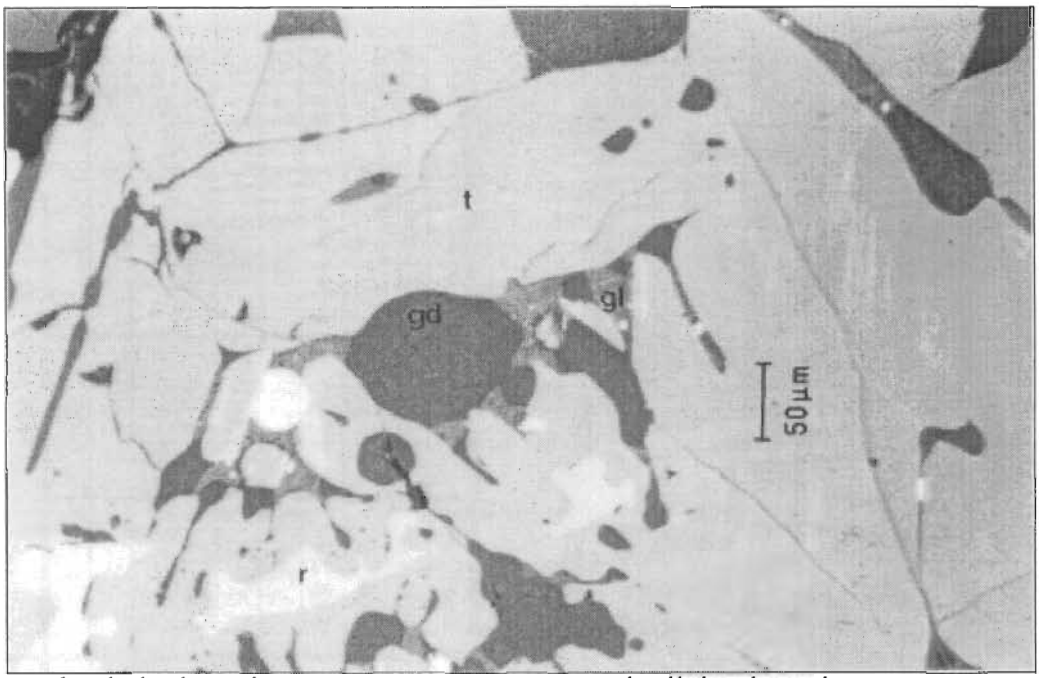

gd – dark glass phase
gl – light glass phase
t – M_3O_5 phase
r – rutile phase

Small amounts of zirconium and chromium were also analysed to be present, but in such small amounts to be ignored for the purposes of this study. The M_3O_5 phases were also analysed for silicon, calcium and sulphur, but only trace amounts of these elements were only found on occasion. It is interesting that the most reduced of these slags, sample DB152 (FeO content of 6.8 per cent and Ti_2O_3 content of 36.8 per cent), has a slight deviation from the M_3O_5 stoichiometry. For this sample a value for M of 3.09 was calculated. A standard deviation value of 0.06 was calculated for M. There however seems to be a mass balance problem when comparing the bulk analysis of the sample (Table 12) with the M_3O_5 phase analysis given in Appendix B. The bulk FeO content of slag DB152 is 6.8 per cent, but the M_3O_5 phase only contains 1.64 per cent Fe (or 2.1 per cent FeO). It therefore seems that the grain that was analysed is not representative of the bulk sample, perhaps even being a Magnéli phase.

It is interesting to note that Borowiec and Rosenqvist (1985) also found an oxygen deficiency in some of their M_3O_5 solid solution phases. This was in their studies of the phase relations in the Fe-Ti-Mg-O system at temperatures below 1100 °C. The oxygen deficiency was found in solid solutions with a $Ti_3O_5/FeTi_2O_5$ molar ratio of approximately greater than 2. They did not suggest any explanation for this.

The Mössbauer data obtained for these slags are shown in Table 13. The Mössbauer spectra of these samples are given in Appendix C, together with the Mössbauer spectra of all the samples in this study. The Mössbauer data show that the majority of the iron content of the slags is present in the A site of the M_3O_5 structure. This confirms the results

Table 12: Bulk chemical analyses of selected slag samples

Sample no.	Analyses (mass %)											
	SiO_2	Al_2O_3	CaO	MgO	MnO	Cr_2O_3	V_2O_5	Fe^0	FeO	TiO_2	Ti_2O_3	Total Ti as TiO_2
DB100	1.41	1.19	0.27	1.03	1.17	0.05	0.45	< 0.1	9.80	53.9	30.4	87.70
DB152	1.76	1.64	0.24	1.02	1.40	0.09	0.42	0.39	6.83	48.4	36.78	89.29
DB156	1.84	1.48	0.27	1.07	1.33	0.09	0.43	0.19	9.42	52.0	30.92	86.40

Table 13: Mössbauer analyses of selected slag samples

Sample number	Sample origin	Hyperfine interaction parameters			Abundance (atom %)	Attribution
		A ($mm.s^{-1}$)	B ($mm.s^{-1}$)	B_{hf} (T)		
DB100	Sample from tap stream	1.16 (2)	3.35 (4)	-	90 (2)	Fe^{2+} compound (ferropseudobrookite; site A)
		1.09 (2)	1.83 (4)	-	10 (2)	Fe^{2+} compound (ferropseudobrookite; site B)
DB152	Sample from tap stream	1.07 (3)	3.00 (5)	-	75 (5)	Fe^{2+} compound (ferropseudobrookite; site A)
		1.07 (2)	1.85 (3)	-	25 (4)	Fe^{2+} compound (ferropseudobrookite; site B)
DB156	Sample from tap stream	1.08 (2)	3.03 (3)	-	82 (5)	Fe^{2+} compound (ferropseudobrookite; site A)
		1.04 (3)	2.0 (5)	-	15 (5)	Fe^{2+} compound (ferropseudobrookite; site B)
		0.49 (3)	0.68 (2)	-	3 (3)	Fe^{3+} compound (pseudobrookite)

Errors are quoted in brackets

obtained by other investigators (see data shown in Table 4 and Table 5). It is also interesting to note that the most reduced slag (DB152, composition closest to Ti_3O_5) has the lowest iron content in the A site. This confirms the findings of Grey and Ward that the iron content in the A site decreases with a decrease in the iron content of the M_3O_5 phase. The data in Table 13 also show that the oxidation state of the iron contained in the high titania slags are +2. For sample DB156 the presence of some Fe^{3+} was indicated. This was however discounted due to the large relative error of the result, with the error being equal to the value.

X-ray diffraction data obtained for the M_3O_5 phase in a typical slag (sample DB156) are shown in Table 14. Only the major peaks are shown, with the detailed set of data given in Appendix D. Also given in Appendix D is the calculated data for the phase. As discussed previously (see Table 6) the two major peaks (at approximately d = 3.50 Å and d = 2.76 Å) for the M_3O_5 phase were also found in this sample. X-ray diffraction patterns for the slag samples given in Table 12 are shown in Appendix E. These patterns also include the pattern for quartz that was used as internal standard.

Table 14: Crystallographic data for sample DB156

h	k	l	d (Å)	I/I_0 (obs)
2	0	0	4.910	36.0
2	0	0	4.898	16.9
1	1	0	3.531	100.0
1	1	0	3.522	51.5
2	0	3	2.760	79.2
2	0	3	2.753	39.1
3	1	0	2.473	20.9
1	1	3	2.425	20.8
2	0	4	2.230	15.1
4	0	2	2.201	18.8
4	0	3	1.975	21.0
0	2	0	1.890	35.1
0	2	0	1.886	18.1
5	1	2	1.644	20.0
2	2	3	1.559	21.0
5	1	3	1.543	18.0

The unit cell parameters obtained for the M_3O_5 phases in the titania slag samples are shown in Table 15. The data shows that low standard deviations were obtained for all the samples. The difference in volume between the highest (DB100) and lowest (DB152) cell volume is approximately 0.2 per cent.

The site occupancies of the cations in the M_3O_5 structure were calculated by using all the available information, together with some assumptions. The results of the calculations are shown in Table 16. The information used, and the assumptions made, are listed below:

- The elemental phase analyses data for the various samples given in Appendix B were used to determine the composition of the M_3O_5 phase in each sample, as well as for the

calculation of the charge balance. To calculate the charge balance the following were taken into consideration:

- Iron is only present in the +2 oxidation state (based on Mössbauer results – see Table 13).
- Magnesium and manganese are only present in the +2 oxidation state, aluminium in the +3 oxidation state.
- Vanadium is present in the +3 oxidation state (see Pistorius and Coetsee, 2000).
- The Ti^{3+} and Ti^{4+} contents were calculated using the composition data. This was done by assuming a charge balance (the oxidation state of oxygen is –2).

- All the V^{3+} and Al^{3+} report to the smaller B site because of their small cation size ($r(Ti^{3+}) > r(V^{3+}) > r(Al^{3+})$), the larger Mn^{2+} cation reports exclusively to the larger A site (see ionic radii, Table 2).
- Fe^{2+} is distributed among the A and B sites according to the Mössbauer results shown in Table 13.
- One third of the Mg^{2+} is present in the B site. This assumption is made on the basis of the data in Table 5 for $Ti_{2.36}Fe_{0.33}Mg_{0.31}O_5$. It is believed that this information for Mg^{2+} is closest to the slags investigated in this study.
- Ti^{4+} preferentially fills the smaller B site (see Table 4 for distribution of Ti^{3+} and Ti^{4+} in Ti_3O_5).
- Ti^{3+} is distributed according to the remaining available spaces.

Table 15: Unit cell data for the M_3O_5 phases in the respective titania slag samples

Lattice parameters	Sample numbers			
	DB100	DB123	DB152	DB156
a (Å)	9.7830 (0.0003)	9.7770 (0.0007)	9.7939 (0.0003)	9.7915 (0.0024)
b (Å)	3.7794 (0.0001)	3.7599 (0.0002)	3.7769 (0.0001)	3.7768 (0.0007)
c (Å)	10.0122 (0.0004)	10.0649 (0.0007)	9.9902 (0.0003)	10.0010 (0.0027)
Cell Volume ($Å^3$)	370.191 (0.026)	369.988 (0.051)	369.542 (0.014)	369.841 (0.113)

Standard deviation values given in brackets

For samples DB100 and DB152 the stoichiometry was calculated to be $M_{3.01}O_5$ and $M_{3.09}O_5$ respectively (see Appendix B). In Table 16 the additional cations were included in the B site for calculation purposes. For example the stoichiometry for DB152 was calculated to be $A_{1.00}B_{2.09}O_5$.

The Ti^{3+} fraction (as a fraction of the total Ti in moles) of the M_3O_5 phase was found to be approximately 0.5 for samples DB100 and DB156 (see Table 16). This might however be too high due to the error associated with the oxygen analysis. Based on the bulk chemical analyses of these samples this value is closer to 0.4 (see Table 12).

2.4.1.2 Rutile phase

Rutile was identified as the second most prevalent phase in the slags as identified by X-ray diffraction. Figure 17 also shows the presence of the rutile phase (r). Microprobe analysis of a typical rutile phase is given in Table 17, showing that the phase consists mainly of titanium as expected. It was however not possible to determine whether all the titanium is in the +4 oxidation state, or whether there is some Ti^{3+} present. This is because the oxygen content of the phase was not determined. The analysis also shows some solubility of manganese and iron in the rutile. Webster and Bright (1961) however found limited solubility of iron in rutile at 1200 °C.

Table 16: Proposed cation distribution in the M_3O_5 phases present in titania slags

Sample no.	A site	B site
DB100	$Fe^{2+}_{0.24}\ Mn^{2+}_{0.01}\ Mg^{2+}_{0.05}\ Ti^{3+}_{0.70}$	$Fe^{2+}_{0.03}\ Mg^{2+}_{0.02}\ Al^{3+}_{0.04}\ V^{3+}_{0.01}\ Ti^{3+}_{0.59}\ Ti^{4+}_{1.32}$
DB152	$Fe^{2+}_{0.05}\ Mn^{2+}_{0.01}\ Mg^{2+}_{0.05}\ Ti^{3+}_{0.89}$	$Fe^{2+}_{0.02}\ Mg^{2+}_{0.02}\ Al^{3+}_{0.09}\ V^{3+}_{0.01}\ Ti^{3+}_{1.07}\ Ti^{4+}_{0.88}$
DB156	$Fe^{2+}_{0.17}\ Mn^{2+}_{0.01}\ Mg^{2+}_{0.03}\ Ti^{3+}_{0.79}$	$Fe^{2+}_{0.03}\ Mg^{2+}_{0.02}\ Al^{3+}_{0.08}\ V^{3+}_{0.01}\ Ti^{3+}_{0.60}\ Ti^{4+}_{1.26}$

Table 17: Microprobe analysis of a typical rutile phase (mass percentages)

Total Ti as TiO_2	MnO	FeO
98.08	0.19	1.72

2.4.1.3 Glass phases

Examples of the glass phases found in titania slags are shown in Figure 17. Two types of glass phases were identified, a light coloured phase (identified by gl) and a dark coloured phase (identified by gd). These two phases were found in close proximity to each other. The bulk chemical analysis of the sample shown in Figure 17 is given in Table 18. In terms of the FeO content of the slag it could be characterised as a typical slag that would be produced for the chloride production route. The impurity content, in particular the CaO and SiO_2 content, is however too high.

A summary of the microprobe analyses of the two glass phases identified is given in Table 19 (details given in Appendix F). From Table 19 it can be seen that the dark coloured glass phase consists mainly of SiO_2 and TiO_2. The composition of the light coloured phase is more complex. The main component is once again SiO_2, with TiO_2, MnO, FeO and CaO all present at levels of approximately 10 to 15 per cent. The composition of this glass phase also appears to be similar to that of the Tyssedal slag (see Table 3).

Table 18: Bulk chemical analysis of sample YS2872

Sample no.	Analyses (mass %)											
	SiO_2	Al_2O_3	CaO	MgO	MnO	Cr_2O_3	V_2O_5	Fe^0	FeO	TiO_2	Ti_2O_3	Total Ti as TiO_2
YS2872	2.56	1.60	0.72	0.55	1.18	0.10	0.42	0.03	9.98	49.1	33.5	86.3

Table 19: SEM analyses of the dark and light coloured glassy samples found in sample YS2872

	Analysis (mass per cent)								
	MgO	Al_2O_3	TiO_2	MnO	FeO	SiO_2	K_2O	CaO	Na_2O
Dark coloured phase	-	3.13	8.21	0.61	1.74	83.61	1.10	1.07	0.78
Light coloured phase	-	5.85	11.48	10.76	11.19	45.82	0.13	14.80	-

2.4.1.4 Metallic iron phases

Two types of metallic Fe particles were identified in the Iscor slags. The most prominent particles were finely disseminated metallic iron globules present in the slag and on the grain boundaries of the Ti-oxide crystals, in the silicate rich glassy matrix. The size of these particles was greater than approximately 15 μm, and as large as 150 μm as determined by SEM analyses (apparent diameter as determined in polished section). These metallic globules are believed to consist of metallic iron droplets caught in the slag. Some of these metallic iron globules contained a Fe-sulphide rich outer margin. Microprobe analyses of this Fe-sulphide phase is shown in Table 20, with the Fe:S molar ratio being 0.68. The Fe-sulphide outer rim also contains small amounts of Mn and Ti. The sulphur found in the slags was always associated with the iron globules. Examples of this are shown in Figure 18. The phenomenon of metallic iron globules containing a Fe-sulphide rich outer margin had previously also been observed by Reznichenko et. al. (1981) and Toromanoff and Habashi (1984).

Table 20: Microprobe analyses of the iron sulphide phase on the rim of an iron globule

Element	Analyses (mass %)
S	44.0
Fe	52.1
Mn	2.2
Ti	1.81

The second type of metallic iron particle present in the slags was found to be present in the rutile phases. It was found that the larger of the rutile crystals contained fine, metallic iron precipitates. The size of these precipitates was less than approximately 3 μm. An example of this is shown in Figure 19. Toromanoff and Habashi (1984) found similar precipitates nucleated during cooling of their slags as a result of the following reaction:

$$2\ Ti^{3+} + Fe^{2+} \rightarrow 2\ Ti^{4+} + Fe^{0} \ldots (J)$$

2.4.2 CHEMICAL ANALYSES OF THE SLAGS

The chemical composition of high titania slags is dependent on the chemical quality of the ilmenite and reductant used for smelting. The extent of reduction during the smelting process obviously also has an effect on the chemical composition of the slags, especially so for the iron and titanium content of the slags. In Table 21 a wide range of slag compositions is given. These slags were prepared in the Iscor pilot plant furnace during various ilmenite smelting campaigns. In these campaigns a variety of ilmenite and reductant feedstocks were used, resulting in the range of chemical compositions shown. Also shown in Table 21 is the insoluble content of some selected slags. This analysis refers specifically to the suitability of a particular slag for the sulphate pigment production process, with a high value indicating that the slag is less suitable for the sulphate process. The rutile content of the slag is important in this regard, as rutile is insoluble in sulphuric acid (Stanaway, 1994). As the rutile content of the slags was not quantified, it was not possible to correlate the data in Table 21 with the rutile content.

Figure 18: Micrograph of metallic iron globules (F) with a Fe-sulphide rich outer margin (S)

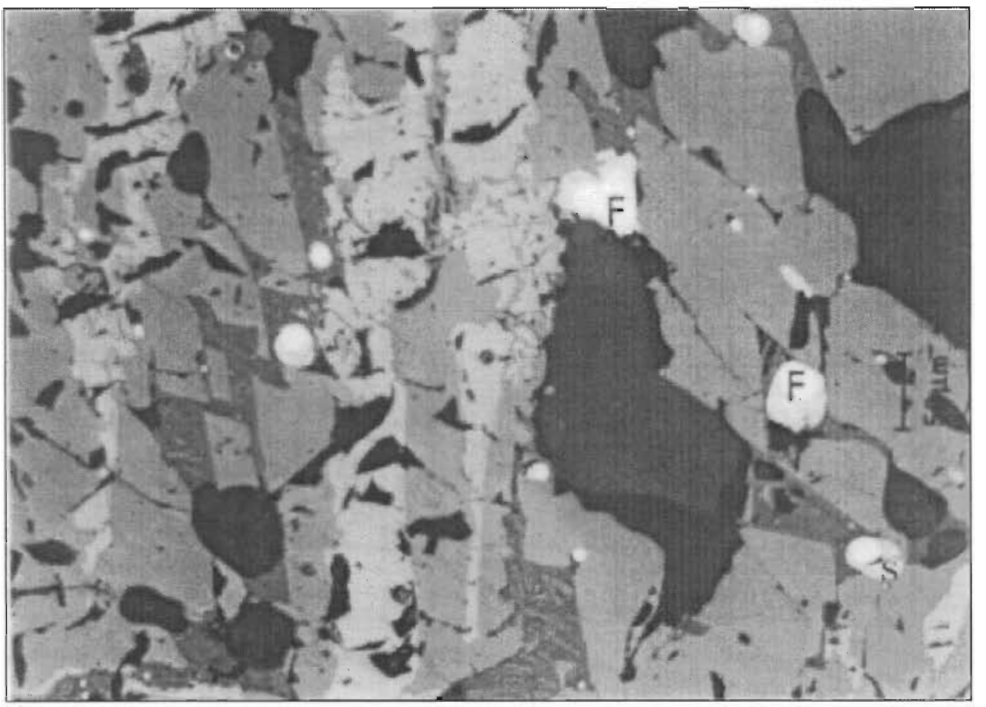

Figure 19: Micrograph of fine metallic iron precipitates (F) within the rutile phase (R)

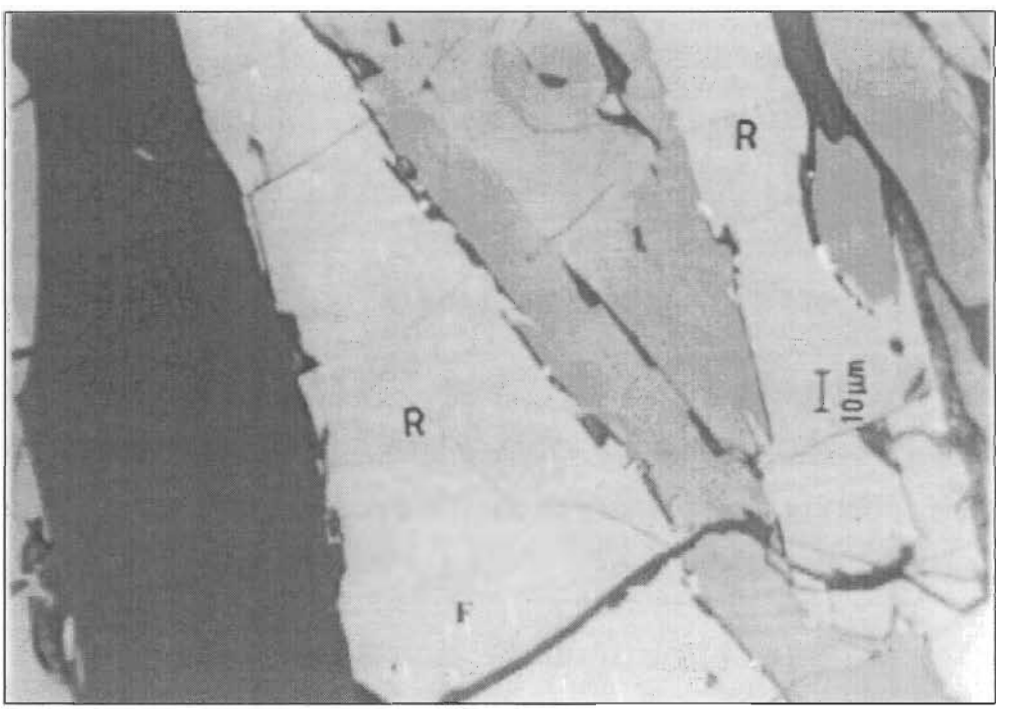

Table 21 : Chemical analyses of various high titania slags produced in the Iscor 3 MVA plasma furnace

Sample no.	Tap Temperature (°C)	Analyses (mass %)															TiO_2 insolubility
		SiO_2	Al_2O_3	CaO	MgO	MnO	Cr_2O_3	V_2O_5	ZrO_2	C	S	Fe^0	FeO	TiO_2	Ti_2O_3	Total Ti as TiO_2	
3176	1641	1.26	0.98	0.10	0.94	1.25	0.13	0.47	-	0.05	0.06	0.06	11.80	55.00	27.90	86.00	-
3179	1662	1.23	1.07	0.12	0.97	1.22	0.12	0.46	-	0.04	0.07	0.17	10.20	51.80	33.20	88.69	-
3191	1669	2.30	1.24	0.25	1.61	1.24	0.09	0.39	-	0.14	0.08	0.13	9.27	54.00	31.00	88.45	-
3206	1735	2.28	1.62	0.47	0.80	1.15	0.10	0.43	-	0.06	0.09	0.06	5.38	45.15	42.20	92.05	3.46
3209	-	2.75	1.59	0.57	0.53	1.24	0.09	0.40	-	0.04	0.04	0.04	10.64	49.50	32.15	85.23	5.17
3215	-	2.10	1.47	0.35	0.93	1.06	0.08	0.43	-	0.02	0.03	0.07	15.65	55.40	22.30	80.18	4.28
3216	1660	1.75	1.11	0.18	0.37	0.86	0.03	0.44	-	0.04	0.05	0.16	13.30	53.00	29.30	85.56	-
3222	1721	1.56	1.04	0.22	1.05	1.03	0.08	0.45	-	-	-	0.20	5.93	47.70	41.70	94.04	-
3228	1706	1.46	1.14	0.39	1.20	1.24	0.11	0.49	-	0.04	0.07	0.06	7.59	39.05	47.00	91.28	5.79
3229	1695	1.48	1.11	0.38	1.20	1.23	0.13	0.51	-	0.05	0.07	0.17	8.58	37.30	47.55	90.14	1.15
4008	1679	1.04	0.58	0.21	1.00	1.23	0.03	0.46	0.35	-	0.06	0.14	11.40	53.60	28.70	85.50	4.05
4009	1668	1.03	0.58	0.22	0.99	1.24	0.03	0.44	0.36	-	0.06	0.09	10.58	56.20	27.50	86.80	5.41
4011	1679	1.03	0.64	0.22	1.52	1.18	0.03	0.47	0.36	-	0.07	0.13	10.19	54.40	29.00	86.60	3.26
4014	1667	1.18	0.66	0.24	1.08	1.22	0.04	0.47	0.36	-	0.09	0.10	11.23	54.50	27.80	85.39	4.57
4016	1676	1.18	0.69	0.21	1.37	1.15	0.03	0.49	0.34	-	0.06	0.09	11.05	56.00	26.90	85.90	-
4022	1678	1.34	0.70	0.24	1.16	1.20	0.03	0.46	0.35	-	0.07	0.09	10.50	56.50	26.70	86.20	3.26
4027	1686	1.26	0.76	0.29	0.99	1.19	0.03	0.47	0.35	-	0.06	0.09	9.64	54.70	28.80	86.70	3.07
4033	1700	0.96	0.69	0.19	1.88	1.05	0.02	0.48	0.34	-	0.06	0.16	8.56	60.60	25.50	88.94	2.90
4040	1679	1.00	0.56	0.19	2.86	1.13	0.03	0.47	0.34	-	0.06	0.27	9.79	55.70	27.30	86.04	1.28
4044	1688	1.32	1.02	0.58	1.99	1.12	0.02	0.47	0.36	-	0.06	0.08	11.31	57.50	24.90	85.17	2.71
6005	1652	1.16	0.71	0.21	2.06	1.20	0.04	0.43	-	-	-	0.23	13.70	55.30	23.30	81.25	-
6006	1639	1.11	0.69	0.19	1.63	1.21	0.04	0.41	-	-	-	0.18	16.10	57.30	19.90	79.47	-
6009	1616	1.09	0.67	0.25	1.40	1.18	0.04	0.41	-	-	-	0.24	17.90	57.90	17.80	77.69	-
6010	1623	1.10	0.67	0.24	1.33	1.17	0.04	0.41	-	-	-	0.23	17.30	58.10	18.20	78.34	-
6012	1648	1.08	0.68	0.20	1.14	1.21	0.04	0.42	-	-	-	0.19	15.70	56.80	21.60	80.81	-

Table 21 : Chemical analyses of various high titania slags produced in the Iscor 3 MVA plasma furnace (Continued)

Sample no.	Tap Temperature (°C)	Analyses (mass %)															TiO_2 insolubility
		SiO_2	Al_2O_3	CaO	MgO	MnO	Cr_2O_3	V_2O_5	ZrO_2	C	S	Fe^0	FeO	TiO_2	Ti_2O_3	Total Ti as TiO_2	
6013	1639	1.17	0.68	0.20	1.16	1.22	0.04	0.42	-	-	-	0.23	14.70	56.10	22.60	81.19	-
6015	1635	1.17	0.67	0.20	1.11	1.27	0.03	0.42	-	-	-	0.32	14.60	57.30	21.90	81.69	-
6021	1688	1.21	0.76	0.23	1.68	1.25	0.03	0.41	-	-	-	0.06	10.50	54.30	28.40	85.81	-
6025	1665	1.63	1.03	0.32	2.62	1.58	0.21	0.40	-	-	-	0.06	10.90	55.40	24.80	81.04	-
6031	1698	1.36	0.81	0.33	1.99	1.30	0.05	0.39	-	-	-	0.03	7.50	49.80	35.40	89.16	-
6033	1707	1.29	0.82	0.29	1.44	1.22	0.04	0.42	-	-	-	0.06	8.80	53.80	31.70	89.04	-
6034	1712	1.26	0.78	0.28	1.31	1.23	0.03	0.42	-	-	-	0.01	8.10	52.90	33.40	89.99	-
6047	1650	2.82	1.17	0.56	1.15	1.37	0.03	0.36	-	-	-	0.03	12.80	53.80	24.10	80.56	-
7066	1695	1.48	0.88	0.31	1.02	1.25	0.04	0.44	-	-	-	0.10	7.80	51.10	35.50	90.55	-
7070	1685	1.48	1.09	0.30	1.01	1.29	0.03	0.44	-	-	-	0.10	9.00	52.40	32.50	88.52	-
7075	1644	1.20	0.87	0.23	0.92	1.13	0.04	0.43	-	-	-	0.20	12.70	55.30	25.90	84.08	-
7080	1698	1.90	1.00	0.26	1.15	1.16	0.03	0.44	-	-	-	0.10	9.00	52.00	32.30	87.89	-
7201	1652	1.27	0.77	0.24	0.99	1.23	0.06	0.44	-	-	-	0.13	12.90	55.50	25.40	83.73	-

The relationship between the FeO and Ti_2O_3 contents of the titania slags from Table 21 is shown in Figure 20. Also shown is the linear regression line drawn for the data. The data from this study was also compared with the data given by various other authors. This comparison is shown in Figure 21. As expected the data from this study compare very well with that given by Pistorius and Coetsee (2000) for South African slags. The data published by Grau and Poggi (1978), and Pistorius and Coetsee (2000) for the Sorel slags also compare well.

As discussed by Pistorius and Coetsee (2000) it can be seen that the linear regression lines for the Sorel slags lie below that of the South African slags. The reason for this is the higher impurity content of the Sorel slags (Pistorius and Coetsee, 2000). Ban (1988) and Ban et. al. (1988) obtained a semi-logarithmic relationship between the Ti_2O_3 and FeO contents of the slags studied by them. Depending on the FeO content of their slags, the Ti_2O_3 content of their slags is markedly different to those of the other investigators. For example, comparing their data for RBM slags with that of this study and with the data of Pistorius and Coetsee (2000) for South African slags the following comments can be made:

- The equation of Ban et. al. (1988) intersects the linear regression lines of this study and the study of Pistorius and Coetsee (2000) at approximately 8 and 23 per cent FeO.
- At 15 per cent FeO the difference in the Ti_2O_3 content between the respective studies is approximately 6 per cent.
- At values lower than 8 per cent FeO the Ti_2O_3 values diverge sharply and can perhaps be explained in the way the different data sets are fitted.

As explained by Pistorius and Coetsee (2000) high titania slag consists mainly of one solid solution phase, with this phase expected to consist of a mixture of the stoichiometric end members $FeTi_2O_5$ and Ti_3O_5. This should therefore result in a linear relationship between the FeO and Ti_2O_3 content in high titania slags. This FeO-Ti_2O_3 relationship for the $FeTi_2O_5$-Ti_3O_5 tie line is also shown in Figure 21. As found by Pistorius and Coetsee (2000) this line lies well above the other data lines. As explained previously, Pistorius and Coetsee (2000) re-calculated the data in their paper to take into account the effect of the impurities (see equations (VII) and (VIII)). Taking this into account their data correlated very well with the FeO-Ti_2O_3 relationship for the $FeTi_2O_5$-Ti_3O_5 tie line. It should however be pointed out at this stage that the correction applied by Pistorius and Coetsee (2000) for the Al_2O_3 content is not relevant to South African slags (see equation (VIII)). This is due to the low Al_2O_3/SiO_2 ratios found in the glass phases for South African slags. This is typified by the results shown in Table 19, where the molar Al_2O_3/SiO_2 ratios varied between 0.02 and 0.07 for the different glass phases. Due to the low levels of these impurities it does however not have a significant impact on the results.

These calculations were also done for the data in this study, also by using equations (VII) and (VIII), followed by the normalisation of the TiO_2, equivalent FeO and equivalent Ti_2O_3 data to 100 per cent. The results obtained for the re-calculated data are shown in Figure 22. Also shown is the linear regression line for the data, with a R^2 value of 0.75 obtained. This is slightly higher than the R^2 value of 0.70 obtained in Figure 20, indicating that the inclusion of the impurities marginally improves the linear regression fit. The results show that the inclusion of the impurities definitely improves the correlation with the $FeTi_2O_5$-Ti_3O_5 tie line composition relationship, with the linear regression line only slightly below the tie line composition. The reason for the difference can possibly be explained by some oxidation of the Ti^{3+} content of the slag on cooling.

Figure 20: Relationship between the FeO and Ti_2O_3 content of titania slag (This study)

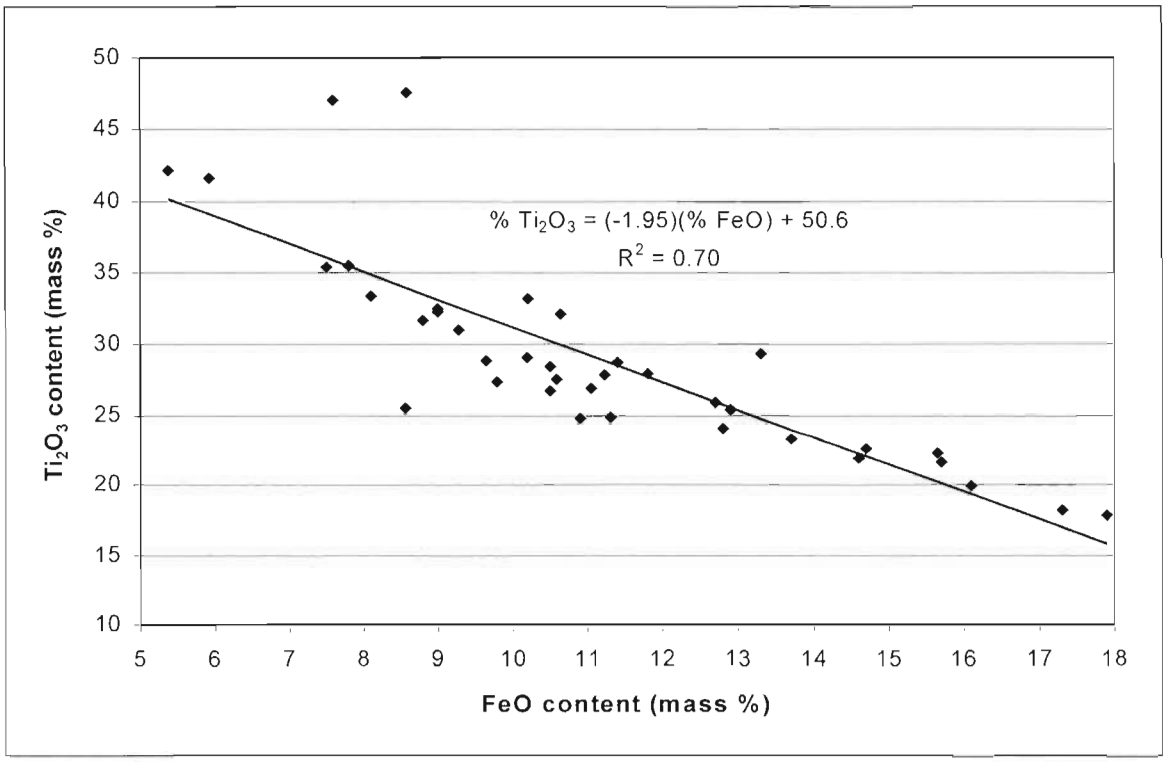

Figure 21 : Comparison of various results for the FeO-Ti_2O_3 relationship in titania slags

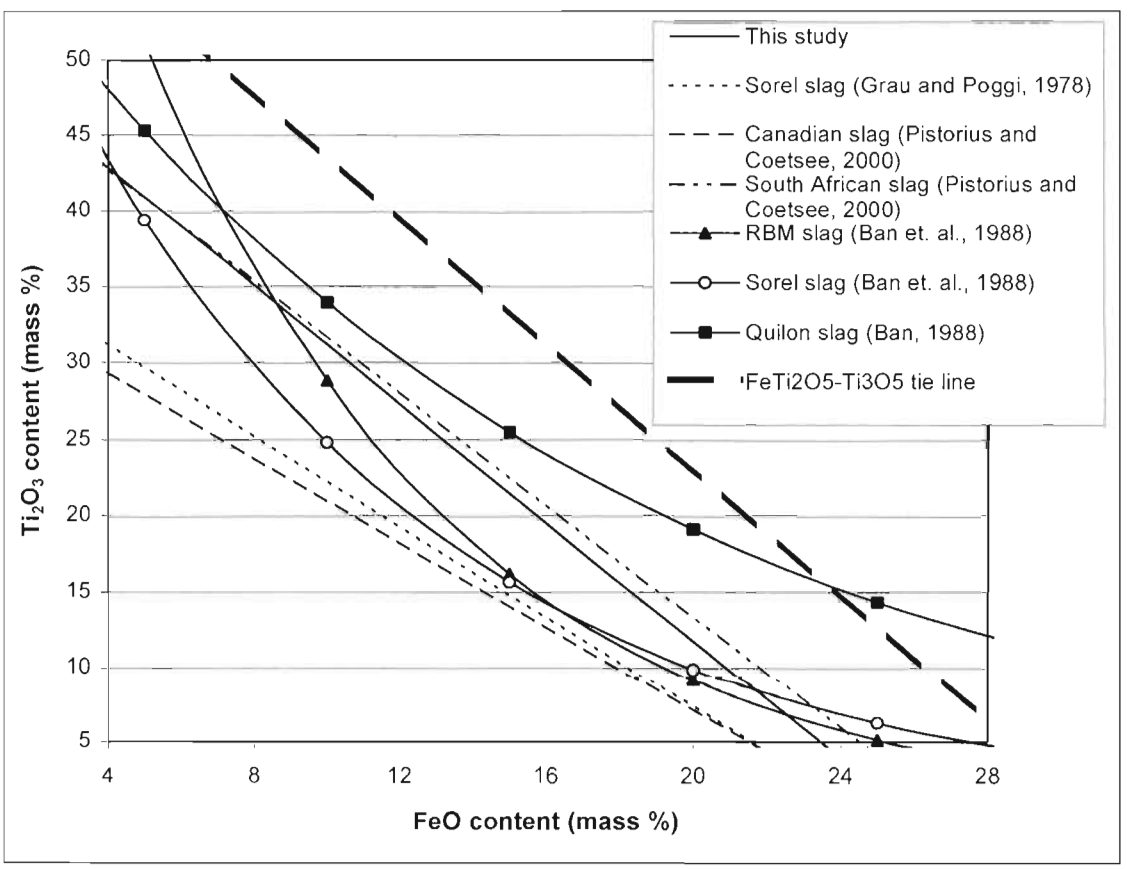

Figure 22: Relationship between the FeO and Ti_2O_3 content of titania slag in this study (Effect of impurities taken into account)

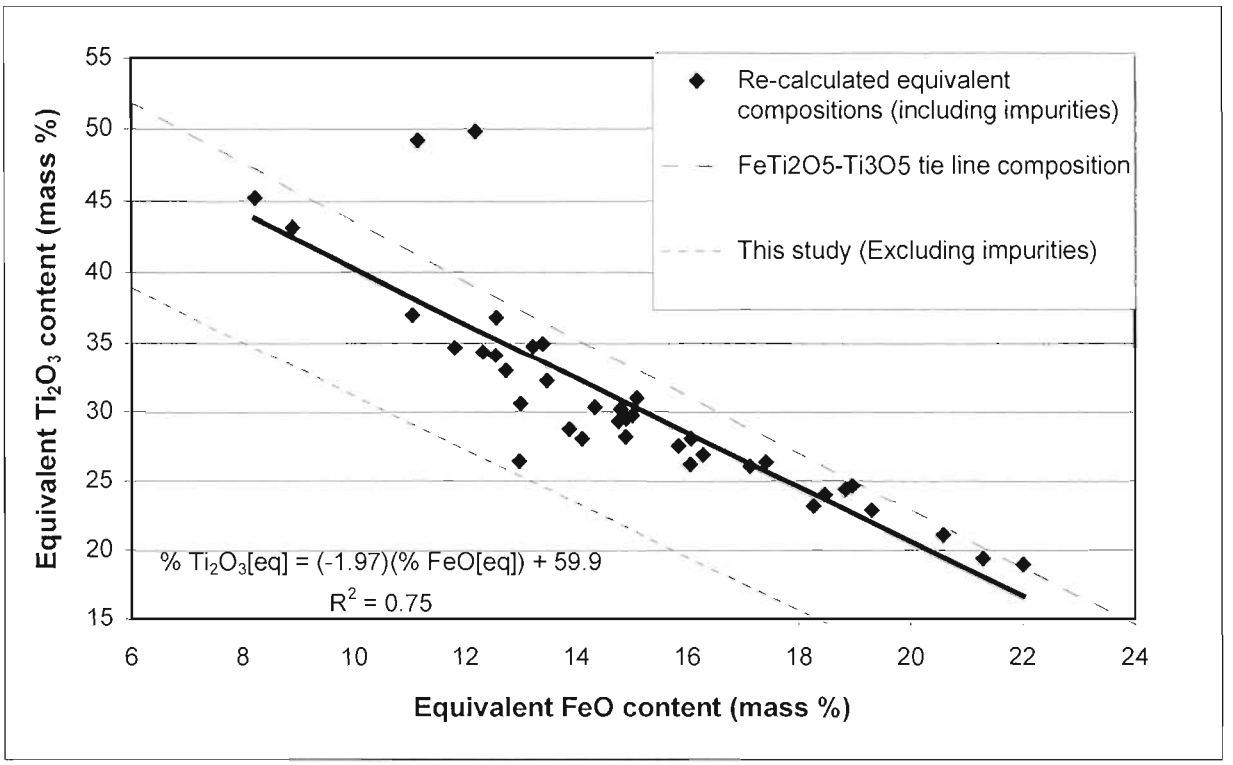

The relationship between the FeO content and the total titanium content of the slag (expressed as TiO_2) was also plotted. This is shown in Figure 23. Also shown is the composition line for the $FeTi_2O_5$-Ti_3O_5 tie line (dashed line). Once again it can be seen that by excluding the impurities in the slag there is a substantial difference between the tie line composition and the linear regression line for the data not including the impurities. The data was re-calculated to include the effect of the impurities. To calculate the equivalent total titanium content expressed as TiO_2 (% TiO_2[eq]), the following equation was used (M_{TiO2} and M_{Ti2O3} the molar mass of the respective compounds):

$$\% TiO_2[eq] = \% TiO_2 + (\% Ti_2O_3[eq])(2M_{TiO2}/M_{Ti2O3}) \ldots(XI)$$

For the calculation of % Ti_2O_3[eq], equation (VIII) was again used. The effect of including the impurities can be seen very clearly in Figure 23. Excellent correlation between the calculated relationship and the tie line composition are observed. This also tends to confirm the earlier contention that the Ti^{3+} content of the slags decreased slightly during the cooling process due to oxidation. The calculated line also has an R^2 value of 0.99, showing the excellent fit of the data. This R^2 value is also substantially higher than the value of 0.75 found for the Ti_2O_3[eq]-FeO[eq] relationship (see Figure 22). The reason for the difference can probably be attributed to the uncertainty involved with the wet chemical technique used for the analysis of the Ti_2O_3 content of the slags.

Figure 23: Relationship between the FeO and total titanium content (expressed as TiO_2) of titania slag in this study

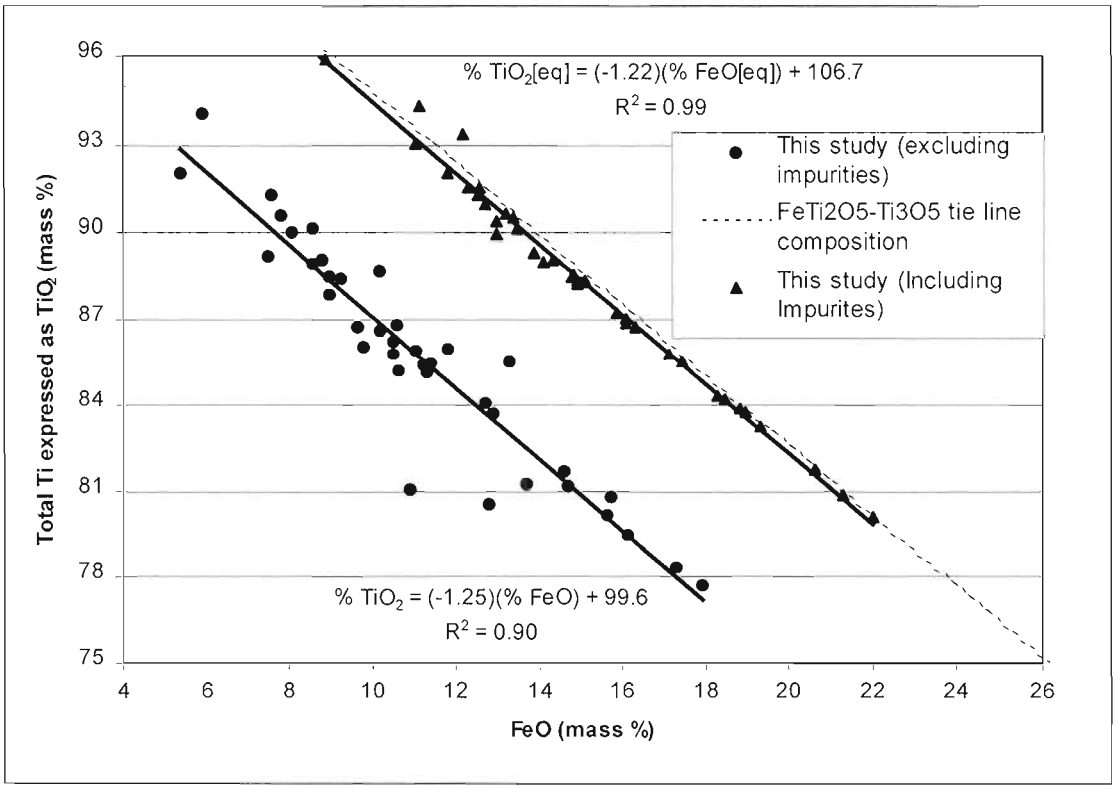

2.4.3 TAPPING TEMPERATURES FOR ILMENITE SMELTING

The tapping temperatures of the various high titania slag samples are also given in Table 21. This tapping temperature data was then plotted on the conjectural $FeTiO_3$-TiO_2-$TiO_{1.5}$ liquidus diagram proposed by Pistorius and Coetsee (2000) as a function of the slag composition. The following equations were used for the calculation of the compositions (n is defined as the number of moles of each species):

$$n(FeO)_{Total} = n(FeO) + n(MgO) + n(MnO) \ldots(XII)$$

$$n(TiO_{1.5})_{Total} = n(TiO_{1.5}) + n(AlO_{1.5}) + n(CrO_{1.5}) + n(VO_{1.5}) \ldots(XIII)$$

$$n(FeTiO_3)_{Total} = n(FeO)_{Total} \ldots(XIV)$$

$$n(TiO_2)_{Residual} = n(TiO_2) - n(FeO)_{Total} \ldots(XV)$$

The total number of moles was then normalised in order to obtain the mole fractions. These equations were used to take into account the effect of the impurities that are part of the slags. The ternary diagram, with the calculated slag compositions, is shown in Figure 24. The tapping temperatures shown in the diagram were divided into the following three temperature regimes:

- Tap temperatures above 1700 °C.
- Tap temperatures between 1700 and 1650 °C.
- Tap temperatures below 1650 °C.

The following comments can be made based on the ternary diagram:

- The bulk of high titania slag consists of the M_3O_5 phase (as illustrated by the Ti_3O_5-$FeTi_2O_5$ tie line). It should therefore be expected that the slag compositions should lie on, or close to this tie line. With an increase in reduction (reducing the FeO content of the slag and increasing the Ti^{3+} content of the slag) the composition of the slag should shift towards the Ti_3O_5 end member. If this diagram is correct it indicates that the liquidus temperature of the slag should increase with an increase in the reduction of the slag.

Figure 24: Tapping temperatures as a function of the slag composition (compositions expressed as mole fractions)

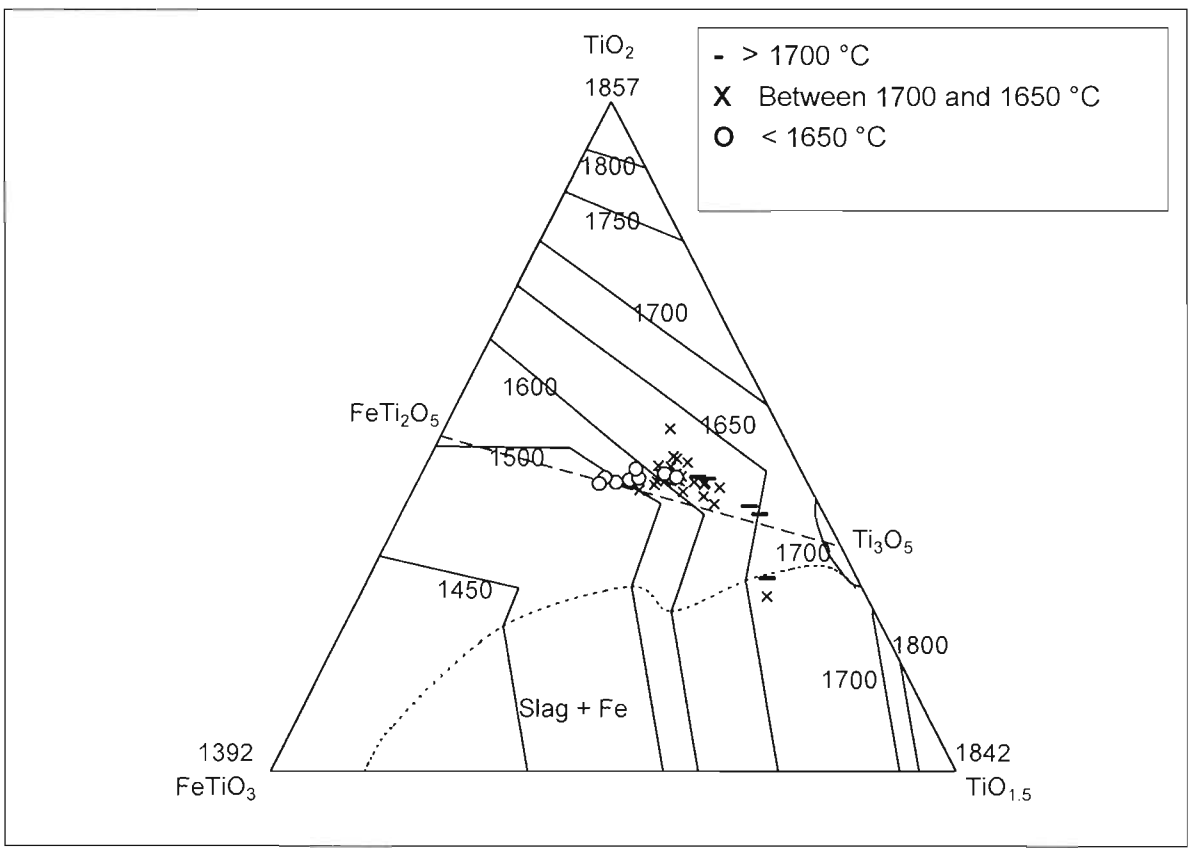

- From the data it can be seen that the tap temperatures above 1700 °C in general are closer to the Ti_3O_5 end member, while the tap temperatures below 1650 °C in general are closer to the $FeTi_2O_5$ end member.
- The data points lie on or above the Ti_3O_5-$FeTi_2O_5$ tie line. This is probably an indication that some of the Ti^{3+} in the slag oxidised on cooling. There are two data points that lie substantially below the Ti_3O_5-$FeTi_2O_5$ tie line (sample numbers 3228 and 3229 from Table 21). The following possible reasons for this can be put forward:
  - It is possible that these compositions were determined incorrectly, as their position in the phase diagram can not be otherwise explained.

- As these two samples contain high levels of Ti_2O_3 it can be postulated that a highly reduced M_2O_3 phase formed. The formation of M_2O_3 phases in high titania slags has previously been suggested by Russian investigators (see Handfield and Charette, 1971).

- In general it seems that the tapping temperatures lie substantially above the proposed liquidus temperatures. For example, all the tapping temperatures between 1650 and 1700 °C (with one exception) are below the 1650 °C temperature isotherm. Some of the tapping temperatures in this range were also plotted close to the 1500 °C isotherm. It therefore seems likely that the difference between the liquidus and tapping temperatures can be ascribed to the "super heat" present in the slags. In general the difference between the liquidus and tap temperatures seems to be between 50 and 100 °C. It should also be emphasised that the tap temperatures are taken in the ladle. In the past it has been found that the temperature in the furnace is somewhat higher (in the order of 20 °C) than the tap temperature. This has however not been quantified in this study.

In Figure 25 the tap temperature of various slags are shown as a function of the FeO content of the slags (data once again from Table 21). A fairly good correlation for this relation was obtained ($R^2 = 0.87$).

Figure 25: Tap temperature of slag as a function of the FeO content of the slag

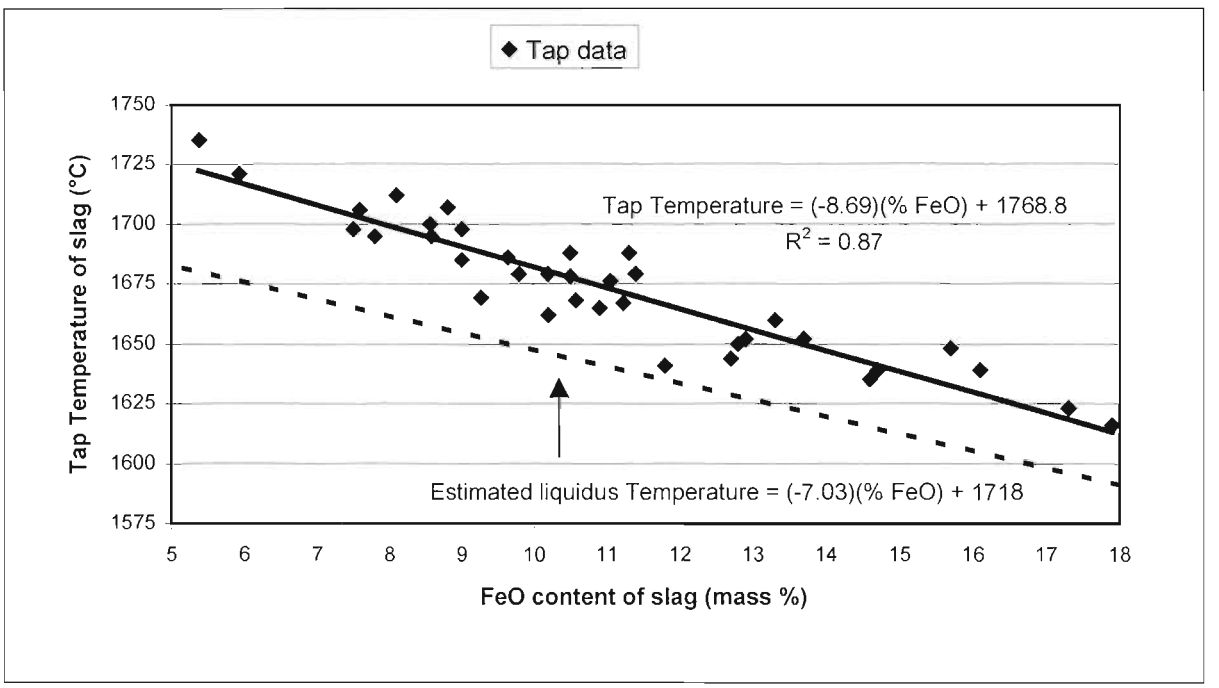

Also shown in Figure 25 is an equation (shown by the dashed line) for the estimated liquidus temperature as a function of the FeO content. Titania slag consists mainly of a M_3O_5 phase with a specific composition, with the composition being defined by the $FeTi_2O_5$ and Ti_3O_5 end members. The liquidus temperatures for these two compositions are available from the data of Eriksson and Pelton (1993) for the FeO-TiO_2 and Ti_2O_3-TiO_2 binary systems. It was assumed that a linear relationship between the liquidus temperatures of these two end members would provide a good estimate of the theoretical liquidus temperatures of the titania slags. The liquidus temperatures for these end members from the relevant phase diagrams are 1500 °C for $FeTi_2O_5$ (31.0 mass per cent FeO; 69 mass per cent TiO_2) and 1718 °C for Ti_3O_5

(64.3 mass per cent Ti_2O_3; 35.7 mass per cent TiO_2). For the calculation of the equation it was assumed that the liquidus temperature for this M_3O_5 tie line (shown schematically in Figure 24) increases linearly from $FeTi_2O_5$ to Ti_3O_5. The effect of impurities on the estimated liquidus line has not been taken into account. For example the liquidus temperature of $MgTi_2O_5$ according to Eriksson and Pelton (1993) is 1657 °C. It can therefore be expected that for slags which contain appreciable amounts of magnesium, that the liquidus temperature would be higher.

It is interesting to note in Figure 25 that the slopes of the estimated liquidus line and the tap temperature line are similar. A slight divergence of the lines takes place as the FeO content of the slags decrease. Assuming that the calculated liquidus temperature equation is correct, it seems that the tap temperature is approximately 25 to 50 °C above the liquidus temperature of the slag that is estimated in this way.

In Figure 26 the tap temperature of the slag is shown as function of the Ti_2O_3 content of the slag. This data shows more scatter than the data for Figure 25 (R^2 = 0.62). This is probably due to the quality of the analytical techniques used for the two components. FeO is analysed by using an accurate instrumental technique such as ICP or XRF, while the Ti_2O_3 content of the slags is determined by a more difficult wet chemistry technique.

Figure 26: Tap temperature of slag as a function of the Ti_2O_3 content

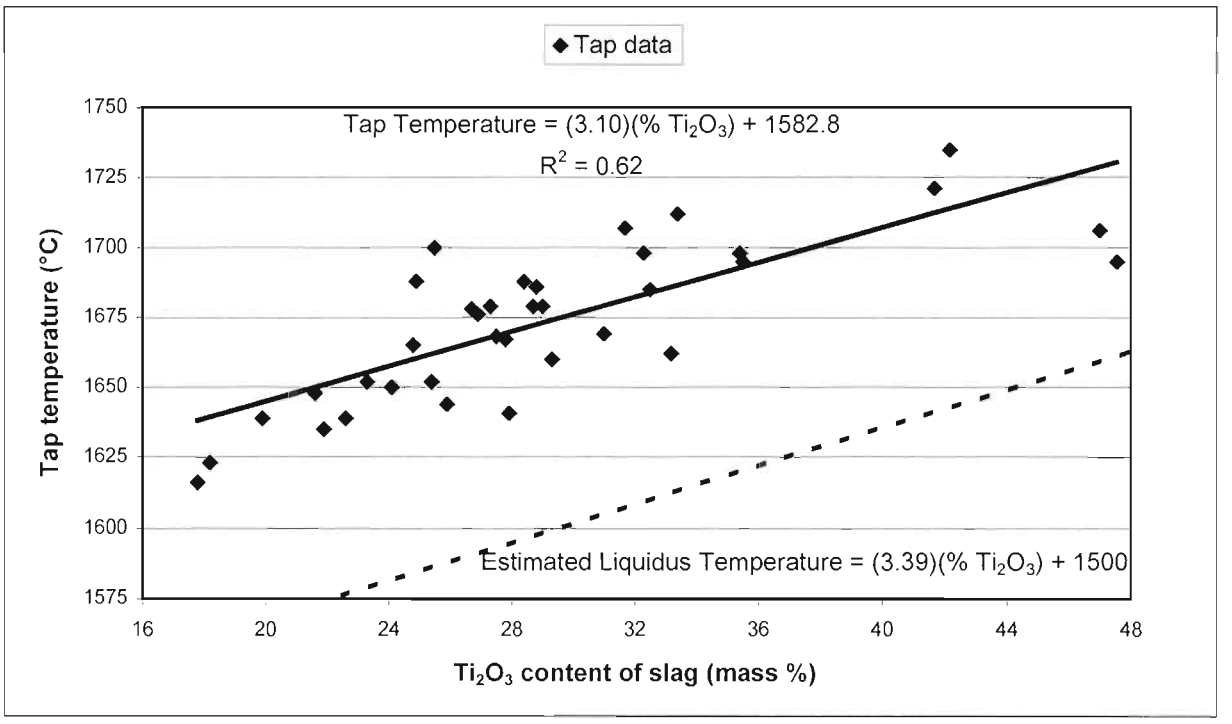

The estimated liquidus temperature is shown as a function of the Ti_2O_3 (dashed line). This was again calculated by using the liquidus temperature data for $FeTi_2O_5$ and Ti_3O_5. According to Figure 26 it seems that the tap temperature is approximately 75 °C higher than the liquidus temperature of the slag, once again assuming that the calculated liquidus temperature relationship is correct.

To investigate the relevance of using a linear liquidus temperature relationship for the $FeTi_2O_5$-Ti_3O_5 tie line, Figure 27 was constructed. For this purpose the data from Pesl and the data from Pistorius and Coetsee were compared with the linear temperature relationship. In each instance the liquidus temperature data for $FeTi_2O_5$ and Ti_3O_5 from Eriksson and Pelton was assumed to be correct. Figure 27 shows that up to a Ti_3O_5 mole fraction of approximately 0.4 (that is approximately 19 mass per cent FeO), very little change in the liquidus temperature is predicted. The figure shows that from a Ti_3O_5 mole fraction of approximately 0.6 (approximately 13 mass per cent FeO), a fairly good correlation is obtained.

Figure 27: Liquidus temperature data for the $FeTi_2O_5$-Ti_3O_5 tie line

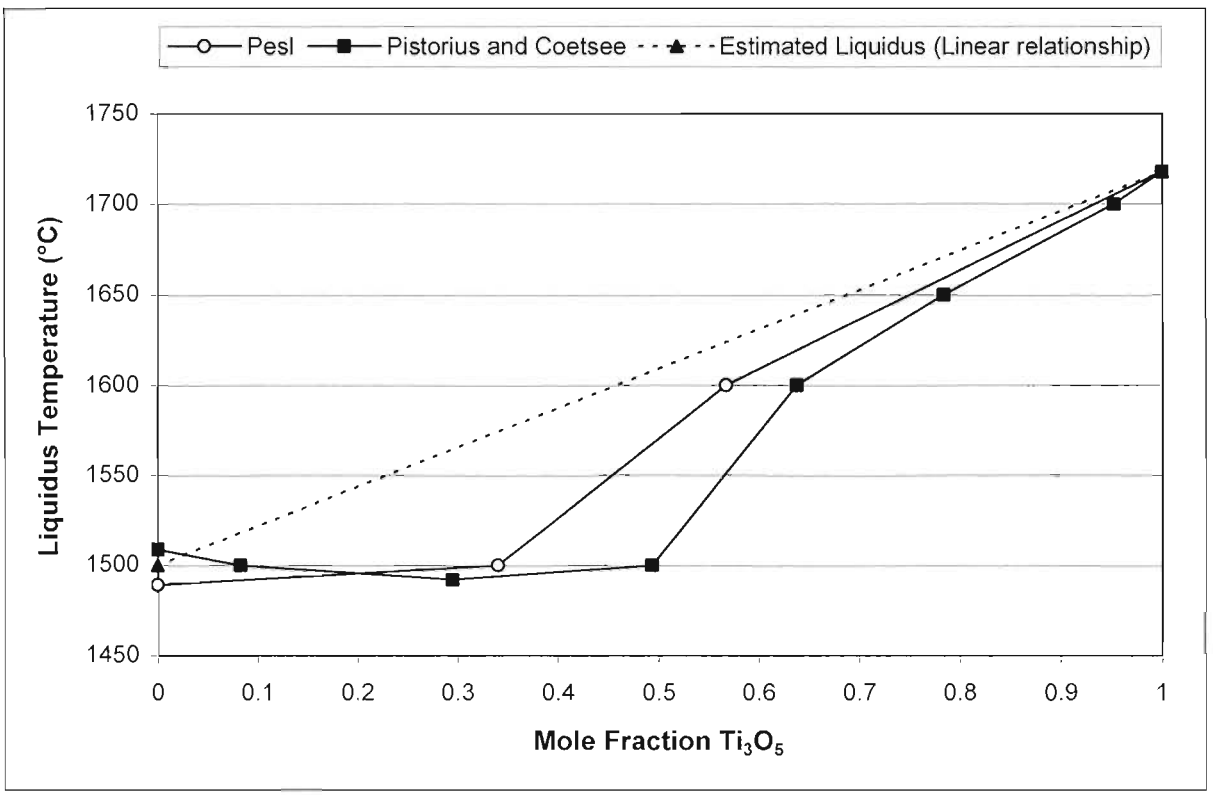

2.5 CONCLUSIONS AND RECOMMENDATIONS

High titania slags consist mainly of a M_3O_5 solid solution phase. In the Fe-Ti-O system this solid solution is continuous only at temperatures above approximately 1350 °C. The M_3O_5 phases found in the spoon samples are therefore only metastable at room temperature. The M_3O_5 phases consist of an orthorhombic, pseudobrookite structure (AB_2O_5). The unit cell contains 4 atoms on the A site, 8 atoms on the B site and 20 oxygen atoms. Mössbauer spectroscopy results shows that the majority of iron is found in the larger A site. The oxidation state of iron in these slags was also confirmed to be +2.

Neutron diffraction studies can also be employed in future to clarify the distribution of iron and titanium in the M_3O_5 structure. The electron densities of iron and titanium are sufficiently similar so that X-ray diffraction cannot always distinguish between them. The scattering cross-section of iron for neutrons is however three times that of titanium and of the opposite sign (Lindsley, 1976).

Two types of glass phases were also found in the high titania slags. These phases consist mainly of SiO_2. The difference between the two types of phases is with regard to the presence of impurities, as well as the levels of these impurities. Reeves and Reeves (1997) mention that the behaviour of silica during the subsequent chlorination process is not understood. It could therefore be worthwhile if the chlorination behaviour of these types of glass phases were studied in future.

Of interest also was the presence of fine metallic precipitates (less than approximately 3 μm) in rutile crystals. It has been suggested that these phases form due to the reaction of Ti_2O_3 and FeO in the slag to form rutile and the metallic iron (Toromanoff and Habashi, 1984). The conditions under which this reaction occurs could also be an area for further study.

Results on the FeO and Ti_2O_3 relationships in the titania slags closely follows the composition of the $FeTi_2O_5$-Ti_3O_5 tie line (as found by Pistorius and Coetsee, 2000). It is also suggested that the tapping temperatures have a "superheat" of approximately 50 °C over the proposed liquidus temperatures. An area of further study could be the determination of the liquidus temperatures along the $FeTi_2O_5$-Ti_3O_5 tie line.

3 THE DECREPITATION OF HIGH TITANIA SLAGS

3.1 BACKGROUND

High titania slag is produced during the smelting of ilmenite in a furnace with a suitable carbonaceous reductant. In this process a large fraction of the iron content of the ilmenite is reduced to metallic iron. The remainder of the material collects in a high titania slag. The iron and slag are tapped through separate tapholes, with the titania slag being the higher value product. The slag is typically tapped into moulds that would yield approximately 20 ton slag blocks. After the slag is cooled, which can last approximately seven to ten days, it is crushed and milled to produce separate fine and coarse products. These products are used in the downstream processing for the production of titanium dioxide pigment. The fine slag product (-106 μm) is used by the sulphate processing route, while the coarser product (-850+106 μm) is used by the chloride processing route (van Niekerk, 1995). The coarse slag product (chloride grade) has a higher value than the fine slag product (sulphate grade). In 1998 the price for typical chloride grade slag was $ 386 per ton, while the price for typical sulphate grade slag was $ 340 per ton (Gambogi, 1998).

During the slag cooling process, which takes place under atmospheric conditions, severe decrepitation of the slag may occur. Decrepitation of the slag is detrimental, because an excess of fine material with average particle diameter of less than 106 μm is produced. It is important to produce a minimum amount of the fine slag, (which is sulphate grade slag, the lower value product) in order to maximize the income that can be derived from titania slag. This part of the investigation was undertaken to study the decrepitation of high titania slag to gain an understanding of the factors affecting decrepitation. In this study decrepitation is defined as the disintegration or crumbling of a material into component parts or smaller fragments. This is graphically illustrated in Figure 28. This figure shows a slag block (approximately 1 ton in size) that has partially decrepitated during the cooling process. The figure shows how the right side of the block has crumbled, with the decrepitated material lying in a heap at the base of the block. Figure 29 shows a micrograph of a typical slag sample that has shown no decrepitation behaviour, while Figure 30 shows a micrograph of a decrepitated slag sample. In comparing these two samples it is obvious that significant changes to the decrepitated material had taken place as shown by the extensive cracking of the decrepitated sample. These changes, and the reasons for these changes, will be investigated in this section.

3.2 LITERATURE SURVEY

3.2.1 DECREPITATION OF SLAGS

Decrepitation of slag is a fairly well known phenomenon, especially for steelmaking slags. Decrepitation of slag occurs due to phase and chemical changes in the slag, and the resultant volume changes associated with these phase changes. Examples of the decrepitation of slags are the following:

Figure 28: Side view of a slag block (tap 68) that had decrepitated (tap ladle in background)

Figure 29: Micrograph of a typical slag sample that has shown no decrepitation

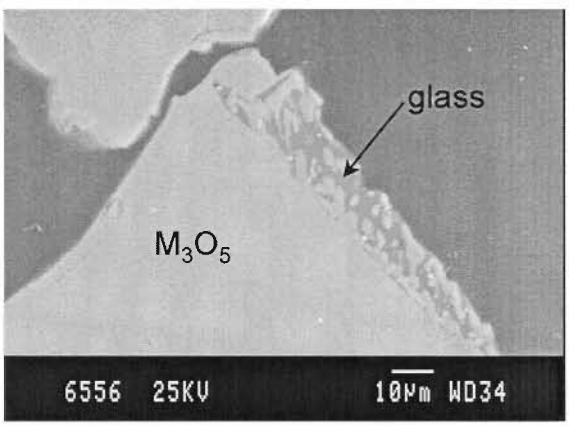

Figure 30: Micrograph of a slag sample that has undergone decrepitation (Sample DB157)

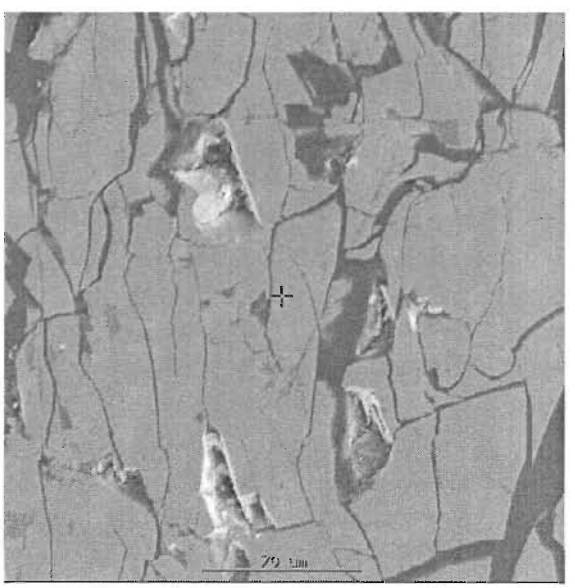

- The decrepitation of steelmaking slags due to an increase in volume of the free lime in the slag during hydration (Okamoto et. al., 1981; Noguchi et. al., 1980). This is particularly a problem in the aggregate industries. To overcome this problem the slag needs to undergo preliminary weathering in heaps prior to use. This allows some of the free lime to be converted to the hydroxide and carbonate (Juckes, 1991).
- A second well-known example is that of the disintegration on cooling of slag containing dicalcium silicate (Ca_2SiO_4). This disintegration is due to a structural transition from the β (monoclinic structure) to γ (rhombohedral structure) polymorph (Grzymek and Derdacka-Grzymek, 1990). From the data given by Grzymek and Derdacka-Grzymek (1990) it can be calculated that this transition is accompanied by an expansion in molar volume of approximately 10 per cent. According to the authors it seems that the addition of a cation with a small ionic radius can delay, or even inhibit the β to γ transition. Examples of these cations are B^{3+}, As^{3+} and Cr^{6+}. A patent has also been registered for the use of boron as a slag modifier to stabilise this type of slag (Harada and Tomari, 1991).

Very little (to the author's knowledge) has been published in the open literature on the oxidation and decrepitation behaviour of high titania slags. Vasyutinskiy and Movsesov (1965) studied the oxidation and grinding of a high titania slag containing 90.1 per cent TiO_2 and 3.47 per cent FeO. They concluded that in order to obtain the maximum reduction in strength of the slag, oxidation of the slag in the temperature region of 500 to 600 °C was required. Vasyutinskiy (1968) followed this up with a more in-depth study of the oxidation of a similar high titania slag. This slag consisted mainly of a M_3O_5 phase, with M denoting the cations present in the phase. This phase can best be represented as a $x[(Fe,Mg,Mn)O.2TiO_2].y[(Ti,Al,Cr)_2O_3.TiO_2]$ solid solution. The experimental results on the oxidation of the slag indicated the following three main stages.

- At temperatures of approximately 300 to 400 °C only slight structural changes in the M_3O_5 phase is observed. X-ray diffraction analysis indicated a distortion of the M_3O_5 crystal lattice.
- At temperatures of up to 750 °C the formation of anatase is observed.
- At higher temperatures the formation of rutile is observed.

The anatase to rutile transformation temperature can range between 400 and 1200 °C, depending on the source of the anatase and the nature of the impurities in it (Shannon and Pask, 1965). Decrepitation of these titania slags was explained by the oxidation of the M_3O_5 phase, resulting in the formation of anatase (Vasyutinskiy, 1968). As the density of anatase is less than the density of the M_3O_5 phase, this results in the rapid cracking of the slag.

Toromanoff and Habashi (1984) investigated the properties of high titania slags (produced at Sorel in Canada). Decrepitation of these slags during cooling was also observed. The slag consisted of a M_3O_5 phase, a glassy phase, rutile (TiO_2) and metallic iron globules. In this Sorel slag 13.1 mass per cent of the total Ti was present as Ti^{3+}. The decrepitation process was explained by the oxidation of the Ti^{3+} present in the slag by Fe^{2+} during the cooling process. It was postulated that this process occurs according to the following reaction:

$$Ti_2O_3 + FeO = 2TiO_2 + Fe^0 \ldots(K)$$
$$\Delta G^0_{1000\,°C} = -\,71.13\ kJ.mol^{-1}$$

Toromanoff and Habashi (1984) concluded that due to the difference in the coefficients of expansion of the metallic iron and the slag, the slag product cracks and decrepitates.

It is also known that ferrous and ferric pseudobrookite decompose at certain temperatures (Haggerty and Lindsley, 1970). It is possible that these decomposition reactions can contribute to the decrepitation of the high titania slags. The decomposition reactions are given below:

$$FeTi_2O_5 = FeTiO_3 + TiO_2 \quad [< 1150\ °C] \ldots(L)$$

$$Fe_2TiO_5 = Fe_2O_3 + TiO_2 \quad [< 585\ °C] \ldots(M)$$

Reid and Ward (1971) found that when a solid solution of Ti_3O_5 in $FeTi_2O_5$ was formed the tendency to decomposition decreased rapidly. It is also known that manganese and magnesium stabilize the M_3O_5 phase (Grey, Reid and Jones, 1974; Borowiec and Rosenqvist, 1981). This may counter the decomposition reactions or change the temperatures at which these occur.

Grey, Cranswick, et. al. (2000) studied the oxidation of synthetic anosovite ($Mg_{0.3}Ti_{2.7}O_5$) for various times at temperatures of 900 °C and lower. These workers found that after oxidation at temperatures below 300 °C, new phases were produced with the general composition of M_nO_{2n-1}, based on unit cell intergrowth of M_3O_5 and anatase structural elements. Structural homogeneity of these phases was restricted to regions of only 100 to 200 Å, due to the low driving force for ordering at these low temperatures. The composition of the dominant phase was found to be M_6O_{11}, although local regions corresponding to compositions of M_5O_9 and M_7O_{13} were also observed. With increasing temperature and oxidation time the x-ray diffraction patterns increasingly adopted the general features of the anatase pattern, although some differences were observed. After prolonged heating at 600 °C the x-ray diffraction patterns showed the start of the anatase to rutile transformation. At 900 °C the main products were rutile and M_3O_5, with traces of anatase. The powder X-ray diffraction patterns they obtained at the lower temperatures are shown in Figure 31, illustrating the differences obtained.

Teller et. al. (pp. 351-367, 1990) studied the thermal decomposition of two slag samples obtained by the high temperature reduction of ilmenite with carbon. The sample compositions were $Ti_{2.52}Fe_{0.33}Mn_{0.05}O_5$ and $Ti_{2.36}Fe_{0.33}Mg_{0.31}O_5$ respectively. Two distinct steps were observed in the decomposition of the metastable titanium-rich pseudobrookite phases. According to the authors the first step involves a phase transition that occurs above 500 °C. This transition is from a high temperature, ordered structure to a low temperature, dis-ordered pseudobrookite phase. This transition involves cation re-distribution whereby ferrous ions are transferred from the A site to the B site in the crystal structure. Before this reaction no iron was found in the B sites (See Table 5 for original distribution of cations in the two sites). At the same time titanium is transferred from the B site to the A site. In the second step the low temperature phase decomposes to metallic iron and an iron-containing, oxygen deficient titanium oxide with the rutile structure. In the light of the recent results obtained by Grey, Cranswick, et. al. (2000) with regard to the formation of a M_6O_{11} phase, and the results obtained in this study, this interpretation by Teller et. al. (pp. 351-367, 1990) needs revision.

3.2.2 PHASES AND PHASE RELATIONS APPLICABLE TO TITANIUM SLAGS AT LOW TEMPERATURES

As the decrepitation of high titania slags is expected to occur at temperatures below 1000 °C (based on practical observations and the available literature), it is relevant to study the phase assemblages that would be expected to be present at these temperatures. In this section the literature relevant to this is listed.

Figure 31: X-ray diffraction patterns for various products (from Grey, Cranswick, et. al., 2000)

(a) $Mg_{0.3}Ti_{2.7}O_5$
(b) Oxidation product from 30 minutes at 300 °C
(c) Oxidation product from 30 minutes at 400 °C
(d) Anatase

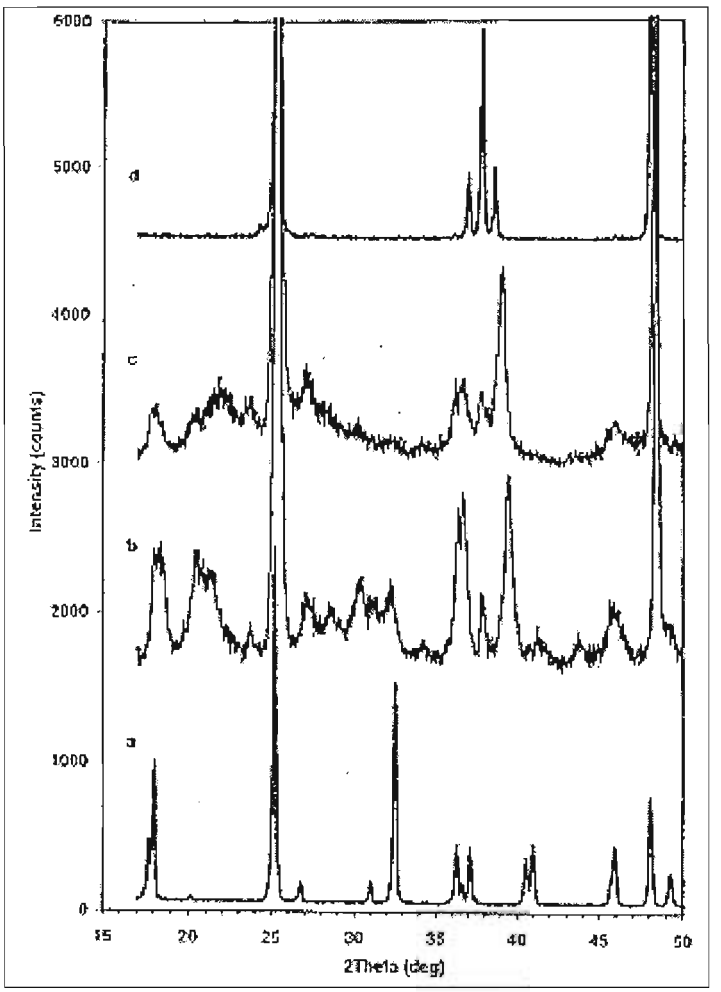

Various investigations have been carried out on oxidation reactions and phase relations in the Fe-Ti-O system at sub-solidus temperatures. These were done particularly to investigate the behaviour of ilmenite under oxidizing conditions. The following principal solid solution series are found in this system (Webster and Bright, 1961):

- The α-oxides ($Fe_mTi_{2-m}O_3$), also referred to as the M_2O_3 phases.
- The spinels ($Fe_nTi_{3-n}O_4$), also referred to as the M_3O_4 phases.
- The orthorhombic oxides ($Fe_pTi_{3-p}O_5$), also referred to as the M_3O_5 phases.
- The titanium oxide phases; rutile (TiO_2), anatase (TiO_2) and the Magnéli phases (Ti_xO_{2x-1})

Trace elements (for example magnesium, manganese, etc.) that are present in ilmenite smelting would also be included in the solid solution series, substituting for iron and titanium in the solid solutions. Information on the various iron and titanium phases present in the system is shown in Table 22.

Borowiec and Rosenqvist (1981) observed the phase relations and oxidation behaviour in the system Fe-Fe_2O_3-TiO_2 at temperatures below 1100 °C. A number of samples were made up by using pure chemical reagents in the required amounts. The samples were sealed in silica tubes under argon and reacted at various temperatures while the oxygen potentials were measured. On completion of the experiments the tubes were quenched and the phase combinations determined by X-ray diffraction analysis. Based on their results they compiled the isothermal phase diagrams shown in Figure 32 and Figure 33. The dashed lines show various values of the mole fraction of titanium ($N_{Ti} = n_{Ti}/(n_{Ti} + n_{Fe})$). This value remains constant for a specific sample whether it is oxidised or reduced. For titania slags the value for N_{Ti} is in the order of 0.90 (calculated for data shown in Table 12), showing that the TiO_2-rich corner of the Fe-Fe_2O_3-TiO_2 system is relevant to titania slags. The approximate position for $N_{Ti} = 0.9$ is also indicated in Figure 32.

For the oxidation of titania slag in the system Fe-Fe_2O_3-TiO_2 at 800 °C (Figure 32), the following phase assemblages could be expected with an increase in the extent of oxidation of a slag sample:

- Metallic iron, together with a succession of two Magnéli phases up to rutile, when all the titanium will be oxidised to Ti^{4+} (various three phase regions).
- Metallic iron, with rutile and ilmenite (three phase region).
- Rutile and α-oxide (two phase region).
- Rutile, α-oxide and pseudobrookite (three phase region).
- Rutile and pseudobrookite (two phase region). By increasing the extent of oxidation of the sample the amount of rutile relative to the amount of pseudobrookite increases. At the same time the amount of Fe^{3+} relative to Fe^{2+} also increases.
- The final phase assemblage will be rutile and Fe_2TiO_5, with all the iron oxidised to Fe^{3+}. For a slag with a value of 0.90 for N_{Ti}, the final phase composition will be 94.4 mole % (84.9 mass %) TiO_2 and 5.6 mole % (15.1 mass %) Fe_2TiO_5.

This reaction sequence does not allow for the presence of impurities, which may stabilise certain phases. From the phase diagram at 800 °C (Figure 32) it is not clear what oxygen partial pressure is required to obtain the final phase assemblage of Fe_2TiO_5 and rutile. For the three phase region (Rutile, α-oxide and pseudobrookite) the equilibrium oxygen potential in Figure 32 is shown as log P_{O2} = -11.41, which is much lower than that for air (log P_{O2} = -0.68). No data is however given for the two phase region, Fe_2TiO_5 and rutile. To obtain an indication of whether high titania slag oxidised in air would attain the Fe_2TiO_5 and rutile phase assemblage the oxygen potential for the following two reactions were calculated as a function of temperature:

$$2\ Ti_3O_5 + O_2 = 6\ TiO_2 \quad ...(N)$$

$$4\ FeTi_2O_5 + O_2 = 2\ Fe_2TiO_5 + 6\ TiO_2 \quad ...(O)$$

Table 22 : Mineralogical data on various iron and titanium phases that could potentially be present in the system under investigation

Stoichiometry	Chemical formula	Mineral name	Crystal system	Density ($g.cm^{-3}$)	Molecular mass ($g.mol^{-1}$)	Molar volume ($cm^3.mol^{-1}$)	References
M_2O_3	$FeTiO_3$	Ilmenite	Rhombohedral	4.72(m)	151.745	32.15	Hölzel (1989)
	Fe_2O_3	Hematite	Rhombohedral	5.26(m)	159.692	30.36	Hölzel (1989)
M_3O_4	Fe_2TiO_4	Ulvöspinel	Cubic	4.77(c)	223.592	46.87	Hölzel (1989)
	Fe_3O_4	Magnetite	Cubic	5.18(m)	231.539	44.70	Hölzel (1989)
M_3O_5	Fe_2TiO_5	Pseudobrookite (ferric)	Orthorhombic	4.39(m)	239.591	54.58	Hölzel (1989)
	$FeTi_2O_5$	Pseudobrookite (ferrous)	Orthorhombic	4.15(c)	231.644	55.82	Akimoto et. al. (1957), Grey and Ward (1973)
	$Fe_{0.5}Mg_{0.5}Ti_2O_5$	Armalcolite	Orthorhombic	3.92(c)	215.877	55.07	Hölzel (1989), Lind and Housley (1972)
	Ti_3O_5	Anosovite	Monoclinic	4.01(c)	223.697	55.78	Grey and Ward (1973)
M_5O_9	$Fe_2Ti_3O_9$	Pseudorutile	Hexagonal	4.01(c)	399.389	99.60	Hölzel (1989)
MO_2	TiO_2	Rutile	Tetragonal	4.23(m)	79.899	18.89	Hölzel (1989)
	TiO_2	Anatase	Tetragonal	3.90(m)	79.899	20.49	Hölzel (1989)

(c) – Calculated from crystallographic data
(m) – Measured data

Figure 32: Phase diagram for the system Fe-Fe_2O_3-TiO_2 at 800 °C. Compositions are in mol-units (From Borowiec and Rosenqvist, 1981)

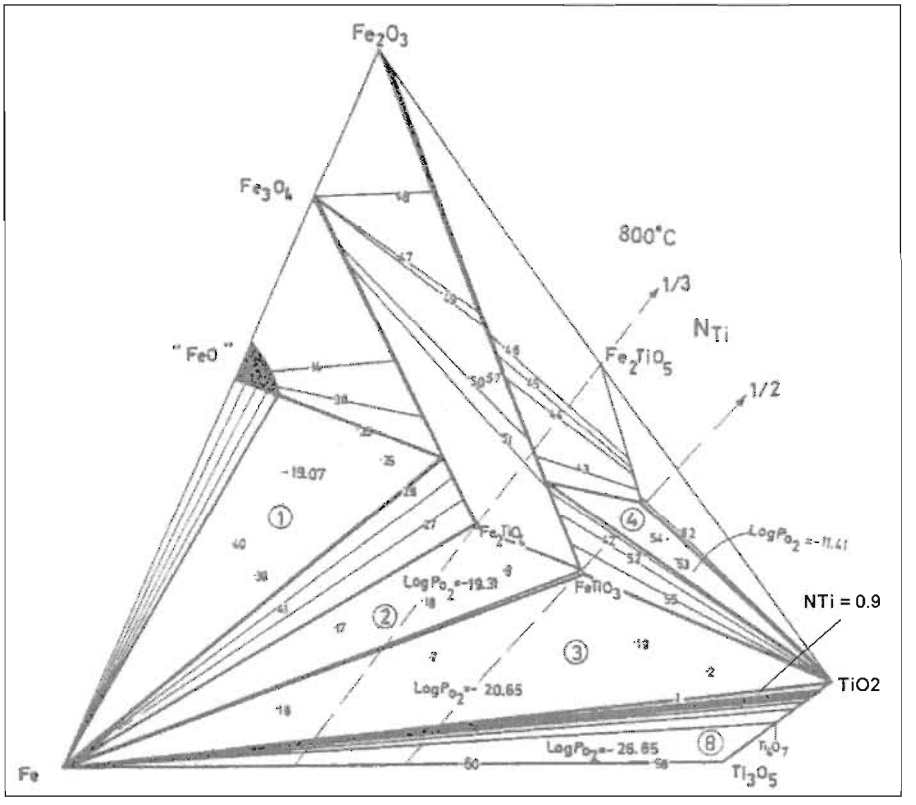

Figure 33 : Phase diagram for the system Fe-Fe_2O_3-TiO_2 at approximately 700 °C. Compositions are in mol-units (From Borowiec and Rosenqvist, 1981)

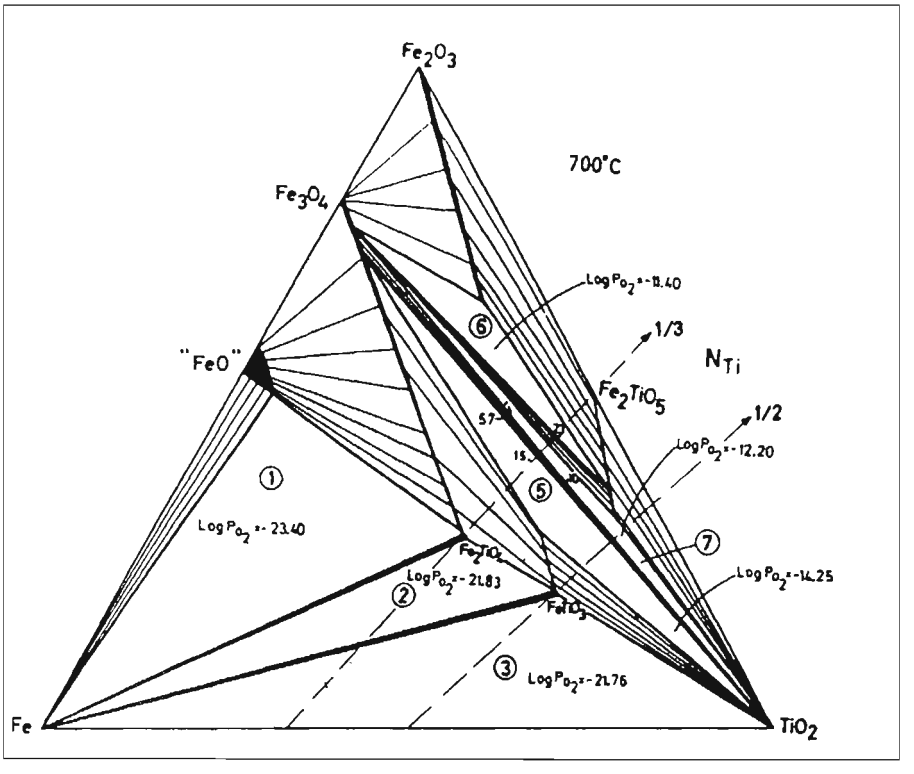

$FeTi_2O_5$ and Ti_3O_5 were used, as these two M_3O_5 phases essentially represent the two end members of the M_3O_5 solid solution obtained in high titania slags. Gibbs free energy data for each compound was obtained from the FACT thermodynamic database (2000) and used to calculate the oxygen potential for the reactions using the following equation (R = gas constant, T = Temperature):

$$P_{O2} = e^{(\Delta G/RT)} \quad ...(XVI)$$

The activities of the solid phases were taken to be equal to one. The calculated results for the two reactions are shown in Figure 34. Figure 34 shows that over the range of temperatures applicable to this study, both reactions (N) and (O) are thermodynamically favorable in air ($\log P_{O2} = -0.68$). Based on this it is reasonable to expect that Fe_2TiO_5 and rutile would be the final phase assemblages at temperatures between 600 and 1000 °C. At lower temperatures the phase assemblages would be different, due to the decomposition of Fe_2TiO_5 (Haggerty and Lindsley, 1970).

Figure 34: The oxygen potential required for the oxidation of relevant M_3O_5 phases

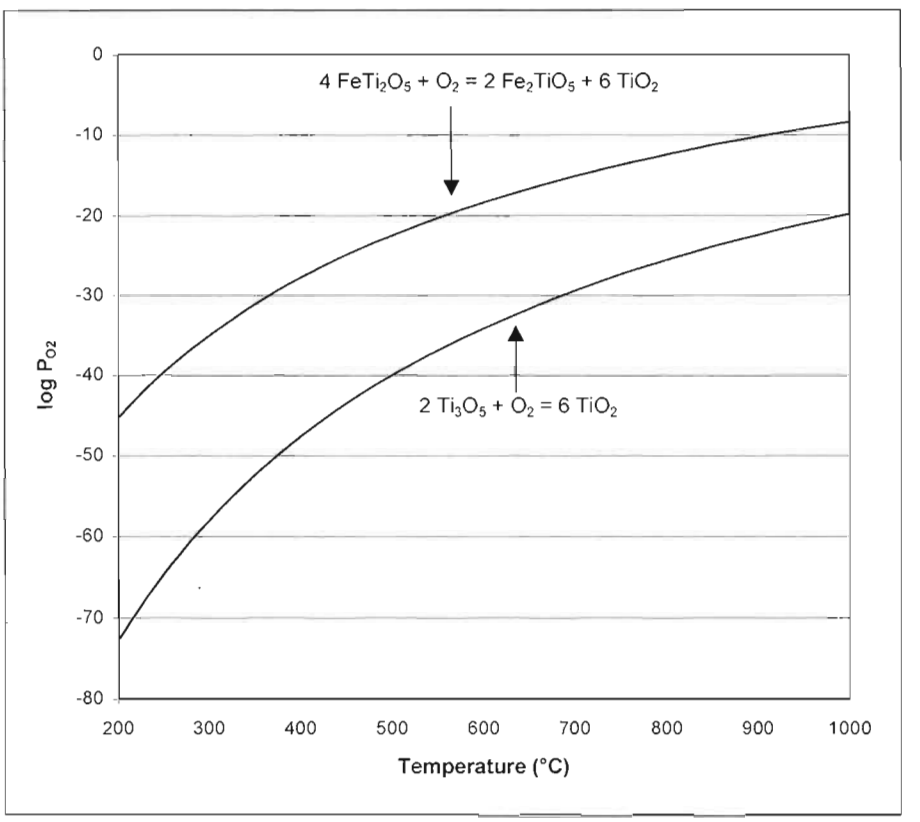

For the oxidation of titania slag at 650 °C (see suggested diagram, Figure 35) the following phase assemblages can be expected for increased oxidation of titania slag:

- Metallic iron, with a succession of two Magnéli phases up to rutile, when all the titanium will be oxidised to Ti^{4+} (various three phase regions). This is not indicated in the phase diagram, but assumed based on Figure 32.
- Metallic iron, with rutile and ilmenite (three phase region).
- Rutile and α-oxide (two phase region).

- Rutile, α-oxide (ilmenite) and spinel (three phase region).
- Rutile and spinel (two phase region).
- Rutile, α-oxide (iron-rich phase) and spinel (three phase region).
- Rutile and α-oxide (two phase region).
- Rutile, α-oxide and pseudobrookite (three phase region).
- Rutile and pseudobrookite (two phase region). Once again by increasing the extent of oxidation of the sample the amount of rutile relative to the amount of pseudobrookite increases. At the same time the amount of Fe^{3+} relative to Fe^{2+} also increases.
- The final phase assemblage will be rutile and Fe_2TiO_5, with all the iron oxidised to Fe^{3+}.

Figure 35 : Suggested phase diagram for the Fe-Fe_2O_3-TiO_2 system at approximately 650 °C. Compositions are in mol-units (from Borowiec and Rosenqvist, 1981)

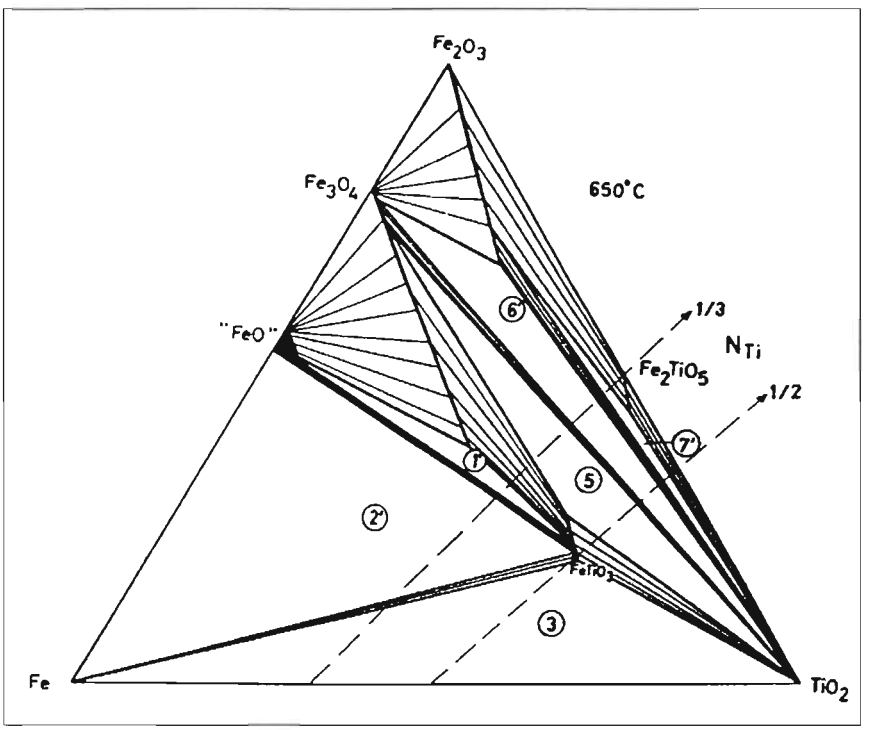

Gupta et. al. (1989) studied the phase relations in the Fe-Fe_2O_3-TiO_2 system at 700 and 900 °C, using a technique similar to that of Borowiec and Rosenqvist (1981). Their proposed isothermal phase diagram at 700 °C is shown in Figure 36. According to the results obtained by Gupta et. al. (1989) the spinel-rutile phase combination in the Fe-Fe_2O_3-TiO_2 system is not stable at 700 °C, explaining the differences between their phase diagram and that of Borowiec and Rosenqvist (1981) as shown in Figure 33. Despite these differences, the fully oxidised condition is given as TiO_2 + Fe_2TiO_5 in both cases.

The phase relations in the Ti_3O_5-Fe_2TiO_5 system as compiled by Borowiec and Rosenqvist (1985) as a function of temperature is shown in Figure 37. This diagram shows that for oxidised pseudobrookite (containing no or little Ti^{3+}), M_2O_3 and TiO_2 are the final phases at equilibrium at low temperatures (below 585 °C). Thus the final oxidation product changes from TiO_2 + Fe_2TiO_5 to TiO_2 + α-oxide at lower temperatures.

Figure 36: Proposed Fe-Fe_2O_3-TiO_2 phase diagram at 700 °C (Gupta et. al., 1989)

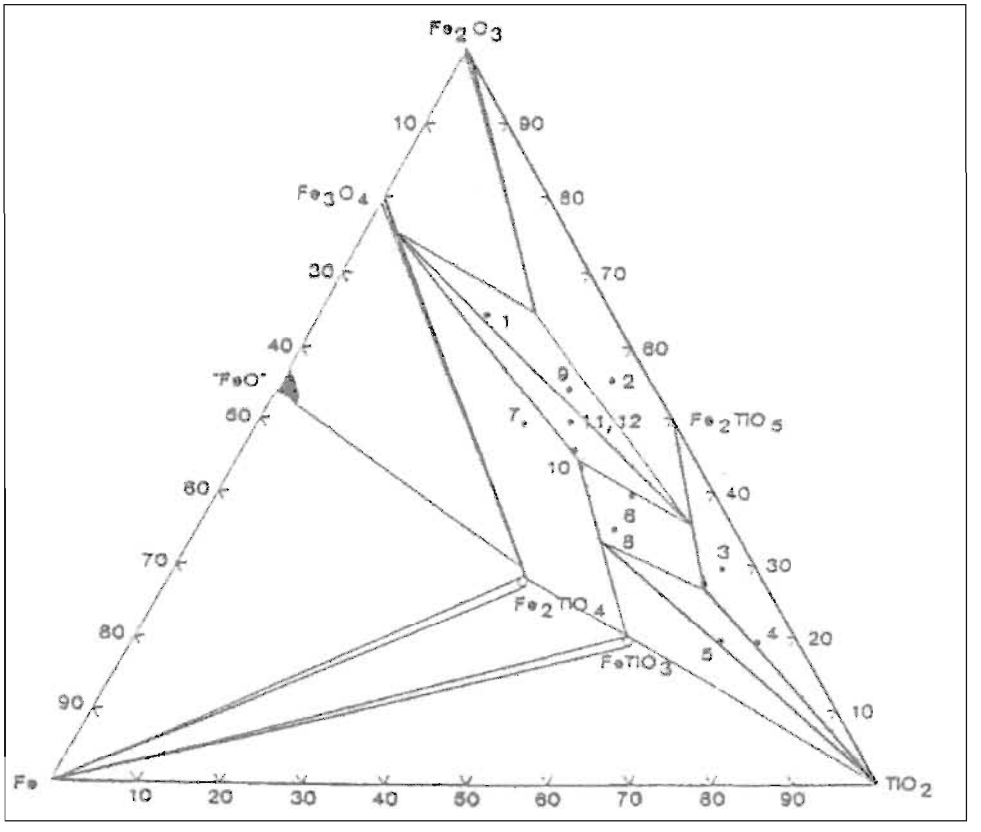

Figure 37: The Ti_3O_5-Fe_2TiO_5 system as a function of temperature (from Borowiec and Rosenqvist, 1985)

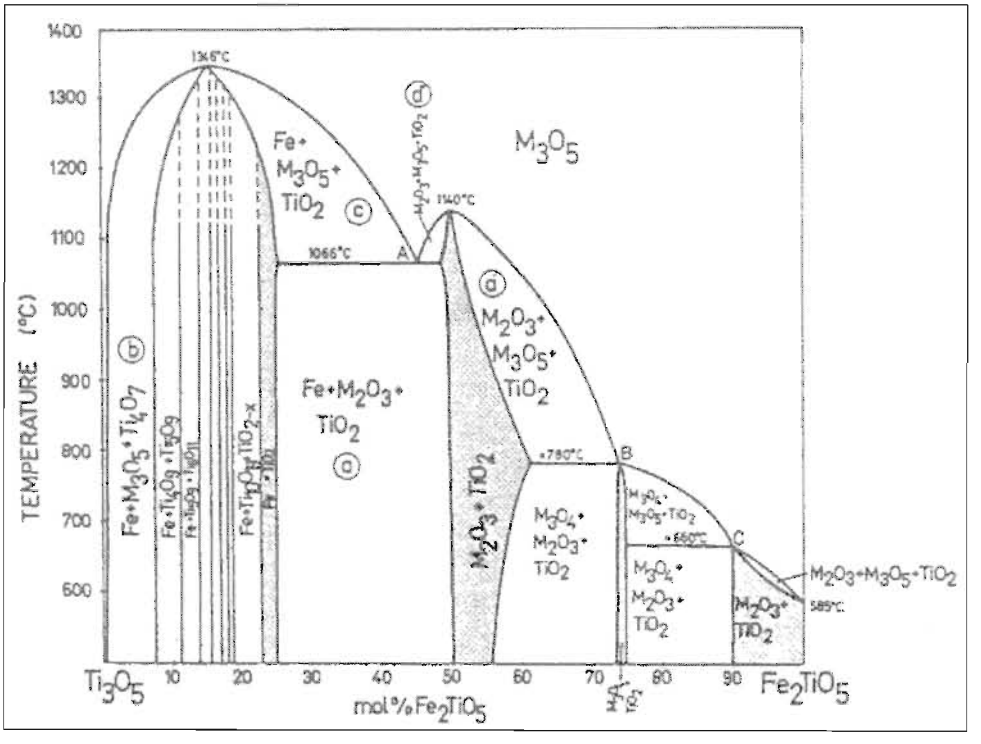

3.3 APPROACH FOR THE STUDY OF DECREPITATION OF TITANIA SLAGS

Based on the available information there are several possible ways in which high titania slags can decrepitate. The following possible reasons for the decrepitation of high titania slags were identified:

a) The formation of a new phase with a higher or lower molar volume. New phases can form by decomposition, or by oxidation. The mineralogical properties of various iron and titanium phases that could potentially exist in the system under investigation are shown in Table 22. Also included in Table 22 are the molar volumes of the various phases, indicating the magnitude of potential volume changes.
b) Polymorphic phase changes of some of the phases already present during cooling.
c) Differences in the coefficients of expansion of the metallic iron and the slag, with the metallic iron formed according to reaction (K). It is also possible that decrepitation of the slag can occur due to differences in the coefficients of expansion of other phases present in the slag.
d) Hydration of selected phases present in the slag. As no hydrated phases were previously observed in high titania slags it was however not considered to be a viable option.
e) Thermal shock of the slag on cooling was also considered as an option for decrepitation of the slag. However, as large blocks are cooled over extended periods of several days or weeks (depending on the size of the block) this was considered unlikely.

To test the various possibilities, high titania slag samples produced during various smelting campaigns in a pilot plant furnace (direct current configuration with a electrical rating of 1.5 MW) were obtained. These samples were then exposed to air under isothermal conditions in an effort to simulate the cooling process at various temperatures. Experiments were carried out between 400 and 1000 °C, as this seemed to be the temperature regime where decrepitation could be expected, both from the literature information and from observations of slag blocks produced at Iscor's pilot plant furnace. The data from these experiments were then compared with information gathered from decrepitated slags obtained during the cooling of large blocks (approximately one ton in size).

3.4 EXPERIMENTAL DETAILS

3.4.1 SLAG SAMPLES USED FOR SMALL-SCALE EXPERIMENTS

Several slag samples were used for the small-scale testwork. The chemical analyses of these samples are shown in Table 23.

3.4.2 TESTWORK ON PRESSED PELLET SAMPLES

3.4.2.1 Preliminary testwork on pressed pellets

As no prior information was available on the oxidation of titania slags to observe decrepitation behaviour, some initial experiments were carried out under a range of

experimental conditions in an attempt to observe the desired decrepitation behaviour and determine the best range of experimental conditions.

Slag DB91 was used as starting material for the preliminary tests (see Table 23 for composition). The slag was milled to a powder prior to use. For each test a pellet (15 mm in diameter) was pressed. The densities of the pellets were calculated using the dimensions of the pellets and the mass of each pellet. Alumina crucibles were used as sample holders. The pellets were placed in a Gallenkamp muffle furnace with silicon carbide elements situated in the roof. All the experiments were carried out in a stagnant air atmosphere. At the completion of each test the pellet was quenched in water. Some of the pellets completely disintegrated into a powder upon quenching, while for other experiments no change to the shape of the pellet was observed. The experimental details of the various preliminary tests are shown in Table 24. It was decided that the pellets for this program would be pressed at 817 atmospheres to obtain the maximum pellet density, using a total of 5.00 g of slag for each pellet.

3.4.2.2 Isothermal testwork on pressed pellets

Based on the results obtained on the preliminary work a detailed test program was drawn up to investigate the decrepitation behaviour of the titania slags, as well as the phase relations present in the samples. Slag DB100 (see Table 23) was used for this test program. The slag was milled to a d_{50} of 121 µm prior to use. Pellets were then pressed for this powder as described earlier. Experiments at 800 and 1000 °C were carried out in the Gallenkamp muffle furnace as described above. Experiments at lower temperatures were carried out in a Carbolite muffle furnace, also in a static air atmosphere. Alumina crucibles were used as sample holders in all instances. For each experiment the furnace was heated to the required temperature before inserting the sample in the furnace. The sample was then kept in the furnace for the required time. At the completion of the experiment the sample was removed from the furnace and quenched in water. On quenching some samples decrepitated to powder, while other samples retained their shape with some surface decrepitation. In some cases no signs of any decrepitation was observed. The samples were then dried at approximately 100 °C.

Temperatures inside the furnaces were verified by using a digital FLUKE multimeter and type K thermocouple probe. The equipment was calibrated as a system from 200 to 1000 °C by a South African National Accreditation System approved laboratory (Laboratory no. 308) using the procedure TEMP 08. The uncertainty of measurement was as follows:

- ± 2 °C for temperatures below 700 °C.
- ± 4 °C for temperatures above 700 °C.

Furnace temperatures were controlled to ± 10 °C of the setpoint temperature.

3.4.3 TESTWORK WITH MINIATURE SLAG BLOCKS

3.4.3.1 Isothermal testwork on miniature slag blocks

It was decided to compare the results obtained with the pressed pellets with those of solid pieces of slag. For this purpose a large solid piece of slag was cut with a diamond coated saw

Table 23 : Analyses of slag samples used for small-scale testwork

Slag no.	Analyses no.	Analyses (mass %)												
		SiO_2	Al_2O_3	CaO	MgO	MnO	Cr_2O_3	V_2O_5	ZrO_2	Fe^0	FeO	TiO_2	Ti_2O_3	Total Ti as TiO_2
7195	DB91	1.05	0.87	0.22	0.95	1.14	0.06	0.48	0.20	< 0.1	10.96	56.32	28.20	87.66
7030	DB100	1.41	1.19	0.27	1.03	1.17	0.05	0.45	0.16	< 0.1	9.80	53.9	30.4	87.70
7036	DB123	3.79	0.89	0.57	0.72	2.02	0.08	0.25	0.42	0.4	14.4	60.6	15.4	77.75
7051	DB136	1.50	0.96	0.25	1.22	1.11	0.05	0.46	0.16	0.13	8.40	52.04	33.92	89.74

Table 24 : Experimental details of the preliminary testwork

Test no.	Mass of pellet (g)	Pressure applied to form pellet (atmospheres)	Temperature (°C)	Time of test (hours)	Density of pellet ($g.cm^{-3}$)	Decrepitation observed
1	5.00	408	1000	46	2.83	No
2	5.00	408	500	71	2.83	Yes
3	5.00	817	750	101	2.99	No
4	4.00	817	750	101	2.96	No
5	5.00	817	350	98	-	Yes

to obtain miniature slag blocks. The blocks were cut in the approximate shape of a cube, with the length of each side ranging between 10 and 13 mm. Based on the mass, and the measured dimensions of nine of these blocks, the average apparent density was calculated to be 3.48 $g.cm^{-3}$ (standard deviation = 0.21). The analysis of the slag is shown in Table 23 (sample DB123). Unfortunately it was found after completion of these tests that the chemical analysis of the miniature slag blocks differed significantly from the slag used for the pressed pellet testwork (believed to be due to mistaken sample identification).

Testwork on the miniature slag blocks was carried out using the same methodology as previously described for the pressed pellet samples.

3.4.3.2 Unidirectional crushing tests on miniature slag blocks

The miniature slag blocks were made as described in the previous section, and were similar in their dimensions. Chemical analysis of these blocks is shown in Table 23 (slag DB136). The blocks were heated at various temperatures (400, 600 and 800 °C) and times (24 and 96 hours) in a muffle furnace. All the experiments were carried out as previously in air. At the completion of the experiments the samples were quenched in water, then dried at approximately 100 °C. All the samples treated at 400 °C decrepitated completely on quenching, with the remainder of the samples retaining their cubic shape.

Both treated and untreated miniature slag blocks were then subjected to unidirectional compression strength tests using a Monsanto Tensometer. A simplified schematic of the equipment used for the unidirectional compression strength testwork is shown in Figure 38. The blocks were fixed to the moving plate with elastic bands. The elastic passed on the side of the blocks, so that the initial contact of the block surface was directly with the fixed plate. With each experiment the plate with the block was moved towards the fixed plate by means of an electric motor at a rate of approximately 6 $mm.s^{-1}$ prior to the sample coming in contact with the fixed plate. After the sample made contact with the fixed plate this rate decreased markedly due to elastic deformation of the testing apparatus. This is discussed in more detail in section 3.5.2.2. The moving plate was stopped approximately 2 mm from the fixed plate using a limit switch. Data on the position of the moving plate and the applied force was collected as a function of time. The data output for the position of the miniature slag block and force applied to the block was recorded as volts, while the time output was in seconds. It was therefore necessary to calibrate the equipment for each series of tests to obtain conversion constants to convert the position and applied force readings to millimeter and kilo-newton respectively. Two series of tests were carried out, consisting of eight tests in each series.

3.4.4 TESTWORK ON THE EFFECT OF DIFFERENT ATMOSPHERES ON DECREPITATION

In order to test the effect of an inert atmosphere on decrepitation several tests were carried out. For this purpose powder samples from sample DB100 (see Table 23 for composition) were used. The experiments were carried out in a vertical silica tube reactor at 370 and 400 °C. The reactor was heated to the required temperature in either argon or air. After the temperature was attained the sample (~ 10 g) was introduced. The samples were heated for periods between 24 and 72 hours. Several experiments were carried out in argon before a leak

in the system was discovered through partial oxidation of these samples. It was still possible to extract some useful information from these tests (discussed later). After repairing the leak another test in argon was completed successfully.

Figure 38: Simplified schematic of the equipment used for the unidirectional crushing tests

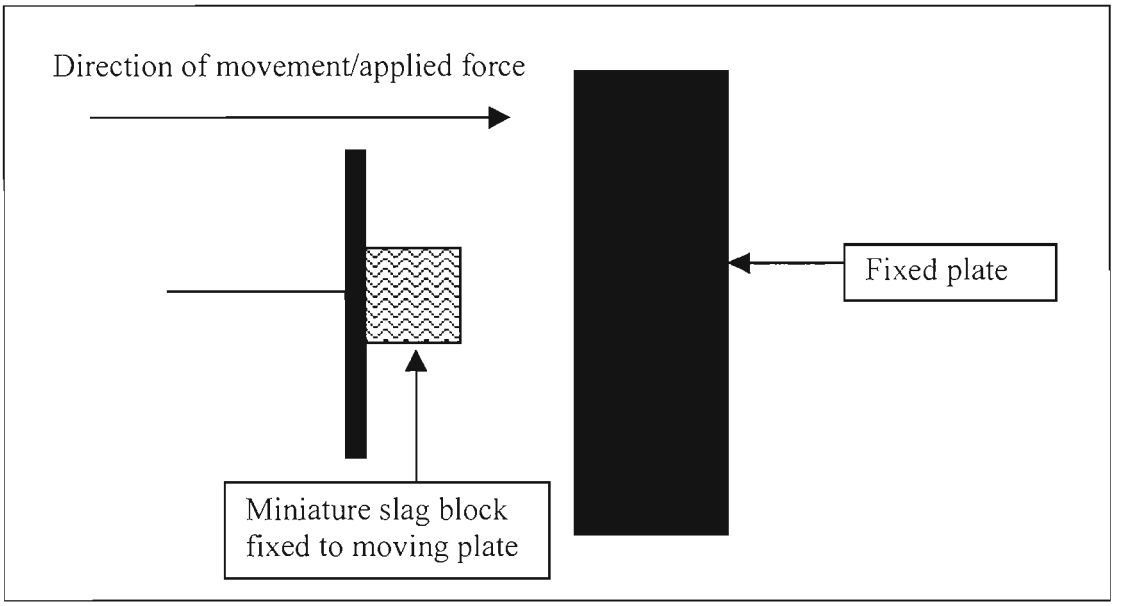

3.4.5 TESTWORK CARRIED OUT DURING THE PILOT PLANT ILMENITE SMELTING CAMPAIGN

3.4.5.1 Determination of the cooling rate of the slag blocks

Ilmenite was smelted in the Iscor pilot plant furnace (direct current configuration; rated at 1.5 MW) to produce titania slag. The slag was tapped at regular intervals, with the approximate tap sizes being one ton. The cooling rates of two of these slag blocks (tap numbers 73 and 79) were measured. This was done by inserting a thermocouple assemblage inside the slag block directly after tapping, and measuring the temperature inside the slag block until a temperature of less than 200 °C was attained. After tapping the slag into the ladle, a channel iron frame (in the shape of a +) was placed across the ladle in which the slag was tapped. This frame had a hole in the center through which the thermocouple assemblage was inserted. For tap 73 the thermocouple assemblage was inserted into the slag approximately four minutes after the taphole was closed, while for tap 79 the thermocouple assemblage was inserted approximately one minute after the taphole was closed. Temperature readings were taken at regular intervals by using a multimeter device. The slag blocks remained in the ladles until the measurements were completed.

The thermocouple assemblage was made up of three different sheaths, placed inside each other. The smallest sheath housed a type S thermocouple. The dimensions of the sheaths were as follows:

- External SiC sheath

  - 600 mm length
  - 44 mm outer diameter (OD)
  - 25 mm inner diameter (ID)
- Outer Alumina sheath
  - Approximately 610 mm in length
  - 17 mm OD
  - 12 mm ID
- Inner Alumina sheath
  - Approximately 620 mm in length
  - 10 mm OD
  - 6 mm ID

The thermocouple assemblage was made in this way, as there was some concern about a single sheath protecting the thermocouple for the duration of the measurements. This concern was however unfounded, as the SiC sheath was found to be intact in both instances after completion of the measurements.

3.4.5.2 Decrepitated slag samples

Decrepitated slag samples were collected from two slag blocks. As the slag blocks decrepitated, small heaps of decrepitated material formed adjacent to the blocks. Grab samples were taken from these heaps over a period of time.

3.4.6 ANALYTICAL TECHNIQUES

The analytical techniques used in the study of the decrepitation of the titania slags were the same that was used as described previously. Elemental phase analyses of various samples are again given in Appendix B.

X-ray diffraction analyses of the oxidised products produced in this section proved to be challenging, as several of the products produced contained overlapping peaks making phase identification difficult. This is particularly so at a d value of approximately 3.50 Å. The approximate d-values shown in Table 25 were used for the identification of the various phases. The d-values (and therefore also the 2θ-values) were slightly shifted for some samples in the accumulation of the patterns. The following explanations are possible in explaining these shifts:

- Displacement of the sample (samples were placed on glass plates) from the focussing circle of the diffractometer (Schreiner and Jenkins, 1982).
- The zero position of the instrument. This can however be excluded as the instrument was calibrated.
- Small changes in the structure of the solid solution phases due to the experimental treatments.

The relationship between the d-values and the 2θ values is given by the well-known Bragg equation:

$$n\lambda = 2d\sin\theta \quad \ldots(XVII)$$

In this study the wavelength (λ) used was that of Cu, at 1.54056 Å. The X-ray diffraction patterns for the relevant samples in this section are given in various Appendices.

Table 25: Peak positions used for phase identification

Phase	d-values (Å)	2θ values
M_3O_5	3.48, 2.75	25.6, 32.5
Ilmenite	3.73, 2.53, 1.72	23.8, 35.5, 53.2
Rutile	3.25	27.4
Anatase	3.52, 2.38, 1.89, 1.70, 1.67	25.3, 37.8, 48.1, 54.0, 55.1
Hematite	2.69	33.3
M_6O_{11}	4.20, 3.50, 2.46, 1.87	21.1, 25.5, 36.5, 48.6

3.5 RESULTS AND DISCUSSION

It is important to make a comment with regard to the Mössbauer results for the samples treated at temperatures of 600 °C and lower. For these samples the Mössbauer data was interpreted as still containing iron in the pseudobrookite (M_3O_5) phase. As will be discussed later, it was however found that changes in the M_3O_5 structure occurred. It is however likely that iron in the changed structure still occupies octahedral sites. This will however need to be confirmed. In the various tables containing the Mössbauer results, the attribution of iron is therefore still indicated as being pseudobrookite. It should however be remembered that this is not a "true pseudobrookite", but a transformed M_3O_5 product. One of the consequences of this might be that the oxidation states inferred from the Mössbauer data are incorrect, or that the errors in the data might be larger.

This is one of the reasons why the oxidation states for specific phases in samples treated at 600 °C and lower were not calculated, as some anomalous results were obtained. The second reason for not calculating the oxidation states for these samples are due to the uncertainty of the oxygen analysis as discussed earlier (see section 2.3.2.1).

3.5.1 RESULTS OBTAINED FROM THE PRESSED PELLET SAMPLES

Sample DB100 was used as starting material for the testwork on the pellet samples. The chemical composition of this sample is shown in Table 23. X-ray diffraction patterns for these samples are given in Appendix G.

3.5.1.1 Results of testwork at 1000 °C

Experiments were carried out at 1000 °C for periods of 24 and 384 hours (samples DB104 and DB106 respectively). All the samples treated at 1000 °C contained slag particles that were porous. This can be seen quite clearly in Figure 39, for the sample heated for 24 hours.

The slag particles in all the samples consisted of a mixture of rutile (dark colour) and M_3O_5 (light colour) phases. This phase assemblage is predicted by the phase diagram obtained by Borowiec and Rosenqvist (1981) at 950 °C. These phases were identified by X-ray diffraction

analyses, with rutile being the major phase present. Mössbauer analyses of the sample treated for 24 hours (sample DB104; see Table 26) indicate the presence of metallic iron and a pseudobrookite (M_3O_5) phase. These products probably formed by disproportionation (reaction (K)) as suggested by Toromanoff and Habashi (1984).

Figure 39: Photograph of a pellet sample treated at 1000 °C for 24 hours (Sample no. DB104)

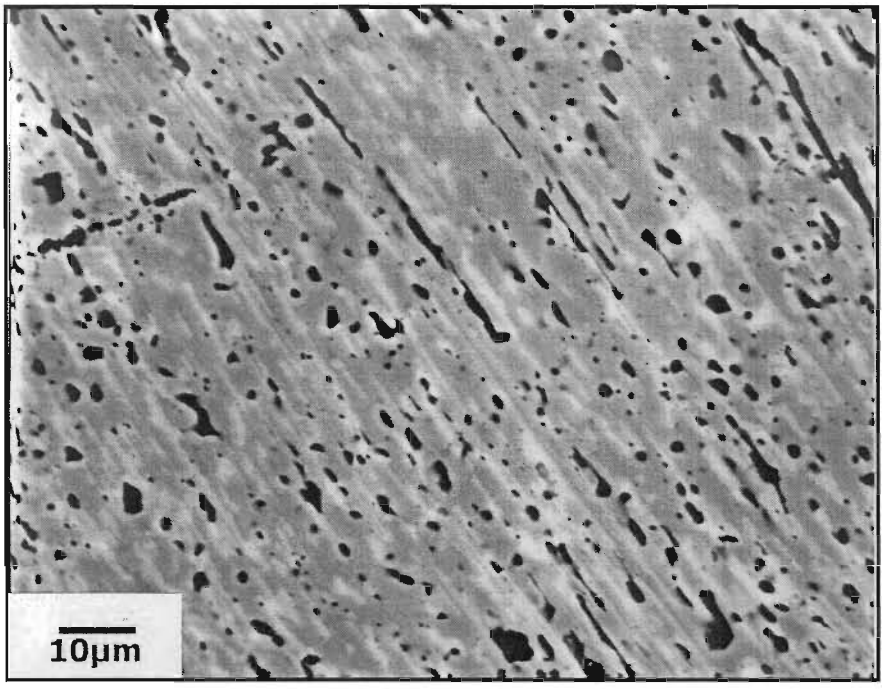

The pseudobrookite phase only contained Fe^{3+}, indicating that this phase was fully oxidised. This was found for both the samples treated at 1000 °C (24 and 384 hours). It seems from the Mössbauer results that the sample treated for 384 hours (DB106) might contain an additional hematite-like phase. This is however not certain, due to the high relative error obtained (the error is equal to the iron abundance). It can be speculated that if the hematite-like phase is present, it could possibly be due to some of the metallic iron being oxidised to hematite.

No decrepitation of these two samples was observed.

3.5.1.2 Results of the testwork at 800 °C

A photograph of the sample treated for 24 hours (DB109) is shown in Figure 40. The slag particles are shown to be finely porous, with the majority of the particles displaying well-defined, iron-enriched outer rims. Rutile and the M_3O_5 solid solution series phase were identified by X-ray diffraction analysis, with these phases intimately mixed together. This is in line with the phase diagram (see Figure 32). It is probable that some anatase is also present, although this could not be confirmed with absolute certainty using X-ray diffraction. From the Mössbauer spectroscopy results shown in Table 26 a hematite-like phase (written as M_2O_3) and metallic iron phase were also identified. The concentrations of these phases were however too low to be identified by X-ray diffraction analysis.

Table 26: Summary of results obtained from Mössbauer spectroscopy for the pressed pellet samples heated at 800 and 1000 °C

Sample no.	Temperature (°C)	Time (hours)	Hyperfine interaction parameters			Abundance (atom %)	Attribution
			Isomeric shift - δ ($mm.s^{-1}$)	Quadropole splitting - Δ ($mm.s^{-1}$)	B_{hf} (T)		
DB100	Starting slag		1.16 (2)	3.35 (4)	-	90 (2)	Fe^{2+} compound (ferropseudobrookite)
			1.09 (2)	1.83 (4)	-	10 (2)	
DB104	1000	24	0.39 (5)	0.75 (4)	-	73 (2)	Fe^{3+} compound (pseudobrookite)
			0.00 (2)	0.014 (4)	33	27 (2)	Metallic iron
DB106	1000	384	0.38 (2)	0.76 (2)	-	84 (2)	Fe^{3+} compound (pseudobrookite)
			0.00	-0.078	32.9	14 (2)	Metallic iron
			0.51 (3)	-0.91 (3)	49.6 (1)	2 (2)	Hematite-like compound (Fe^{3+})
DB109	800	24	0.38 (2)	0.74 (5)	-	69 (2)	Fe^{3+} compound (pseudobrookite)
			0.02 (2)	-0.01 (3)	33.0 (1)	20 (2)	Metallic Fe
			0.36 (2)	-0.12 (5)	50.3 (2)	11 (2)	Hematite-like compound (Fe^{3+})
DB105	800	384	0.38 (2)	0.75 (5)	-	80 (2)	Fe^{3+} compound (pseudobrookite)
			0.116(2)	-0.08 (3)	32.9 (1)	13 (2)	Metallic iron
			0.46 (2)	-0.18 (5)	50.4 (2)	11 (2)	Hematite-like compound (Fe^{3+})

Errors are quoted as percentage (in parenthesis)
B_{hf} – internal magnetic field

The iron present in the M_2O_3 phase was identified as being trivalent by the Mössbauer spectroscopy results. Once again only the presence of Fe^{3+} and Fe^0 are indicated. The presence of metallic iron is once again believed to be due to reaction (K) as mentioned previously.

Figure 40: Photograph of a pellet sample treated at 800 °C for 24 hours (sample DB109)

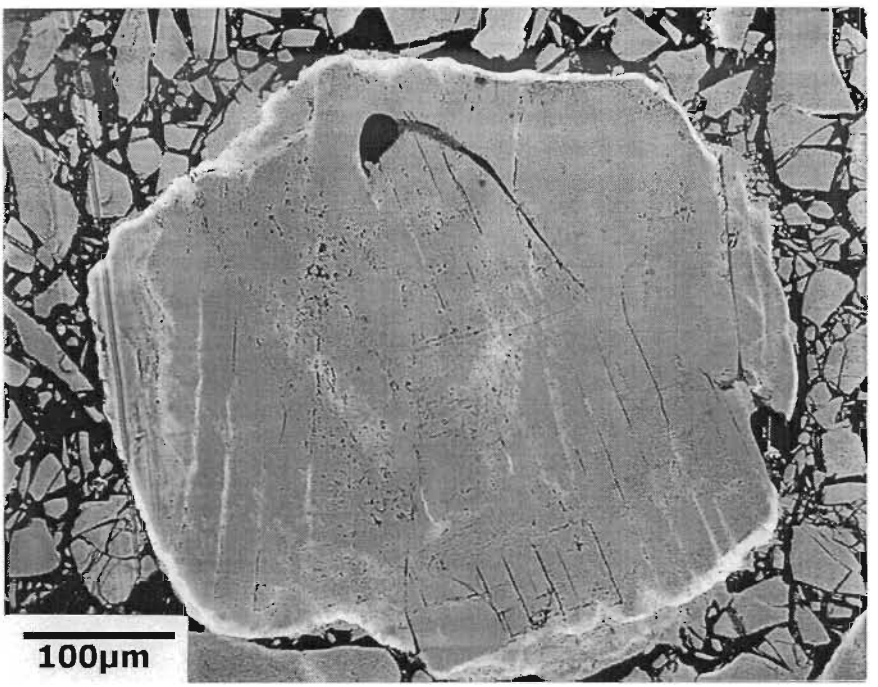

For a sample treated at 384 hours (DB105) both rutile and the M_3O_5 phase were identified by X-ray diffraction. It is however noticeable that the X-ray diffraction pattern (Appendix G) had become indicative of a more amorphous structure compared to sample DB109, indicating increasing disorder in the crystal structure of the phases. Metallic iron and M_2O_3 phases were also identified using Mössbauer spectroscopy (see Table 26). A photograph of this sample is shown in Figure 41. The slag particles in this sample appear to be more porous compared to the sample treated for 24 hours. This sample also displays a well-defined iron enriched outer rim. A phase analysis of the rim showed a M/O molar ratio of 0.66, as expected for the α-oxide (M_2O_3). The chemical composition of the rim phase was calculated to be as follows:

$$Fe^{2+}_{0.38}\,Fe^{3+}_{1.14}\,Al^{3+}_{0.02}\,Mn^{2+}_{0.02}\,Mg^{2+}_{0.02}\,Ti^{4+}_{0.42}\,O^{2-}_{3}$$

The oxidation state of iron was calculated by assuming a charge balance, as well as assuming the oxidation states of the other cations as indicated. It was assumed that only Fe^{2+} and Fe^{3+} are present, with the composition of the phase showing that it is essentially a M_2O_3 solid solution. However, according to the Mössbauer results the hematite-like phase only contained Fe^{3+}. If this is correct, it implies that there must be some Ti^{3+} present in order to maintain the charge balance. This scenario is considered most unlikely. From the composition and charge balance it does seem more likely that some Fe^{2+} is present. The end members of the solid solution are Fe_2O_3 (iron as Fe^{3+}) and $FeTiO_3$ (iron as Fe^{2+}). At 800 °C this solid solution is still continuous (see Figure 32). The composition of the rim phase is closer to the hematite

end member. This is illustrated by taking the solid solution end members into account, and re-writing the composition of the rim phase as follows:

$$0.42\left[\left(Fe_{0.90}^{2+}Mn_{0.05}^{2+}Mg_{0.05}^{2+}Ti_{1.00}^{4+}\right)O_{3}^{2-}\right]\bullet 0.01\left[Al_{2}^{3+}O_{3}^{2-}\right]\bullet 0.57\left[Fe_{2}^{3+}O_{3}^{2-}\right]$$

Figure 41: Photograph of a pellet sample treated at 800 °C for 384 hours (sample DB105)

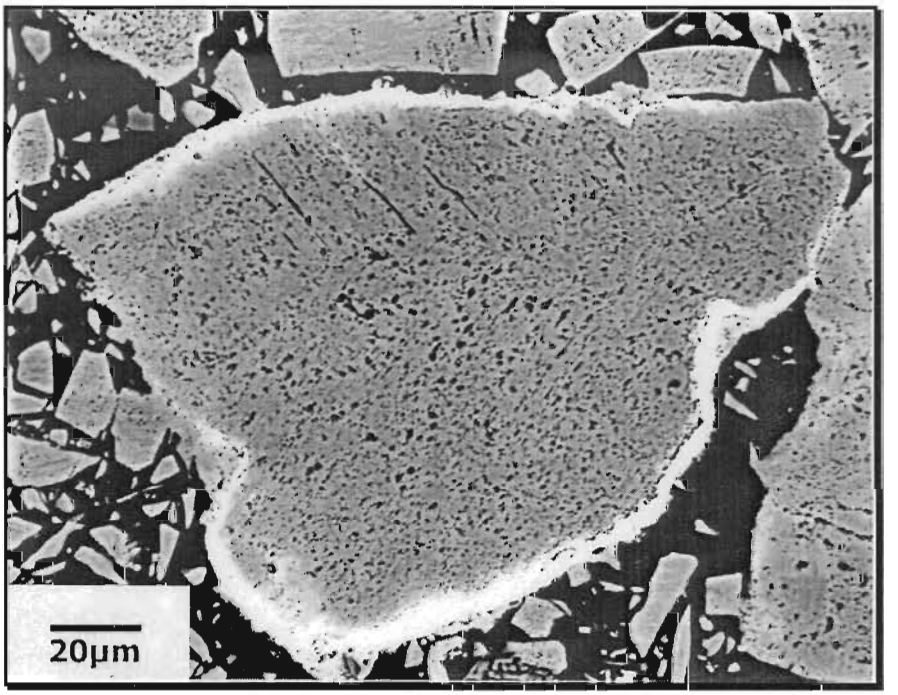

According to the phase diagram in Figure 32, the final phase assemblage at equilibrium at 800 °C should be TiO_2 (rutile) and Fe_2TiO_5 (pseudobrookite). This indicates that the rim is not in equilibrium with the core.

Of interest is the high level of porosity that is observed in the samples treated at the higher temperatures. This is illustrated for example in Figure 39 and Figure 41. Two possible reasons for this phenomenon are presented:

- A reduction in volume due to phase changes. Consider for example reaction (P) that could be expected to occur:

$$4FeTi_2O_5 + O_2 = 2Fe_2TiO_5 + 6TiO_2 \ldots(P)$$

  Using the data from Table 22 the starting volume for the reaction can be calculated to be 223.3 cm^3 (for 4 moles of $FeTi_2O_5$), while the finishing volume is calculated to be either 222.5 cm^3 (based on rutile) or 232.1 cm^3 (based on anatase). This result indicates only a marginal decrease (0.4 per cent) in the expected volume in the case of rutile, while in the instance of anatase being produced an increase (3.9 per cent) in the volume is calculated. Based on the X-ray diffraction results, rutile is the dominant phase in these samples. To create porosity in a sample a decrease in the volume is required. Therefore reaction (P) does not give an explanation for the observed porosity. A similar calculation was carried

out for the oxidation of Ti_3O_5 to TiO_2. This also resulted in an increase in the volume. Any inaccuracies of the data contained in Table 22 might however change the scenario. The effect of temperature (i.e. the thermal expansion coefficients) on the data in Table 22 might also change the results.

- Porosity could also develop due to the migration of cations (specifically iron) to the surface of the particles, thereby causing the development of pores in the interior of the particles. Such migrations were observed in some cases, with iron-rich rims observed in some samples (see for example Figure 41). This explanation seems more likely than the first one. This is however not a likely cause in the case of oxidation at 1000 °C where no iron-rich rim had formed.
- Another possibility is the contribution of short-range migration to porosity. The initial phase is a single, homogeneous phase (M_3O_5). Through a process of nucleation and growth, rutile and a second M_3O_5 phase is formed. The grain growth requires a diffusion process that can lead to porosity. This explanation will also account for porosity found at 1000 °C where no iron-rich rims had formed.

3.5.1.3 Results of the testwork at 600 °C

A photograph of the sample treated for 24 hours (DB115) is shown in Figure 42. The large slag particles in this sample display a zoned texture, with iron enriched outer margins, titanium-rich mantle zones and large cores with a dense and smooth appearance. An example of a large particle (approximately 400 µm by 550 µm in size) is shown in Figure 42. As mentioned previously, the d_{50} of the milled slag used for making the pellets is 121 µm. This indicates that these large particles are not representative of the sample used. Figure 43 shows the iron and titanium analyses (by WDS) from the centre of such a large particle to the rim of the particle. This figure illustrates the change in composition of iron and titanium over the three phases. Both rutile and anatase were clearly identified by X-ray diffraction analyses. Iron enrichment also occurs at the edges of the cracks. Fine metallic iron precipitates were also found to be present. The smaller particles (majority of the sample) were completely transformed to the titanium-rich phase, with iron-rich rims. Mössbauer data for this sample (Table 27) also shows the presence of a hematite-like phase. This was also confirmed by the X-ray diffraction analysis. It is interesting to note that the M_3O_5 peak at a 2θ-value of 32.5 degrees had almost completely disappeared, while the peak at a 2θ-value 25.5 degrees still showed the highest intensity. The ratio for these two peaks ($I_{2\theta=32.5}/I_{2\theta=25.5}$) for the starting material (DB100, see Appendix G) is 0.52, while for sample DB115 the ratio is 0.06. This difference can be explained by the near disappearance of the original M_3O_5 phase and the formation of anatase (main peak at a 2θ-value of 25.5 degrees).

The compositions of the various zones are given below. The typical composition of the core region was as follows, with a total of 3.07 cations obtained for every 5 oxygen atoms:

$$Fe_{0.21}Al_{0.05}V_{0.01}Mn_{0.01}Mg_{0.10}Ti_{2.69}O_5$$

A typical composition of the mantle zone is as follows (oxygen content normalised to 2):

$$Fe_{0.01}Al_{0.01}V_{0.01}Mg_{0.03}Ti_{1.01}O_2$$

There are a total of 1.07 cations for every 2 oxygen atoms.

Figure 42: Photograph of a pellet sample treated at 600 °C for 24 hours (sample DB115)

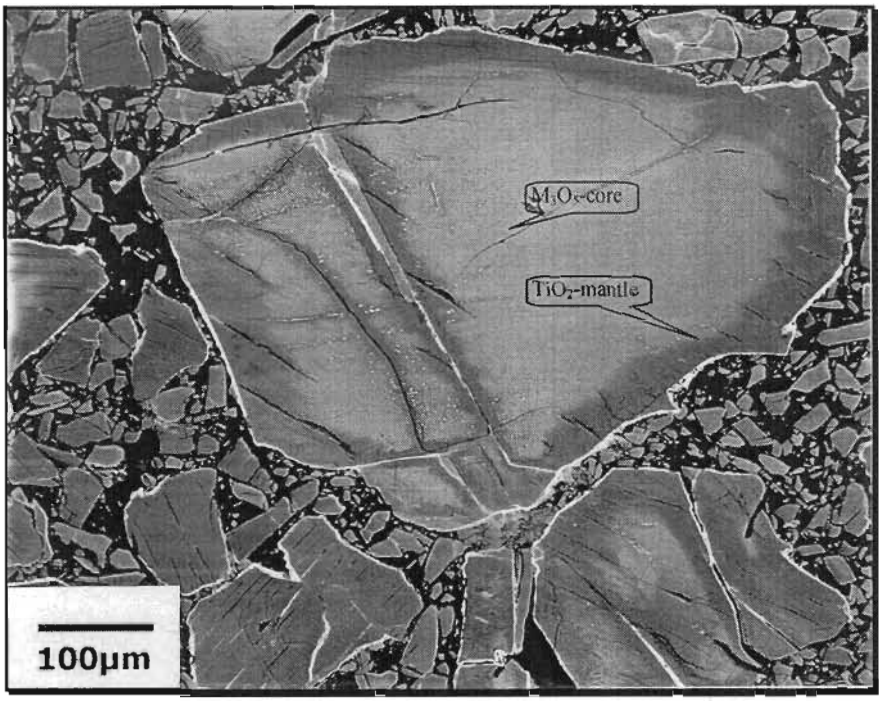

Figure 43: Iron and titanium analyses from the centre to the rim of a typical particle treated at 600 °C for 24 hours (sample DB115)

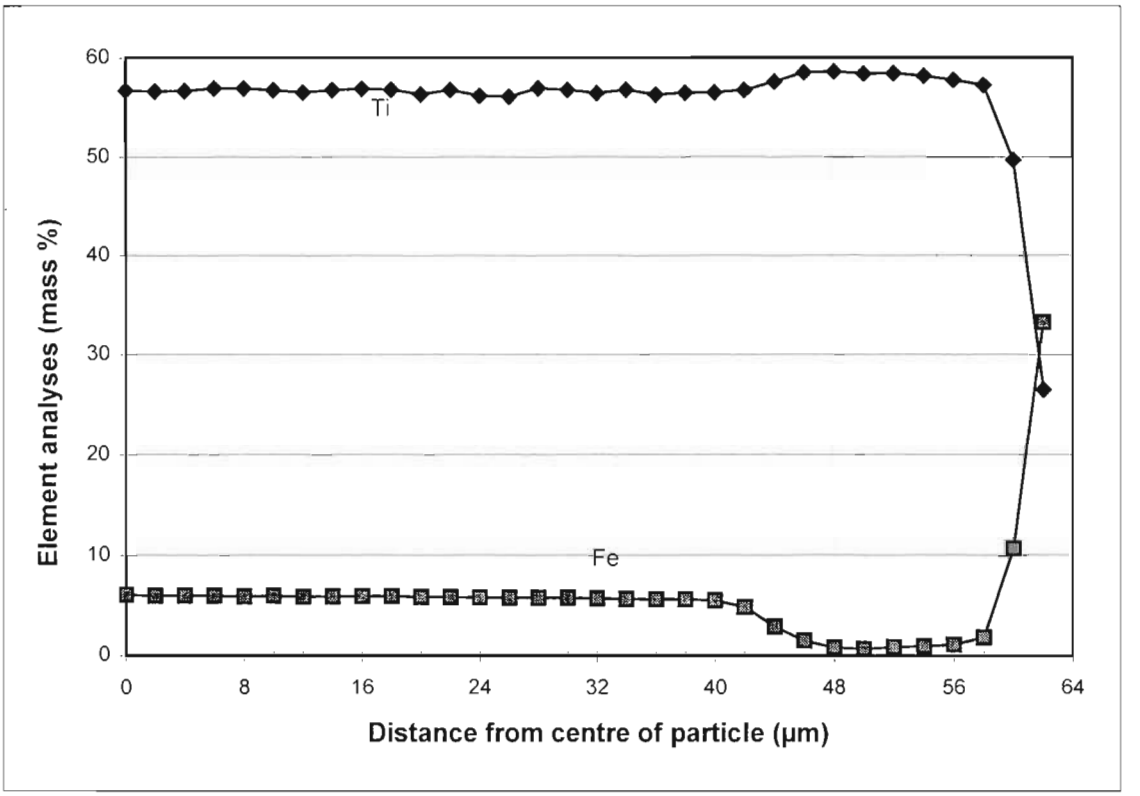

Table 27: Summary of results obtained from Mössbauer spectroscopy for the pressed pellet samples heated at 400 and 600 °C

Sample no.	Temperature (°C)	Time (hours)	Hyperfine interaction parameters			Abundance (atom %)	Attribution
			Isomeric shift - δ ($mm.s^{-1}$)	Quadropole splitting - Δ ($mm.s^{-1}$)	B_{hf} (T)		
DB100	Starting slag		1.16 (2)	3.35 (4)	-	90 (2)	Fe^{2+} compound (ferropseudobrookite)
			1.09 (2)	1.83 (4)	-	10 (2)	
DB115	600	24	0.39 (1)	0.66 (2)	-	47 (2)	Fe^{3+} compound (pseudobrookite)
			1.07 (1)	3.07 (4)	-	11 (2)	Fe^{2+} compound (ferropseudobrookite)
			0.38 (2)	-0.20 (2)	50.8 (2)	42 (2)	Hematite-like compound (Fe^{3+})
DB114	600	384	0.39 (2)	0.68 (2)	-	55 (2)	Fe^{3+} compound (pseudobrookite)
			0.38 (3)	-0.20 (3)	50.8 (1)	45 (2)	Hematite-like compound (Fe^{3+})
DB128	400	48	0.32 (1)	0.65 (2)	-	37 (2)	Fe^{3+} compound (pseudobrookite)
			1.09 (1)	3.07 (4)	-	43 (2)	Fe^{2+} compound (ferropseudobrookite)
			1.00 (2)	2.23 (2)	-	20 (2)	
DB125	400	384	0.39	0.68	-	55 (2)	Fe^{3+} compound (pseudobrookite)
			1.09	3.05	-	45 (2)	Fe^{2+} compound (ferropseudobrookite)

Errors are quoted as percentage (in parenthesis)
B_{hf} – internal magnetic field

A typical composition of the rim phase is as follows (oxygen content normalised to 3):

$$Fe_{1.64}Al_{0.06}Mn_{0.01}Mg_{0.02}Ti_{0.29}O_3$$

There are a total of 2.02 cations for every 3 oxygen atoms.

A photograph of the sample treated for 384 hours (DB114) is shown in Figure 44. The particles consist predominantly of the anatase and rutile as identified by X-ray diffraction analysis. As for sample DB115 the X-ray diffraction pattern also indicates that the M_3O_5 phase had almost disappeared. The slag particles are finely porous. According to the Mössbauer spectroscopy results shown in Table 27 a hematite-like compound (M_2O_3 phase) containing only Fe^{3+} was also identified. This was also confirmed by the X-ray diffraction results. This correlates with the iron-rich rims observed in Figure 44. The M_3O_5 phase (pseudobrookite) was also identified by Mössbauer spectroscopy, with this phase only containing Fe^{3+}.

Figure 44: Photograph of a pellet sample treated at 600 °C for 384 hours (sample DB114)

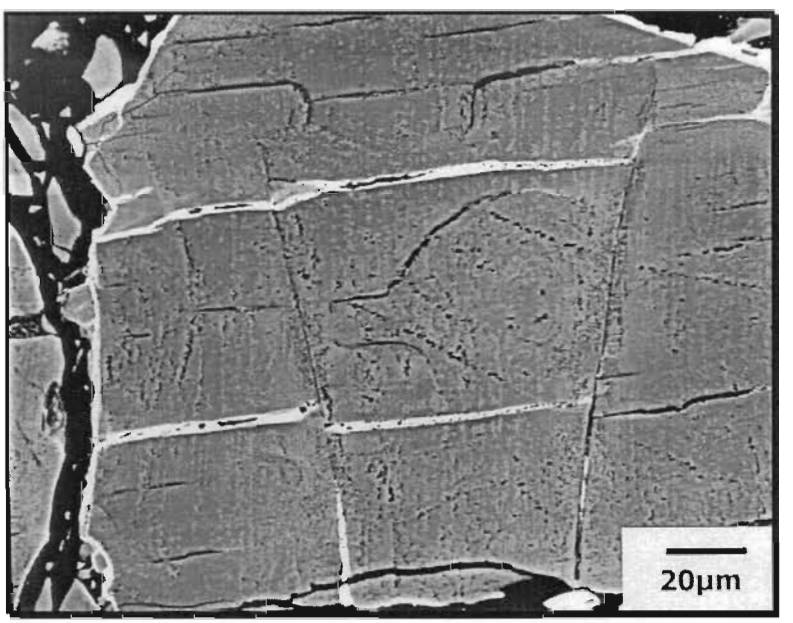

In general, only minor decrepitation of the samples treated at 600 °C was observed. This decrepitation occurred on the surface of the pellets, with the surface crumbling away.

3.5.1.4 Results of the testwork at 400 °C

All the samples treated at 400 °C decrepitated completely on quenching. This was also found for the sample treated for 2 hours (DB129). A photograph of a sample treated at 400 °C for 2 hours is shown in Figure 45. This photograph shows that extensive cracking of the particles had taken place when compared to the samples treated at 600 °C and higher temperatures. A sample treated for 96 hours is shown in Figure 46. The same type of cracks is observed in this sample, although the area density of the cracks seems to be slightly higher based on visual observation.

Figure 45: Photograph of a pellet sample treated at 400 °C for 2 hours (sample DB129)

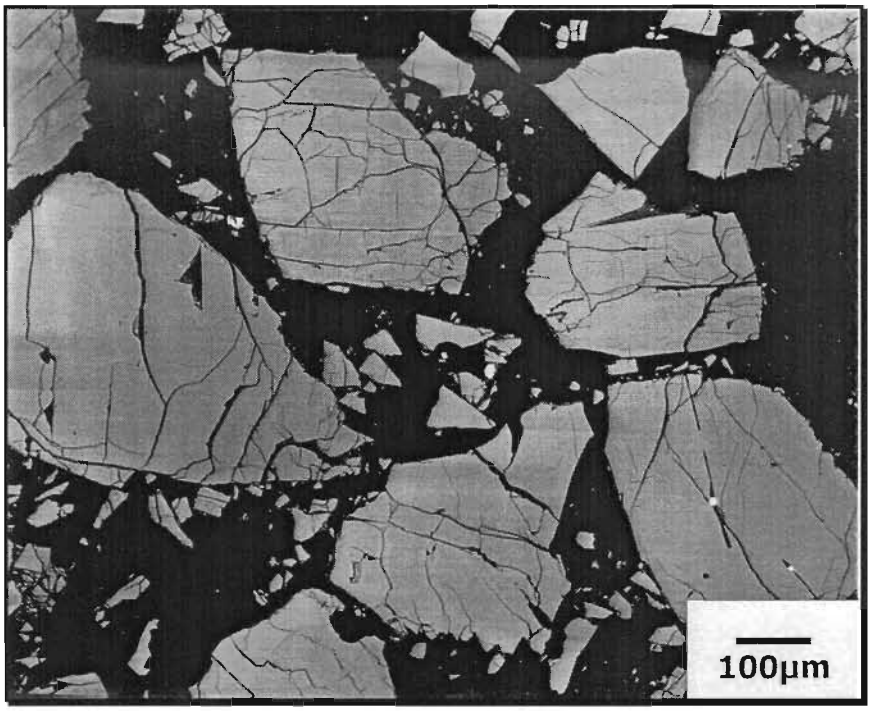

Figure 46: Photograph of a pellet sample treated at 400 °C for 96 hours (sample DB122)

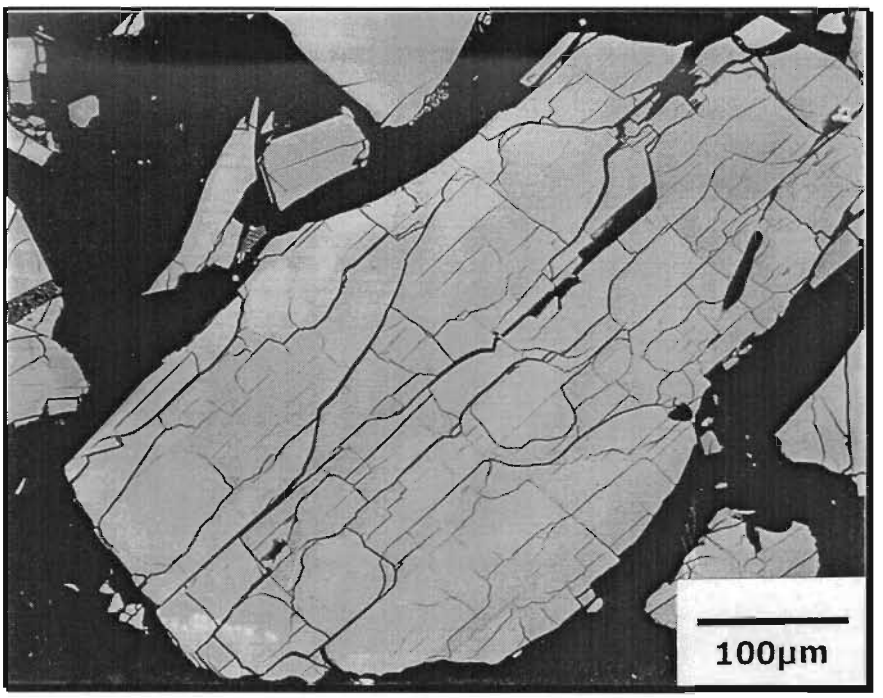

The X-ray diffraction patterns of some samples treated at 400 °C are also given in Appendix G. What is immediately noticeable is that the diffraction patterns show that the samples have became more amorphous when compared to the pattern for the starting material (DB100). This indicates increasing disorder in the crystal structure of the phases present. Also noticeable is the almost complete disappearance of the M_3O_5 peak at a 2θ-value of 32.5 degrees, whilst the peak at a 2θ-value of 25.3-25.6 degrees remains as the peak with the highest intensity. The results obtained for the various samples are summarised in Table 28, with the $I_{2\theta=32.5}/I_{2\theta=25.5}$ ratio also being plotted. The $I_{2\theta=32.5}/I_{2\theta=25.5}$ ratio is taken as an indication of the presence of the M_3O_5 phase. The results show that after 24 hours it seems that the M_3O_5 phase had almost completely disappeared. The question can then be asked what replaces the M_3O_5 phase?

Table 28: A summary of the relative peak intensities for the various samples treated at 400 °C for various times

Sample no.	Time (Hours)	2θ-value (degrees)	Intensity of the peak at a 2θ-value of ~ 25.5 degrees	2θ-value (degrees)	Intensity of the peak at a 2θ-value of ~ 32.5 degrees	$I_{2\theta=32.5}/I_{2\theta=25.5}$
DB100	0	25.6	3021.6	32.8	1564.7	0.518
DB129	2	25.6	896.4	32.7	262.5	0.293
DB121	24	25.6	753.2	32.3	57.0	0.076
DB128	48	25.7	1659.0	32.7	149.0	0.090
DB125	384	25.7	1462.6	32.9	102.6	0.070

Also noticeable is the appearance of a broad peak at a 2θ-value of approximately 21.1 degrees. This is similar to the peak obtained by Grey, Cranswick, et. al. (2000) as shown in Figure 31 for $Mg_{0.3}Ti_{2.7}O_5$ oxidised at low temperatures. Rietveld refinement of the M_6O_{11} intergrowth phase by Grey, Cranswick, et. al. (2000) show that the two major peaks for the M_6O_{11} phase are present at 2θ-values of 25.5 and 48.6 degrees respectively. At a 2θ-value of approximately 21.1 degrees some of the lesser peaks are also present. The position of these peaks correlates reasonably well with the data obtained for the samples treated at 400 °C. It can therefore be postulated that the disappearance of the M_3O_5 phase in the samples treated at 400 °C can be explained by the M_3O_5 phase being transformed into a M_6O_{11} phase. It seems that small amounts of anatase are also present in the oxidised pellet samples. This was also found by Grey, Cranswick, et. al. (2000) in their samples.

Mössbauer spectroscopy data of selected samples treated at 400 °C are shown in Table 27. These results show that a significant portion of the iron content is still in the +2 oxidation state. This is so even for the sample treated at 384 hours, indicating the slow rate of oxidation.

From point analysis of the bulk phase for the sample treated at 384 hours (Sample DB125, point a in Figure 47) the following compositions was calculated (oxygen content normalised to 5):

$$Fe_{0.22}Al_{0.04}V_{0.01}Mn_{0.01}Mg_{0.05}Ti_{2.50}O_5$$

Figure 47: Photograph of sample treated at 400 °C for 384 hours (DB125)

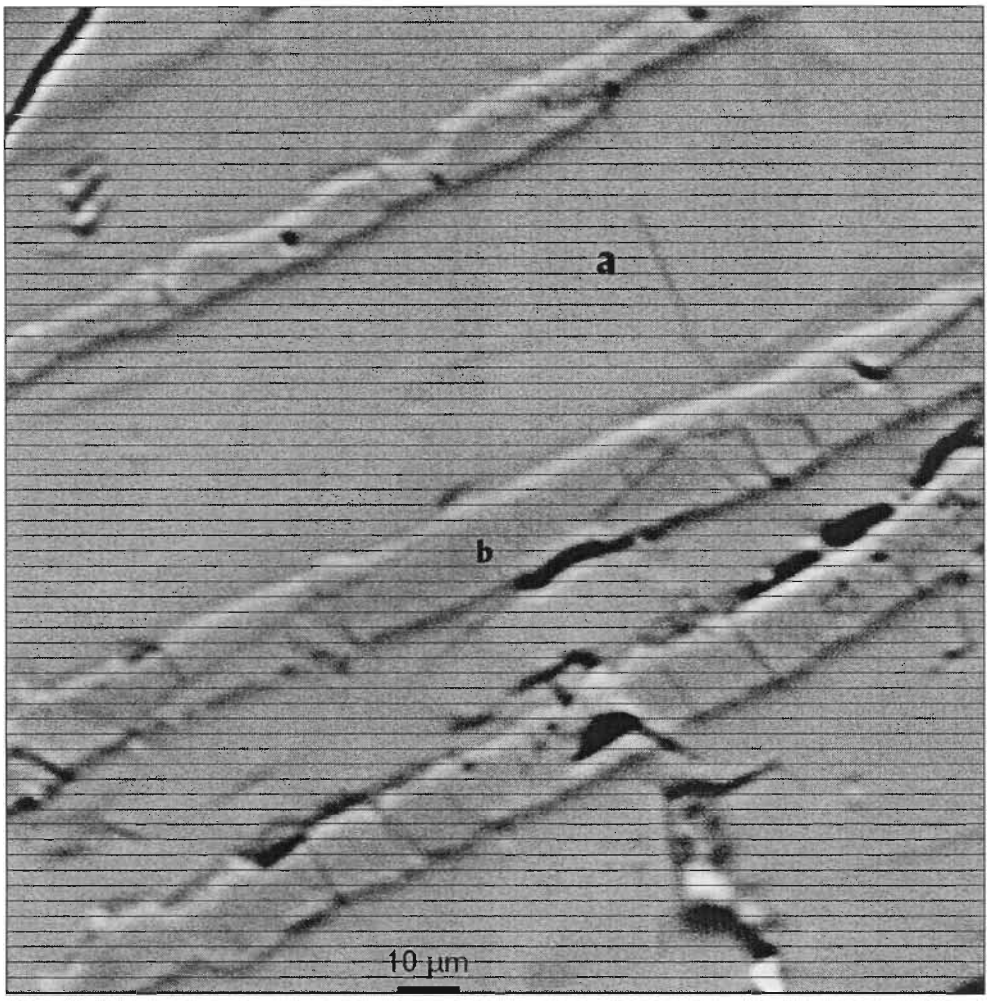

There are a total of 2.83 cations for every 5 oxygen atoms. When compared to the starting material (DB100) it can be seen that the oxygen to cation ratio of the bulk phase had increased. The X-ray diffraction pattern of the sample however shows almost none of a M_3O_5 phase to be present, and the cation to oxygen ratio is lower than can be expected for a M_3O_5 phase. As discussed previously it was not possible to obtain consistent meaningful data for the composition and oxidation states of the cations by using a combination of the relevant Mössbauer and phase analyses. To illustrate some of these uncertainties some calculations were carried out for the bulk phase of sample DB125. These calculations are shown in Appendix H.

Also shown in Figure 47 are lamellae observed in the bulk phase. The composition of these lamellae as given by point b in Figure 47 was calculated as follows (oxygen content normalised to 2):

$$Fe_{0.01}Al_{0.01}V_{0.01}Mg_{0.01}Ti_{1.04}O_2$$

There are a total of 1.08 cations for every 2 oxygen atoms. It should be noted that besides the oxygen analysis problem discussed earlier, these lamellae are thin (approximately 10 µm) and therefore difficult to analyse without some interference from the matrix which can influence the analysis.

3.5.2 RESULTS OBTAINED FROM THE TESTWORK WITH MINIATURE SLAG BLOCKS

3.5.2.1 Isothermal testwork on the miniature slag blocks

Sample DB123 was used as starting material for this testwork. The chemical composition of this sample is shown in Table 23. X-ray diffraction patterns of these samples are given in Appendix I.

A) Results of the testwork at 800 °C

The block sample treated at 800 °C for 24 hours (DB124) contained three distinct zones. These zones were as follows:

- The first zone is the outer rim zone. This zone can be seen in Figure 48. Iron migration occurred towards the outer margins of the slag block. This zone is characterised by alternate dense and porous sub-zones.

Figure 48: Photograph of the outer rim of a miniature block sample treated at 800 °C for 24 hours (sample DB124)

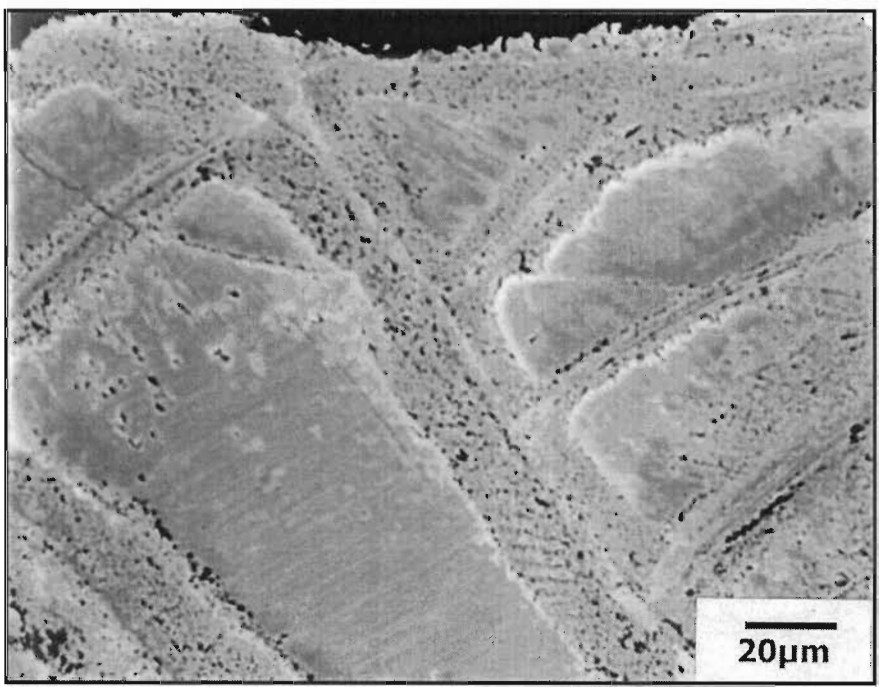

- The second zone is the mantle zone. This zone can be seen in Figure 49. The zone consists predominantly of a mixture of TiO_2 (darker colour) and the M_3O_5-solid solution phase, with abundant fine-grained iron enriched M_3O_5-precipitates (whitish coloured) concentrating along cracks. This zone is not that clearly distinguishable from the outer rim zone.
- The third zone is the core of the block, with the zone being approximately 1 mm in length. This is shown in Figure 50. The core is finely porous and contains an abundance of fine metallic iron precipitates. The core is in general dual phased, consisting of a mixture of

TiO_2 and the M_3O_5-solid solution phase. The metallic iron (bright white) is in general associated with TiO_2.

Figure 49: Photograph of the mantle zone of a miniature block sample treated at 800 °C for 24 hours (sample DB124)

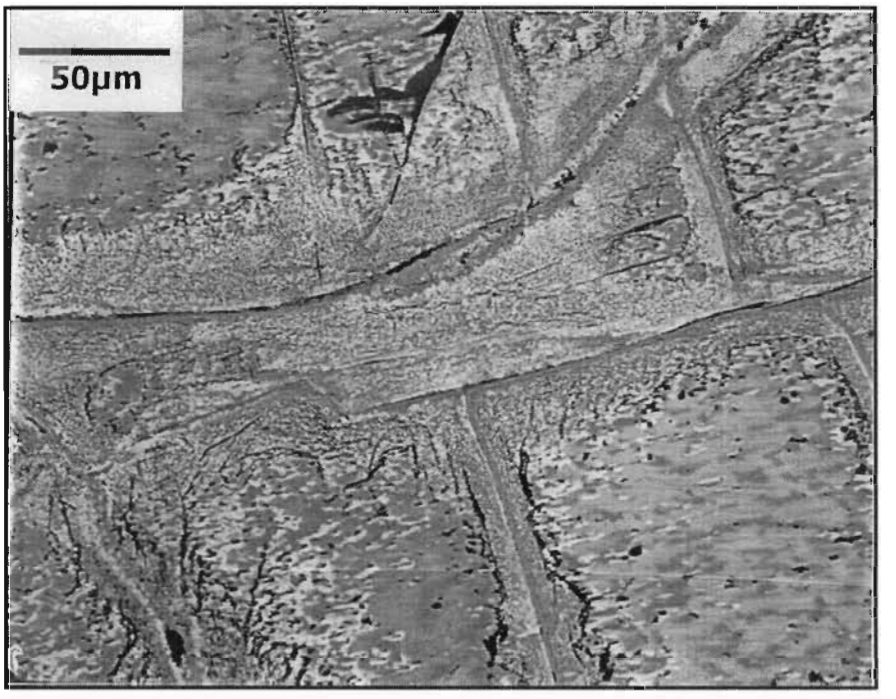

Figure 50: Photograph of the core of a miniature block sample treated at 800 °C for 24 hours (sample DB124)

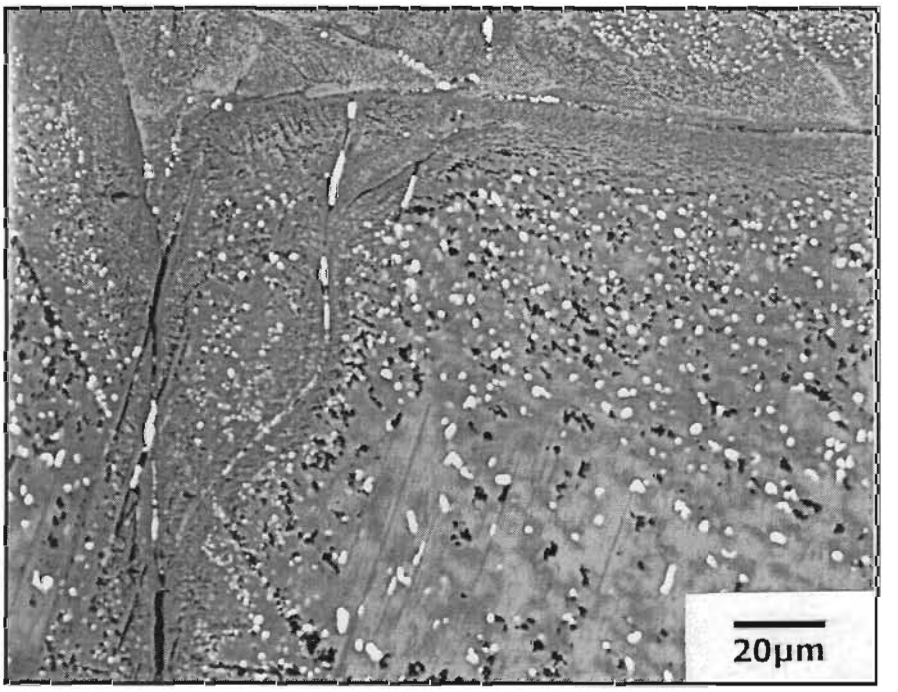

Mössbauer spectroscopy (see Table 29) of the sample shows the presence of pseudobrookite and ilmenite. Ilmenite was also confirmed by X-ray diffraction as indicated by the peaks with

Table 29: Summary of results obtained from Mössbauer spectroscopy for a miniature block sample heated at 800 °C

Sample no.	Temperature (°C)	Time (hours)	Hyperfine interaction parameters			Abundance (atom %)	Attribution
			Isomeric shift - δ ($mm.s^{-1}$)	Quadropole splitting - Δ ($mm.s^{-1}$)	B_{hf} (T)		
DB124	800	24	0.35	0.62	-	41 (3)	Fe^{3+} compound (pseudobrookite)
			1.08	3.05	-	20 (2)	Fe^{2+} compound (ferropseudobrookite)
			1.11	0.70	-	39 (2)	Ilmenite-like compound (Fe^{3+})

Errors are quoted as percentage (in parenthesis)
B_{hf} – internal magnetic field

2θ-values of 23.8, 35.5 and 53.2 degrees (see Appendix I). Rutile was identified as the main phase present, with M_3O_5 as a secondary phase. No decrepitation of this sample was observed.

When comparing sample DB124 with the equivalent pellet sample (24 hours at 800 °C, DB109) several differences are noted:

- The visual appearances of the samples are different (compare Figure 40 with Figure 48, Figure 49 and Figure 50), with sample DB124 showing an elaborate zoned structure.
- From the Mössbauer results sample DB124 contains ilmenite (also confirmed by X-ray diffraction analysis), while sample DB109 contains a hematite-like phase.

B) Results of the testwork at 400 °C

X-ray diffraction patterns for the miniature block samples treated at 400 °C are shown in Appendix I. These results show that the main phases present in these samples are M_3O_5 (or a structural modification there-of) and rutile. Some anatase might also be present. No broad peak at a 2θ-value of approximately 21.1 degrees was observed for these samples (see Appendix G for comparison with the pellet samples). The diffraction patterns of the miniature slag blocks do seem to indicate that the samples after treatment are more amorphous than the starting material. This can be seen by the broadening of the peaks, as well as the increase in the noise levels of the background. It is also noticeable that the miniature block samples contain a significant amount of rutile, while the pellet samples contained a negligible amount of rutile. Another difference between these two types of samples is the disappearance of the M_3O_5 peak at a 2θ-value of 32.5 degrees for the pellet samples, while this peak is still found in the diffraction patterns for the miniature slag blocks. A summary of the peak intensities of the miniature slag blocks is shown in Table 30.

Table 30: A summary of the relative peak intensities for various miniature block samples treated at 400 °C for various times

Sample no.	Time (Hours)	2θ-value (degrees)	Intensity of the peak at a 2θ-value of ~ 25.5 degrees	2θ-value (degrees)	Intensity of the peak at a 2θ-value of ~ 32.5 degrees	$I_{2\theta=32.5}/I_{2\theta=25.5}$
DB123	0	25.7	1691.1	32.7	1042.7	0.617
DB130	6	25.8	1393.7	32.8	666.6	0.478
DB131	24	25.8	551.9	32.8	252.0	0.457
DB133	96	25.7	1174.8	32.7	322.5	0.275
DB132	384	25.7	1155.0	32.7	290.8	0.252

A comparison between the relative intensities of the pellet samples and the miniature block samples are given in Figure 51. The following differences in Figure 51 can be noted:

- It seems that the rate of change of the peak intensity ratio of the blocks is smaller than that of the pellets. This can be seen by comparing the results of the two types of samples obtained after 24 hours. For the pellet samples it is evident that the relative peak intensity is already at a minimum value of 0.076 (14.7 per cent of the value obtained for the starting

material), while for the miniature block sample a value of only 0.457 (74.1 per cent of the value obtained for the starting material) was obtained.

- It also seems that the miniature blocks reach equilibrium at a higher peak ratio level than the pellet samples. For the pellet sample reacted at 384 hours a value of 0.070 (13.5 per cent of the value obtained for the starting material) was obtained, while for the miniature block sample reacted at 384 hours a value of 0.252 (40.8 per cent of the value obtained for the starting material) was obtained.

Figure 51: A comparison of the peak intensity ratios ($I_{2\theta=32.5}/I_{2\theta=25.5}$) for the pellet and miniature block samples treated at 400 °C.

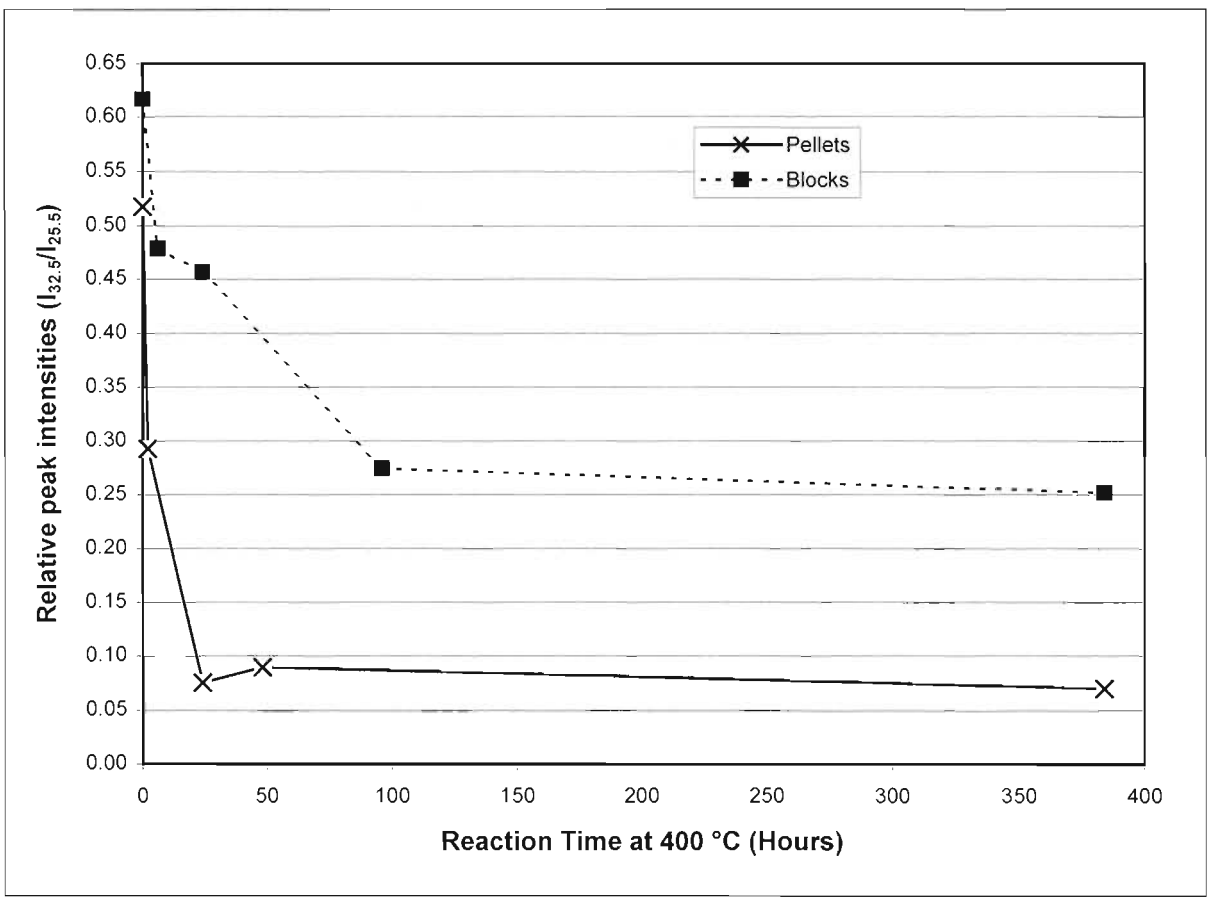

In explaining the different results obtained between the two types of samples, the following differences between the two types of samples should be noted:

- The pellet samples has a higher porosity than that of the miniature block samples. This can result in higher reaction rates if oxygen transfer plays a limiting role in the respective reactions. This is unlikely, given the long reaction times used.
- The chemistry of the respective starting materials is also different. This is shown in Table 23. For the pellet samples the starting material (DB100) contained 9.8 per cent FeO, while the starting material for the miniature block samples (DB123) contained 14.4 per cent FeO. This is considered to be the more likely cause.

The chemistry of the respective starting materials probably also explains the differences between the pellet and miniature block samples obtained at 800 °C, as discussed earlier.

The photograph of the miniature slag block sample heated for 6 hours at 400 °C (DB130) is shown in Figure 52. The photograph displays a section of the block consisting predominantly of the M_3O_5 solid solution phase containing abundant fine-grained, needle-like rutile exsolution lamellae displaying preferred orientation. Cracking of the block can be observed. It should be noted that the cracks do not in any way seem to be associated or aligned with the rutile needles, with some rutile needles even divided into smaller fragments due to cracking perpendicular to the needles. Figure 53 shows a photograph of a sample treated for 96 hours at 400 °C (DB133). Once again extensive cracking of the sample can be observed. The composition of the bulk phase of the block sample treated for 384 hours was as follows (oxygen content normalised to 5):

$$Fe_{0.55}\ Al_{0.03}\ V_{0.01}\ Mg_{0.04}\ Zr_{0.01}\ Ti_{2.29}\ O_{5}$$

It was not possible to determine the oxidation states of the various cations, as no data on the Fe^{2+} and Fe^{3+} content of the sample was available (Mössbauer spectroscopy was not carried out on the sample). There is a total of 2.96 cations for every 5 oxygen atoms in this phase (i.e. close to stoichiometric M_3O_5).

The composition of the rutile phase for the sample DB132 was determined to be as follows (oxygen content normalised to 2):

$$Ti_{1.03}O_2$$

Figure 52: Photograph of a miniature block sample treated at 400 °C for 6 hours (sample DB130)

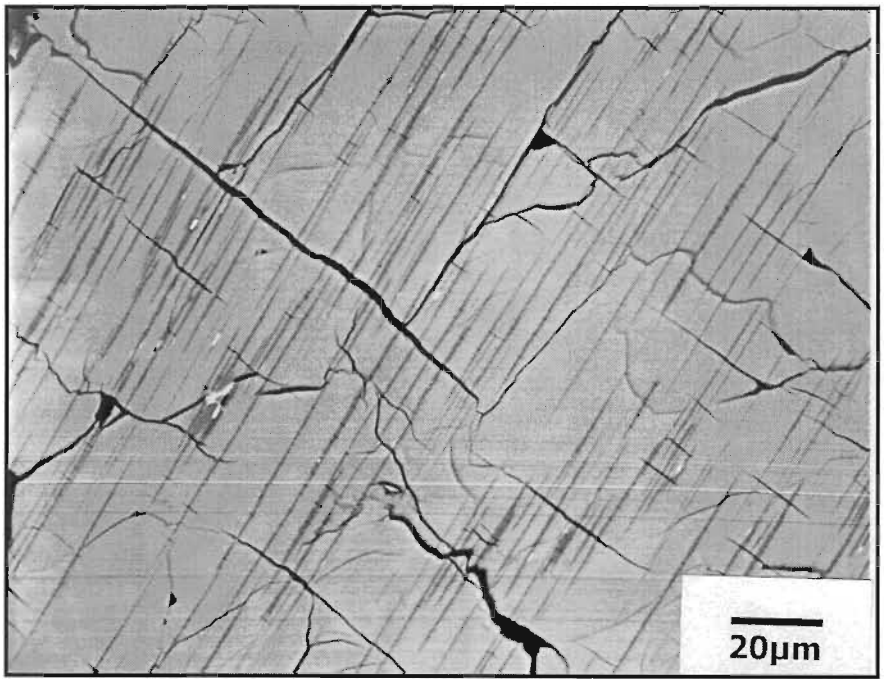

Figure 53: Photograph of a miniature block sample treated at 400 °C for 96 hours (sample DB133)

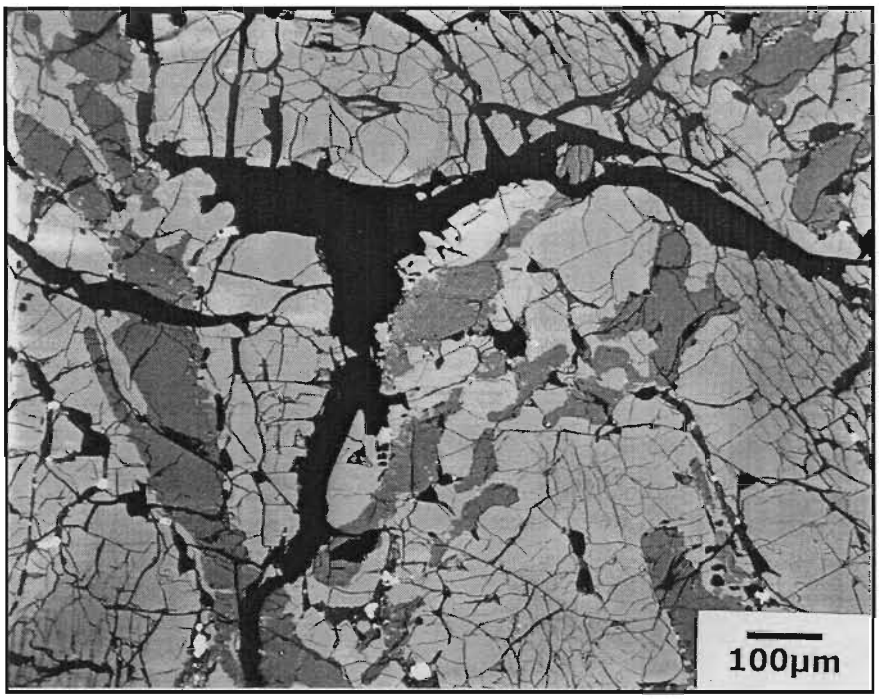

Only limited decrepitation of these miniature slag blocks treated at 400 °C was observed. For the sample treated for 6 hours (DB130) no decrepitation was observed, while for the samples treated for 24 and 96 hours (DB131 and DB133 respectively) only decrepitation on the surface of the blocks were observed. For the sample treated for 384 hours the block broke in two pieces on quenching, indicating a decrease in the strength of the block. However, compared to the pellet samples the observed decrepitation was mild.

3.5.2.2 Results of the unidirectional crushing tests

In an attempt to quantify the effect of decrepitation on the physical strength of the slag it was decided to carry out unidirectional crushing tests on some miniature slag blocks. The starting composition of these blocks is given in Table 23 (sample DB136). The data from the crushing tests were converted to obtain information on the following aspects:

- The total crushing energy for each experimental condition.
- The maximum force required for crushing the blocks for each experimental condition.
- The size distribution of the miniature slag blocks after crushing.

Details of the raw data, and the conversion of the data, is given in Appendix J. Also shown in Appendix J is a statistical analysis of the data.

Figure 54 shows a typical result for the displacement of the miniature slag block as a function of time, while Figure 55 shows the force applied as a function of time for the same sample. This block was treated for 24 hours at 600 °C. Approximately 8 seconds after the recording of data was started, the moving plate was set in motion (see point A; Figure 54). After approximately 10 seconds the miniature slag block made contact with the fixed plate (at point

B in Figure 54). Between points B (10.0 s; 7.1 mm) and C (10.5 s; 6.2 mm) the rate of displacement decreases markedly, with a displacement of only 0.9 mm measured between the two points. This small displacement is related to the increase in the applied force, which causes elastic deformation of the test frame. At point C it seems that the block fractures due to the stress placed on it, with the majority of the material falling away. Point C also coincides with the maximum applied force (see Figure 55). The displacement between points C and D (10.6 s; 2.1 mm) is 4.1 mm. Between points D and E no displacement of the moving plate takes place. This can be explained by a certain amount of play present in the equipment. Between points C and D the moving plate shoots forward due to the release of the pressure when the block fractures. After a time delay (approximately 0.5 seconds in this instance) the slack is taken up again and the moving plate starts moving forward again at point E.

For comparison purposes the graphs obtained for a sample treated at 800 °C for 24 hours are shown in Figure 56 and Figure 57. The major difference between the samples seems to be the maximum force required for the samples (6.13 kN compared to 4.70 kN), indicating that the sample treated at 800 °C is much harder to crush.

Figure 58 shows a summary of the results obtained for the various experimental conditions. The statistical analyses done in Appendix J show that only the following significant differences between the various experimental conditions with regard to the total energy required for crushing were calculated:

- The samples treated at 800 °C for 24 hours required significantly more energy to crush than the other samples.

The following results between the various experimental conditions were found with regard to the maximum force applied to the miniature slag blocks:

- The untreated slag samples required significantly less force to crush than the samples treated at 600 °C for 24 hours and the samples treated at 800 °C for 24 hours.
- The samples treated at 600 °C for 24 hours required significantly more force to crush than the samples treated at 600 °C for 96 hours.
- The samples treated at 600 °C for 24 hours required significantly less force to crush than the samples treated at 800 °C for 24 hours.
- The samples treated at 600 °C for 96 hours required significantly less force to crush than the samples treated at 800 °C for 24 hours.
- No significant difference in the force required for crushing the blocks were found between the untreated slag samples and the samples treated at 600 °C for 96 hours.

The size distributions of the slag blocks after crushing were also evaluated. The percentage slag less than 500 μm was used as indicator. These results are shown in Figure 59. The following significant results were obtained:

- The untreated slag samples contained significantly more –500 μm material after crushing than the samples treated at 600 °C for 24 and 96 hours, as well as the samples treated at 800 °C for 24 hours.
- The samples treated at 600 °C for 24 hours also contained significantly more –500 μm material than the samples treated at 600 °C for 96 hours and the samples treated at 800 °C for 24 hours.

No significant difference in size between the samples treated at 600 °C for 96 hours and the samples treated at 800 °C for 24 hours were found.

Figure 54: Displacement of the miniature slag block treated at 600 °C for 24 hours as a function of time (test no. 6241)

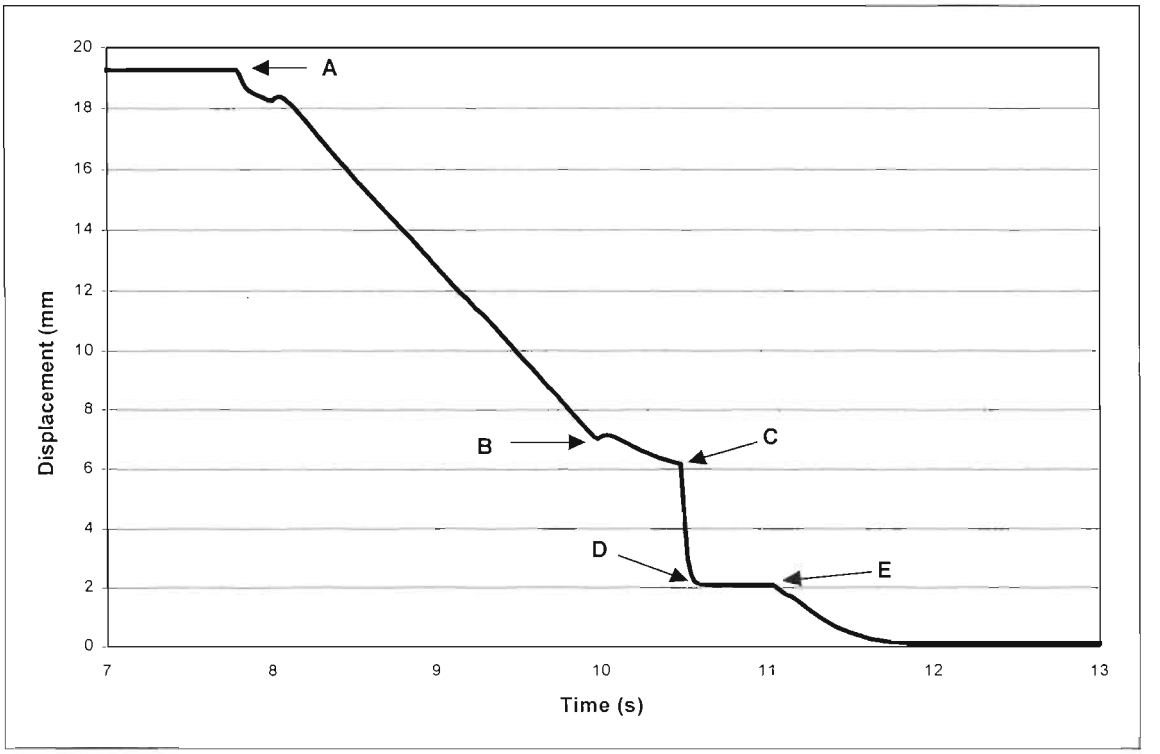

Figure 55: Measurement of the force applied as a function of time for a miniature slag block treated at 600 °C for 24 hours (test no. 6241)

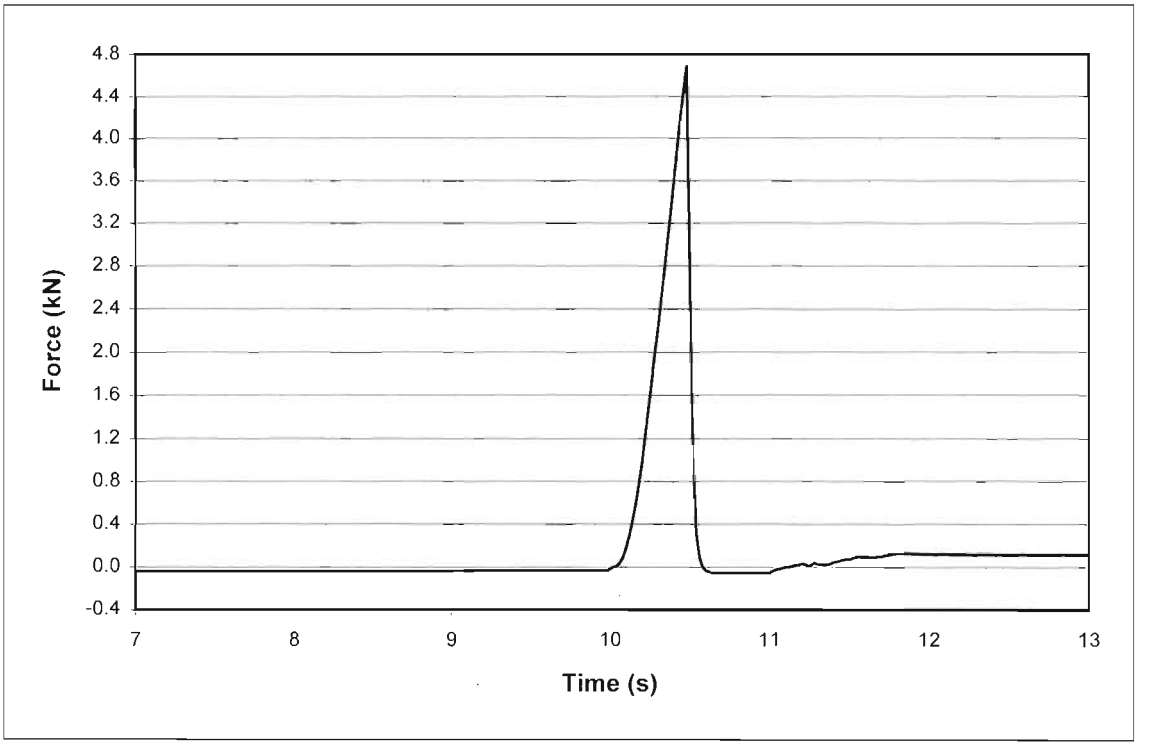

Figure 56: Displacement of the miniature slag block treated at 800 °C for 24 hours as a function of time (test no. 8243)

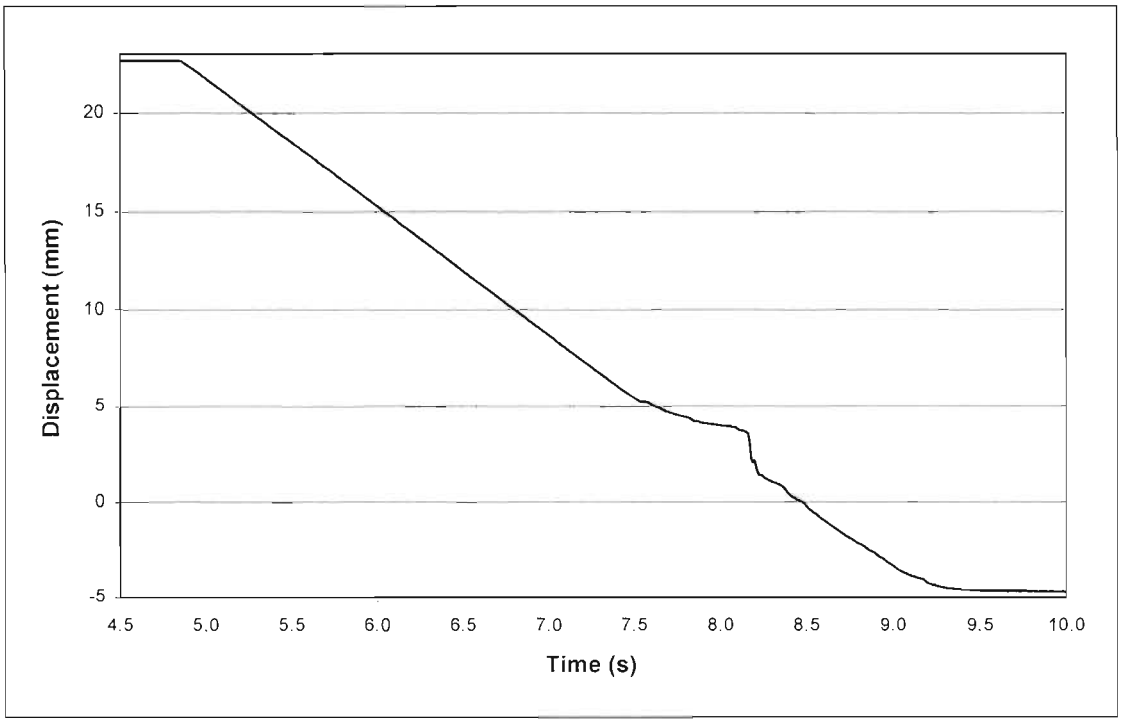

Figure 57: Measurement of the force applied as a function of time for a miniature slag block treated at 800 °C for 24 hours (test no. 8243)

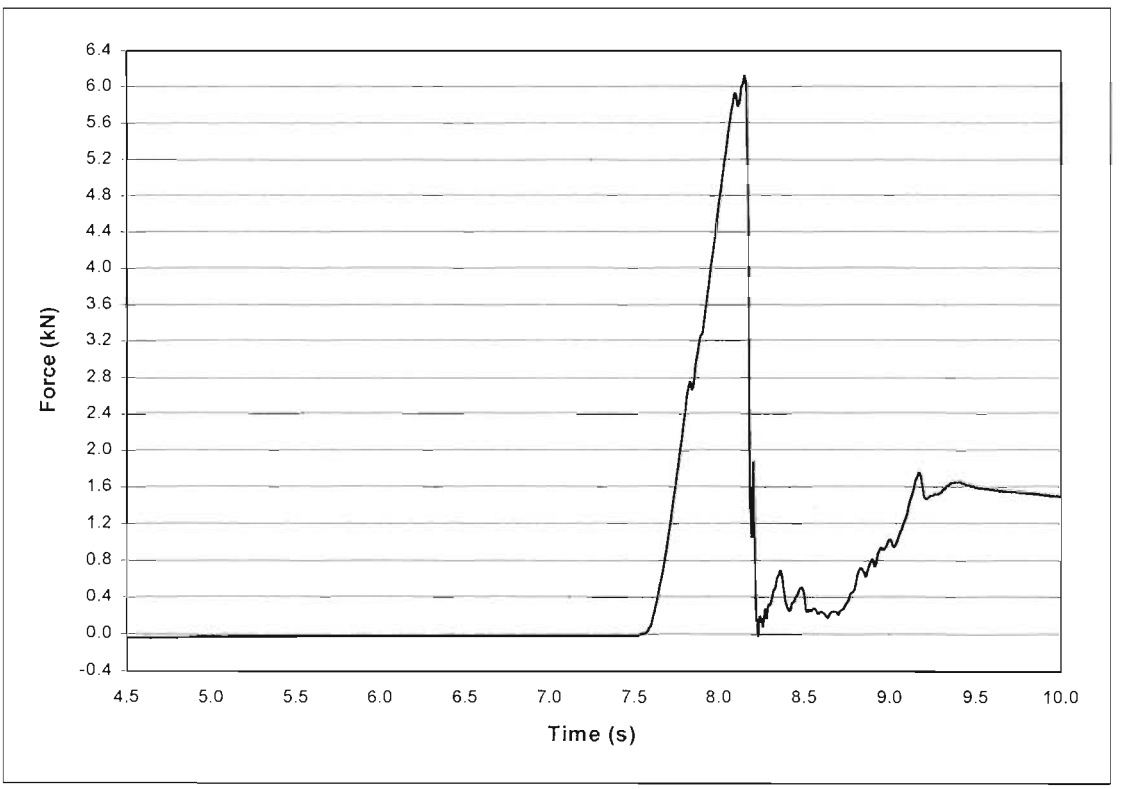

Figure 58: The total energy required and the maximum force applied for the crushing of the miniature slag blocks

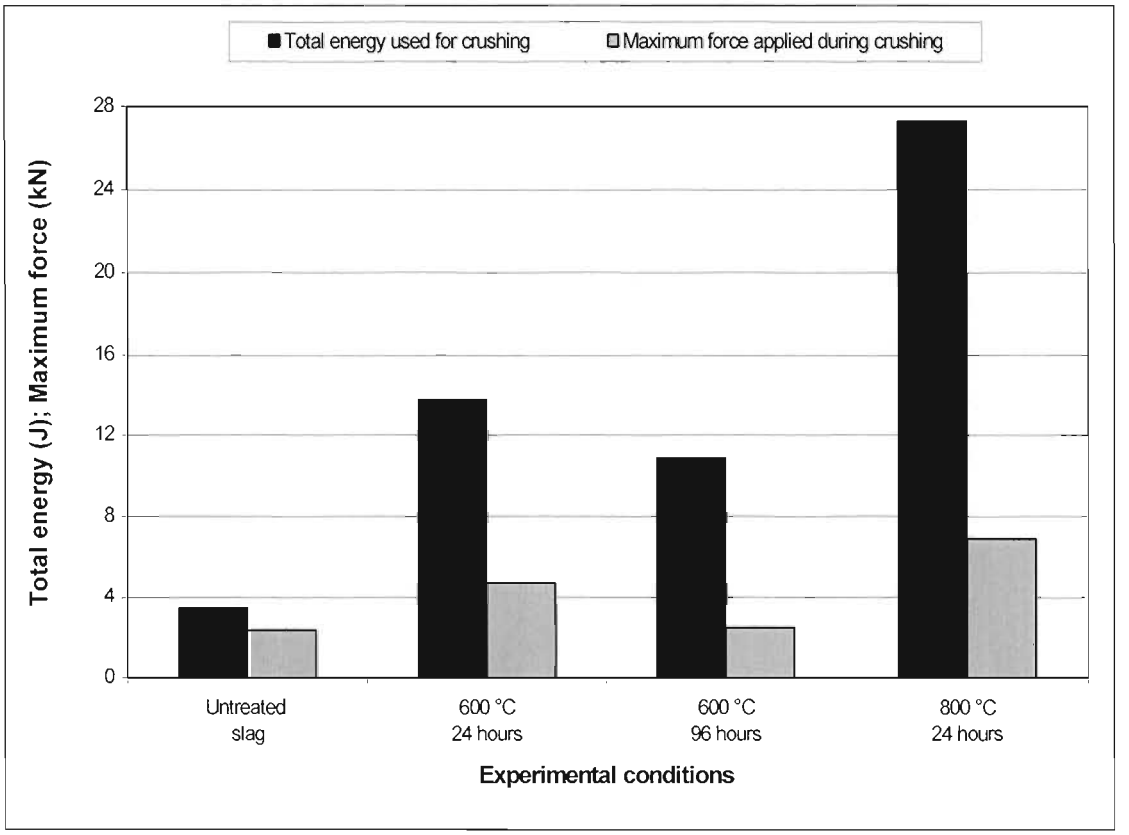

Figure 59: Size distribution of the miniature slag blocks after the crushing tests

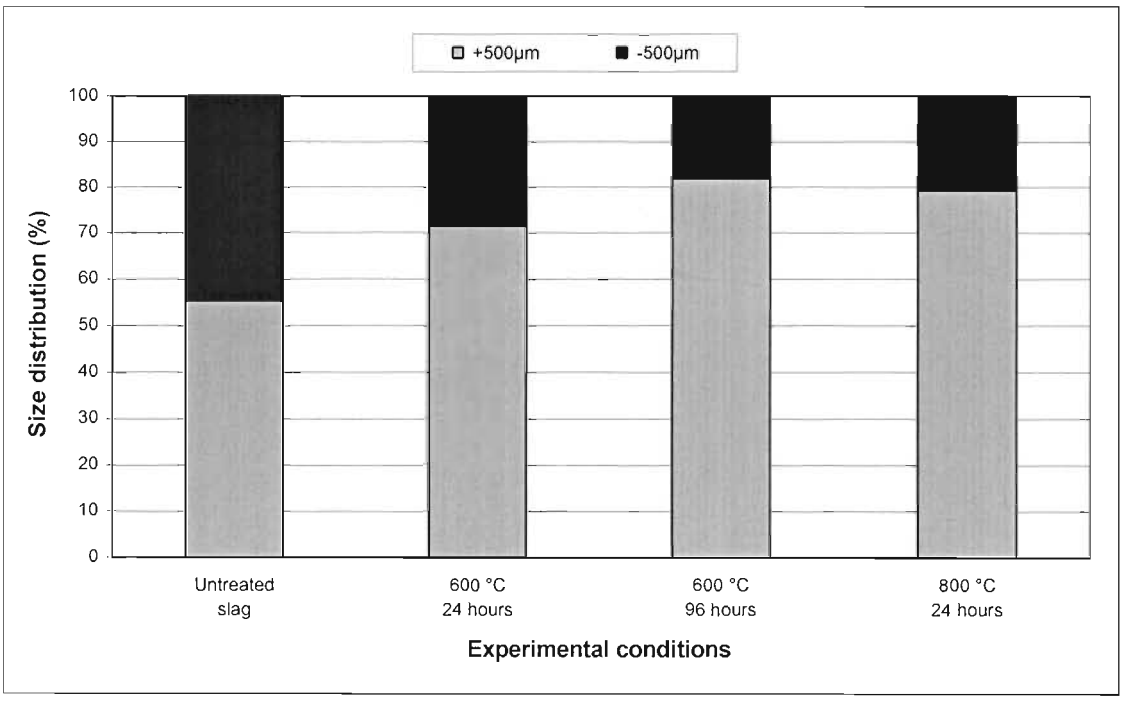

It was only possible to carry out crushing tests on the miniature slag blocks treated at 600 and 800 °C as the blocks treated at 400 °C decrepitated completely on quenching. This was somewhat surprising, as the miniature slag blocks discussed in the previous section (starting material DB123, see Table 23 for composition) did not decrepitate on quenching. X-ray diffraction data from one of the samples prepared for 24 hours at 400 °C for the crushing testwork are given in Appendix K. The sample was separated into two size fractions after decrepitating on quenching. Sample DB145 represents the –1 mm size fraction, while sample DB146 represents the +1 mm size fraction. Also shown in Appendix K is the X-ray diffraction pattern for the –212 μm size fraction one of the untreated slag samples (DB139, slag 2 as shown in Table 46, Appendix J).

The size fraction was obtained subsequent to the crushing test. Sample DB139 is essentially the starting material for samples DB145 and DB146. Once again the broad peak at a 2θ-value of approximately 21.1 degrees is observed for samples DB145 and DB146, indicating the presence of the M_6O_{11} phase. This peak was also found in the pellet samples treated at 400 °C, but not for the miniature block samples treated at 400 °C discussed in the previous section.

The likely explanation of the different results is therefore the difference in chemical composition of the respective starting materials. The samples that showed the appearance of the M_6O_{11} phase contained 9.8 and 8.4 per cent FeO in their respective starting materials (see samples DB100 and DB136, Table 23), while the samples that did not show this phase contained 14.4 per cent FeO in their starting material. This sample obviously also contains the least amount of Ti^{3+}. It appears that the formation of the M_6O_{11} phase is driven by the oxidation of Ti^{3+} to Ti^{4+} at low temperatures in the M_3O_5 structure. It seems that the formation of the M_6O_{11} phase is sensitive to the composition of the slag, with the slag containing 14.4 % FeO being too iron-rich for the M_6O_{11} phase to form in significant amounts.

3.5.3 RESULTS FROM TESTWORK IN DIFFERENT ATMOSPHERES

For the tests carried out in different atmospheres sample DB100 in the form of a powder was used as starting material. The experimental conditions of the tests are shown in Table 31, with the chemical analyses of the various samples given in Table 32. Where Ar+Air is indicated as the atmosphere, it indicates experiments that were carried out in the reactor where it was subsequently discovered that a leak was present in the system. Also shown in Table 31 is a summary of the results extracted from the X-ray diffraction patterns (patterns given in Appendix L). As described previously the $I_{2\theta=32.5}/I_{2\theta=25.5}$ ratio is again taken as an indication of the presence of the M_3O_5 phase. The Ti_2O_3 content of the samples in Table 32 is taken as the extent of oxidation of the samples. Thus for the starting material (DB100) the Ti_2O_3 content was determined to be 30.4 per cent, while for the sample heated in air for 72 hours the Ti_2O_3 content was analysed as being less than 1 per cent. At these low levels of Ti_2O_3 it could also be expected that all or most of the iron would be oxidised to Fe^{3+}, with similar results that could be expected for the pellet and miniature slag block samples treated under similar conditions. No Mössbauer spectroscopy analysis was however carried out on these samples. The samples heated in Ar+Air showed an intermediate level of oxidation, with Ti_2O_3 levels of approximately 20 per cent. The sample treated only in Ar also showed some oxidation, with a Ti_2O_3 level of 26.4 per cent compared to 30.4 per cent for the starting material. The possibility

Table 31: A summary of the relative peak intensities for samples treated in various atmospheres

Sample no.	Temperature (°C)	Time (Hours)	Atmosphere	2θ-value (degrees)	Intensity of the peak at a 2θ-value of ~ 32.5 degrees	2θ-value (degrees)	Intensity of the peak at a 2θ-value of ~ 25.5 degrees	$I_{2\theta=32.5}/I_{2\theta=25.5}$
DB100	Starting material			25.6	3021.6	32.8	1564.7	0.518
DB196	400	24	Ar	25.2	472.6	32.4	214.5	0.454
DB186	400	24	Ar+Air	25.5	504.5	32.7	203.3	0.403
DB185	370	24	Ar+Air	25.2	414.0	32.4	152.5	0.368
DB184	400	24	Air	25.2	426.3	32.3	115.0	0.270
DB193	400	48	Air	25.4	378.4	32.4	24.5	0.065
DB194	400	72	Air	25.3	376.5	32.3	24.1	0.064

Table 32: Analyses of the samples treated in various atmospheres

Sample no.	Analyses (mass %)												
	SiO_2	Al_2O_3	CaO	MgO	MnO	Cr_2O_3	V_2O_5	ZrO_2	Fe^0	FeO	TiO_2	Ti_2O_3	Total Ti as TiO_2
DB100	1.41	1.19	0.27	1.03	1.17	0.05	0.45	0.16	< 0.1	9.80	53.9	30.4	87.70
DB196	1.81	1.18	0.25	1.27	1.14	0.10	0.45	-	< 0.1	9.79	57.6	26.4	
DB186	1.46	1.14	0.27	1.24	1.09	0.10	0.45	-	< 0.1	9.61	65.0	21.5	
DB185	1.32	1.12	0.25	1.24	1.08	0.09	0.46	-	< 0.1	9.54	67.1	18.6	
DB184	1.50	1.16	0.27	1.25	1.11	0.10	0.46	-	< 0.1	9.58	70.4	14.9	
DB193	1.78	1.16	0.28	1.21	1.09	0.09	0.43	-	< 0.1	9.45	85.3	< 1	
DB194	1.72	1.11	0.23	1.17	1.06	0.09	0.42	-	< 0.1	9.19	85.3	< 1	

that some air leakage into the experimental set-up occurred to cause this oxidation can not be excluded. Ti_2O_3 can of course also be oxidised by Fe^{2+} in the disproportionation reaction that has been mentioned several times.

Evaluating the results obtained in Table 31 and Table 32, a direct correlation between the extent of oxidation and the decrease in the M_3O_5 content (as exemplified by the decrease in the $I_{2\theta=32.5}/I_{2\theta=25.5}$ ratio) becomes apparent. This is illustrated in Figure 60. Also shown is a linear regression fit with a R^2 value of 0.99, indicating the excellent correlation obtained. Comparing samples DB196 (treated for 24 hours in Ar) and DB184 (treated for 24 hours in air), the latter appears to have a substantial number of cracks compared to sample DB196.

These results also provide a possible solution for preventing the decrepitation of titania slags. From the results it can be inferred that decrepitation can be avoided if the slag is cooled down under an inert atmosphere. This will probably only be necessary at relatively low temperatures of less than 600 to 700 °C.

Figure 60: Correlation between the Ti_2O_3 content and the ratio of X-ray diffraction intensities at 2θ-values of 32.5 and 25.5 degrees

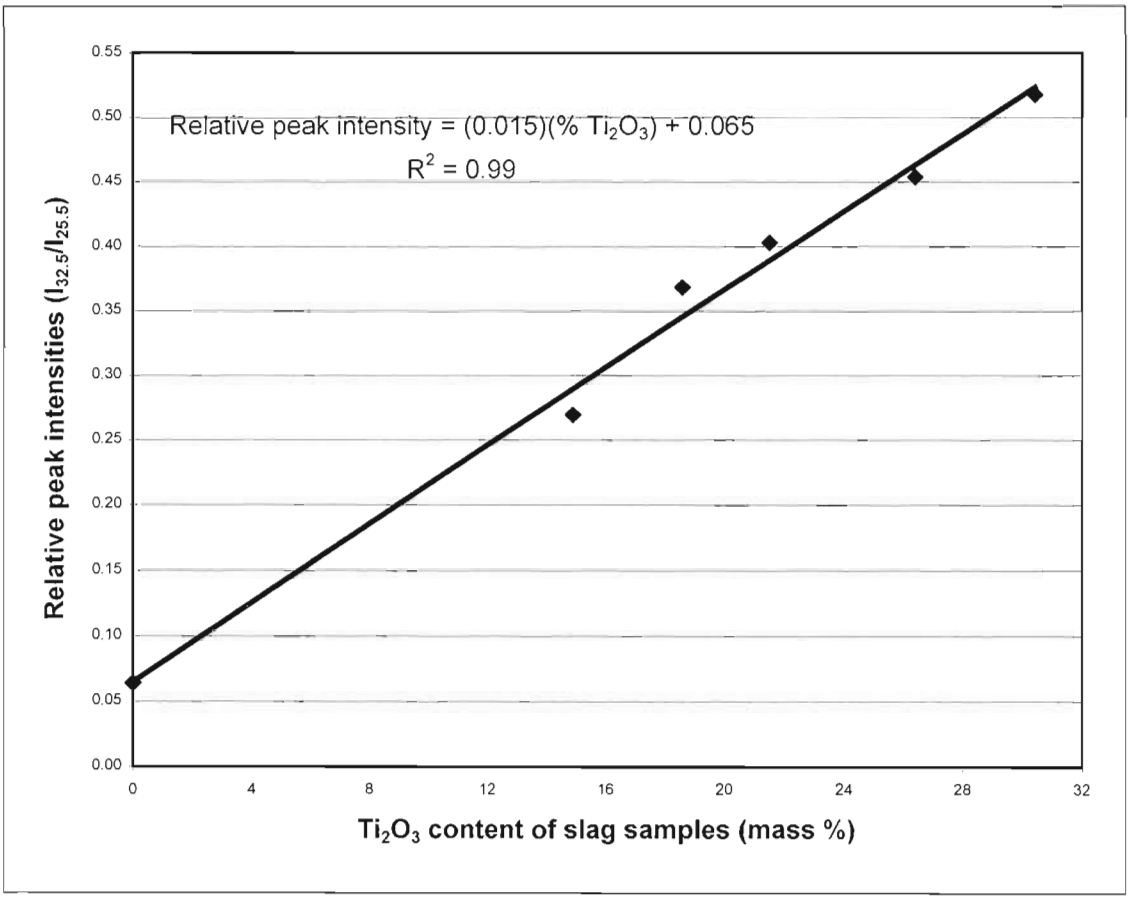

3.5.4 RESULTS FROM THE DATA OBTAINED DURING THE MAY 2000 SMELTING CAMPAIGN

The decrepitation phenomenon on large, slow-cooled slag blocks during the smelting campaign was studied, as this closely approximates the situation that could be expected on an industrial scale plant. In this campaign decrepitated slag was obtained directly from cooled liquid slag. This is different to the small-scale tests described previously, where quenched liquid slag was re-heated at various temperatures in order to study decrepitation. This part of the study is therefore also important in assessing the relevance of the small-scale testwork.

It also appears from observations that the decrepitation of the slag blocks is a relatively low temperature phenomenon. Decrepitation of the blocks only seemed to occur after the blocks had stopped glowing red, possibly indicating that the decrepitation reactions only occur at temperatures below 700-800 °C. This corroborates the results obtained from the small-scale tests, where significant decrepitation of the titania slag was only obtained below 600 °C.

3.5.4.1 Cooling rate of slag blocks

The temperature measurements obtained for the cooling of the two slag blocks are shown in Figure 61. The calculated cooling rates for the two slag blocks are also shown in Figure 62. Due to the protective sheath configurations (described previously) enclosing the thermocouples, the response time of the thermocouples were relatively slow. For tap 73, 63 minutes elapsed (after the closing of the taphole) before the maximum temperature of 1654 °C was registered. This is a difference of 18 °C when compared to the measured tap temperature of 1672 °C. For tap 79, 76 minutes elapsed (also relative to the closing of the taphole) prior to registering a maximum temperature of 1662 °C. This is a difference of 14 °C when compared to the tap temperature of 1676 °C.

The cooling rate of tap 79 was higher than that of tap 73, despite tap 79 (1029 kg) being approximately sixteen per cent larger than tap 73 (889 kg). The chemical compositions of the two taps are fairly similar, and it is not expected that this would make a significant difference in the respective cooling rates. The analyses of the two slags are shown in Table 33. The difference in the cooling rates can rather be explained by the relative position of the thermocouple assemblages in the slag blocks. The positions of the thermocouple assemblages for the two taps are shown in Figure 63. From the diagrams it is evident that the thermocouple assemblage for tap 79 is much closer to the bottom of the ladle, a distance of 157 mm compared to 245 mm for tap 73. It was also calculated that the closest distance to the side of the ladle for tap 79 was approximately 244 mm, while for tap 73 this distance was approximately 301 mm. It therefore seems reasonable to expect the measured cooling rate of tap 79 to be faster than those of tap 73. The maximum cooling rates of between 2 and 2.2 °C per minute for the blocks were attained after 8 to 10 hours. After this the cooling rates of the blocks decreased rapidly, with values of less than 0.2 °C per minute obtained at the completion of the measurements.

Very little interaction between the SiC thermocouple sheath material and titania slag was found (For details see Appendix M). It can therefore be recommended that these types of sheaths again be used in future for similar applications.

Figure 61: Temperature measurements obtained for the cooling of two slag blocks

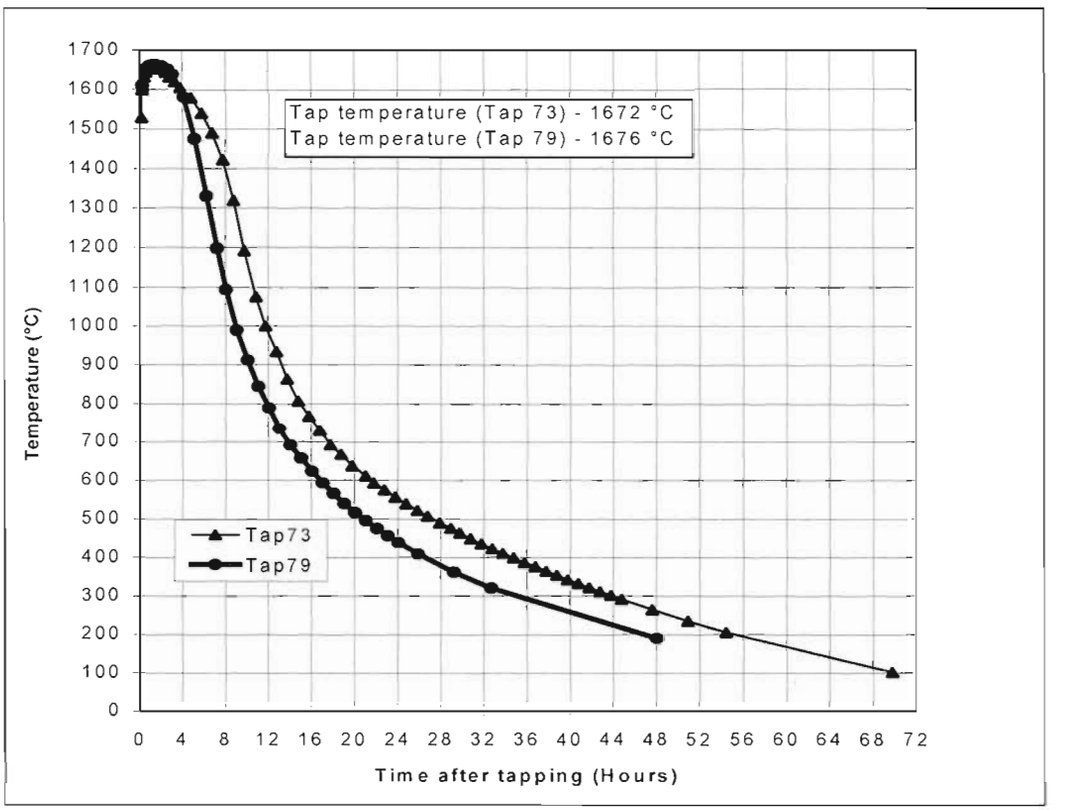

Figure 62: Cooling rates calculated for the two slag blocks

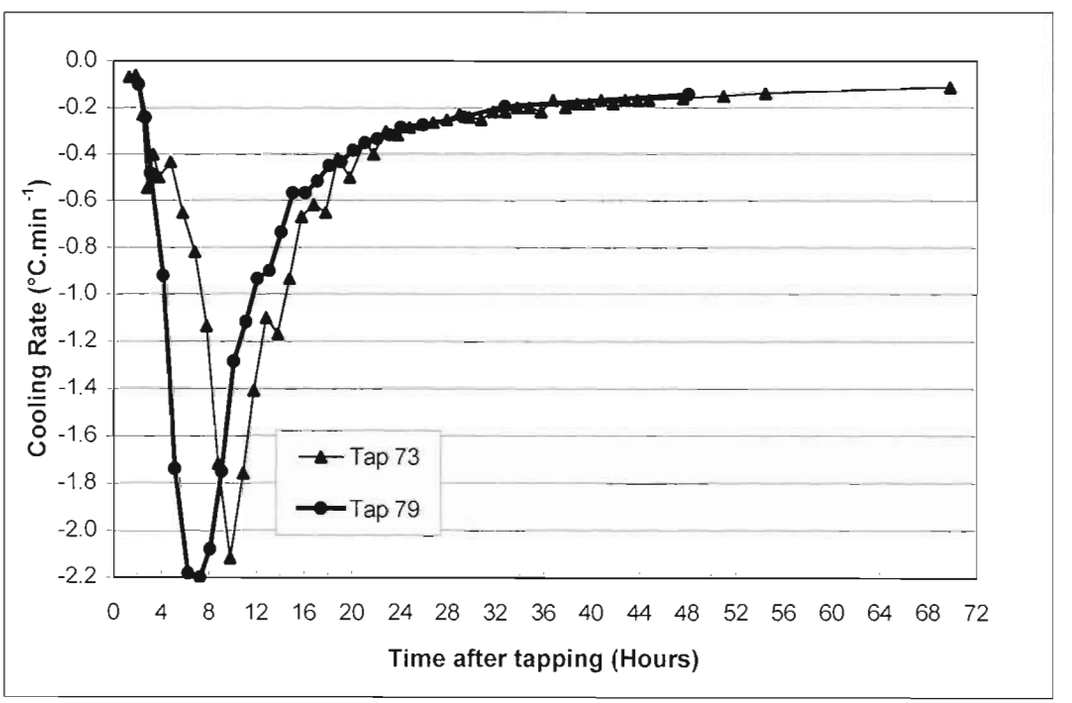

Table 33: Chemical analyses of taps 73 and 79

Tap no.	Chemical analyses (mass %)								
	SiO_2	Al_2O_3	CaO	MgO	MnO	Cr_2O_3	V_2O_5	Total Fe as FeO	Total Ti as TiO_2
73	1.62	1.33	0.26	0.94	1.25	0.11	0.46	10.90	85.94
79	1.65	1.40	0.27	1.01	1.29	0.11	0.45	9.26	87.36

Figure 63: Positioning of the thermocouple assemblages in the slag ladles for determining the cooling rate of the slag taps (not drawn to scale)

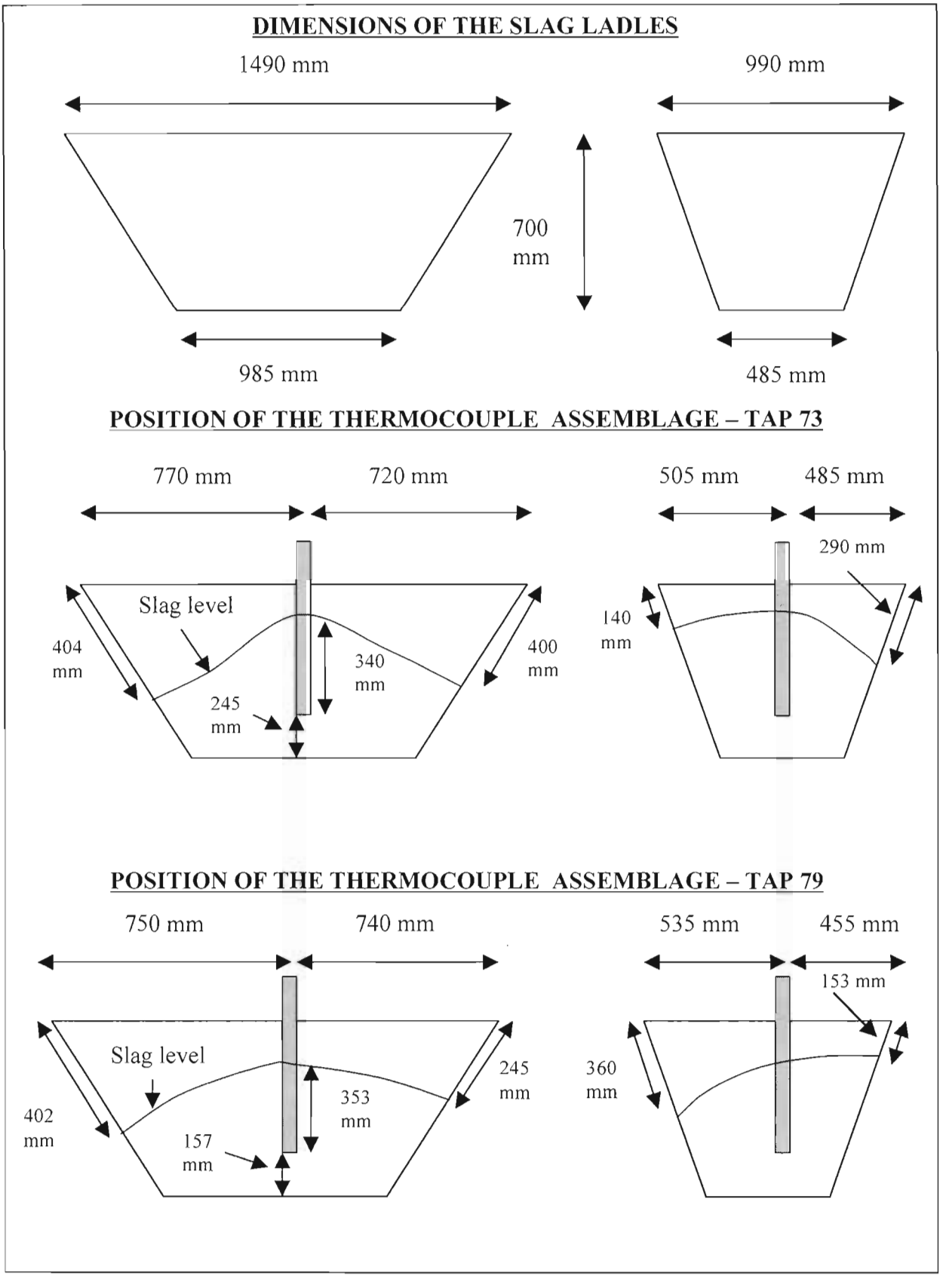

3.5.4.2 Characterisation of decrepitated slag samples from slag blocks

Decrepitated slag samples were obtained from two slag blocks, tap 68 and tap 70. Figure 64 and Figure 28 show different views of tap 68 to illustrate the effect of decrepitation on these large slag blocks. It can be seen that a substantial portion of the block had decrepitated, with the slag material crumbling away. In the background of Figure 28 a ladle can be seen of the type into which slag was tapped.

The chemical analyses of the various samples obtained from taps 68 and 70 are shown in Table 34 and Table 35. In each instance a sample obtained from the tap stream was analysed. Samples of the decrepitated material were taken after different intervals from different locations of the decrepitated slag blocks. Mössbauer analyses were also carried out on the samples (see Table 36 and Table 37). The Mössbauer results were used to calculate the Fe^{3+} content of the slags where applicable. It is apparent from the analyses that the decrepitated material had undergone some oxidation. This can be seen by the decrease of the Ti_2O_3 content of the slags over a period of time. This is illustrated clearly in Figure 65. At the lower Ti_2O_3 content levels it was found that Fe^{2+} had also started to oxidise to Fe^{3+}. This can be seen for example for sample DB155 in Table 34.

A micrograph of decrepitated sample DB157 (description and analysis given in Table 35) is shown in Figure 30. The similarities with the pellet samples treated at 400 °C is striking (see Figure 45 and Figure 46), with all the samples showing extensive cracking.

Figure 64: Front view of a slag block (tap 68) that had decrepitated

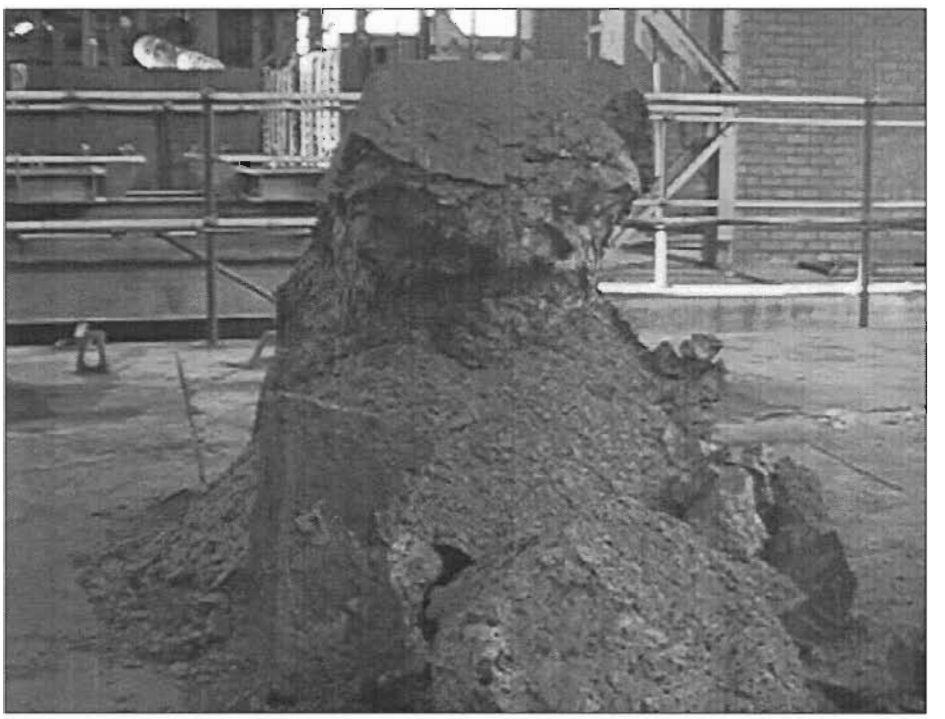

Table 34: Analyses of decrepitated slag samples taken from tap 68

Analyses no.	Origin of Sample	Analyses (mass %)													
		SiO_2	Al_2O_3	CaO	MgO	MnO	Cr_2O_3	V_2O_5	Fe^0	FeO	Fe_2O_3	TiO_2	Ti_2O_3	Total Ti as TiO_2	Insoluble TiO_2 content
DB152	Tap stream	1.76	1.64	0.24	1.02	1.40	0.09	0.42	0.39	6.83	-	48.4	36.78	89.29	0.71
DB153	Wide side of block (16.6 hours after tapping)	1.65	1.62	0.22	1.31	1.30	0.09	0.41	0.13	7.58	-	64.0	17.71	83.70	3.24
DB154	Narrow side of block (16.2 hours after tapping)	2.21	1.60	0.27	1.11	1.42	0.08	0.39	0.18	7.28	-	61.9	22.97	87.40	3.76
DB155	Narrow side of block (36.7 hours after tapping)	2.70	1.57	0.34	1.10	1.70	0.10	0.33	0.16	7.40	1.23	72.4	9.69	83.20	5.39

Table 35: Analyses of decrepitated slag samples taken from tap 70

Analyses no.	Origin of Sample	Analyses (mass %)													
		SiO_2	Al_2O_3	CaO	MgO	MnO	Cr_2O_3	V_2O_5	Fe^0	FeO	Fe_2O_3	TiO_2	Ti_2O_3	Total Ti as TiO_2	Insoluble TiO_2 content
DB156	Tap stream	1.84	1.48	0.27	1.07	1.33	0.09	0.43	0.19	9.42	-	52.0	30.92	86.40	1.04
DB157	Wide side of block (36.7 hours after tapping)	1.73	1.43	0.25	1.06	1.23	0.09	0.43	0.28	8.45	0.81	76.6	8.07	85.60	0.69

Table 36: Mössbauer analyses of the decrepitated samples taken from tap 68

Sample number	Sample origin	Hyperfine interaction parameters			Abundance (atom %)	Attribution
		Isomeric shift - δ ($mm.s^{-1}$)	Quadropole splitting - Δ ($mm.s^{-1}$)	B_{hf} (T)		
DB152	Tap stream	1.07 (3)	3.00 (5)	-	75 (5)	Fe^{2+} compound (ferropseudobrookite; site A)
		1.07 (2)	1.85 (3)	-	25 (4)	Fe^{2+} compound (ferropseudobrookite; site B)
DB153	Wide side of block (16.6 hours after tapping	1.07 (3)	3.06 (4)	-	65 (5)	Fe^{2+} compound (ferropseudobrookite; site A)
		1.03 (4)	1.90 (5)	-	35 (5)	Fe^{2+} compound (ferropseudobrookite; site B)
DB154	Narrow side of block (16.2 hours after tapping)	1.08 (2)	3.0 (2)	-	62 (4)	Fe^{2+} compound (ferropseudobrookite; site A)
		1.04 (3)	1.90 (5)	-	38 (5)	Fe^{2+} compound (ferropseudobrookite; site B)
DB155	Narrow side of block (36.7 hours after tapping)	1.07 (2)	3.08 (2)	-	41 (4)	Fe^{2+} compound (ferropseudobrookite; site A)
		1.00 (3)	2.0 (5)	-	46 (5)	Fe^{2+} compound (ferropseudobrookite; site B)
		0.49 (3)	0.68 (2)	-	13 (3)	Fe^{3+} compound (pseudobrookite)

Errors are quoted as percentage (in parenthesis)

Table 37: Mössbauer analyses of the decrepitated samples taken from tap 70

Sample number	Sample origin	Hyperfine interaction parameters			Abundance (atom %)	Attribution
		Isomeric shift - δ ($mm.s^{-1}$)	Quadropole splitting - Δ ($mm.s^{-1}$)	B_{hf} (T)		
DB156	Tap stream	1.08 (2)	3.03 (3)	-	82 (5)	Fe^{2+} compound (ferropseudobrookite; site A)
		1.04 (3)	2.0 (5)	-	15 (5)	Fe^{2+} compound (ferropseudobrookite; site B)
		0.49 (3)	0.68 (2)	-	3 (3)	Fe^{3+} compound (pseudobrookite)
DB157	Wide side of block (36.7 hours after tapping	1.07 (2)	3.0 (2)	-	65 (5)	Fe^{2+} compound (ferropseudobrookite; site A)
		1.04 (2)	1.69 (3)	-	27 (3)	Fe^{2+} compound (ferropseudobrookite; site B)
		0.49 (3)	0.68 (2)	-	8 (5)	Fe^{3+} compound (pseudobrookite)

Errors are quoted as percentage (in parenthesis)

Figure 65: The Ti_2O_3 content of decrepitated campaign slag samples taken at various times

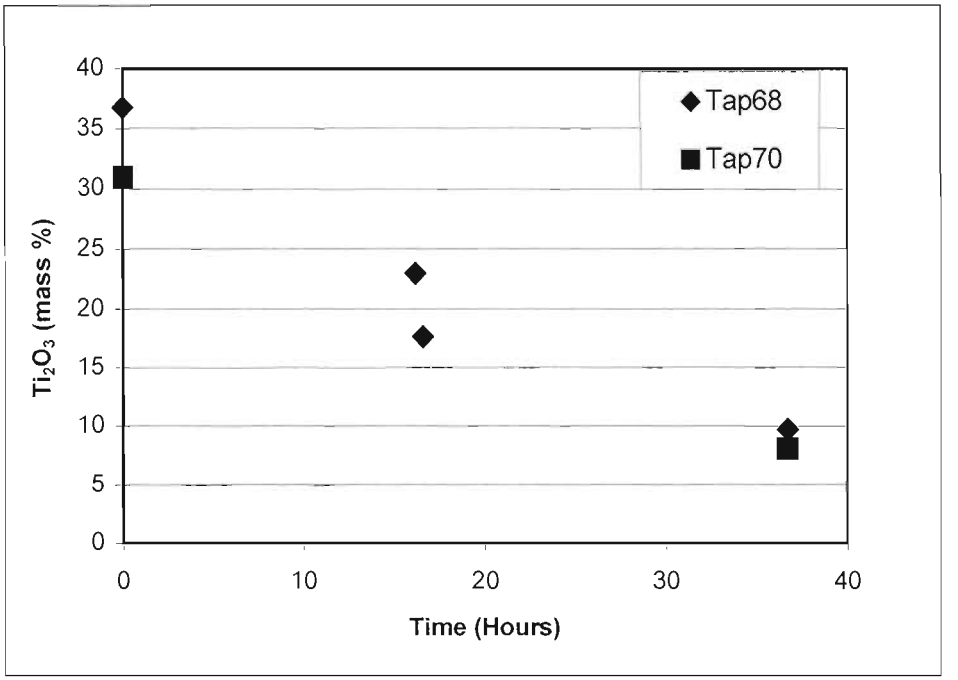

The insoluble TiO_2 content of the decrepitated samples was also analysed. These results give an indication of the insoluble content of the slag for the sulphate processing route. The maximum insoluble content specification for the sulphate processing route is 4 per cent. For tap 68 the insoluble content increases as the slag is oxidised, with a value of 5.4 per cent obtained for the most oxidised sample. For tap 70 this relationship is not apparent, with the oxidised slag having a slightly lower value than the starting slag.

The Mössbauer results also show that the distribution of iron in the A and B sites of the structure changes from the starting material to the decrepitated material. This can be seen in Table 36, where 75 per cent of the iron for the tap stream sample (DB152) is in the A site, with the remainder in the B site. For decrepitated sample DB154 it can be seen that only 62 per cent of the iron now resides in the A site, while 38 per cent of the iron is in the B site.

X-ray diffraction patterns of the various decrepitated samples obtained during the smelting campaign are given in Appendix N. Once again it can be seen from the patterns that the decrepitated slag samples appear more amorphous that the starting materials. As with the small-scale testwork it is again observed that the intensity of the peak at approximately 32.5 degrees decreases relative to the intensity of the peak at a 2θ-value of approximately 25.5 degrees. This is shown in Table 38 and Table 39 for taps 68 and 70 respectively. Also noticeable from the X-ray diffraction patterns is the appearance of the broad peak at a 2θ-value of approximately 21 to 22 degrees for the decrepitated samples. This is especially noticeable for sample DB157.

This is similar to the results obtained for the pellet samples treated at 400 °C, where it was postulated that the disappearance of the M_3O_5 phase is associated with the formation of a

M_6O_{11} phase. Based on these results it therefore appears that the small-scale testwork gives similar results to that obtained in the campaign testwork.

Table 38: A summary of the relative peak intensities for the decrepitated slag samples obtained during the campaign from tap 68

Sample no.	Description	2θ-value (degrees)	Intensity of the peak at a 2θ-value of ~ 25.5 degrees	2θ-value (degrees)	Intensity of the peak at a 2θ-value of ~ 32.5 degrees	$I_{2\theta=32.5}/I_{2\theta=25.5}$
DB152	Tap stream	25.2	543.3	32.4	274.7	0.506
DB153	Wide side of block (16.6 hours after tapping)	25.3	400.3	32.4	130.7	0.327
DB154	Narrow side of block (16.2 hours after tapping)	25.2	425.7	32.3	148.7	0.349
DB155	Narrow side of block (36.7 hours after tapping)	25.4	373.3	32.3	53.4	0.143

Table 39: A summary of the relative peak intensities for the decrepitated slag samples obtained during the campaign from tap 70

Sample no.	Description	2θ-value (degrees)	Intensity of the peak at a 2θ-value of ~ 25.5 degrees	2θ-value (degrees)	Intensity of the peak at a 2θ-value of ~ 32.5 degrees	$I_{2\theta=32.5}/I_{2\theta=25.5}$
DB156	Tap stream	25.2	466.4	32.4	256.0	0.549
DB157	Wide side of block (36.7 hours after tapping)	25.4	447.6	32.3	68.0	0.152

Sieve analyses of grab samples taken from the two decrepitated slag blocks (taps 68 and 70) were carried out to get an indication of the size distribution of the decrepitated material. The size distribution results are shown in Table 40 and Figure 66. Approximately 25 per cent of the samples was smaller than 106 µm in size. This is an unacceptably high value. The reason for that is that a size fraction of less than 106 µm is not acceptable for the chloride process for the production of pigment, but only for the sulphate processing route. After the slag cooling process, the slag also undergoes a crushing and milling process. During this process it can be expected that the decrepitated material will be milled finer still, thereby compounding the problem.

The chemical and Mössbauer analyses of two size fractions from tap 68 (see Table 40) are given in Table 41 and Table 42 respectively. These results seem to indicate that the –106 µm size fraction had undergone more change. This is indicated by the slightly lower Ti^{3+} analysis,

as well as the greater disorder of the iron atoms in the various sites as determined by the Mössbauer analysis.

Table 40: Size distribution of decrepitated slag samples obtained from two slag blocks

Sieve fraction (μm)	Tap 68		Tap 70	
	Mass (g)	Percentage (%)	Mass (g)	Percentage (%)
+2000	37.3	4.2	15.1	2.1
-2000+1180	12.2	1.4	4.9	0.7
-1180+850	68.0	7.7	11.2	1.6
-850+600	111.5	12.7	51.6	7.3
-600+425	114.6	13.0	73.9	10.5
-425+300	94.1	10.7	82.2	11.7
-300+212	107.4	12.2	102.6	14.6
-212+150	77.7	8.8	77.5	11.0
-150+106	73.3	8.3	75.0	10.7
-106	185.2	21.0	209.9	29.8
Total	**881.3**	**100.0**	**703.9**	**100.0**

Figure 66: Size distribution of decrepitated slag

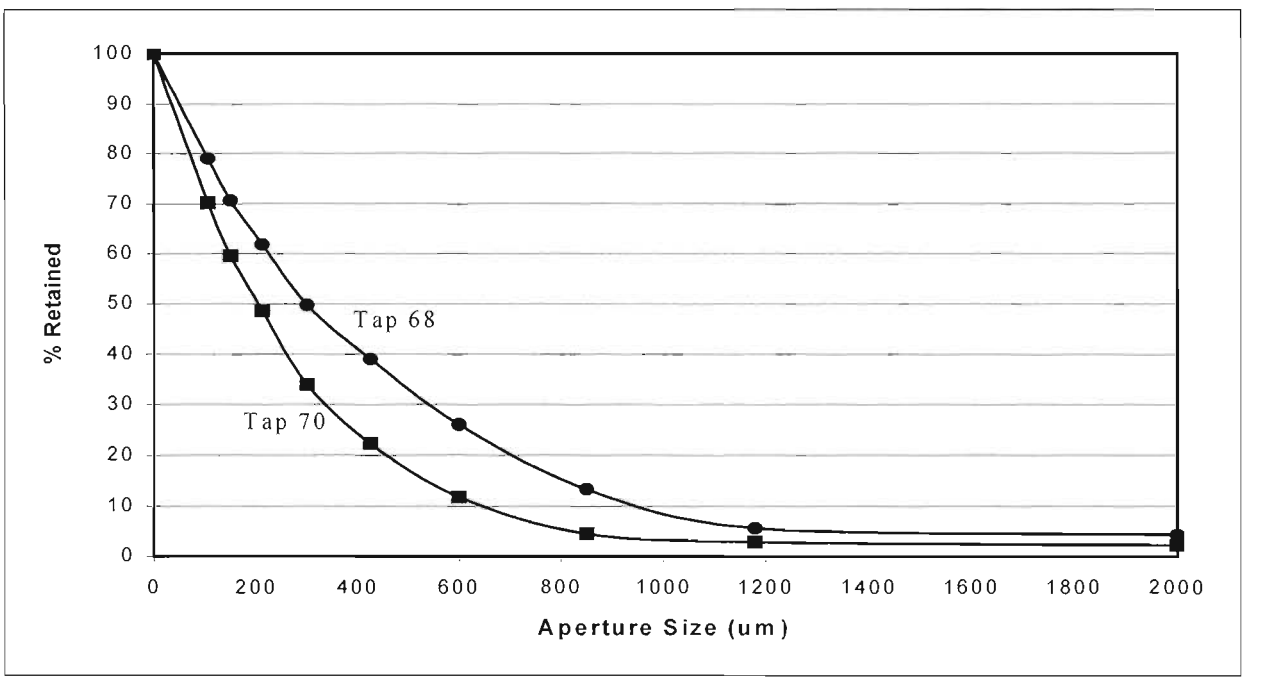

The specific density of some of the decrepitated samples was also determined. Details of these results are shown in Appendix O, with a summary of the results given in Table 43. The estimated uncertainty was based on the following errors:

- The reproducibility of the instrument.
- The sample mass, with a lower sample mass having a larger error.
- The temperature at which the density determinations were carried out.
- The particle size of the samples.

Table 41: Analyses of selected samples obtained from the size distribution analyses shown in Table 40

Analyses no.	Origin of Sample	Analyses (mass %)												
		SiO_2	Al_2O_3	CaO	MgO	MnO	Cr_2O_3	V_2O_5	Fe^0	FeO	Fe_2O_3	TiO_2	Ti_2O_3	Total Ti as TiO_2
DB152	Tap stream	1.76	1.64	0.24	1.02	1.40	0.09	0.42	0.39	6.83	-	48.4	36.78	89.29
DB175	Tap 68, -850+600 µm size fraction	3.24	1.51	0.44	0.87	1.77	0.10	0.30	<0.1	7.63	1.05	76.67	5.76	83.07
DB178	Tap 68, -106 µm size fraction	2.00	1.57	0.28	1.07	1.75	0.10	0.38	<0.1	7.49	2.35	81.92	4.18	86.57

Table 42: Mössbauer analyses of two size fractions obtained from the size distribution analyses shown in Table 40

Sample number	Sample origin	Hyperfine interaction parameters			Abundance (atom %)	Attribution
		Isomeric shift - δ ($mm.s^{-1}$)	Quadropole splitting - Δ ($mm.s^{-1}$)	B_{hf} (T)		
DB152	Tap stream	1.07 (3)	3.00 (5)	-	75 (5)	Fe^{2+} compound (ferropseudobrookite; site A)
		1.07 (2)	1.85 (3)	-	25 (4)	Fe^{2+} compound (ferropseudobrookite; site B)
DB175	Tap 68, -850+600 µm size fraction	1.07 (3)	3.07 (4)	-	62 (5)	Fe^{2+} compound (ferropseudobrookite; site A)
		1.01 (4)	1.85 (5)	-	27 (5)	Fe^{2+} compound (ferropseudobrookite; site B)
		0.30 (2)	0.87 (3)	-	11 (5)	Fe^{3+} compound (pseudobrookite)
DB178	Tap 68, -106 µm size fraction	1.07 (2)	3.04 (3)	-	39 (5)	Fe^{2+} compound (ferropseudobrookite; site A)
		1.07 (3)	2.03 (5)	-	39 (5)	Fe^{2+} compound (ferropseudobrookite; site B)
		0.27 (3)	0.80 (2)	-	22 (3)	Fe^{3+} compound (pseudobrookite)

Errors are quoted as percentage (in parenthesis)

Although the results are not statistically significant based on the estimated uncertainty, there does however seem to be a general trend. Both decrepitated samples DB155 and DB157 seem to have lower densities than their respective starting materials (DB152 and DB156). It is also noticeable that the finer size fraction (DB178) has a lower density than the coarser size fraction. These results do seem to indicate that the decrepitation of titania slag is associated with a change in the density of the slag (and therefore also the volume).

Table 43: Comparison of the densities of decrepitated samples with their respective starting materials

Sample no.	Sample description	Average Density ($g.cm^{-3}$)	Estimated uncertainty ($g.cm^{-3}$)
DB152	Tap stream - tap 68	3.9546	0.028
DB155	Narrow side of block – tap 68 (36.7 hours after tapping)	3.9432	0.092
DB156	Tap stream - tap 70	3.9670	0.028
DB157	Wide side of block – tap 70 (36.7 hours after tapping	3.9397	0.047
DB175#	Tap 68, -850+600 µm size fraction	3.9403	0.028
DB178#	Tap 68, -106 µm size fraction	3.9266	0.028

- Samples obtained from size distribution analyses as shown in Table 40.

3.6 GENERAL COMMENTS, CONCLUSIONS AND RECOMMENDATIONS

From the results obtained in this study it appears that the samples treated at 400 °C had the largest propensity to decrepitate. This propensity to decrepitate decreased markedly with an increase in temperature, with samples treated at 600 °C and higher temperatures showing minimal to no signs of decrepitation. It was found that the microstructure of decrepitated slag samples produced on a laboratory scale were similar to that of the samples obtained from the large-scale slag blocks.

A potential mechanism for the decrepitation of the high titania slags mentioned initially is the possibility of a polymorphic phase change of one of the phases present in the slag. It is for example known that Ti_3O_5 undergoes a reversible phase transformation at 190 °C (Grey and Ward, 1973). In various samples produced by Haggerty and Lindsley (1970) crystals in the pseudobrookite field frequently showed a tendency to form a rim with a lower reflectivity compared to the core. No variation in the iron and titanium concentration was found across the core and the rim in their study. The investigators therefore inferred that the rim represented a quenched polymorphic inversion product of pseudobrookite.

From the results obtained in this study, it seems that a more likely explanation for the decrepitation behaviour is the observed changes in the phase assemblages at temperatures below 600 °C.

As discussed previously, Vasyutinskiy (1968) found that a distortion of the M_3O_5 crystal lattice occurred on oxidation of the slag samples at temperatures of approximately 400 °C. The X-ray diffraction data of Teller et. al. (1990, pp. 351-367) for their samples after heating

also shows distortion of the M_3O_5 crystal structure. The Mössbauer results obtained in this study tend to confirm the idea that the crystal structure of the M_3O_5 phase found in the starting material changes when heated at 400 °C (see Table 27 for results). The Mössbauer spectra shown in Appendix C for example illustrates the differences in the Mössbauer spectra for the starting slag (DB100) and for the pellet sample treated for 384 hours at 400 °C (DB125). The X-ray diffraction results of the severely decrepitated samples indicate the presence of a M_6O_{11} phase. Anatase was also found to be present in these samples. These phases were also previously found by Grey, Cranswick, et. al. (2000) for $Mg_{0.3}Ti_{2.7}O_5$ samples oxidised at these low temperatures. They stated that oxidation of their samples produced new phases of general composition based on unit cell intergrowth of M_3O_5 and anatase structural elements. The structural homogeneity was restricted to regions of approximately 100 to 200 Å, due to the low driving force for ordering at these temperatures. It can be assumed that the decrepitation of the samples at the temperatures below 600 °C is caused by the formation of the large number of cracks observed in these samples. It is postulated that these cracks are formed due to volume changes on formation of these new M_nO_{2n-1} phases. Unfortunately no information was found on the volume changes associated with the oxidation of M_3O_5 to M_6O_{11}. From the density data in Table 43 it seems that the decrepitated material has a lower density, and therefore a higher volume, than that of the starting materials which only contain the M_3O_5 phase.

Based on the above conclusions from this study the question can be asked as to why these M_nO_{2n-1} phases only seem to form at temperatures below 600 °C. This is an aspect for further investigation. The following thoughts suggest that this might be due to kinetic limitations at these low temperatures:

- From the isothermal Fe-Fe_2O_3-TiO_2 phase diagrams presented by Borowiec and Rosenqvist (1981) it was concluded for temperatures as low as 650 °C, Fe_2TiO_5 and TiO_2 should be the phases attained at equilibrium for the oxidation of titania slag (see for example Figure 35 for the diagram at 650 °C). No data was however available at lower temperatures.
- As discussed earlier (see reaction (M)) it is also well known that Fe_2TiO_5 decomposes at 585 °C to form Fe_2O_3 and TiO_2 (Haggerty and Lindsley, 1970). This is also illustrated in Figure 37 for the Ti_3O_5-Fe_2TiO_5 system. It can therefore be suggested that at low temperatures the equilibrium phases after complete oxidation of titania slag should be M_2O_3 and TiO_2 phases. From the data of Haggerty and Lindsley (1970) this should be at a temperature of below 585 °C. As seen earlier the effect of impurities on the stability of the M_3O_5 phase probably plays a significant role in the determination of this decomposition temperature.
- For sample DB125 it was however found that this "equilibrium" is not attained after heating the particular pellet sample for 16 days at 400 °C in air. This is indicated by the presence of Ti^{3+} and Fe^{2+} in the bulk phase as found from data from the elemental analyses and Mössbauer data for this sample. From the X-ray diffraction results M_6O_{11} and anatase are the major phases present.
- At temperatures above 600 °C the expected equilibrium phases are different, with ferric pseudobrookite and TiO_2 to be expected. After heating samples for 16 days at temperatures of 800 and 1000 °C these were indeed found to be the main phases present. At 600 °C rutile and anatase was identified as the main phases present, with the M_3O_5 phase almost completely disappearing.

From the temperature measurements of the slag blocks during cooling it was established that from tapping, the slag blocks took approximately 18 to 24 hours to cool down to 550 °C (see

Figure 61). To cool down from 550 to 200 °C approximately another 30 hours was required, providing ample time for partial oxidation of the slag. It also seems that when decrepitation of the slag at these temperatures is initiated, the decrepitated material breaks off from the block, thereby exposing fresh slag to the atmosphere for further oxidation.

An aspect that warrants further investigation is the effect of the chemistry of the starting slag on the decrepitation of the slag. It seems from the results of this study that the propensity to decrepitate decreases with an increase in the FeO content of the slag and a decrease of the Ti_2O_3 content of the slag. The reason for this is not understood at this stage.

Another aspect that warrants further work is the application of Mössbauer spectroscopy in understanding the transformations that occur. In this study the data obtained on the decrepitated slags was modeled as having a pseudobrookite structure. In some instances the X-ray diffraction results showed that the M_3O_5 phase had disappeared, with a M_6O_{11} phase forming. The interpretation of the Mössbauer data in the light of the X-ray diffraction data therefore needs to be confirmed. It is still possible that the Mössbauer data is applicable, as the local environment of the iron atoms in the two phases could be similar. Another interesting aspect that was noted with the Mössbauer investigations was the increase in the line width from the starting materials to that of the decrepitated material. According to Hearne (2000) this can probably be ascribed to increasing disorder in the structure of the M_3O_5 phase. This was however not followed up in this study.

4 ACKNOWLEDGEMENTS

The author would like to make the following acknowledgements:

- Professors Kobus Geldenhuis and Chris Pistorius for their inputs and encouragement during the study.
- Corelie Visser and Leonie Reyneke with their assistance with X-ray diffraction and mineralogical investigations.
- Dr. Giovanni Hearne and Dr. Antoine Mulaba for carrying out the Mössbauer spectroscopy.
- Dr. Villie Viljoen and co-workers for carrying out the electron microprobe analyses.
- Professor Johan de Villiers and Dr. Johan Nell for interesting and useful discussions.
- Iscor for providing me with the opportunity to do this study.
- The Innovation fund (Project no. 32215) of the South African Department of Arts, Culture, Science and Technology for partial funding of the project.
- My family (Robyn, Mark and Gail) for their patience and support over the last couple of months while I was completing the study.

5 REFERENCES

Akimoto S., Nagata T. and Katsura T. "The $TiFe_2O_5$-Ti_2FeO_5 solid solution series", *Nature, Vol. 179, No. 4549, 5 January 1957, pp. 37-38.*

Anderson A.T., Bunch T.E., Cameron E.N., Haggerty S.E., Boyd F.R. Finger L.W., James O.B., Keil K., Prinz M., Ramdohr P. and El Goresy A. "Armalcolite: A new mineral from the Apollo 11 samples", *Proceedings of the Apollo 11 Lunar Science Conference, Vol. 1, 1970, pp.55-63.*

5 REFERENCES

Akimoto S., Nagata T. and Katsura T. "The $TiFe_2O_5$-Ti_2FeO_5 solid solution series", *Nature, Vol. 179, No. 4549, 5 January 1957, pp. 37-38.*

Anderson A.T., Bunch T.E., Cameron E.N., Haggerty S.E., Boyd F.R. Finger L.W., James O.B., Keil K., Prinz M., Ramdohr P. and El Goresy A. "Armalcolite: A new mineral from the Apollo 11 samples", *Proceedings of the Apollo 11 Lunar Science Conference, Vol. 1, 1970, pp.55-63.*

Anonymous "South Africa will remain world's leading slag producer", *South African Mining: Coal, Gold and Base Minerals, Sept 1997, p. 25.*

Anonymous "Namakwa Sands embarks on Phase 2", *South African Mining: Coal, Gold and Base Minerals, February 1998, p. 19.*

Ban B-C. "Reduction and melting of Quilon ilmenite in the DC arc furnace", *Erzmetall, 41(5), 1988, pp. 278-284 (Iscor translation Service 94-06-454).*

Ban B. Ch., Heil J., Krone K., Krüger J. and Lüderitz E. "Upgrading titaniferrous materials by DC arc smelting and processing of products in a plasma heated fluidized bed reactor", *Sixth world conference on titanium, France 1988, pp. 685-695.*

Battle T.P., Nguyen D. and Reeves J.W. "The processing of titanium-containing ores", *Extractive Metallurgy of Copper, Nickel and Cobalt. Vol. 1: Fundamental Aspects, Denver, Colorado. Reddy R.G. and Weizenbach R.N. (ed.). The Minerals, Metals and Materials Society, Warrendale, Pennsylvania, 1993, pp. 925-943.*

Borowiec K. "Sulphidization of solid titania slag", *Scandinavian Journal of Metallurgy, 20, 1991, pp. 198-204.*

Borowiec K. and Rosenqvist T. "Phase relations and oxidation studies in the system Fe-Fe_2O_3-TiO_2 at 700-1100 °C", *Scandinavian Journal of Metallurgy, 10, 1981, pp. 217-224.*

Borowiec K. and Rosenqvist T. "Phase relations and oxygen potentials in the Fe-Ti-Mg-O system", *Scandinavian Journal of Metallurgy, 14, 1985, pp. 33-43.*

Bowles J.F.W. "Definition and range of composition of naturally occurring minerals with the pseudobrookite structure", *American Mineralogist, Vol. 73, 1988, pp. 1377-1383 and references contained there-in.*

Brown N.E. and Navrotsky A. "Structural, thermodynamic, and kinetic aspects of disordering in the pseudobrookite-type compound karrooite, $MgTi_2O_5$", *American Mineralogist, Vol. 74, 1989, pp. 902-912.*

Desrosiers R., Ajersch F. and Grau A. "Electrical conductivity of industrial slags of high titania content", *International symposium on metallurgical slags; Halifax, Nova Scotia. 24-27 August 1980.*

Du Plooy H. "Melting point determinations on TiO_2-rich slags", *M.Eng Dissertation, University of Pretoria. 1997.*

Eriksson G. and Pelton A.D. "Critical evaluation and optimization of the thermodynamic properties and phase diagrams of the MnO-TiO_2, MgO-TiO_2, FeO-TiO_2, Ti_2O_3-TiO_2, Na_2O-TiO_2 and K_2O-TiO_2 systems", *Metallurgical Transactions B, Vol. 24B, 1993, pp. 795-805.*

FACT Thermodynamic database. http://www.crct.polymtl.ca/fact/fact.htm, October 2000.

Fisher J.R. "Developments in the TiO_2 pigments industry which will drive the demand for TiO_2 mineral feedstocks", *Heavy Minerals 1997. Johannesburg, South African Institute of Mining and Metallurgy, 1997, pp.207-218.*

Formanek L., Lommert H. and Beyzavi A.N. "Synthetic rutile manufacture by the SL/RN-Becher process", *Heavy Minerals 1997. Johannesburg, South African Institute of Mining and Metallurgy, 1997, pp. 161-168.*

Gambogi J. "Titanium", *Minerals Yearbook, United States Geological Survey, Vol. 1 – Metals and Minerals (1998).*

Grau A.E. "Liquidus temperatures in the TiO_2-rich side of the FeO-TiO_2 system", *Canadian Metallurgical Quarterly, Vol. 18, 1979, pp. 313-321.*

Grau A. and Poggi D. "Physico-chemical properties of molten titania slags", *Metallurgical Society of CIM, Annual Volume, Incorporating Canadian Metallurgical Quarterly, vol. 17 (1-4), 1978, pp. 97-102.*

Grey I.E. "Mineral sands to materials", *Chemistry in Australia, Vol. 59, April 1992, pp. 158-161.*

Grey I.E., Cranswick L.M.D., Li C., White T.J. and Bursill L.A. "New M_3O_5-Anatase intergrowth structures formed during low-temperature oxidation of anosovite", *Journal of Solid State Chemistry, vol. 150, 2000, pp. 128-138.*

Grey I.E. and Merritt R.R. "Stability relations in the pseudobrookite solid solution $Fe_yTi_{3-y}O_5$", *J. Sol. State Chem., 37, 1981, pp. 284-293.*

Grey I.E., Reid A.F. and Jones D.G. "Reaction sequences in the reduction of ilmenite: 4 - interpretation in terms of the Fe-Ti-O and Fe-Mn-Ti-O phase diagrams", *Trans. Instn. Min. Met., 83, 1974, pp. C105-C111.*

Grey I.E. and Ward J. "An X-ray and Mössbauer study of the $FeTi_2O_5$-Ti_3O_5 system", *Journal of Solid State Chemistry, 7, 1973, pp. 300-307.*

Grzymek J. and Derdacka-Grzymek A. "Physicochemical basis of sinter-disintegration complex method of aluminium oxide and cement production", *Light Metals 1990, Anaheim, California, 18-22 Feb. 1990, Published by The Minerals, Metals & Materials Society, Warrendale, Pennsylvania, 1990, pp. 149-155.*

Gupta S.K., Rajakumar V. and Grieveson P. "Phase relations in the system Fe-Fe_2O_3-TiO_2 at 700 °C and 900 °C", *Canadian Metallurgical Quarterly, Vol. 28, No. 4, 1989, pp. 331-335.*

Habashi F. (Editor) "Handbook of Extractive Metallurgy", *WILEY-VCH, VCH Verlagsgesellschaft mbH, Weinheim, Federal Rebublic of Germany, 1997, p. 1143.*

Handfield G. and Charette G.G. "Viscosity and structure of industrial high TiO_2 slags", *Canadian Metallurgical Quarterly, Vol. 10, No. 3, 1971, pp. 235-243 and references contained there-in.*

Handfield G., Charette G.G. and Lee H.Y. "Viscosity of industrial titania slags", *Light Metals, AIME, New York, 1971, pp. 591-601*

Haggerty S.E and Lindsley D.H. "Stability of the pseudobrookite (Fe_2TiO_5) – ferropseudobrookite ($FeTi_2O_5$) series", *Carnegie Inst. Washington Yearbook, 68, 1970, pp. 247-249.*

Harada M. and Tomari M. "Method of modifying steel slag", *United States Patent No. 5 019 160, 28 May 1991.*

Hearne G., *University of the Witwatersrand, Private Communication, September 2000.*

Hölzel A.R. "Systematics of minerals", *1st Edition, Published by Mainz, 1989.*

Howell D.C. "Fundamental statistics for the behavioral sciences", *2nd Edition, PWS-KENT Publishing Company, Boston, 1989.*

Huheey J.E. "Inorganic Chemistry: Principles of Structure and Reactivity", *Third Edition, Harper & Row Publishers, New York, 1983, pp. 73-76.*

Juckes L.M. "Investigation of the connection between test results found in the laboratory on volume stability and the values found in practice for LD slags", *Commission of the European Communities – Technical Steel Research, Report No. EUR13430, 1991, 57 pages.*

Lee H.Y. and Poggi D. "Mine, mill and smelting complex at Richards Bay, South Africa", *Can. Metall. Q., 1978, 17(1-4), pp. 93-96.*

Lind M.D. and Housley R.M. "Crystallization studies of lunar igneous rocks: Crystal structure of synthetic armalcolite", *Science, 175, 4 February 1972, pp. 521-523.*

Lindsley D.H. "The crystal chemistry and structure of oxide minerals as exemplified by the Fe-Ti oxides", *Min. Soc. Amer., Reviews in Mineralogy, Vol. 3, Oxide Minerals, 1976, pp. L1-L60.*

McLoughlin B.C., Bernard N.G., Bultitude-Paull J., Franklin R., Sahajwalla V. and Moon J. "Pig iron from chemically precipitated iron oxide", *1ST ISS Australian Section Meeting Proceedings, 1998, pp. 43-50.*

Mulaba A. and Hearne G. "Mössbauer hyperfine interaction parameters of selected iron-titanium compounds and iron-oxides", *Private Communication, September 1999.*

Navrotsky A. "Thermodynamics of formation of some compounds with the pseudobrookite structure and of the $FeTi_2O_5$-Ti_3O_5 solid solution series", *American Mineralogist, vol. 60, 1975, pp. 249-256.*

Noguchi F., Nakamura T., Ueda Y. and Yanagase T. "Behaviour of phosphorus and sulphur in slag melts during CaO dissolution", *Australia/Japan Extractive Metallurgy Symposium, Sydney, Australia, 16-18 July 1980, Published by Australasian Institute of Mining and Metallurgy, Parkville, Victoria, 1980, pp. 479-486.*

Okamoto A., Futamura E. and Kawamura K. "Hydration behaviour of LD slag at autoclave test", *Trans. Iron Steel Inst. Japan, Vol. 21, No. 1, Jan. 1981, pp. 16-24.*

Pesl J. "Thermodynamics and phase equilibria in the Fe-Ti-O system at 1500 ° and 1600 °C and metal-slag equilibria pertinent to ilmenite reduction", *PhD-thesis, University of the Witwatersrand, Johannesburg, South Africa. June 1997.*

Pistorius P.C. and Coetsee C. "The relationship between FeO and Ti_2O_3 in ilmenite smelter slags", *Conference Proceedings, Sixth International conference on Molten Slags, Fluxes and Salts; Stockholm, Sweden-Helsinki, Finland; 12-17 June 2000 and references contained there-in.*

Reeves J.W. and Reeves R.G. "Misconceptions about titanium ore chlorination", *Heavy Minerals 1997. Johannesburg, South African Institute of Mining and Metallurgy, 1997, pp. 203-206.*

Reid A.F. and Ward J.C. "Solid solution in the $FeTi_2O_5$-Ti_3O_5 system", *Acta Chem. Scand., 25(4), 1971, pp. 1475-1476.*

Reznichenko V.A., Karyazin I.A., Il'yashenko S.F. and Olyunina T.V. "Metallic inclusions in high-titanium slags", *Russian Metallurgy (4), 1981, pp. 16-20.*

Schreiner W.N. and Jenkins R. "Automatically correcting for specimen displacement error during XRD search/match identification", *Advances in X-ray Analysis, Vol. 25 (Eds. J.C. Russ, C.S. Barrett, D.E. Leyden, P.K. Predecki), Plenum Publishing Co. (New York), 1982, pp. 231-236.*

Shannon R.D. and Pask J.A. "Kinetics of the Anatase-Rutile transformation", *Journal of the American Ceramics Society, Vol. 48 (No. 8), 1965, pp. 391-398 and references contained there-in.*

Shirane G., Cox D.E. and Ruby S.L. "Mössbauer study of isomer shift, quadrupole interaction, and hyperfine field in several oxides containing Fe^{57}", *Physical Review, 125(4), 1962, pp. 1158-1165.*

Skillen A. "Mineral sands – Crash of the Ti-tans", *Industrial Minerals, Aug. 1992, pp. 19-33.*

Sommerville I.D. and Bell H.B. "The behaviour of titania in metallurgical slags", *Canadian Metallurgical Quarterly, Vol. 21, No. 2, 1982, pp. 145-155.*

Stanaway K.J. "Overview of titanium dioxide feedstocks", *Mining Engineering, Dec. 1994, pp. 1367-1370.*

Stevens J.G., Khasanov A.M., Miller J.W., Pollak H. and Li Z. "Mössbauer Mineral Handbook", *Mössbauer Effect Data Center, 1998.*

Swinden D.J. and Jones D.G. "Arc-furnace smelting of Western Australia beach sand ilmenite", *Trans. Instn. Min. Metall. C, Vol. 87, 1978, pp. C83-C87.*

Teller R.G., Antonio M.R., Grau A.E., Gueguin M. and Kostiner E. "Structural analysis of metastable pseudobrookite ferrous titanium oxides with neutron diffraction and mössbauer spectroscopy", *Journal of Solid State Chemistry, 88, 1990, pp. 334-350.*

Teller R.G., Antonio M.R., Grau A.E., Gueguin M. and Kostiner E. "The chemistry of the thermal decomposition of pseudobrookite ferrous titanium oxides", *Journal of Solid State Chemistry, 88, 1990, pp. 351-367.*

Tioxide Southern Africa "Adding brightness to life", *Information leaflet obtained October 1997.*

Toromanoff I. And Habashi F. "The composition of a titanium slag from Sorel", *Journal of the Less-Common Metals, 97, 1984, pp. 317-329.*

Van Niekerk W.H., *Iscor, Private Communication, June 1995.*

Vasyutinsky N.A. "Kinetics and mechanism of the oxidation of a titanium slag", *Russian Metallurgy (4), 1968, pp. 29-34.*

Vasyutinsky N.A. and Movsesov E.E. "Oxidation and grinding of titanium slag", *Russian Metallurgy (1), 1965, PP. 56-57.*

Virgo D. and Huggins F.E. "Cation distributions in some compounds with the pseudobrookite structure", *Carnegie Institution of Washington Year Book, vol. 74, 1975, pp. 585-590.*

Webster A.H. and Bright N.F.H. "The system iron-titanium-oxygen at 1200 °C and oxygen partial pressures between 1 atm. and $2x10^{-14}$ atm.", *J. Am. Ceram. Soc., 44, 1961, pp. 110-116.*

Wechsler B.A., Prewitt C.T. and Papike J.J. "Chemistry and structure of lunar and synthetic armalcolite", *Earth and Planetary Science Letters, 29, 1976, pp. 91-103.*

Appendix A: Data obtained from Grau and Poggi used for calculation of equations and in figures

Table 44: Chemical analyses of Sorel slags (measured from Figure 2 in Grau and Poggi, 1978)

Equivalent TiO_2 [Total Ti expressed as TiO_2] (mass %)	FeO (mass %)	Ti_2O_3 (mass %)
69.1	14.5	15.2
69.1	15.5	16.5
71.6	13.1	16.8
71.6	13.3	17.7
72.2	12.0	17.6
73.2	12.7	17.3
73.6	10.5	21.4
74.4	10.9	22.5
74.5	9.6	19.9
75.6	8.9	24.2
75.8	8.9	19.9
77.5	9.3	27.3
79.0	6.9	29.4

Appendix B: Normalised elemental phase analyses results of various samples

- **Sample DB100 (Sample from tap stream) – Point analyses of the M_3O_5 phase (2 µm intervals)**

	Analysis (mass per cent)											
	Mg	Al	Zr	V	Mn	O	Ti	Fe	Cr	Si	Ca	S
Analysis 1	0.92	0.47	0.24	0.20	0.36	35.01	55.85	6.86	0.06	0.01	0.01	0.01
Analysis 2	1.15	0.43	0.35	0.21	0.34	34.93	55.71	6.78	0.07	0.03	0.00	0.00
Analysis 3	0.44	0.47	0.21	0.23	0.33	35.10	56.30	6.85	0.07	0.00	0.00	0.01
Analysis 4	1.11	0.37	0.32	0.21	0.34	35.17	55.61	6.80	0.06	0.00	0.01	0.00
Analysis 5	0.81	0.40	0.18	0.24	0.34	35.16	55.92	6.87	0.06	0.00	0.01	0.02
Analysis 6	1.27	0.44	0.30	0.22	0.34	34.62	55.90	6.83	0.06	0.01	0.00	0.01
Analysis 7	0.54	0.39	0.26	0.23	0.33	35.99	55.47	6.66	0.06	0.05	0.01	0.01
Analysis 8	0.77	0.43	0.21	0.27	0.34	36.56	54.84	6.50	0.06	0.03	0.01	0.01
Analysis 9	0.85	0.39	0.20	0.25	0.34	36.33	54.32	7.24	0.06	0.01	0.00	0.01
Analysis 10	1.12	0.54	0.29	0.27	0.33	36.38	54.40	6.60	0.06	0.01	0.00	0.00
Analysis 11	0.42	0.44	0.28	0.28	0.37	36.25	55.18	6.72	0.05	0.00	0.01	0.01
Analysis 12	0.85	0.38	0.13	0.27	0.34	35.39	55.82	6.74	0.06	0.01	0.01	0.00
Analysis 13	0.64	0.45	0.28	0.25	0.35	35.22	55.86	6.88	0.06	0.00	0.01	0.01
Analysis 14	0.45	0.48	0.22	0.26	0.37	35.15	56.12	6.87	0.06	0.01	0.01	0.01
Average	0.81	0.43	0.25	0.24	0.34	35.52	55.52	6.80	0.06	0.01	0.01	0.01
Standard Deviation	0.28	0.05	0.06	0.03	0.01	0.64	0.61	0.17	0.00	0.01	0.00	0.00

Calculated composition (normalising O to 5): $Mg_{0.07}Al_{0.04}V_{0.01}Mn_{0.01}Ti_{2.61}Fe_{0.27}O_5$ ($M_{3.01}O_5$)

- **Sample DB152 (Sample from tap stream) – Point analyses of the M_3O_5 phase**

	Analysis (mass per cent)											
	Mg	Al	Zr	V	Mn	O	Ti	Fe	Cr	Si	Ca	S
Analysis 1	0.12	1.01	0.06	0.13	0.23	35.70	60.97	1.75	0.02	0.00	0.00	0.00
Analysis 2	1.06	1.20	0.09	0.12	0.21	35.20	60.33	1.77	0.02	0.00	0.00	0.00
Analysis 3	0.78	1.06	0.08	0.13	0.22	35.35	60.55	1.80	0.02	0.00	0.00	0.00
Analysis 4	1.26	1.13	0.09	0.14	0.26	35.36	60.19	1.54	0.03	0.00	0.00	0.00

Analysis 5	1.26	1.07	0.14	0.14	0.25	35.54	60.03	1.53	0.03	0.00	0.00	0.00
Analysis 6	0.85	1.02	0.13	0.17	0.23	35.55	60.48	1.54	0.02	0.00	0.00	0.00
Analysis 7	0.07	0.93	0.05	0.17	0.23	36.23	60.73	1.55	0.02	0.00	0.00	0.00
Average	0.77	1.06	0.09	0.14	0.23	35.56	60.47	1.64	0.02	0.00	0.00	0.00
Standard Deviation	0.50	0.09	0.03	0.02	0.02	0.34	0.32	0.13	0.00	0.00	0.00	0.00

Calculated composition (normalising O to 5): $Mg_{0.07}Al_{0.09}V_{0.01}Mn_{0.01}Ti_{2.84}Fe_{0.07}O_5$ ($M_{3.09}O_5$)

- **Sample DB156 (Sample from tap stream) – Point analyses of the M_3O_5 phase**

	Analysis (mass per cent)											
	Mg	Al	Zr	V	Mn	O	Ti	Fe	Cr	Si	Ca	S
Analysis 1	0.79	1.09	0.08	0.18	0.52	34.84	55.62	6.83	0.05	0.00	0.01	0.00
Analysis 2	1.04	1.15	0.12	0.24	0.40	34.96	56.00	6.03	0.04	0.00	0.01	0.00
Analysis 3	0.49	1.07	0.09	0.21	0.39	35.64	56.17	5.90	0.04	0.00	0.01	0.00
Analysis 4	0.76	0.98	0.16	0.19	0.38	35.42	57.21	4.84	0.04	0.00	0.00	0.00
Analysis 5	0.19	1.05	0.07	0.24	0.38	35.74	57.27	5.01	0.04	0.00	0.01	0.00
Analysis 6	0.00	1.13	0.11	0.29	0.26	35.99	57.71	4.49	0.02	0.00	0.00	0.00
Average	0.54	1.08	0.10	0.22	0.39	35.43	56.66	5.52	0.04	0.00	0.01	0.00
Standard Deviation	0.40	0.06	0.03	0.04	0.08	0.45	0.84	0.88	0.01	0.00	0.00	0.00

Calculated composition (normalising O to 5): $Mg_{0.05}Al_{0.08}V_{0.01}Mn_{0.01}Ti_{2.65}Fe_{0.20}O_5$ ($M_{3.00}O_5$)

- **Sample DB105 (Pellet treated at 800 °C for 384 hours) – Point analyses of the rim phase**

	Analysis (mass per cent)											
	Mg	Al	Zr	V	Mn	O	Ti	Fe	Cr	Si	Ca	S
Analysis 1	0.29	0.32	0.02	0.13	0.56	31.04	12.87	54.75	0.01	0.00	0.03	0.00

Calculated composition (normalising O to 3): $Mg_{0.02}Al_{0.02}V_{0.00}Mn_{0.02}Ti_{0.42}Fe_{1.52}O_3$ ($M_{2.00}O_3$)

- **Sample DB115 (Pellet treated at 600 °C for 24 hours) – Point analyses of the core region**

	Analysis (mass per cent)											
	Mg	Al	Zr	V	Mn	O	Ti	Fe	Cr	Si	Ca	S
Analysis 1	0.89	0.61	0.04	0.30	0.26	35.05	56.94	5.86	0.04	0.00	0.00	0.00
Analysis 2	1.12	0.54	0.06	0.28	0.22	35.02	56.79	5.93	0.04	0.00	0.00	0.00

Analysis 3	1.70	0.69	0.07	0.29	0.18	34.67	56.52	5.84	0.04	0.00	0.00	0.00
Analysis 4	1.14	0.68	0.09	0.31	0.20	34.87	56.79	5.87	0.04	0.00	0.00	0.00
Average	1.21	0.63	0.07	0.29	0.22	34.90	56.76	5.87	0.04	0.00	0.00	0.00
Standard Deviation	0.34	0.07	0.02	0.01	0.04	0.17	0.18	0.04	0.00	0.00	0.00	0.00

Calculated composition (normalising O to 5): $Mg_{0.10}Al_{0.05}V_{0.01}Mn_{0.01}Ti_{2.69}Fe_{0.21}O_5$ ($M_{3.07}O_5$)

- **Sample DB115 (Pellet treated at 600 °C for 24 hours) – Point analyses of the mantle zone**

	Analysis (mass per cent)											
	Mg	Al	Zr	V	Mn	O	Ti	Fe	Cr	Si	Ca	S
Analysis 1	0.84	0.44	0.12	0.37	0.24	38.52	58.60	0.82	0.03	0.00	0.01	0.00
Analysis 2	1.49	0.41	0.11	0.38	0.25	38.30	58.38	0.63	0.03	0.00	0.01	0.00
Analysis 3	0.45	0.54	0.07	0.40	0.23	38.98	58.43	0.85	0.05	0.00	0.01	0.00
Average	0.92	0.47	0.10	0.39	0.24	38.60	58.47	0.76	0.04	0.00	0.01	0.00
Standard Deviation	0.53	0.07	0.03	0.02	0.01	0.34	0.12	0.12	0.01	0.00	0.00	0.00

Calculated composition (normalising O to 2): $Mg_{0.03}Al_{0.01}V_{0.01}Mn_{0.00}Ti_{1.01}Fe_{0.01}O_2$ ($M_{1.07}O_2$)

- **Sample DB115 (Pellet treated at 600 °C for 24 hours) – Point analyses of the rim phase**

	Analysis (mass per cent)											
	Mg	Al	Zr	V	Mn	O	Ti	Fe	Cr	Si	Ca	S
Analysis 1	0.63	1.55	0.07	0.06	0.11	30.42	4.14	62.83	0.01	0.13	0.01	0.03
Analysis 2	0.09	0.92	0.00	0.05	0.32	29.04	2.72	66.81	0.01	0.00	0.01	0.04
Average	0.36	1.23	0.04	0.05	0.22	29.73	3.43	64.82	0.01	0.06	0.01	0.04
Standard Deviation	0.39	0.45	0.05	0.01	0.15	0.98	1.00	2.81	0.00	0.09	0.00	0.01

Calculated composition (normalising O to 3): $Mg_{0.02}Al_{0.06}V_{0.00}Mn_{0.01}Ti_{0.29}Fe_{1.64}O_3$ ($M_{2.02}O_3$)

- **Sample DB125 (Pellet treated at 400 °C for 384 hours) – Point analyses of the bulk phase**

	Analysis (mass per cent)											
	Mg	Al	Zr	V	Mn	O	Ti	Fe	Cr	Si	Ca	S
Analysis 1	0.30	0.52	0.12	0.37	0.21	36.81	55.14	6.49	0.03	0.00	0.01	0.00
Analysis 2	0.92	0.51	0.08	0.38	0.17	36.83	54.85	6.23	0.03	0.00	0.01	0.00
Average	0.61	0.52	0.10	0.38	0.19	36.82	55.00	6.36	0.03	0.00	0.01	0.00

Standard Deviation	0.44	0.01	0.03	0.00	0.03	0.02	0.21	0.18	0.00	0.00	0.00	0.00

Calculated composition (normalising O to 5): $Mg_{0.05}Al_{0.04}V_{0.01}Mn_{0.01}Ti_{2.50}Fe_{0.22}O_5$ ($M_{2.83}O_5$)

- **Sample DB125 (Pellet treated at 400 °C for 384 hours) – Point analyses of the lamellae present in the bulk phase**

	Analysis (mass per cent)											
	Mg	Al	Zr	V	Mn	O	Ti	Fe	Cr	Si	Ca	S
Analysis 1	0.10	0.36	0.14	0.31	0.05	38.36	60.03	0.62	0.02	0.00	0.00	0.00
Analysis 2	0.34	0.38	0.09	0.41	0.01	38.28	60.15	0.31	0.02	0.00	0.01	0.01
Average	0.22	0.37	0.11	0.36	0.03	38.32	60.09	0.47	0.02	0.00	0.01	0.00
Standard Deviation	0.17	0.02	0.03	0.07	0.03	0.06	0.08	0.22	0.00	0.00	0.00	0.00

Calculated composition (normalising O to 2): $Mg_{0.01}Al_{0.01}V_{0.01}Mn_{0.00}Ti_{1.04}Fe_{0.01}O_2$ ($M_{1.08}O_2$)

- **Sample DB132 (Block sample treated at 400 °C for 384 hours) – Point analyses of the M_3O_5 phase**

	Analysis (mass per cent)											
	Mg	Al	Zr	V	Mn	O	Ti	Fe	Cr	Si	Ca	S
Analysis 1	0.36	0.39	0.40	0.15	0.83	35.11	47.72	14.95	0.06	0.00	0.03	0.00
Analysis 2	0.56	0.37	0.38	0.13	0.77	34.95	47.80	14.95	0.07	0.00	0.02	0.00
Analysis 3	0.68	0.38	0.28	0.19	0.76	35.29	47.39	14.96	0.06	0.00	0.01	0.00
Analysis 4	0.49	0.37	0.45	0.12	0.96	34.99	47.09	15.44	0.06	0.00	0.02	0.01
Average	0.52	0.38	0.38	0.14	0.83	35.09	47.50	15.07	0.06	0.00	0.02	0.00
Standard Deviation	0.13	0.01	0.07	0.03	0.09	0.15	0.33	0.24	0.00	0.00	0.01	0.00

Calculated composition (normalising O to 5): $Mg_{0.04}Al_{0.03}Zr_{0.01}V_{0.01}Mn_{0.03}Ti_{2.29}Fe_{0.55}O_5$ ($M_{2.96}O_5$)

- **Sample DB132 (Block sample treated at 400 °C for 384 hours) – Point analyses of the TiO_2 phase**

	Analysis (mass per cent)											
	Mg	Al	Zr	V	Mn	O	Ti	Fe	Cr	Si	Ca	S
Analysis 1	0.00	0.02	0.52	0.10	0.00	39.80	59.44	0.07	0.04	0.00	0.00	0.00
Analysis 2	0.20	0.00	0.54	0.15	0.00	38.94	60.11	0.01	0.04	0.00	0.00	0.00
Analysis 3	0.00	0.01	0.58	0.09	0.01	38.67	60.59	0.00	0.04	0.00	0.00	0.00
Analysis 4	0.00	0.01	0.59	0.13	0.01	38.84	60.36	0.00	0.04	0.00	0.00	0.00
Average	0.05	0.01	0.56	0.12	0.01	39.06	60.13	0.02	0.04	0.00	0.00	0.00

Standard Deviation	0.10	0.01	0.03	0.03	0.01	0.50	0.50	0.03	0.00	0.00	0.00	0.00

Calculated composition (normalising O to 2): $Ti_{1.03}O_2$ ($M_{1.03}O_2$)

Appendix C: Mössbauer spectra of samples in this study

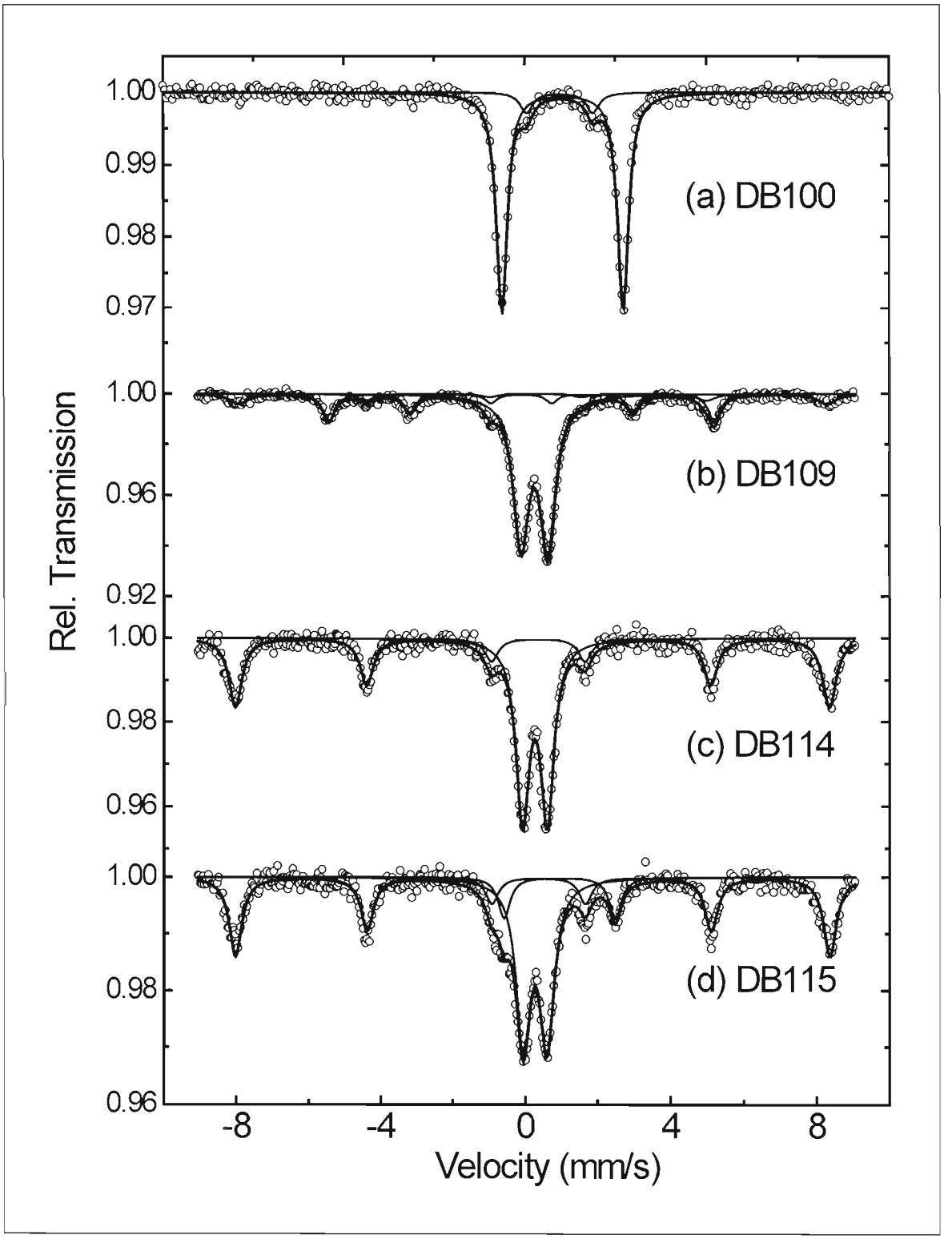

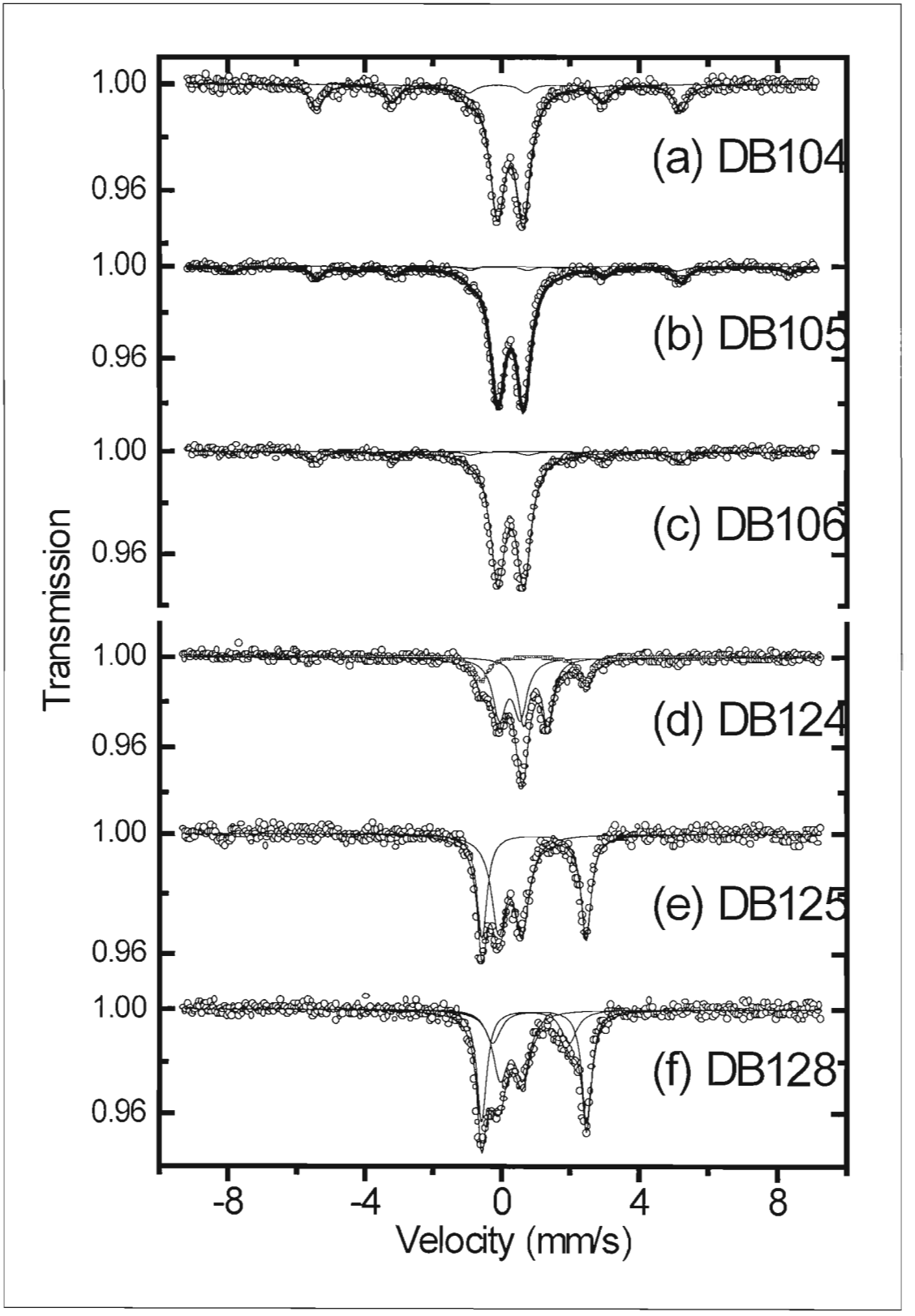
Transmission
1.00
0.96
(a) DB104
(b) DB105
(c) DB106
(d) DB124
(e) DB125
(f) DB128
-8
-4
0
4
8
Velocity (mm/s)

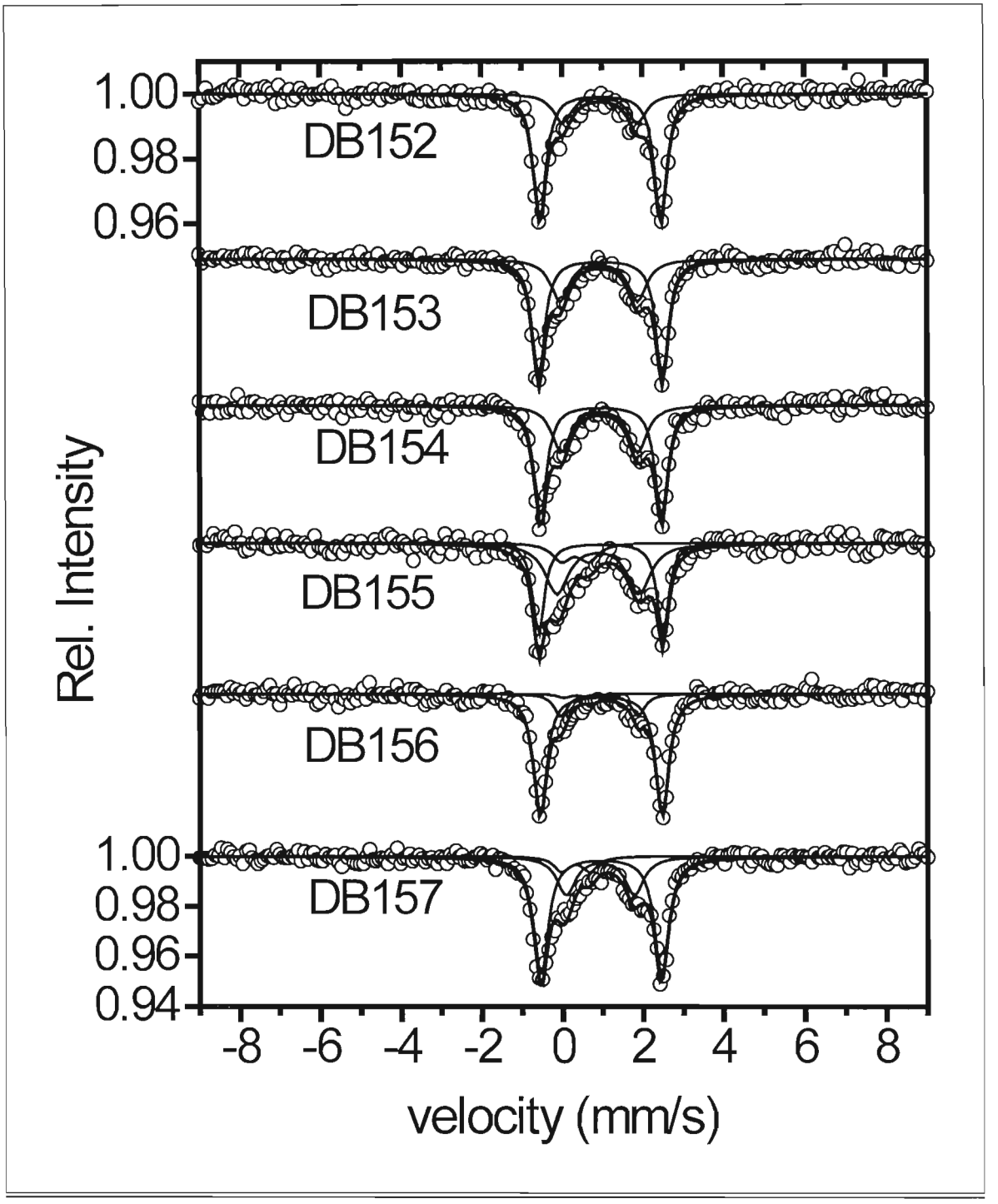
1.00
0.98
0.96
DB152
DB153
DB154
DB155
DB156
1.00
0.98
0.96
0.94
DB157
Rel. Intensity
-8
-6
-4
-2
0
2
4
6
8
velocity (mm/s)

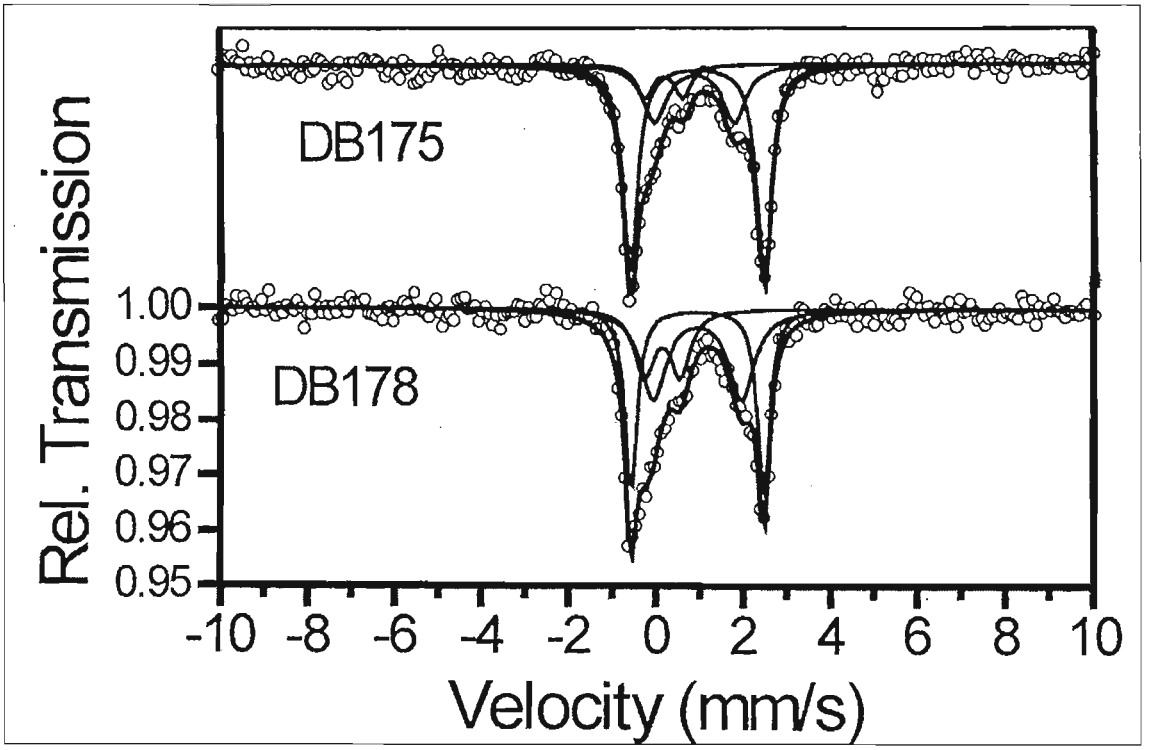
DB175
DB178
Rel. Transmission
1.00
0.99
0.98
0.97
0.96
0.95
-10
-8
-6
-4
-2
0
2
4
6
8
10
Velocity (mm/s)

Appendix D: Crystallographic data for sample DB156

h	k	l	d (Å)	I/I_0 (obs)	I/I_0 (calc)	h	k	l	d (Å)	I/I_0 (obs)	I/I_0 (calc)
0	0	2	5.015	9.8	6.6	2	0	6	1.579	2.9	2.9
0	0	2	5.003	4.7	3.3	2	0	6	1.575	1.6	1.4
2	0	0	4.910	36.0	40.7	2	2	3	1.559	21.0	20.2
2	0	0	4.898	16.9	20.2	3	1	5	1.556	9.2	9.4
1	1	0	3.531	100.0	100.0	2	2	3	1.555	9.9	10.0
1	1	0	3.522	51.5	49.7	3	1	5	1.552	4.5	4.7
2	0	2	3.505	11.6	11.4	5	1	3	1.543	18.0	17.0
2	0	2	3.497	5.5	5.7	5	1	3	1.539	7.9	8.5
1	1	1	3.330	11.0	11.0	1	1	6	1.508	4.5	4.6
1	1	1	3.322	4.9	5.5	1	1	6	1.504	2.1	2.3
1	1	2	2.885	5.9	3.8	4	2	0	1.496	2.4	2.9
1	1	2	2.878	2.9	1.9	4	2	0	1.493	1.0	1.5
2	0	3	2.760	79.2	71.7	6	0	3	1.467	1.0	1.6
2	0	3	2.753	39.1	35.7	2	2	4	1.441	4.3	4.7
0	0	4	2.504	2.8	2.6	2	2	4	1.438	2.2	2.3
0	0	4	2.498	1.4	1.3	4	2	2	1.434	6.6	6.4
3	1	0	2.473	20.9	21.0	4	2	2	1.430	3.0	3.2
3	1	0	2.467	11.1	10.4	5	1	4	1.428	2.5	2.7
4	0	0	2.451	7.2	7.3	5	1	4	1.425	1.0	1.3
4	0	0	2.445	3.4	3.6	3	1	6	1.383	5.6	4.8
1	1	3	2.425	20.8	22.6	3	1	6	1.379	2.4	2.4
1	1	3	2.419	9.6	11.3	2	0	7	1.372	3.1	3.5
3	1	1	2.401	1.4	1.4	2	0	7	1.369	1.5	1.7
2	0	4	2.230	15.1	14.1	4	2	3	1.365	7.4	8.5
2	0	4	2.224	8.2	7.0	4	2	3	1.362	3.6	4.2
3	1	2	2.217	2.1	1.7	1	1	7	1.325	2.2	2.7
3	1	2	2.211	1.0	0.9	2	2	5	1.323	4.2	5.0
4	0	2	2.201	18.8	15.8	1	1	7	1.322	1.1	1.3
4	0	2	2.196	9.7	7.8	2	2	5	1.320	2.1	2.5
1	1	4	2.041	1.0	0.2	7	1	1	1.301	3.8	5.5
3	1	3	1.987	4.6	4.5	7	1	1	1.298	1.8	2.7
3	1	3	1.982	2.4	2.2	7	1	2	1.270	6.7	5.3
4	0	3	1.975	21.0	20.4	7	1	2	1.266	3.3	2.7
4	0	3	1.970	10.4	10.2	6	0	5	1.265	2.7	2.3
0	2	0	1.890	35.1	33.3	6	0	5	1.262	1.4	1.1
0	2	0	1.886	18.1	16.6	0	2	6	1.250	8.0	6.4
2	0	5	1.853	10.9	9.0	1	3	0	1.249	3.2	2.7
2	0	5	1.849	5.7	4.5	0	2	6	1.247	3.8	3.2
2	2	0	1.764	3.9	3.5	1	3	0	1.246	1.6	1.3
2	2	0	1.759	1.9	1.7	3	1	7	1.237	1.0	1.0
3	1	4	1.759	10.4	9.7	6	2	1	1.226	3.2	2.7
3	1	4	1.754	5.1	4.8	6	2	1	1.223	1.4	1.4
5	1	1	1.714	1.5	0.5	2	2	6	1.212	2.0	1.7

0	0	6	1.668	11.0	10.9	2	2	6	1.209	1.0	0.9
0	0	6	1.664	6.1	5.4	8	0	2	1.189	2.2	1.5
2	2	2	1.663	2.1	1.8	8	0	2	1.187	1.7	0.8
2	2	2	1.659	1.0	0.9	3	3	0	1.175	2.6	1.6
5	1	2	1.644	20.0	19.3	3	3	0	1.172	1.4	0.8
5	1	2	1.639	10.0	9.6	1	3	3	1.170	3.6	2.0
6	0	0	1.633	1.3	1.0	1	3	3	1.167	1.9	1.0
6	0	1	1.612	5.0	4.3	6	2	3	1.158	2.7	1.5
6	0	1	1.608	2.5	2.1	6	2	3	1.156	1.6	0.7

Appendix E: X-ray diffraction patterns of the slag samples shown in Table 12

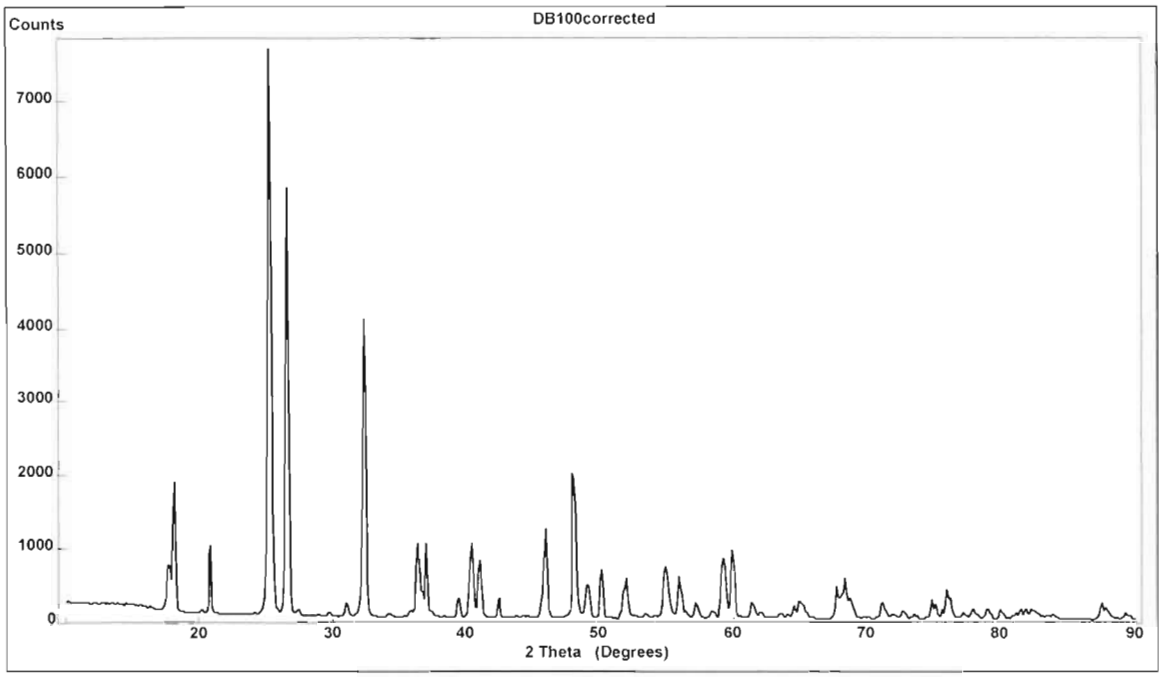

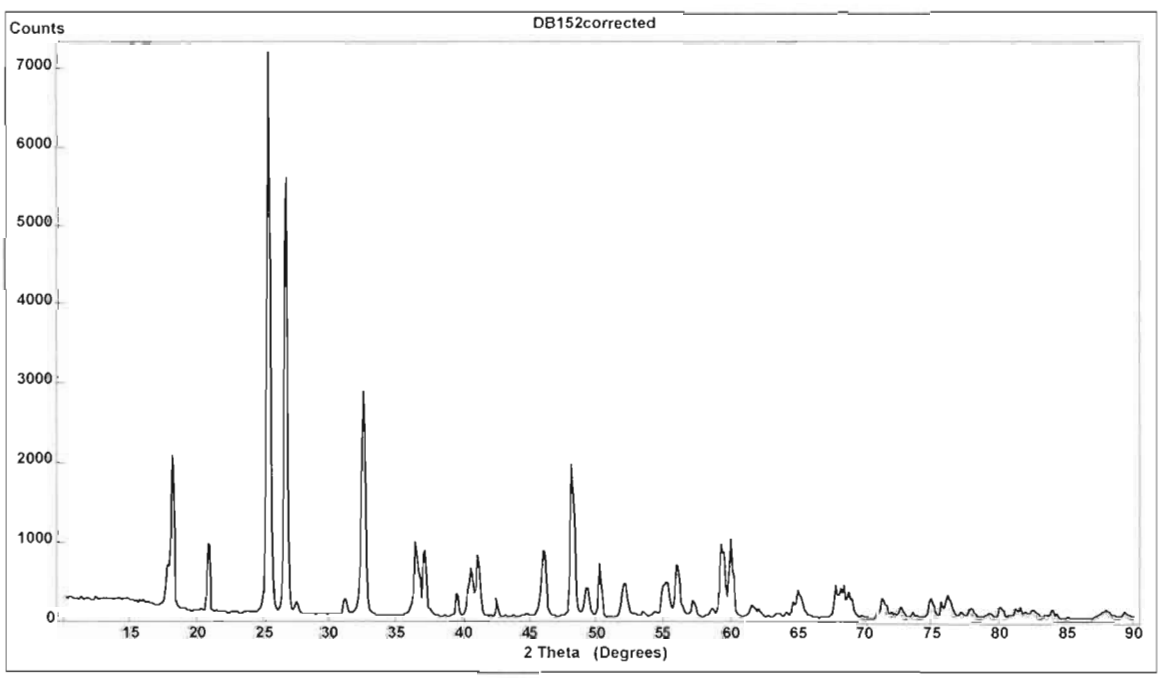

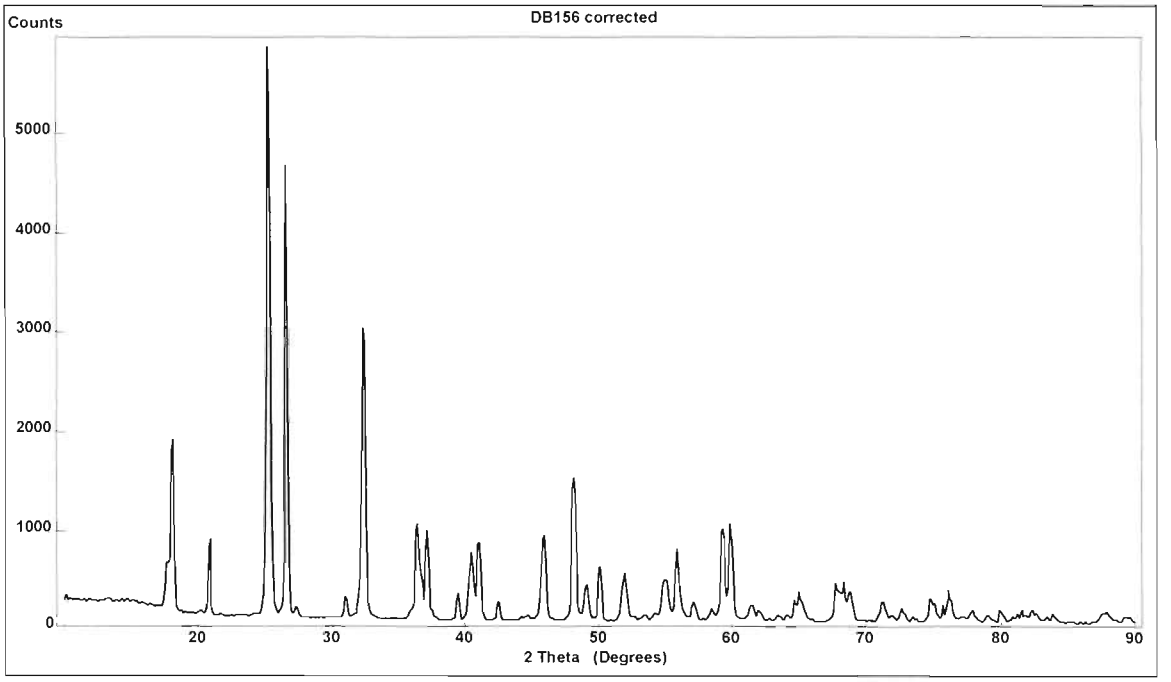
DB156 corrected
Counts
5000
4000
3000
2000
1000
0
20
30
40
50
60
70
80
90
2 Theta (Degrees)

Appendix F: Normalised oxide phase analyses results of various samples

- **Sample YS2872 (Air-cooled spoon sample from tap stream) – Dark coloured glass phase**

	Analysis (mass per cent)								
	MgO	Al_2O_3	TiO_2	MnO	FeO	SiO_2	K_2O	CaO	Na_2O
Analysis 1	-	2.83	8.72	0.44	1.75	83.40	1.20	1.01	0.65
Analysis 2	-	3.03	7.15	0.76	1.62	84.38	0.84	1.32	0.91
Analysis 3	-	3.52	8.77	0.64	1.86	83.05	1.27	0.89	-
Average	-	3.13	8.21	0.61	1.74	83.61	1.10	1.07	0.78
Standard Deviation	-	0.36	0.92	0.16	0.12	0.69	0.23	0.22	0.18

- **Sample YS2872 (Air-cooled spoon sample from tap stream) – Light coloured glass phase**

	Analysis (mass per cent)								
	MgO	Al_2O_3	TiO_2	MnO	FeO	SiO_2	K_2O	CaO	Na_2O
Analysis 1	-	6.41	11.17	9.61	7.34	48.75	0.23	16.49	-
Analysis 2	-	5.99	12.53	10.65	6.29	46.59	0.10	17.84	-
Analysis 3	-	5.82	10.11	11.30	16.68	43.88	0.07	12.14	-
Analysis 4	-	5.17	12.11	11.47	14.46	44.07	-	12.72	-
Average	-	5.85	11.48	10.76	11.19	45.82	0.13	14.80	-
Standard Deviation	-	0.52	1.08	0.84	5.15	2.31	0.09	2.80	-

APPENDIX G: X-ray diffraction patterns for the pellet samples

The following abbreviations are used for the identification of phases:

M3 – M_3O_5 phase R – Rutile H – Hematite
M6 – M_6O_{11} phase A – Anatase

Sample DB100: Starting material for tests with pellets

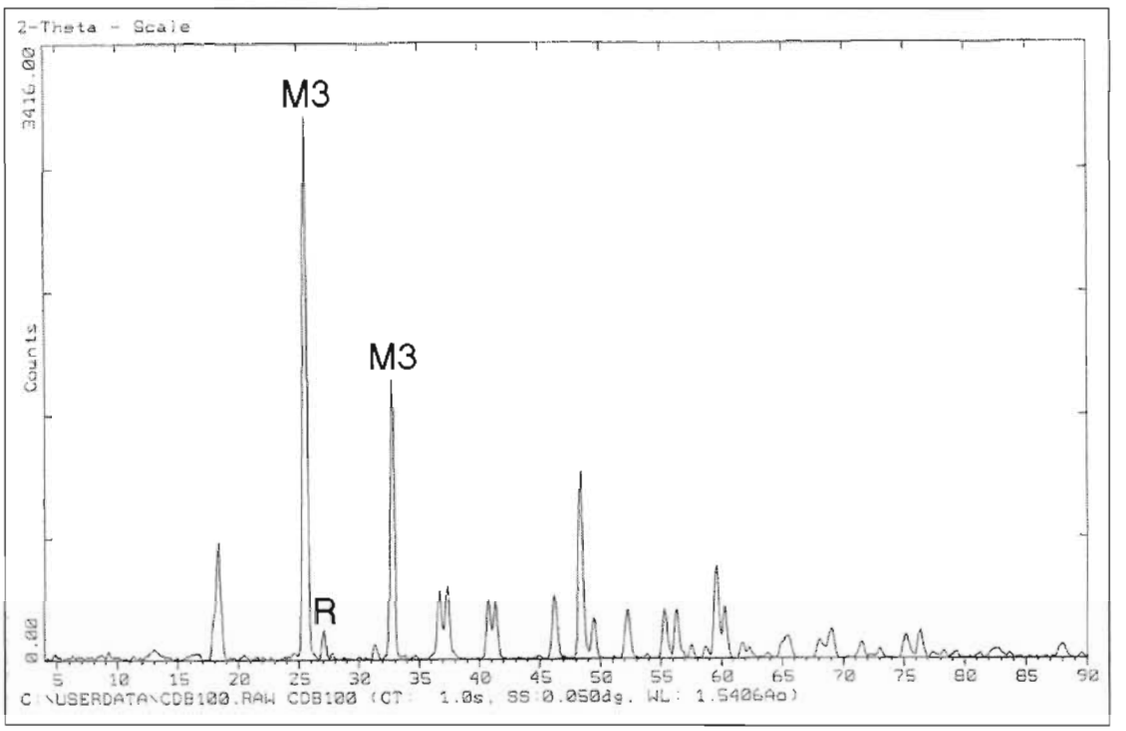

Sample DB104: Pellet; 1000 °C; 24 hours

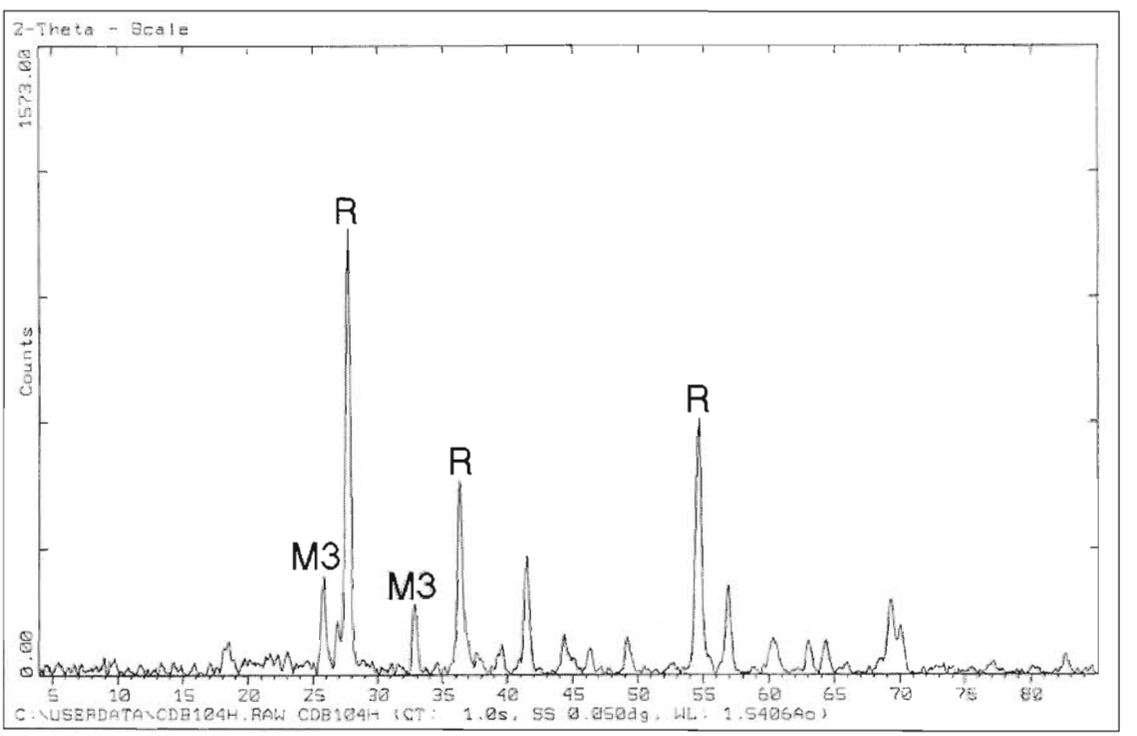

Sample DB106: Pellet; 1000 °C; 384 hours

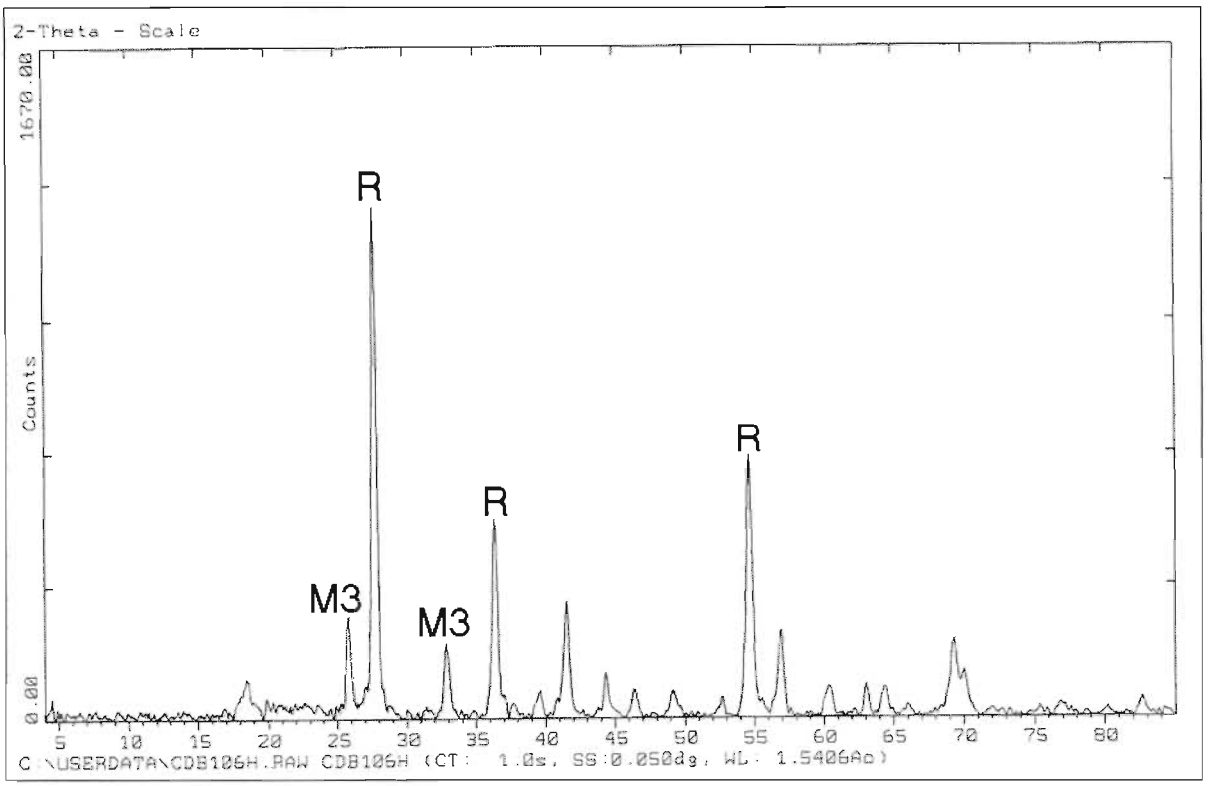

Sample DB109: Pellet; 800 °C; 24 hours

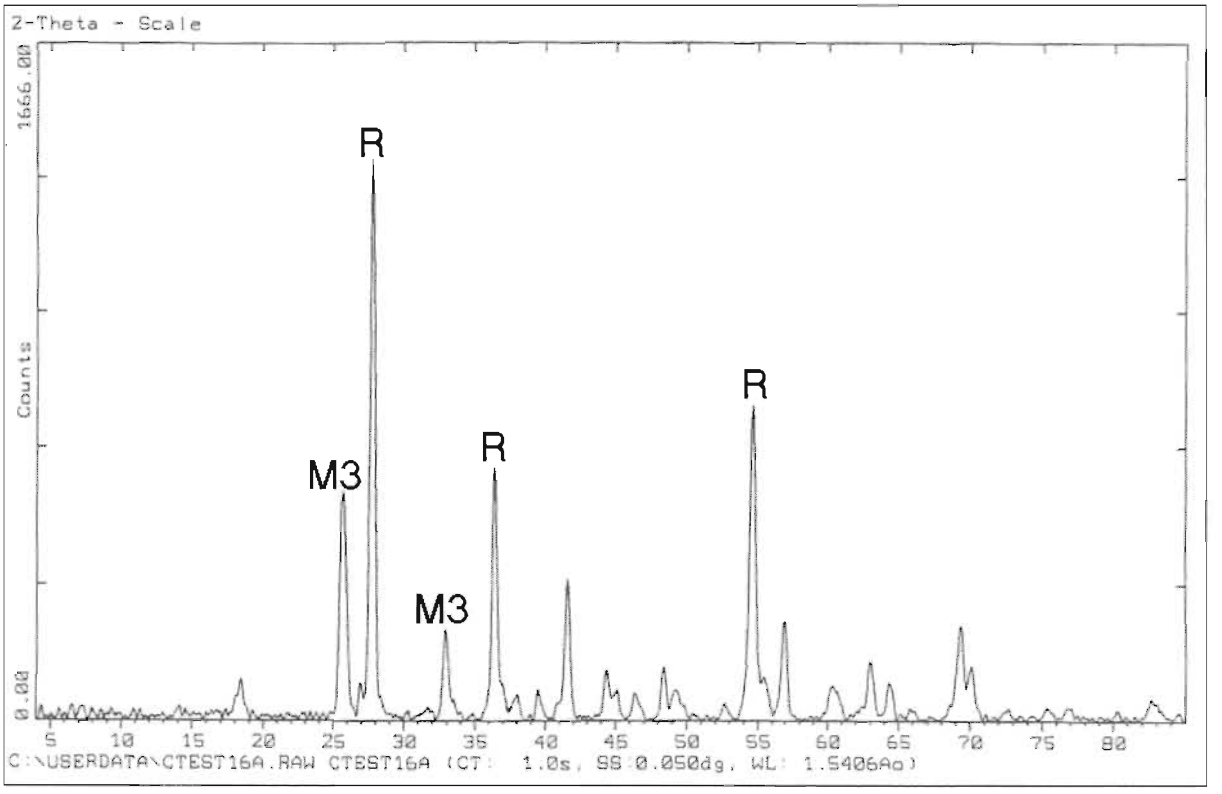

Sample DB105: Pellet; 800 °C; 384 hours

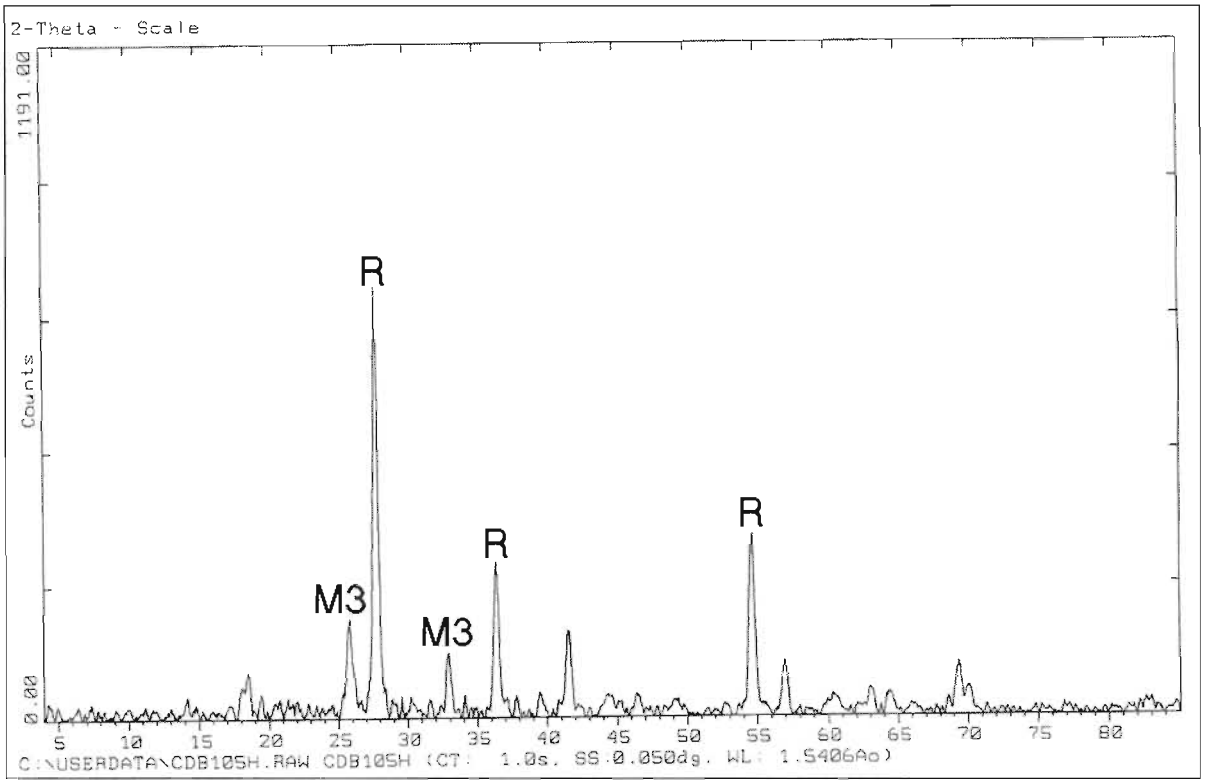

Sample DB115: Pellet; 600 °C; 24 hours

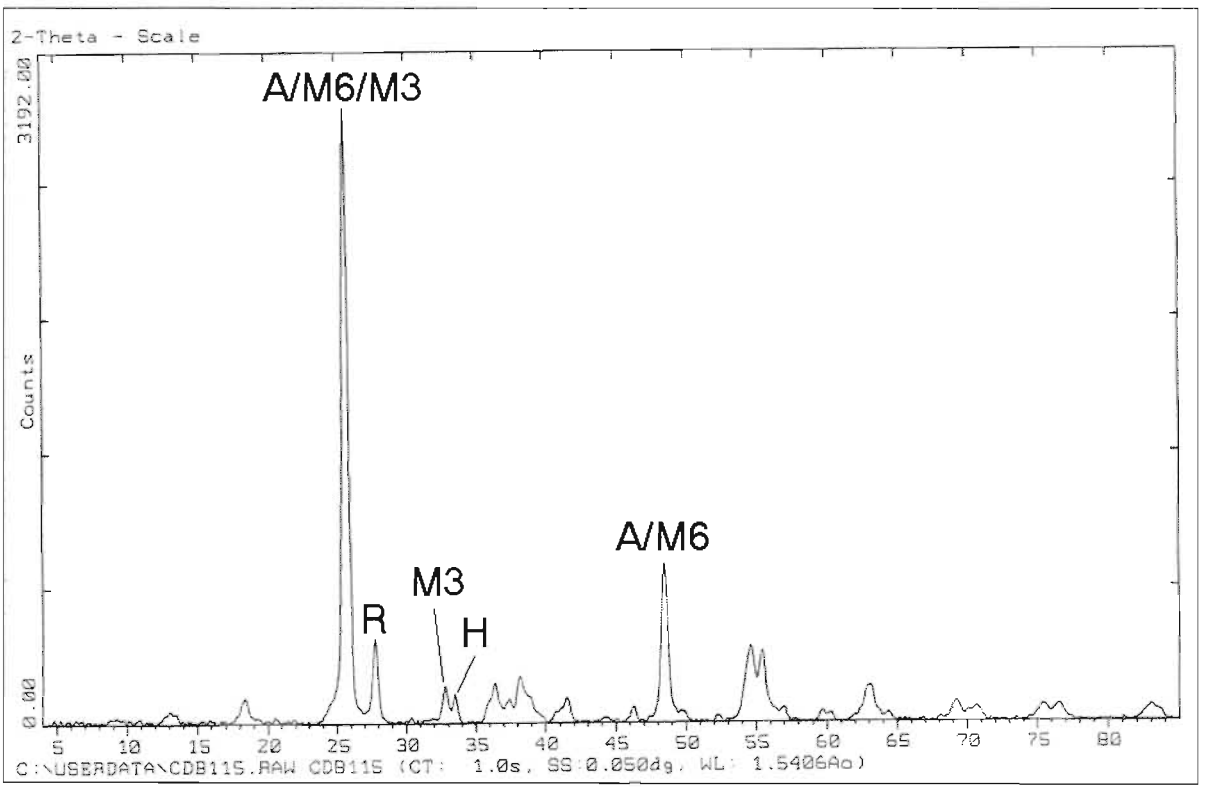

Sample DB114: Pellet; 600 °C; 384 hours

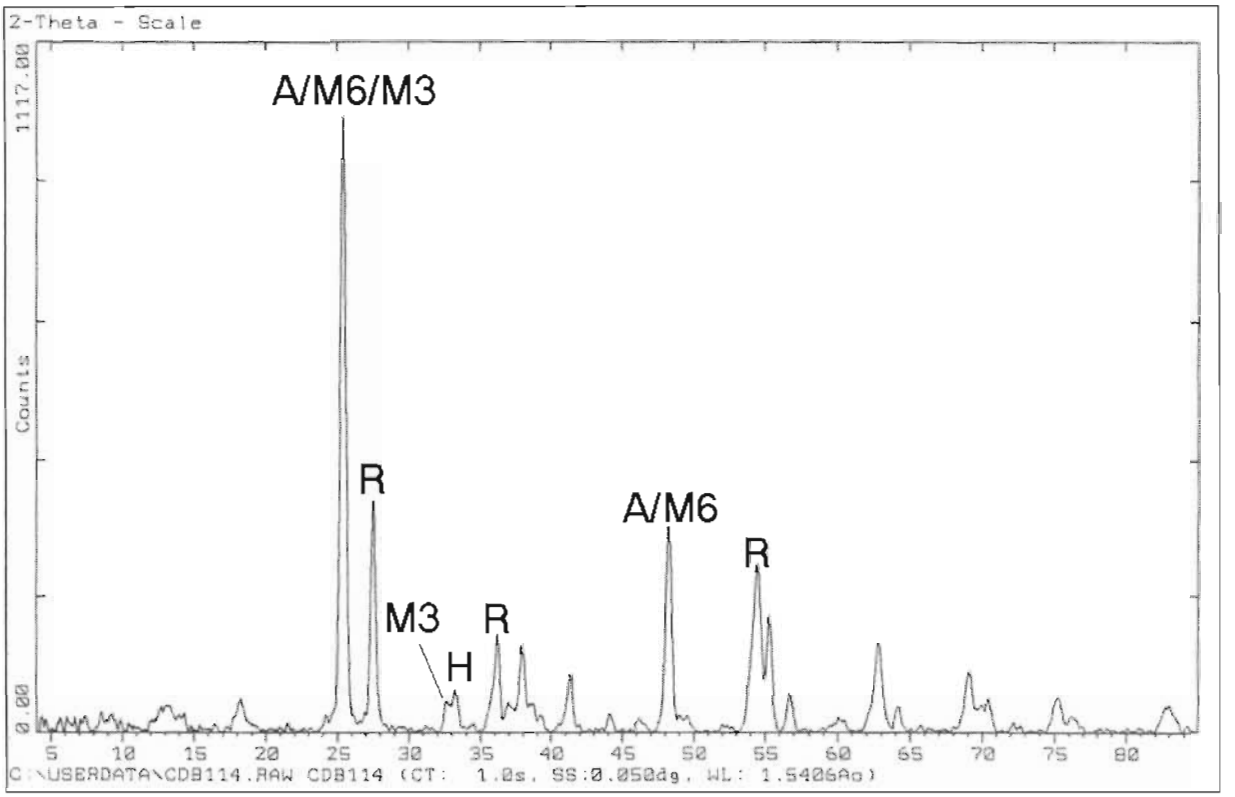

Sample DB121: Pellet; 400 °C; 24 hours

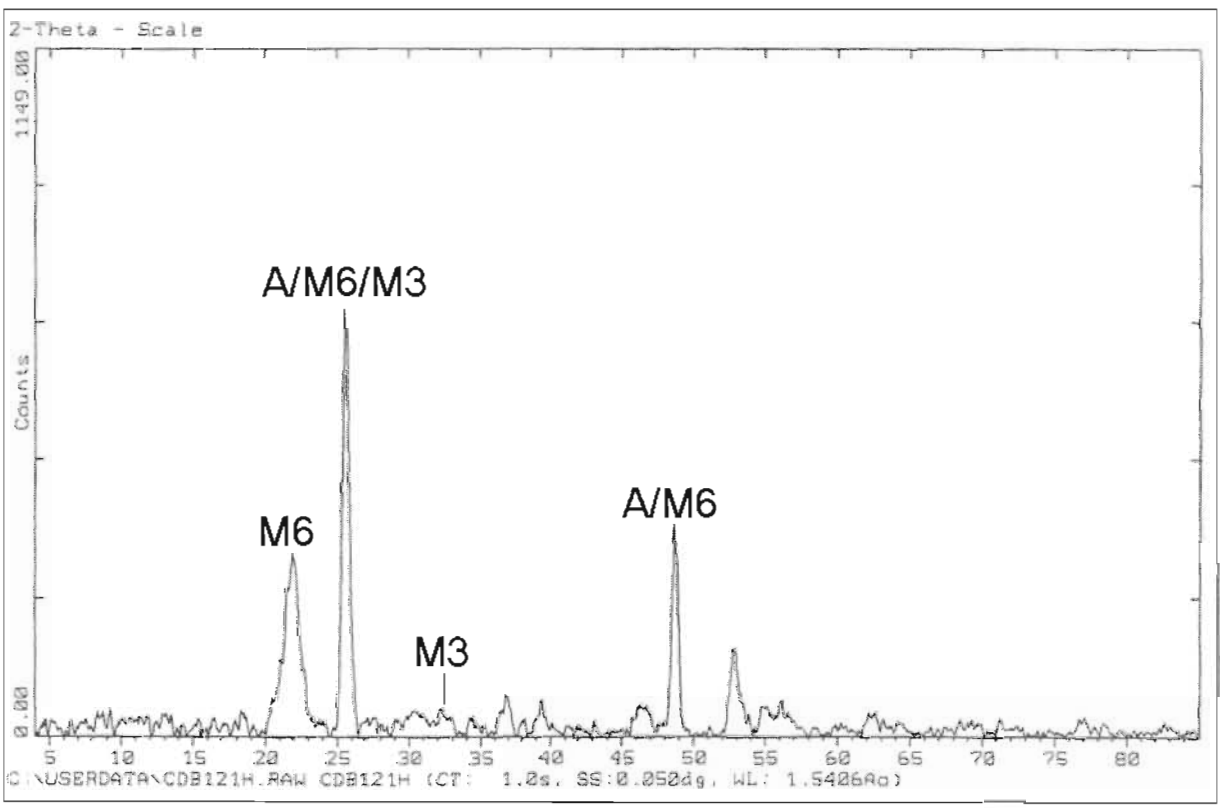

Sample DB128: Pellet; 400 °C; 48 hours

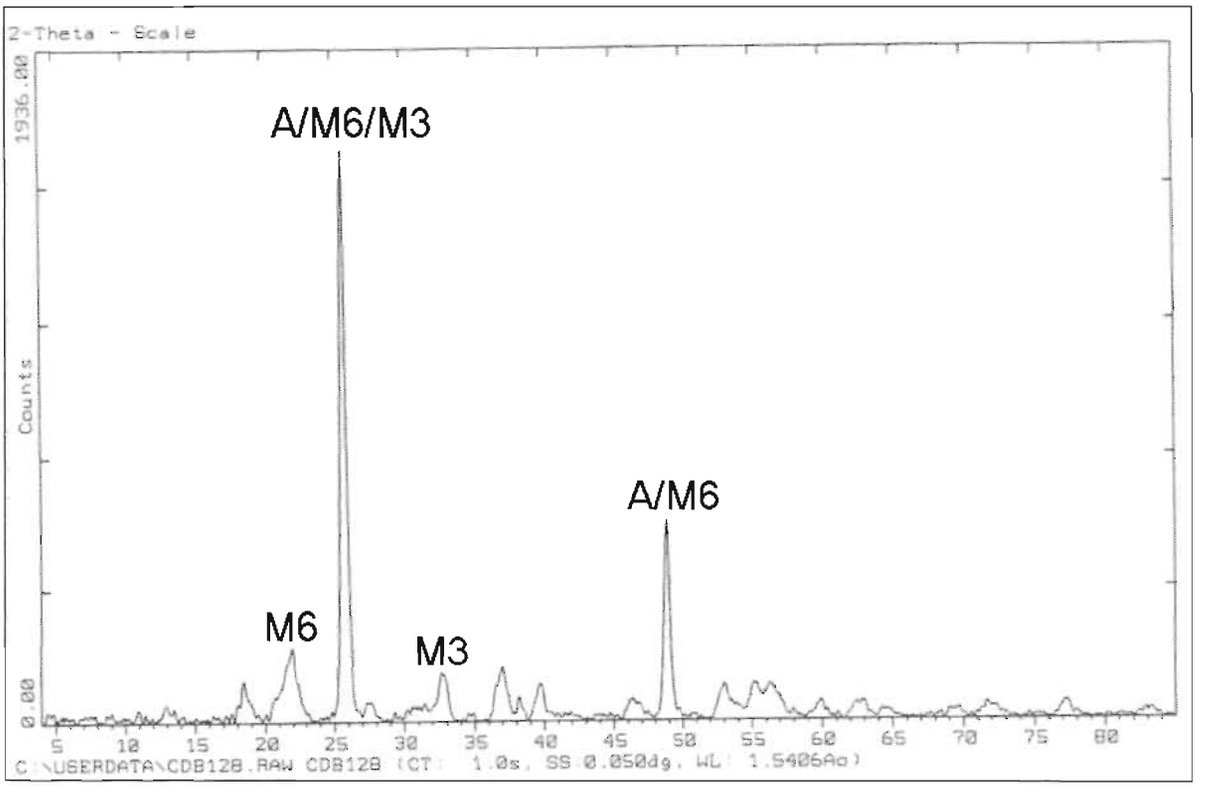

Sample DB125: Pellet; 400 °C; 384 hours

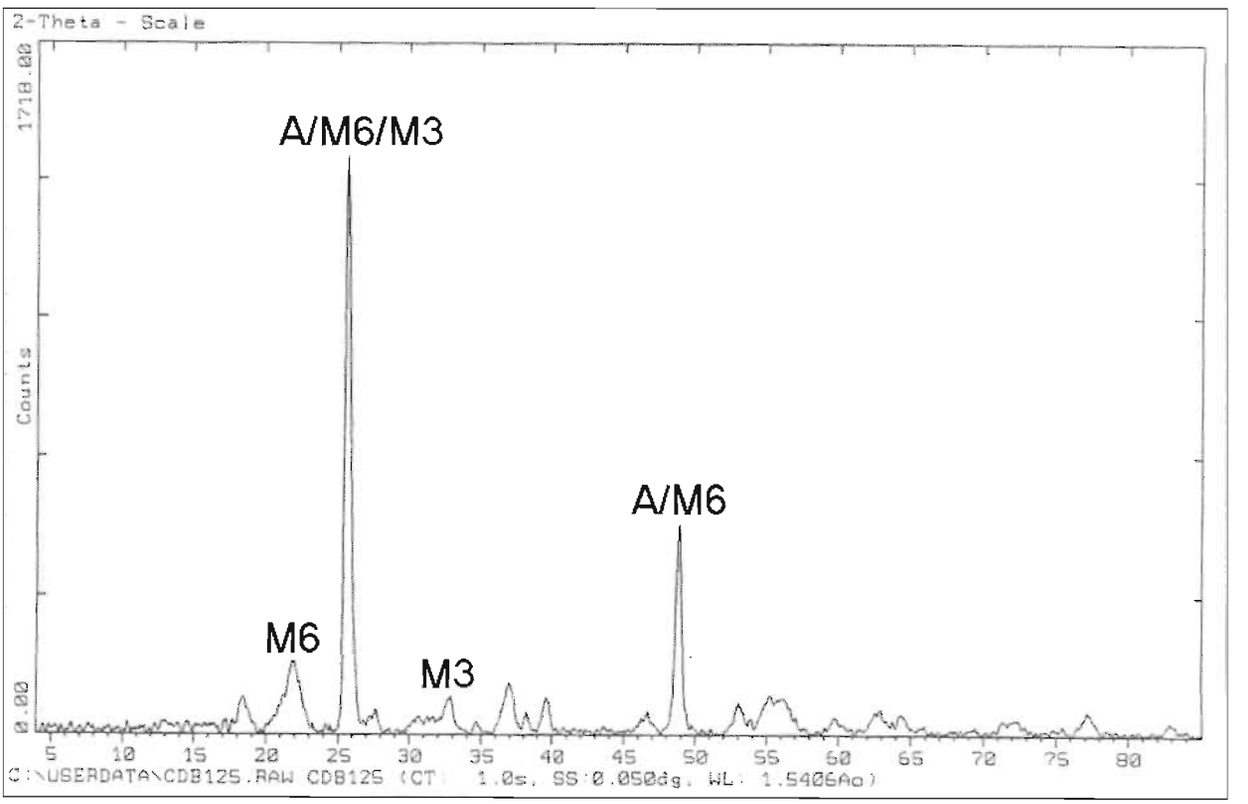

Appendix H: Calculation of the composition and cation oxidation states for sample DB125 (bulk phase)

From the X-ray diffraction results for this sample we know that both M_6O_{11} and anatase phases are present. According to Grey, Cranswick, et. al. (2000) the M_6O_{11} structure comprises planar intergrowth of M_3O_5 compositional blocks with the pseudobrookite-type structure and MO_2 compositional blocks with the anatase-type structure. The calculations were therefore carried out to write the compositions in these terms. The M_3O_5 phase was calculated in terms of the solid solution end members. Various scenarios were calculated based on the given assumptions.

Calculation 1

Assumptions:

- All the iron is present as Fe^{2+}.
- The O content as given in Appendix B is correct.

Based on the assumptions the following composition can be calculated:

$$0.56\left[Ti^{4+}_{1.00}O^{2-}_{2}\right] \bullet 0.25\left[Ti^{4+}_{1.00}\left(V^{3+}_{0.03}Al^{3+}_{0.10}Ti^{3+}_{1.87}\right)O^{2-}_{5}\right] \bullet 0.19\left[\left(Mg^{2+}_{0.18}Mn^{2+}_{0.04}Fe^{2+}_{0.78}\right)Ti^{4+}_{2}O^{2-}_{5}\right]$$

Calculation 2

Assumptions:

- The Mössbauer data from Table 27 is used for the calculation of the oxidation state of iron.
- The O content as given in Appendix B is correct.

Based on the assumptions the following composition can be calculated:

$$0.56\left[Ti^{4+}_{1.00}O^{2-}_{2}\right] \bullet 0.29\left[Ti^{4+}_{1.00}\left(V^{3+}_{0.02}Al^{3+}_{0.09}Ti^{3+}_{1.89}\right)O^{2-}_{5}\right] \bullet 0.11\left[\left(Mg^{2+}_{0.31}Mn^{2+}_{0.06}Fe^{2+}_{0.63}\right)Ti^{4+}_{2}O^{2-}_{5}\right] \bullet 0.04\left[Fe^{3+}_{2.00}Ti^{4+}_{1.00}O^{2-}_{5}\right]$$

Calculation 3

Assumptions:

- The Mössbauer data from Table 27 is used for the calculation of the oxidation state of iron.
- The oxygen content as given in Appendix B is incorrect, with the oxygen content underestimated by 2 per cent. Based on this the composition of the phase changes from $Mg_{0.05}Al_{0.04}V_{0.01}Mn_{0.01}Ti_{2.50}Fe_{0.22}O_5$ ($M_{2.83}O_5$) to $Mg_{0.05}Al_{0.04}V_{0.01}Mn_{0.01}Ti_{2.38}Fe_{0.21}O_5$ ($M_{2.70}O_5$), with the oxygen content normalised to 5 in both instances.

Based on the assumptions the following composition can be calculated:

$$0.79\left[Ti^{4+}_{1.00}O^{2-}_{2}\right] \bullet 0.10\left[Ti^{4+}_{1.00}\left(V^{3+}_{0.05}Al^{3+}_{0.21}Ti^{3+}_{1.74}\right)O^{2-}_{5}\right] \bullet 0.08\left[\left(Mg^{2+}_{0.33}Mn^{2+}_{0.07}Fe^{2+}_{0.60}\right)Ti^{4+}_{2}O^{2-}_{5}\right] \bullet 0.03\left[Fe^{3+}_{2.00}Ti^{4+}_{1.00}O^{2-}_{5}\right]$$

The following comments can be made on these calculations:

- Where the Mössbauer data is used, with both Fe^{2+} and Fe^{3+} present, chemical equilibrium has not been attained due to the co-existence of Fe^{3+} and Ti^{3+}.
- From these calculations it does seem that Ti^{3+} is still present in the samples.
- It seems that the error in the oxygen analysis will have the greatest impact on the calculation of the composition.

APPENDIX I: X-ray diffraction patterns for the miniature block samples

The following abbreviations are used for the identification of phases:

M3 – M_3O_5 phase	R – Rutile	I – Ilmenite
M6 – M_6O_{11} phase	A – Anatase	

Sample DB123: Starting material for tests with pellets

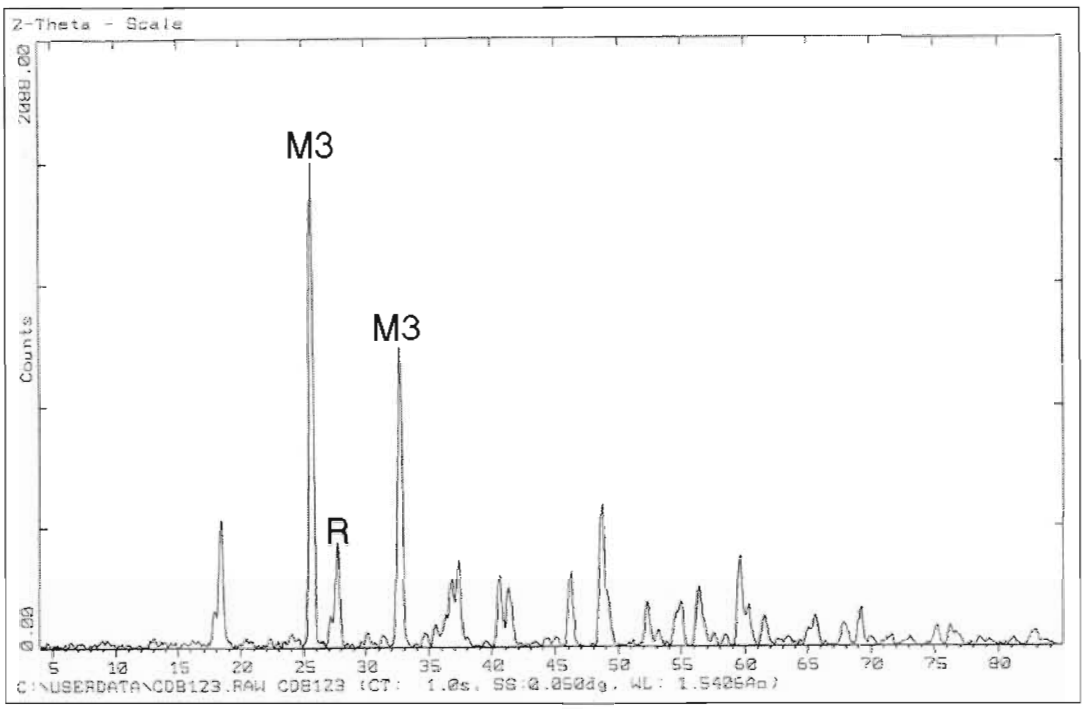

Sample DB124: Miniature Block; 800 °C; 24 hours

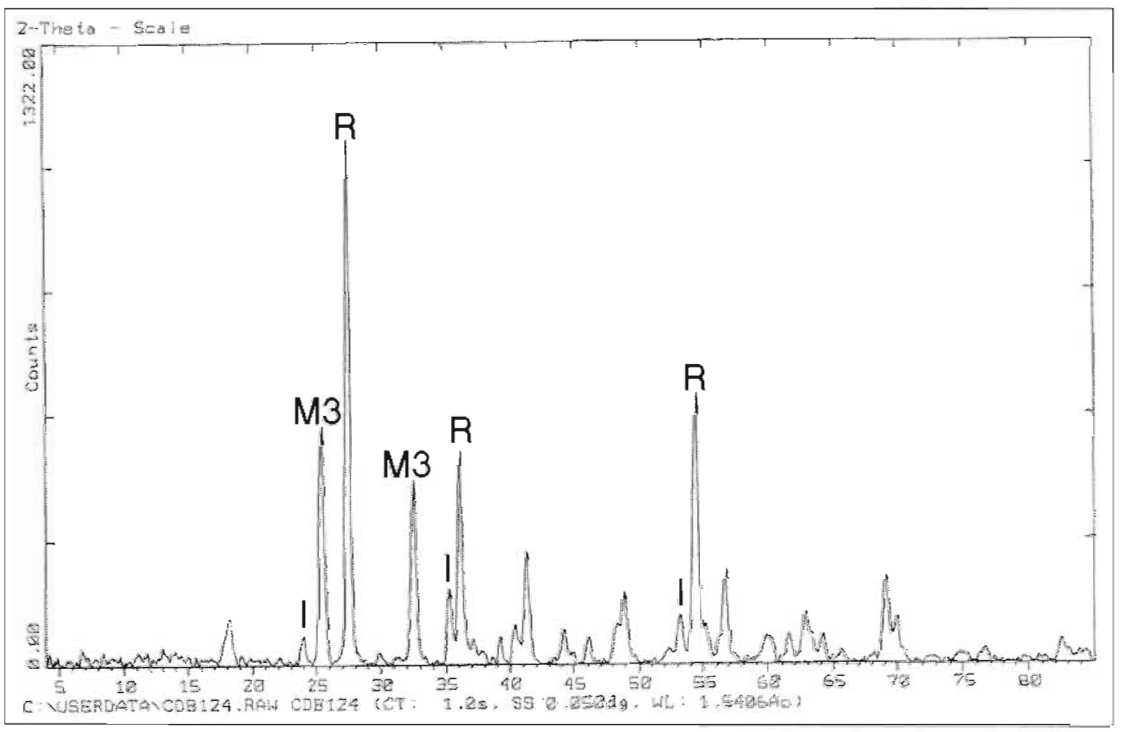

Sample DB130: Miniature Block; 400 °C; 6 hours

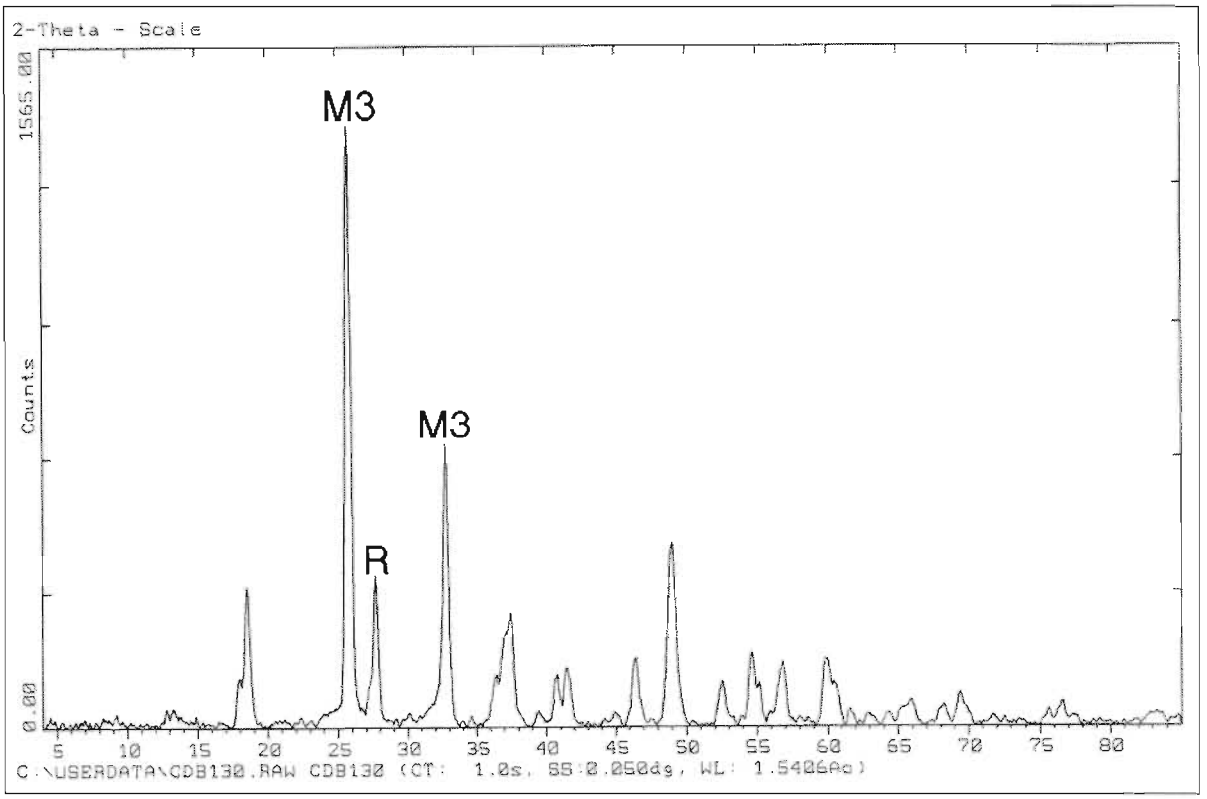

Sample DB131: Miniature Block; 400 °C; 24 hours

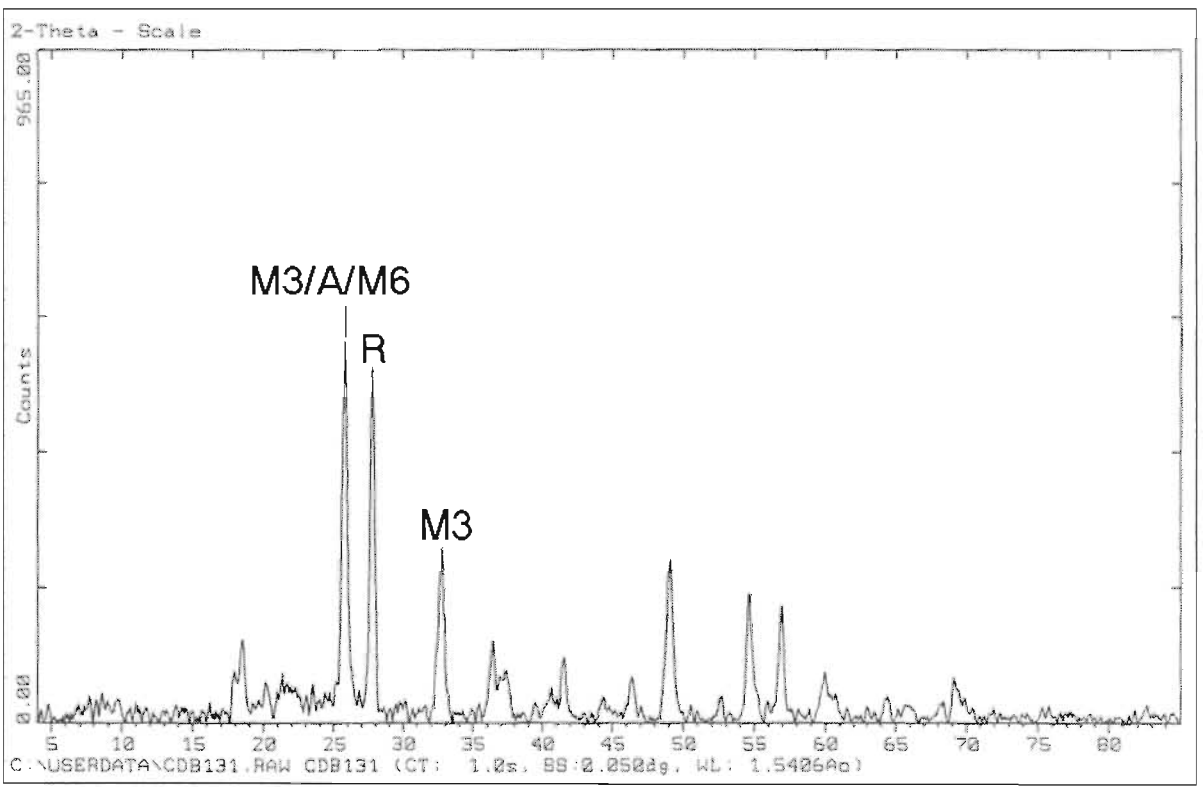

Sample DB133: Miniature Block; 400 °C; 96 hours

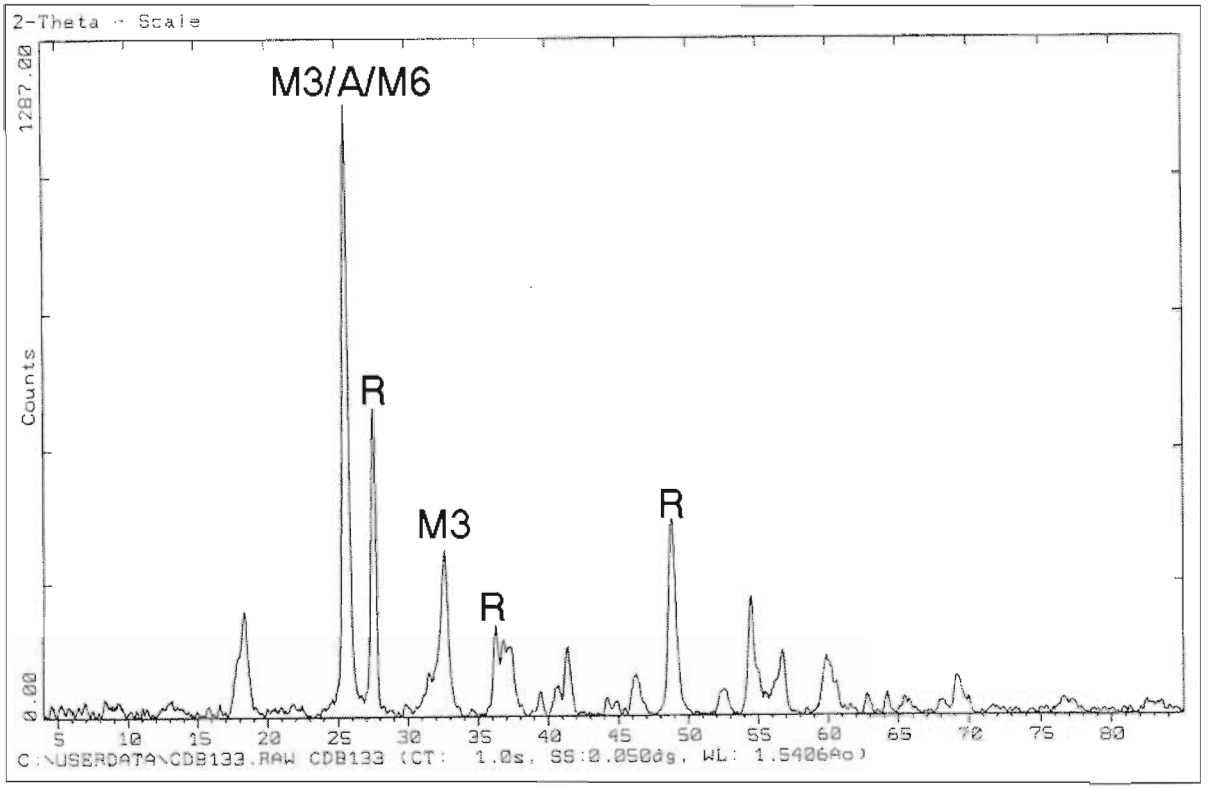

Sample DB132: Miniature Block; 400 °C; 384 hours

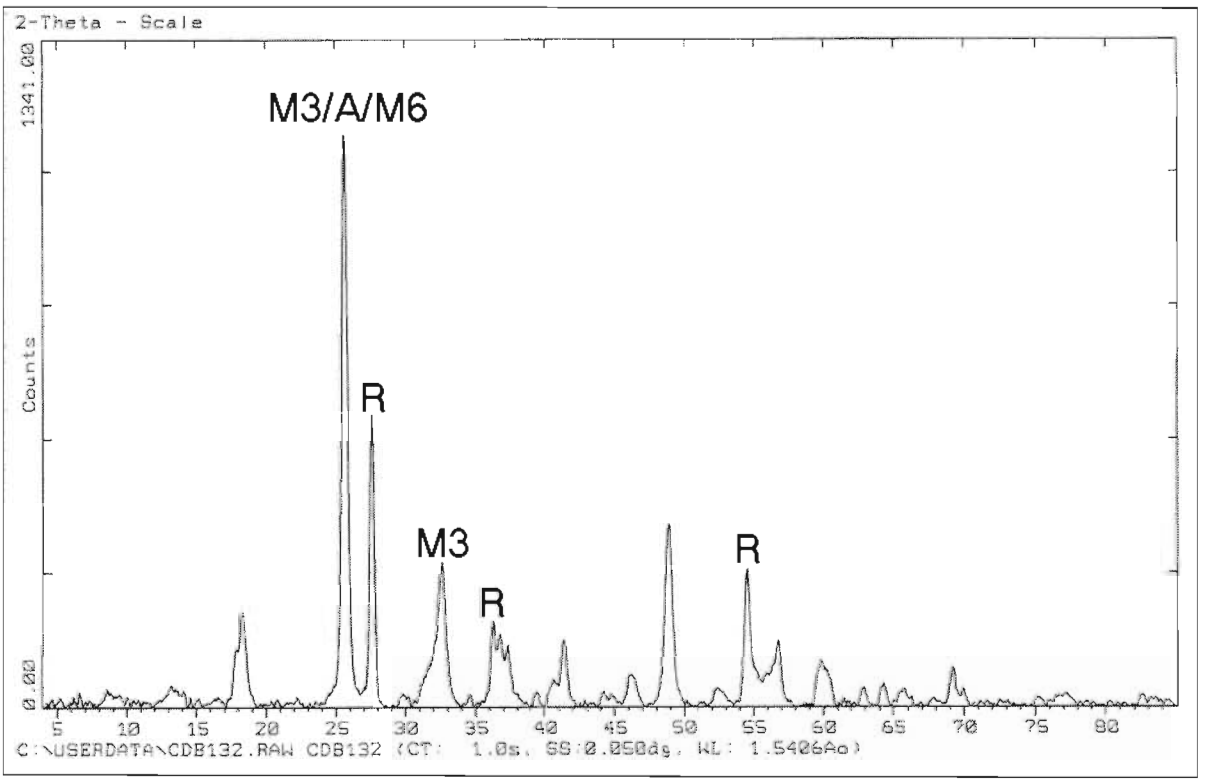

Appendix J: Statistical analyses of the data obtained from the crushing testwork on miniature slag blocks

1. Results for statistical analyses

The various results obtained from the crushing of the miniature slag blocks are given in Table 45 and Table 46. The integral area value in Table 45 was obtained by determing the area under the graph (Force as a function of time) obtained for each experiment (see Figure 55 for an example of such a graph). The slope values were obtained by determining the slope of the displacement as a function of time (see Figure 54 for an example). Calibration constants were used to convert the data to from volts to the required units. The total crushing energy was calculated as the product of the integral area and the slope value for each experiment. The absolute value was used, as the negative values are only a result of the reference point used for the displacement. The maximum force applied during the crushing of each miniature slag block is also shown in Table 45.

The sieve analyses of the miniature slag blocks after the completion of each experiment is shown in Table 46. It was decided to use the -500 μm sieve fraction to differentiate between the various experimental conditions.

2. Introduction to statistical analyses used

All the data generated for the various samples were subjected to the one-way analysis of variance (ANOVA) technique. This technique deals with the differences between sample means. The following two assumptions are made:
a) It is assumed that each set of data is normally distributed around the population mean.
b) It is assumed that each population of scores has the same variance.

The following calculations were made to compute the ANOVA summary tables (i; j - represents the various experimental groups):
$T_j = \Sigma X_j$ (X - data point)
$N = \Sigma n_j$ (n_j - number of data points in each experimental group)
$G = \Sigma X = \Sigma T_j$
$df_{Total} = N-1$
$df_{Group} = k-1$
$df_{Error} = df_{Total} - df_{Group}$
$SS_{Total} = \Sigma X^2 - G/N$ (SS – Sums of squares)
$SS_{Group} = \Sigma(T_j^2/n_j)$
$SS_{Error} = SS_{Total} - SS_{Group}$
$MS_{Group} = SS_{Group}/ df_{Group}$ (df – Degrees of freedom; MS – Mean squares [calculation of the variance])
$MS_{Error} = SS_{Error}/ df_{Error}$
$F = MS_{Group}/MS_{Error}$

Table 45: Results obtained from the crushing strength testwork

Test no.	Temperature of test (°C)	Duration of test (hours)	Maximum Force measured during crushing test (kN)	Average maximum force measured during crushing tests (kN)	Integral value (kN.s)	Slope value ($mm.s^{-1}$)	Total crushing energy – Absolute values (J)	Average crushing energy for each condition (J)	Standard deviation
Slag1	-	-	1.65	2.36	0.2923	-5.6036	1.6379	2.31	0.65
Slag2	-	-	3.29		0.5455	-5.4992	2.9998		
Slag3	-	-	2.24		0.4309	-6.3254	2.7256		
Slag4	-	-	2.25		0.2997	-6.3160	1.8929		
6241	600	24	4.70	4.71	0.9753	-5.2388	5.1094	6.26	2.46
6242	600	24	6.90		1.9217	-5.1199	9.8388		
6243	600	24	3.52		0.7031	-6.1462	4.3214		
6244	600	24	3.72		0.9085	-6.3483	5.7675		
6961	600	96	2.27	2.49	0.5395	-5.7561	3.1054	3.82	0.93
6962	600	96	2.43		0.6697	-5.5655	3.7272		
6963	600	96	2.01		0.5246	-6.2248	3.2655		
6964	600	96	3.23		0.8351	-6.1871	5.1668		
8241	800	24	8.66	6.87	24.9287	-2.1537	53.6891	22.65	20.71
8242	800	24	-		2.3781	-5.7333	13.6342		
8243	800	24	6.13		1.9484	-6.1132	11.9109		
8244	800	24	5.82		1.8427	-6.1744	11.3775		

Table 46: Sieve analyses of the slag after crushing

Test no.	Temperature of test (°C)	Duration of test (hours)	Sieve analysis of slag after crushing (mass %)					Average of the -500 µm sieve analyses (%)
			+1 mm	-1mm+500 µm	-500 µm+212 µm	-212 µm+75 µm	-75 µm	
Slag1	-	-	39.54	18.92	25.98	12.06	3.51	44.64
Slag2	-	-	40.34	17.27	25.05	13.80	3.54	
Slag3	-	-	29.39	17.03	30.72	18.92	3.93	
Slag4	-	-	40.31	18.64	25.00	13.17	2.88	
6241	600	24	48.43	23.78	17.62	7.58	2.59	28.40
6242	600	24	48.37	22.68	17.29	8.94	2.72	
6243	600	24	50.43	21.54	16.49	8.88	2.66	
6244	600	24	47.28	23.90	18.08	8.59	2.15	
6961	600	96	69.55	14.16	9.34	5.14	1.81	18.08
6962	600	96	73.66	12.36	8.12	4.32	1.54	
6963	600	96	70.36	15.57	7.69	5.25	1.13	
6964	600	96	54.12	17.91	15.09	9.05	3.82	
8241	800	24	61.27	18.47	10.78	6.29	3.19	20.67
8242	800	24	63.42	16.30	10.67	5.93	3.68	
8243	800	24	57.39	18.46	14.03	6.44	3.68	
8244	800	24	66.74	15.26	9.94	5.44	2.62	

For the purpose of the calculations the following nomenclature was used:
1: Untreated slag
2: Slag treated at 600 °C for 24 hours
3: Slag treated at 600 °C for 96 hours
4: Slag treated at 800 °C for 24 hours

The following null hypothesis were made for each scenario:

$$H_0: \mu_1 = \mu_2 = \mu_3 = \mu_4$$

In each instance the null hypothesis was rejected. Because of this the protected t test (also known as Fisher's least significant difference test) was used to investigate hypotheses involving means of individual groups.

The following equation (for comparing two means) was used to calculate t (using the means of each group and the number of data points in each group):

$$t = \frac{\overline{X_i} - \overline{X_j}}{\sqrt{MSError(\frac{1}{ni} + \frac{1}{nj})}}$$

Details of the statistical techniques used are given extensively by Howell.

3. Statistical analyses of the total energy required for crushing

The total crushing energy required for crushing the miniature slag blocks were compared on the basis of the experimental treatment of the respective slag blocks. The ANOVA summary for the total crushing energy is given in Table 47. As F is less than the critical F statistic ($F_{calculated} = 3.24 < F_{0.05;3;12} = 3.49$), we must accept H_0 at the level of $\alpha = 0.05$. This implies that there are no significant differences between the means of the various experimental groups.

If we however relax the conditions to $\alpha = 0.10$, $F_{0.10;3;12}$ is calculated to be 2.61. We therefore expect to exceed a F of 2.61 only 10 per cent of the time if H_0 were true. Under these conditions we can reject H_0 and use the protected t test to distinguish between the means of the various experimental groups.

Table 47: ANOVA summary of total energy required for the crushing of miniature slag blocks

Source	Df	SS	MS	F
Groups	3	1061.03	353.68	3.24
Error	12	1309.15	109.10	
Total	15	2370.18		

The critical t statistic (two tailed) used for the protected t test is $t_{0.10;12} = \pm 1.782$. The results obtained from comparing the various means are shown in Table 48. The table shows that only

the mean of the slag treated at 800 °C is significantly different to the means of the other slag samples (where H_0 is rejected). No significant differences were observed between the mean of the untreated slag samples and the means of the samples treated at 600 °C. These insensitive results are mainly due to the high value of 109.1 calculated for MS_{Error}.

Table 48: Summary of the results for the protected t test for the total energy required for crushing the miniature slag blocks

H_0	t	Result
$\mu_1 = \mu_2$	-0.53	Accept H_0
$\mu_1 = \mu_3$	-0.20	Accept H_0
$\mu_1 = \mu_4$	-2.75	Reject H_0
$\mu_2 = \mu_3$	0.33	Accept H_0
$\mu_2 = \mu_4$	-2.22	Reject H_0
$\mu_3 = \mu_4$	-2.55	Reject H_0

4. Statistical analysis of the maximum force measured during crushing

The maximum force measured during crushing of the miniature slag blocks were compared on the basis of the experimental treatment of the respective slag blocks. The ANOVA summary for the maximum force measured during crushing is given in Table 49. As F is greater than the critical F statistic ($F_{calculated} = 11.97 > F_{0.05;3;11} = 3.59$), we can therefore reject H_0. As we reject H_0, we can use the protected t test to distinguish between the means of the various experimental groups.

Table 49: ANOVA summary of maximum force required for crushing of miniature slag blocks

Source	df	SS	MS	F
Groups	3	46.61	15.54	11.97
Error	11	14.27	1.30	
Total	14	60.88		

The critical t statistic (two tailed) used for the protected t test is $t_{0.05;11} = \pm 2.201$. The results for the comparison of the various means are shown in Table 50.

Table 50: Summary of the results for the protected t test for the maximum force measured during crushing of the miniature slag blocks

H_0	**t**	**Result**
$\mu_1 = \mu_2$	-2.92	Reject H_0
$\mu_1 = \mu_3$	-0.16	Accept H_0
$\mu_1 = \mu_4$	-5.19	Reject H_0
$\mu_2 = \mu_3$	2.76	Reject H_0
$\mu_2 = \mu_4$	-2.48	Reject H_0
$\mu_3 = \mu_4$	-5.04	Reject H_0

The table shows that only the following set of means is not significantly different:

- Between the untreated slag and the slag treated at 600 °C for 96 hours.

5. Statistical analysis of the sieve analyses of the slag after crushing

The -500 µm sieve fractions of the samples obtained after the crushing of the miniature slag blocks were compared on the basis of the experimental treatment of the respective slag blocks. The ANOVA summary for this comparison is shown in Table 51. As F is greater than the critical F statistic ($F_{calculated} = 26.23 > F_{0.05;3;11} = 3.49$), we can therefore reject H_0. As we reject H_0, we can use the protected t test to distinguish between the means of the various experimental groups.

Table 51: ANOVA summary of percentage slag less than 500 µm after crushing

Source	Df	SS	MS	F
Groups	3	1716.60	572.20	26.23
Error	12	261.74	21.81	
Total	15	1978.34		

The critical t statistic (two tailed) used for the protected t test is $t_{0.05;12} = \pm 2.179$. The results for the comparison of the various means are shown in Table 52. The table shows that only the following set of means is not significantly different:

- Between the slag treated at 600 °C for 96 hours and the slag treated at 800 °C for 24 hours.

Table 52: Summary of the results for the protected t test for the percentage of slag less than 500 µm after crushing

H_0	t	Result
$\mu_1 = \mu_2$	4.92	Reject H_0
$\mu_1 = \mu_3$	8.04	Reject H_0
$\mu_1 = \mu_4$	7.26	Reject H_0
$\mu_2 = \mu_3$	3.12	Reject H_0
$\mu_2 = \mu_4$	2.34	Reject H_0
$\mu_3 = \mu_4$	-0.79	Accept H_0

APPENDIX K: X-ray diffraction patterns of samples used in unidirectional crushing testwork

The following abbreviations are used for the identification of phases:
M3 – M_3O_5 phase R – Rutile M6 – M_6O_{11} phase A – Anatase

Sample DB139: Untreated sample (Slag 2), -212 µm fraction

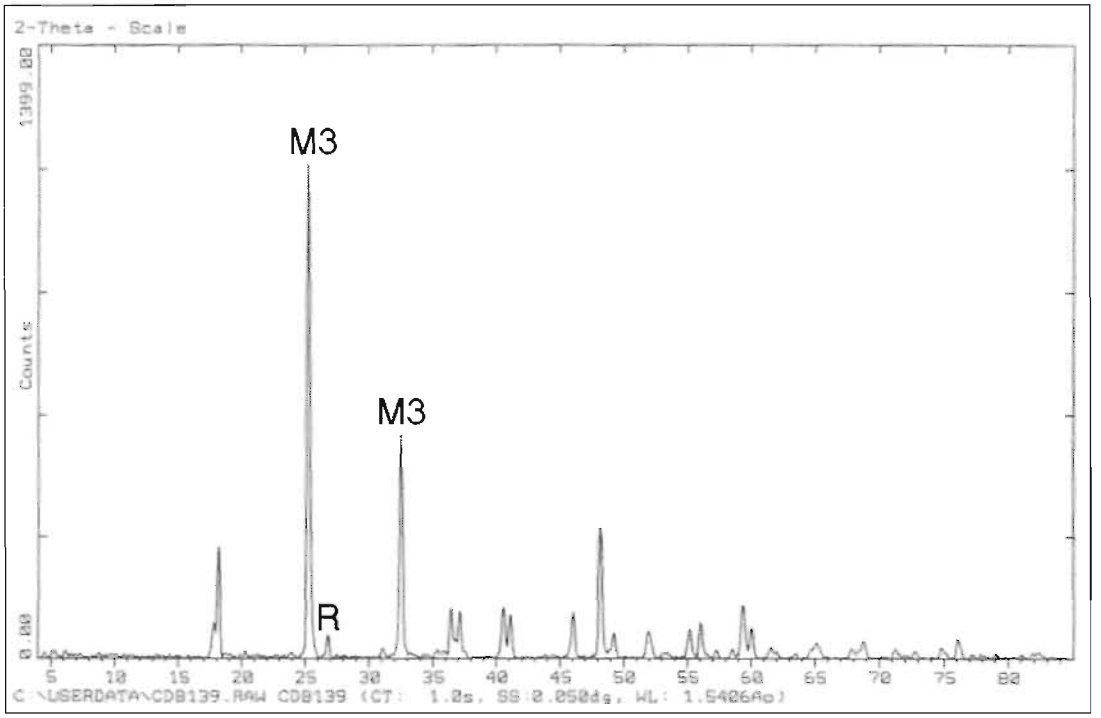

Sample DB145: Sample treated for 24 hours at 400 °C (-1 mm fraction obtained after decrepitation on quenching)

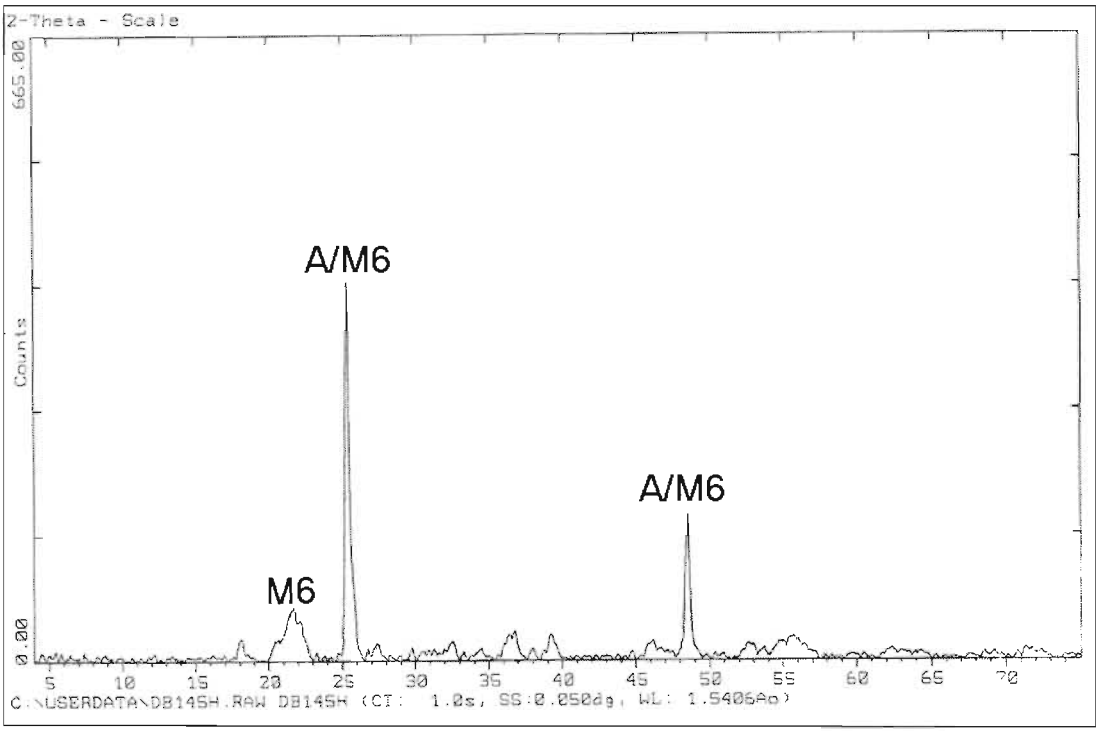

Sample DB146: Sample treated for 24 hours at 400 °C (+1 mm fraction obtained after decrepitation on quenching)

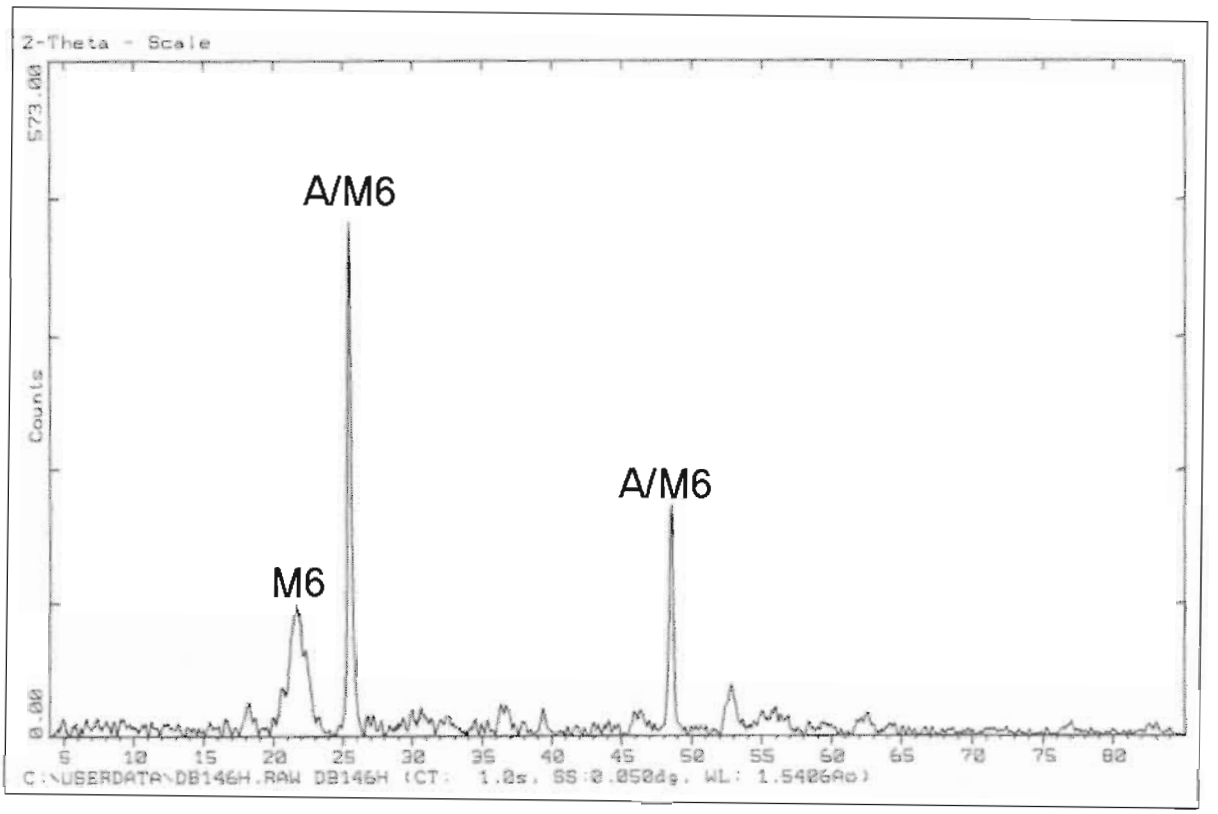

APPENDIX L: X-ray diffraction patterns of samples treated in different atmospheres

The following abbreviations are used for the identification of phases:
M3 – M_3O_5 phase R – Rutile M6 – M_6O_{11} phase A – Anatase

Sample DB184: Powder sample treated in air for 24 hours at 400 °C (Starting material DB100)

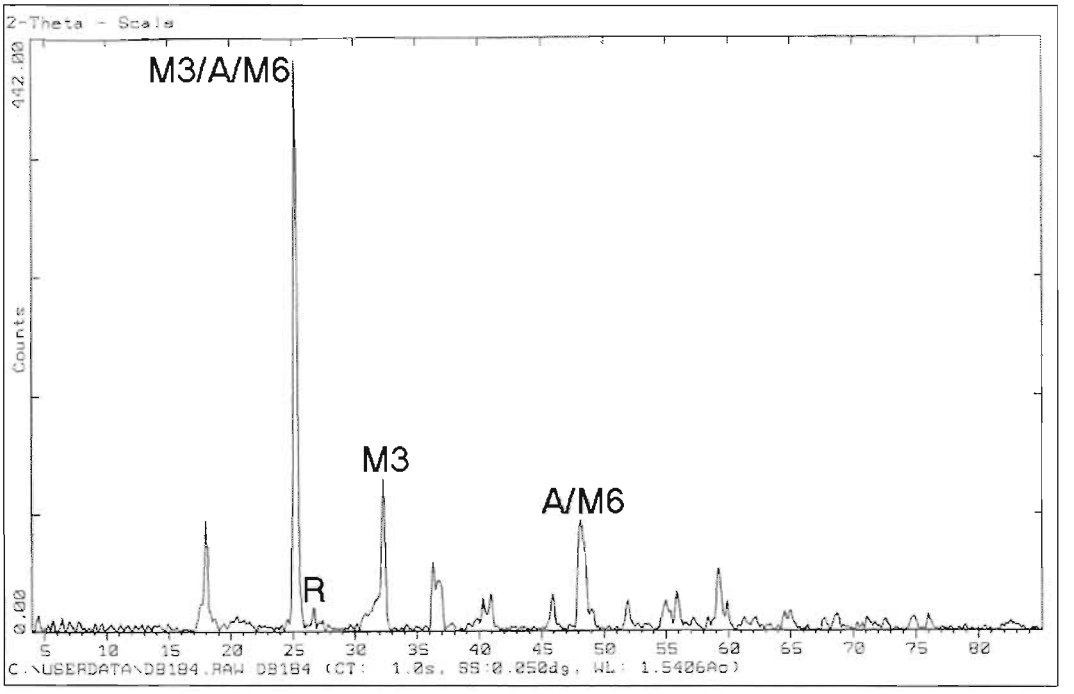

Sample DB196: Powder sample treated in argon for 24 hours at 400 °C (Starting material DB100)

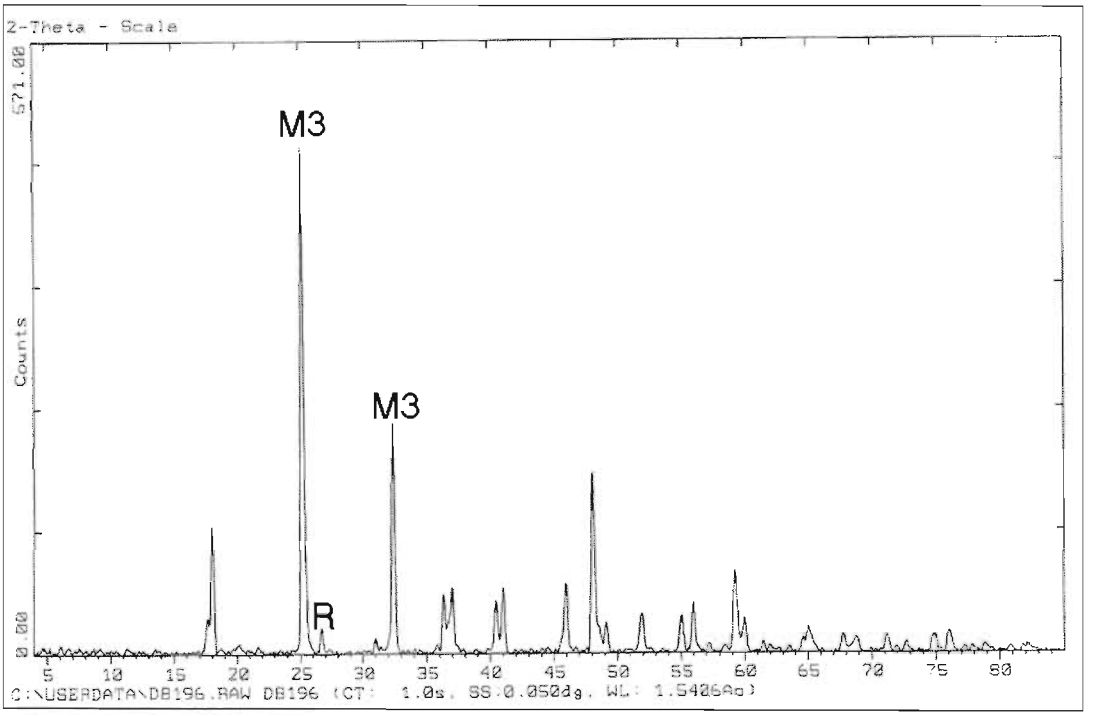

Appendix M: Investigation into the interaction between the SiC sheath material and titania slag

1. Introduction

For the determination of the cooling rate of the slag blocks during the 3MVA smelting campaign a thermocouple configuration was used with SiC as the outer sheath. At the completion of the cooling tests the sheath material was recovered to investigate whether any chemical reaction had taken place between the SiC sheath material and the titania slag. The SiC sheath material was in direct contact with the titania slag over a period of several days. The results obtained from the sheath used in tap 73 are given below. Over the test period a maximum temperature of 1654 °C was measured by the thermocouple (see Figure 61 for data on the cooling of the slag blocks).

2. Results

Figure 67 shows a photograph of the polished block prepared from a piece of the SiC sheath material contained in the slag. The interface between the sheath material and the titania slag appears to be well defined and relatively sharp. Some material from the slag/sheath interface were analysed by X-ray diffraction showing the following results:
Main phase – M_3O_5
Minor phase – Silicon carbide
Trace – Rutile.

Figure 67: Photograph of the polished block prepared from a piece of the sheath material embedded in the slag

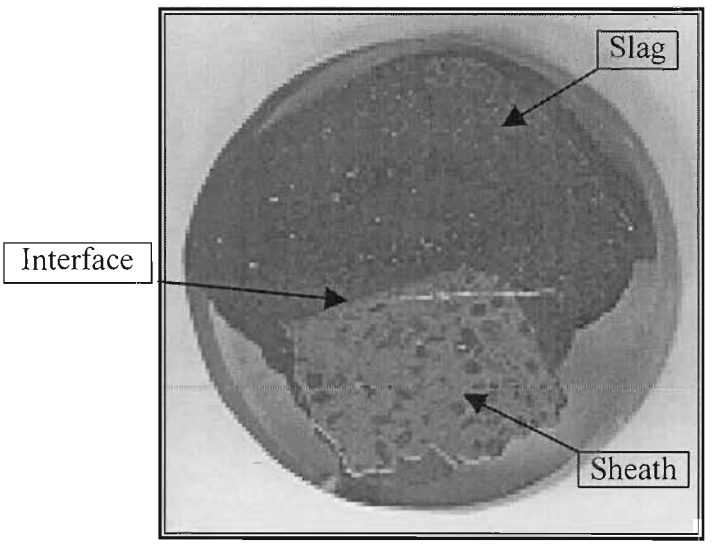

The sheath material consists of coarse-grained SiC particles contained in a fine SiC matrix. The sheath material seems to be slightly porous. This can be seen in Figure 68. In Figure 69 a photograph of the sheath/slag interface is shown. In the top right of the photograph the SiC sheath can be observed, while in the bottom left the titania slag can be seen. In-between a reaction zone, approximately 250 μm in width can be observed. This interface is characterised

by the presence of SiC particles, a ferro-silicon phase (containing trace amounts of titanium), titanium oxide rich slag and a silicon oxide rich glass phase. Trace amounts of fine-grained titanium carbide were also observed to be present in some areas of the interface (not shown in the figures).

Figure 68: Micrograph of the SiC sheath material (back-scattered electron image)

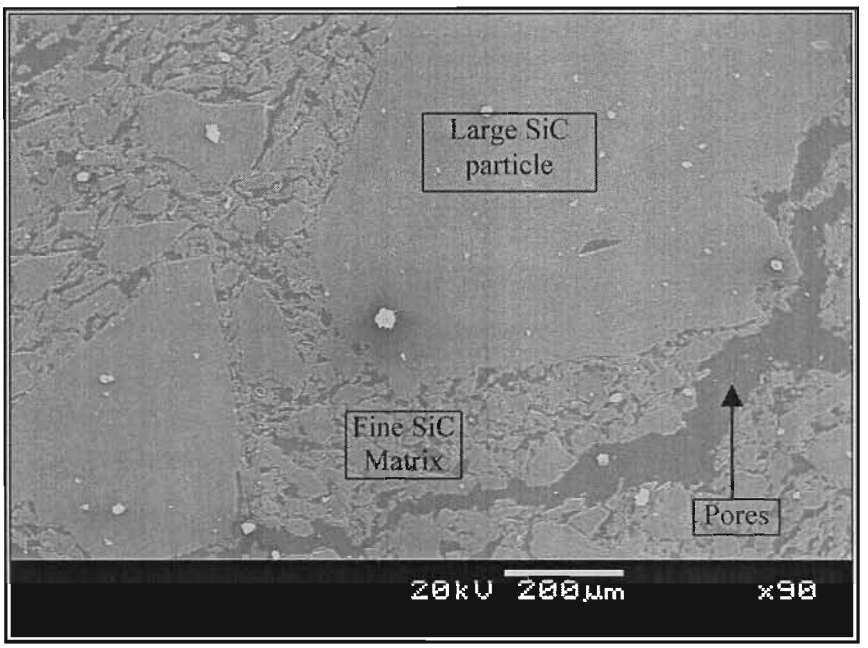

Figure 69: Micrograph of the sheath/slag interface

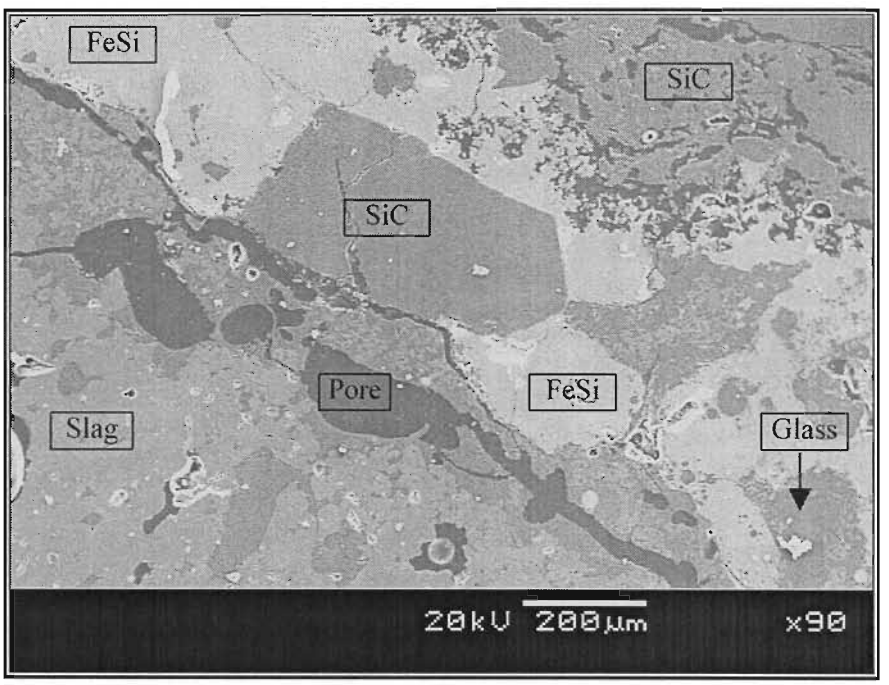

3. Conclusions

The SiC sheaths maintained their integrity and no catastrophic failure of the two sheaths occurred. From these results it seems that some chemical reactions took place at the interface between the slag and the sheath. This was however restricted to a small zone of approximately 250 μm. It seem that the M_3O_5 slag reacted with the SiC in the sheath to form ferro-silicon and silica rich glass phases, with some traces of TiC also present. The compositions of these phases were not investigated. It can be recommended that the SiC sheath material be used again for future testwork of this nature.

APPENDIX N: X-ray diffraction patterns for the decrepitated slag samples obtained during the ilmenite smelting campaign

The following abbreviations are used for the identification of phases:
M3 – M_3O_5 phase R – Rutile M6 – M_6O_{11} phase A – Anatase

Sample DB152: Starting material obtained from tap stream (tap 68)

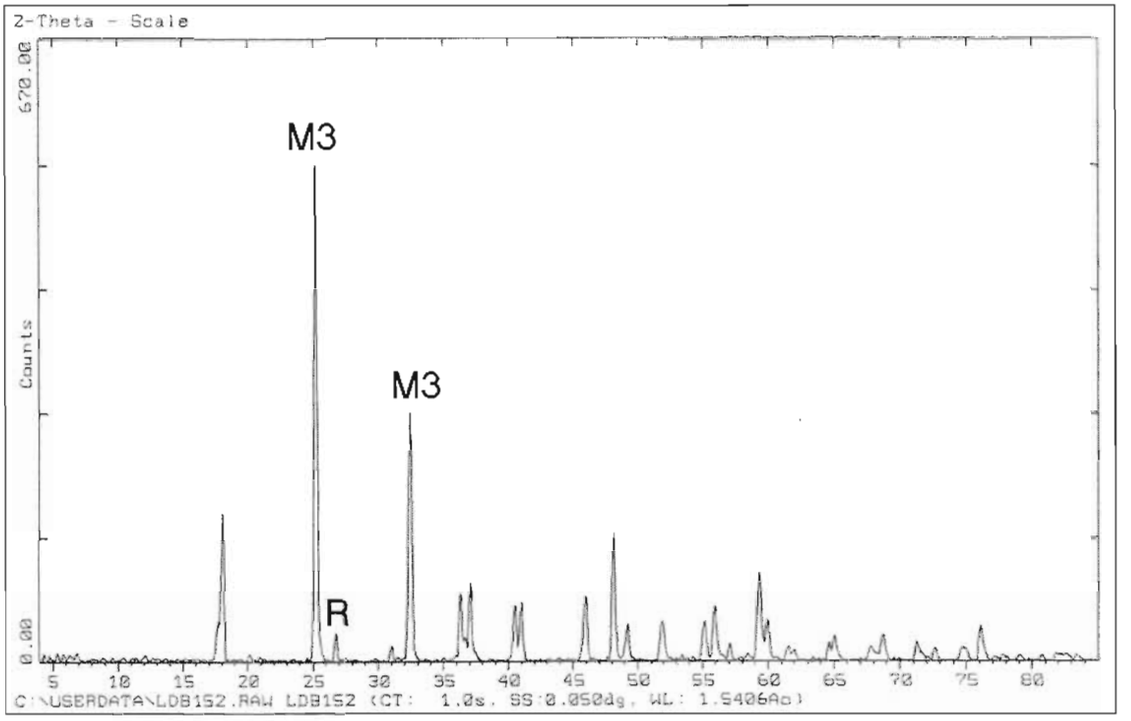

Sample DB153: Decrepitated sample from tap 68

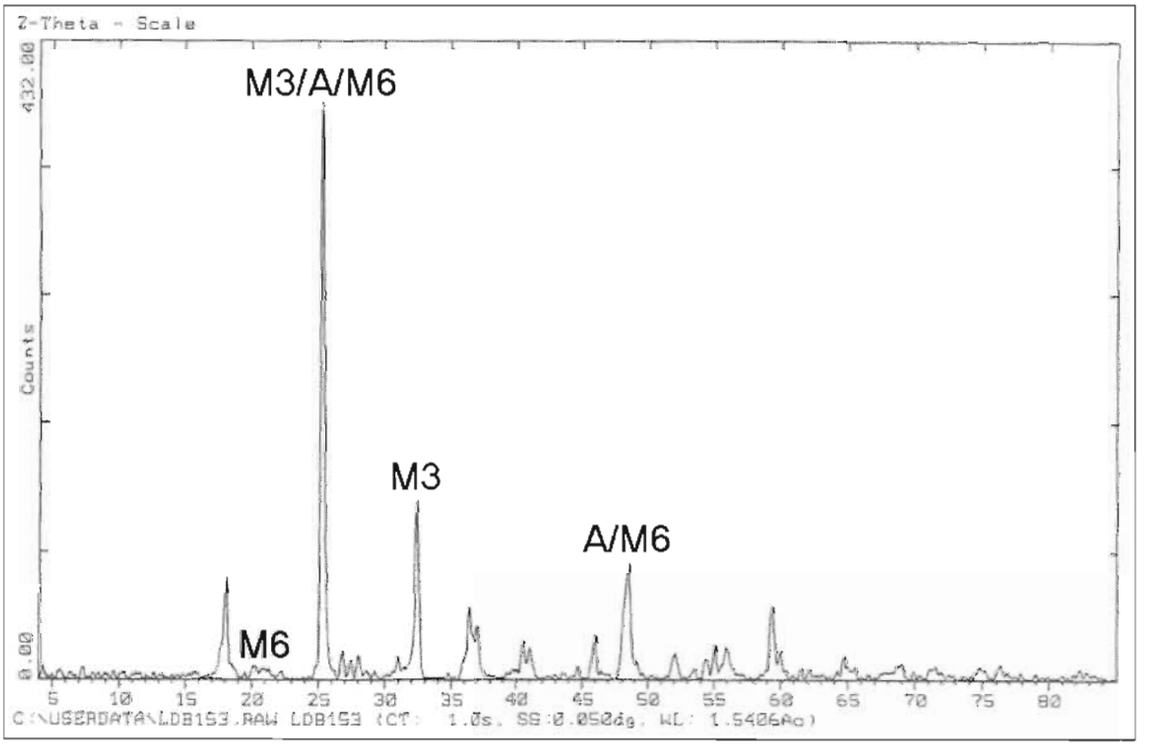

Sample DB154: Decrepitated sample from tap 68

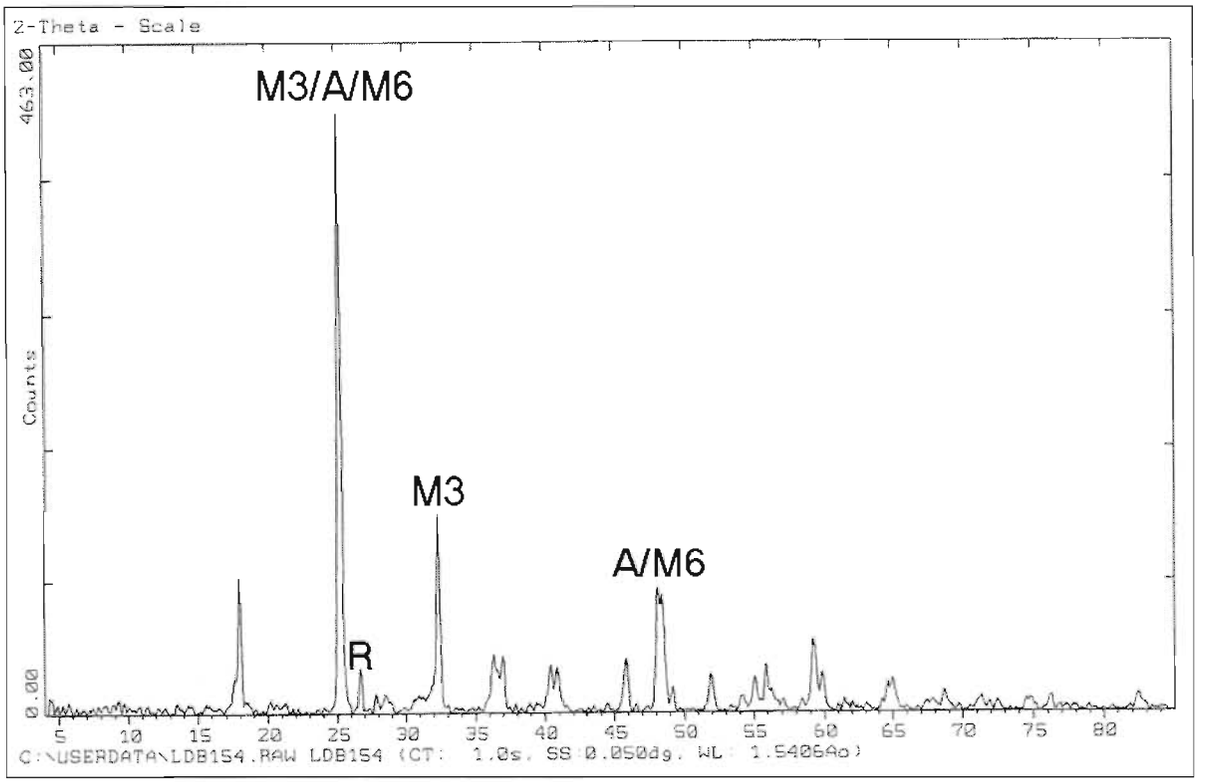

Sample DB155: Decrepitated sample from tap 68

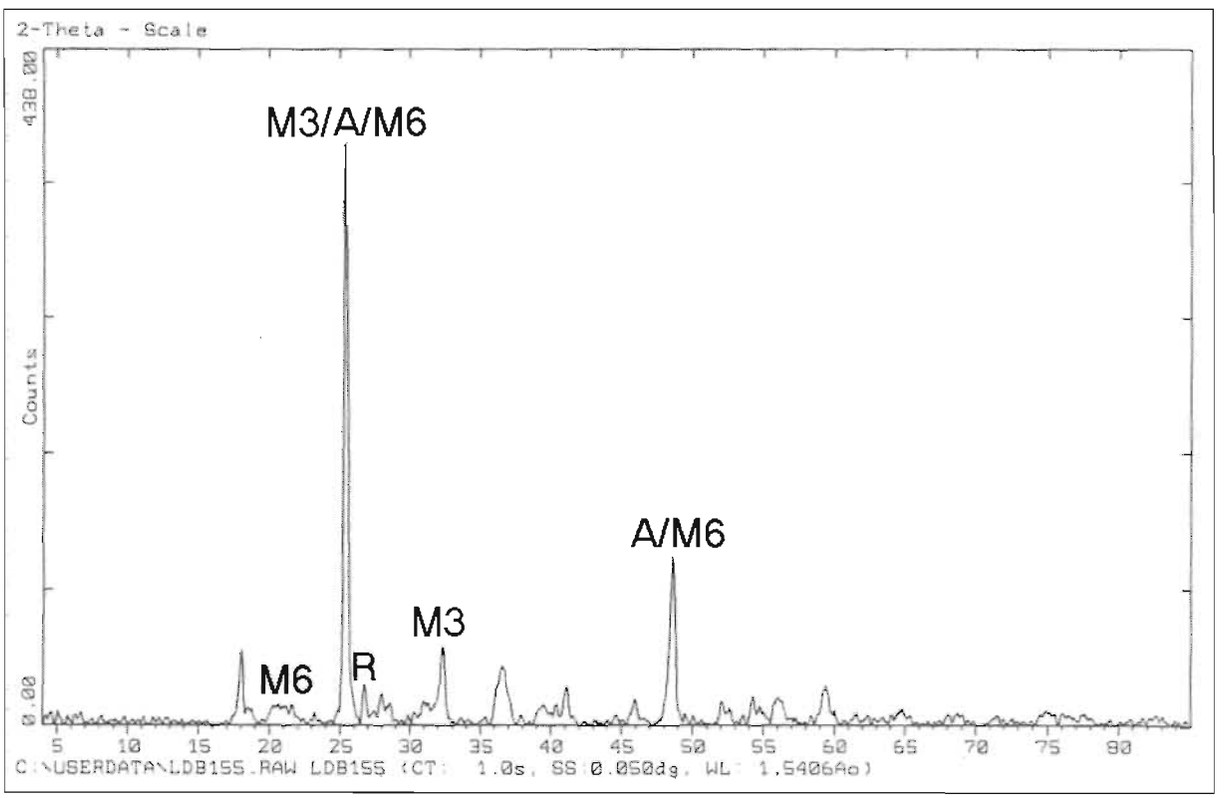

Sample DB156: Starting material obtained from tap stream (tap 70)

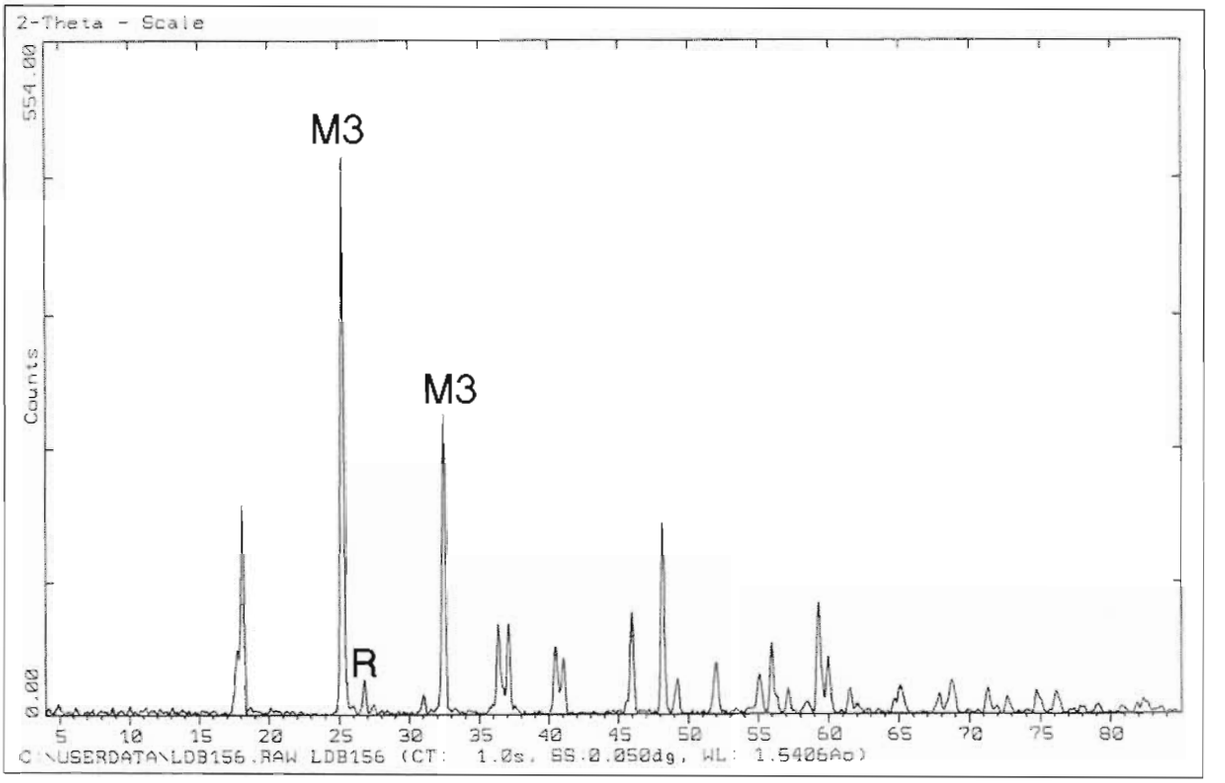

Sample DB157: Decrepitated sample from tap 70

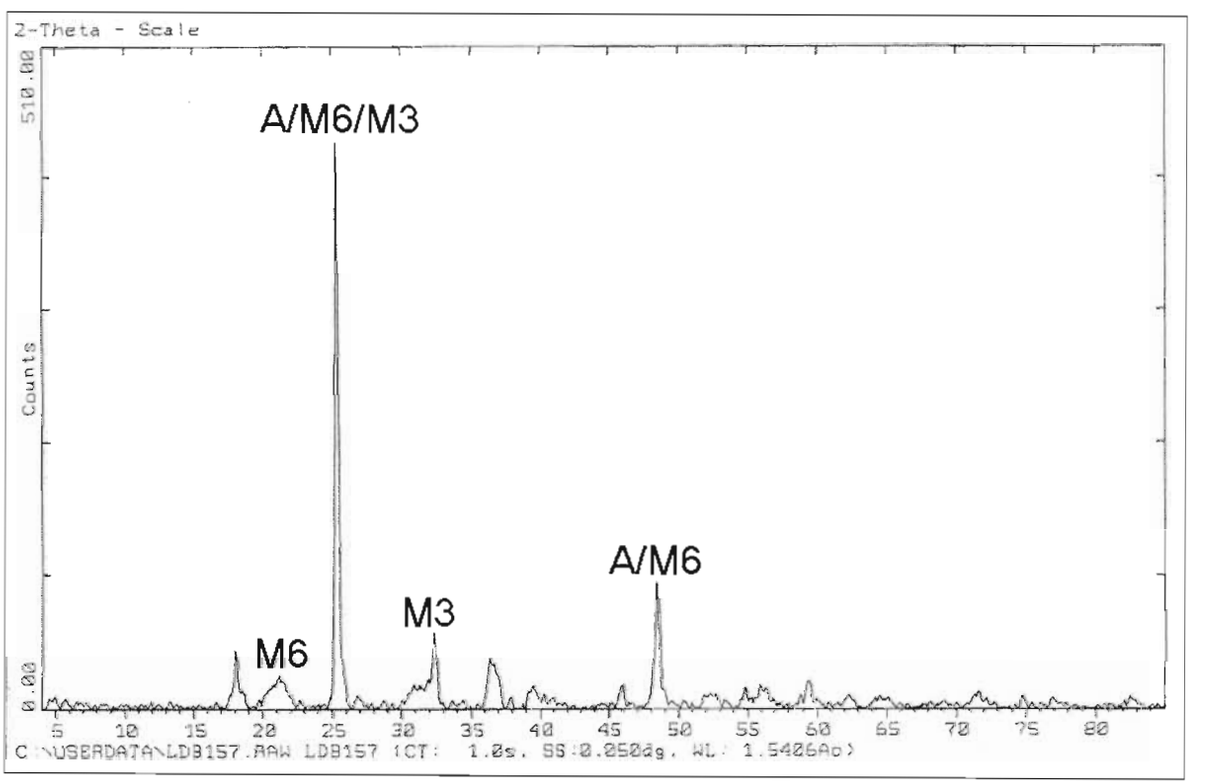

Appendix O: Data from density measurements

UNIVERSITEIT VAN PRETORIA
UNIVERSITY OF PRETORIA
YUNIBESITHI YA PRETORIA

MINTEK
200 Hans Strijdom Drive, Randburg
Telegrams: Minteksa, Johannesburg
Telex: 4-24867 SA Tel: (011) 709-4111
Fax: (011) 709-4564
All correspondence to:
Private Bag X3015Randburg 2125, South Africa

In your Reply please quote: 4189801

Mr Deon Bessinger
Iscor R&D
P.O. Box 450
Pretoria
South Africa
0001

Dear Deon

Density Measurements

I have pleasure in presenting you with our results of the density measurements for the six samples submitted.

The samples were pulverised in a rotating disc mill for 60 seconds to equalise their particle size distributions. The samples were dried overnight at 140°C to remove moisture, and cooled under vacuum to degas the surfaces of the particles and minimise surface porosity effects. A known mass (approximately 16g if available) of material was placed in a helium stereopychnometer and purged for 10 cycles before the volume of the samples was measured at ambient temperature. Ten volume measurements were made per sample and the results averaged. The density was calculated from the volume measurement and sample mass (Table 1). Prior to making the measurements, the instrument was calibrated using a standard of known volume. The uncertainty in the precision of the measurement is also shown in Table 1 and was estimated by taking into account reproducibility, sample mass, temperature fluctuations and particle size distribution. Samples DB 152 and 155 have relatively large errors because the measurements were made using a relatively small sample mass in comparison to the other measurements.

Table 1. Density (g/cm^3 or equivalent units)

	DB 152	DB 155	DB 156	DB 157	DB 175	DB 178
1	3.9540	3.9434	3.9676	3.9400	3.9404	3.9285
2	3.9547	3.9429	3.9676	3.9397	3.9406	3.9288
3	3.9556	3.9442	3.9678	3.9406	3.9410	3.9282
4	3.9550	3.9435	3.9679	3.9397	3.9409	3.9279
5	3.9553	3.9421	3.9676	3.9394	3.9398	3.9272
6	3.9551	3.9441	3.9672	3.9404	3.9403	3.9263
7	3.9545	3.9433	3.9666	3.9392	3.9404	3.9261
8	3.9545	3.9439	3.9661	3.9395	3.9402	3.9252
9	3.9542	3.9413	3.9661	3.9391	3.9402	3.9241
10	3.9533	3.9431	3.9656	3.9390	3.9392	3.9240
Mean	3.9546	3.9432	3.9670	3.9397	3.9403	3.9266
Stdev	0.0007	0.0009	0.0008	0.0005	0.0005	0.0018
Uncertainty	0.028	0.092	0.028	0.047	0.028	0.028

Please feel free to contact me if you want to discuss the result in more detail.
Yours sincerely

Steve McCullough
MINERALOGY